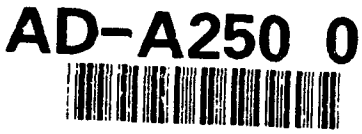

(1)

A COMPARATIVE STUDY OF THE

DYNAMIC PERFORMANCE OF THREE BIVANES

A Thesis

Submitted to the Faculty

of

Purdue University

by

William Gettis Coats, Jr.

In Partial Fulfillment of the

Requirements for the Degree

of

Master of Science

May 1991

REPORT DOCUMENTATION PAGE

Form Approved
OMB No. 0704-0188

1. AGENCY USE ONLY (Leave blank)	2. REPORT DATE	3. REPORT TYPE AND DATES COVERED
	May 1991	THESIS/~~DISSERTATION~~

4. TITLE AND SUBTITLE
A Comparative Study of the Dynamic Performance of Three Bivanes

5. FUNDING NUMBERS

6. AUTHOR(S)
William G. Coats, Jr., Capt

7. PERFORMING ORGANIZATION NAME(S) AND ADDRESS(ES)
AFIT Student Attending: Purdue University

8. PERFORMING ORGANIZATION REPORT NUMBER
AFIT/CI/CIA- 91-107

9. SPONSORING/MONITORING AGENCY NAME(S) AND ADDRESS(ES)
AFIT/CI
Wright-Patterson AFB OH 45433-6583

10. SPONSORING/MONITORING AGENCY REPORT NUMBER

11. SUPPLEMENTARY NOTES

12a. DISTRIBUTION/AVAILABILITY STATEMENT
Approved for Public Release IAW 190-1
Distributed Unlimited
ERNEST A. HAYGOOD, Captain, USAF
Executive Officer

12b. DISTRIBUTION CODE

13. ABSTRACT *(Maximum 200 words)*

14. SUBJECT TERMS

15. NUMBER OF PAGES
165

16. PRICE CODE

17. SECURITY CLASSIFICATION OF REPORT	18. SECURITY CLASSIFICATION OF THIS PAGE	19. SECURITY CLASSIFICATION OF ABSTRACT	20. LIMITATION OF ABSTRACT

I dedicate this work to you, Ruth, and our four boys
Benjamin, Charley, Sam, and Paul.
You all have tolerated a lot.

ACKNOWLEDGMENTS

I am delighted to finally be writing this page. I want to thank the many who brought me to this point. I appreciate Dr. Snow's integrity and leadership as he led me through the work of this study. I am grateful to Dr. Vincent for stepping in for the Saudi Arabia bound Lt Col Snow. His wise and comforting counsel in response to my moments of distress, and his down-to-earth attitude was and is a huge source of encouragement. I thank Dr. Petty for his timely guidance and excellent comments concerning this thesis. I thank Dr. Wood for the use of his wind tunnel and his constructive criticisms. I valued Dr. Baker's guidance pertaining to this study and particularly his money that paid for it.

I thank C. J. Fuqua, Inc. for the release mechanism an lots of technical advice. I also thank Charley Crow for machining the static test jigs. I also want to thank Mrs. Helen Henry and Mrs. Michelle Akridge for their tremendous amounts of help and their interest in my family.

There is absolutely no way I could have accomplished these two years without my wife, Ruth, and our four boys, Benjamin, Charley, Sam, and Paul. While cooking many a supper, Ruth listened when I paced the kitchen floor mulling over programming code. Ruth showed me the difference between the important and the urgent. Ruth and the boys prayed for me often, and God answered those prayers. During this time, Benjamin learned how to read, Charley learned his letters and their sounds, Sam learned his numbers, and Paul was born. I have missed much, and I hope I never have to miss out on my family again.

I thank Tom McClellan for his turbulence advice, and Don Lund for his "Lotus-Eating" expertise and showing me how to perform a wind tunnel experiment. I thank Carl Daudt and Tom Davies for their programming help and spiritually uplifting words. My In-laws and those at Upper Room Christian Fellowship obviously were praying for me. I owe a lot to a very important person, Mrs. Lynn W. Crider, who taught her son the joy of learning when many thought he could not learn. She believed in me.

TABLE OF CONTENTS

LIST OF TABLES

LIST OF FIGURES

Figure Page

Figure Page

Figure Page

Figure Page

Figure Page

Figure Page

Figure Page

LIST OF ABBREVIATIONS AND SYMBOLS

Abbreviation	Description
ASTM	American Society for Testing and Materials
CW	Clockwise
CCW	Counterclockwise
DC	Direct Current
EPA	Environmental Protection Agency
LVDT	Linear Variable Displacement Transducer (Climatronics)
PSID	Pounds per Square Inch Differential

Symbol	Description
A	Amplitude of a peak
A	Projected area of the fin onto the plane of attack
C_L	Lift coefficient
D	Delay distance
T_D	Time when D occurs
F	Force
T	Torque
U	Wind speed
V_{az}	Azimuth voltage
V_{el}	Elevation voltage
ΔV	Voltage error produced by bent wiper in a potentiometer
θ	Azimuth wind angle
ϕ	Elevation wind angle
T_i	Times of the zero-crossings
τ_j	Times of the peaks
ζ	Damping ratio
ω_n	Natural frequency
ω_d	Damped frequency
λ_n	Natural wavelength
λ_d	Damped wavelength
Λ_0	Velocity of the vane at the equilibrium angle

1. INTRODUCTION

The need for data on the fluctuations of both azimuth and elevation wind directions has increased in recent years particularly for the measurement of atmospheric turbulence. Instruments used for this purpose can be expensive and are often vulnerable to the harsh natural environment. One instrument promoted as being rugged with accurate response to wind fluctuations over extended periods of time, is the bi-directional wind vane or bivane. After testing the Brookhaven National Laboratory (BNL) Bivane, D. A. Mazzarella determined that the bivane can respond to atmospheric eddies that are significant in the dispersion of smoke (Mazzarella, 1952). In this context, the United States Environmental Protection Agency (USEPA) is in need of an inexpensive and durable means to measure wind fluctuations that would characterize dispersion of atmospheric contaminants. Therefore, they are funding the present research to find out if bivanes can indeed meet the requirements necessary to accomplish this objective. One part of this objective is to examine which one best responds to changes in wind direction. A second part will be to determine how well the bivane can measure vertical flux of horizontal momentum using procedures outlined in Chimonas (1980). This paper addresses the first part.

1.1 Description of Bivanes

A bivane is a wind sensing instrument that measures the horizontal or azimuthal angle and the vertical or elevation angle of the wind direction (from now on, the term wind direction will refer to both azimuthal and elevation wind angles). A bivane is composed of four parts: a vane assembly or sensor, two transducers, signal conditioning electronics, and a data logging/display system. The vane assembly (typically a boom and tail or a possibly more inventive design) physically aligns itself with the wind direction by pivoting about two axes. Thus, the bivane moves about in two planes: horizontal and vertical. It pivots

ABSTRACT

Coats, William Gettis, Jr. M.S., Purdue University, May 1991. A comparative study of the dynamic performance of three bivanes. Major Professor: John T. Snow. Acting Major Professor: Dayton G. Vincent.

The dynamic performances of three multi-directional wind vanes, or bivanes, are studied and compared for the purpose of determining which bivane responds the fastest to changes in wind direction, with acceptable accuracy. The manufacturers of these bivanes are the R. M. Young Co., Teledyne Geotech, and Climatronics Corp. The procedures for testing the bivanes include evaluations on the static and dynamic characteristics of each bivane, and comparing how well each conforms to published standards. The static tests determined the accuracy and linearity of each bivane. Deviations from the ideal linear response were used to correct the dynamic test data.

The dynamic tests were performed in the large Civil Engineering wind tunnel at wind speeds of 5 and 10 m s^{-1}. The bivanes were released from six positions and allowed to return to the equilibrium angle. All three bivanes produced second-order underdamped responses necessary to rapidly adjust to a change in wind direction. Using the times of the first peak and second zero-crossing, the damping ratio, ζ, and natural wavelength, λ_n, were calculated. The ζ and λ_n described how well and fast the bivane responds to changes in wind direction. Apart from technical irregularities in a portion of the electronics, the Climatronics Dual Annulus Bivane responded the quickest and appears to be the best bivane for yielding wind components. In a subsequent study, the wind measurements from this bivane will be used to compute vertical flux of horizontal momentum in accordance with the techniques described by Chimonas (1980).

about the axis that is normal to the horizontal (vertical) plane measuring an azimuthal (elevation) wind angle, θ (ϕ). Two transducers (one for azimuth and one for elevation) translate the mechanical signals of the vane assembly into two electrical signals. Signal conditioning electronics inputs azimuth and elevation electrical signals produced by the transducers and outputs two discrete electrical signals associated with the vane assembly position. A data logging/display system translates these two output signals into a useable form.

The R. M. Young Company, Teledyne Geotech, and Climatronics Corporation manufacture the three bivanes considered in this research. Each employs different vane assemblies, transducers, and signal conditioners. All three outputs were sampled with the same data logging system.

1.1.1 R. M. Young Gill Bivane Model 17003

The R. M. Young Company of Traverse City, Michigan produced the Gill Bivane Model 17003 (Figure 1) specifically for micrometeorological research to sense rapid fluctuations in wind direction near the earth's surface (R. M. Young Co. Catalog, 1989 and R. M. Young Co. Gill Bivane Instructions,1979). The boom of the vane assembly is made of aluminum alloy and the fin is made of low density foamed polystyrene (current production of Gill Bivanes use low density expanded polystyrene or EPS for the fin). Stainless steel and plastic complete the housing and mechanical parts of the bivane.

The design of the Gill Bivane is straightforward with a rectangular shaped bracket on the vane assembly which sits on a horizontal axle so that the vane assembly directly governs the axle's movement. The horizontal axle transfers the vertical movement of the vane using a bead chain and pulley. The bead chain grants free azimuthal movement of the vane without the chain winding up. The chain is threaded down the hollow portion of a plastic shaft that is inside the post of the housing. The chain is connected to another pulley with the same diameter of the first pulley on the horizontal axle. A counterweight on the lower pulley keeps the chain taught, eliminating backlash. The lower pulley is attached to 1000 ohm potentiometer. Via this pulley and chain system, the potentiometer's wiper directly corresponds to the elevation angle of the vane. The output range produced is 0 to 12 volts DC.

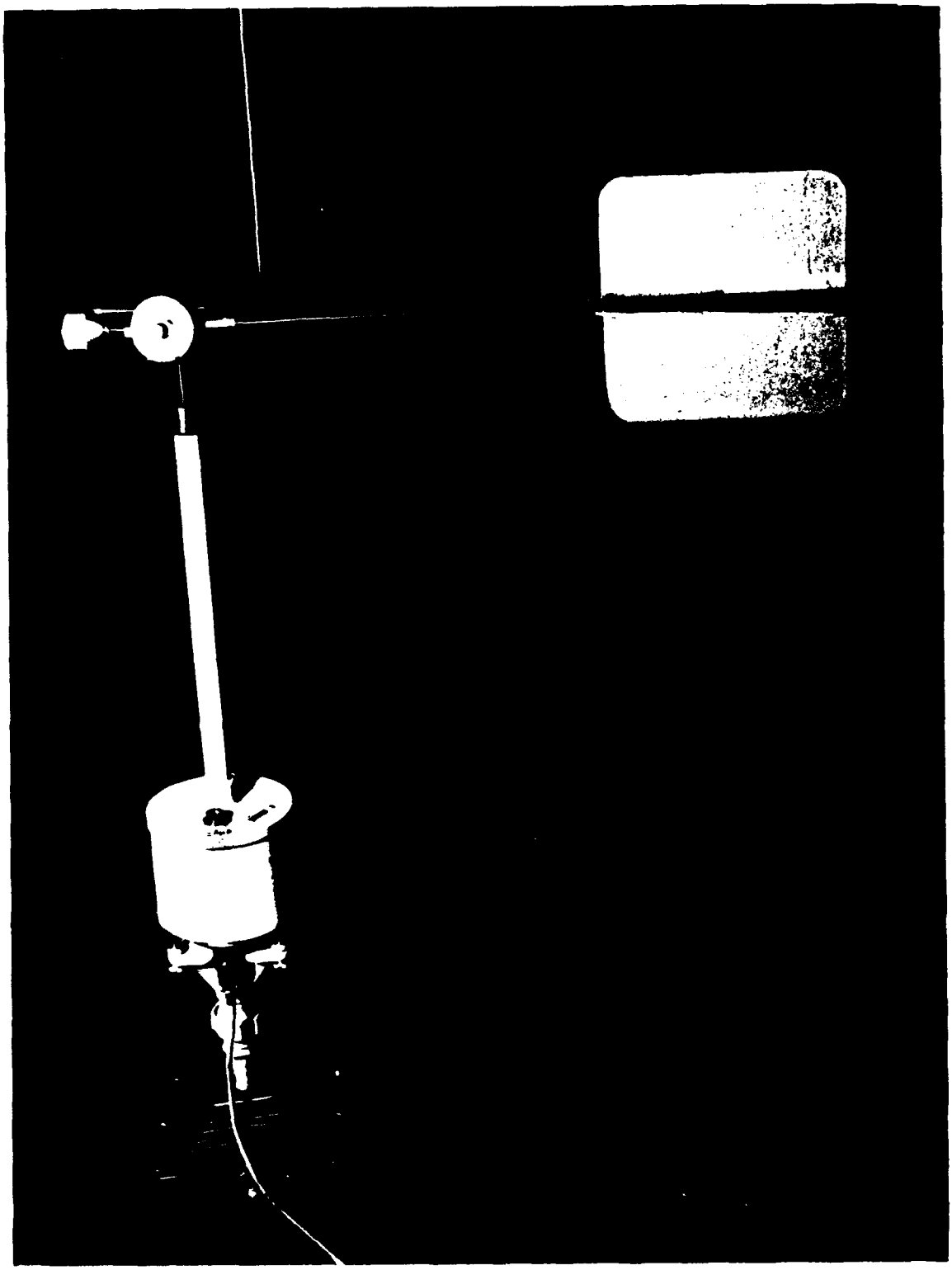

Figure 1. The R. M. Young Gill Bivane Model 17003.

Attached to the horizontal axle housing is a vertical axle that allows the vane to move horizontally. This vertical axle connects to a plastic shaft or tube located inside the housing post. A gear system on the lower end of the shaft connects to another 1000 ohm potentiometer and its wiper directly corresponds to the vane's azimuthal position. The output range for azimuthal angles is also 0 to 12 volts DC, representing 0° to 355°.

The R. M. Young bivane is the largest of the three sensors tested. Its vane assembly is 76.2 cm in length with its cruciform fin measuring 23 x 23 cm. The tail is that portion of the vane assembly which is from the pivot point to the end of the fin and measures 64.8 cm. The forward portion of the vane assembly from the pivot point is 11.4 cm in length. Each cruciform plate is approximately 0.5 cm thick. The entire vane assembly has a mass of 478.7 g. The diameter of the post holding the vane assembly is 2.7 cm and is 40 cm in length. A much thinner secondary post extends 4.5 cm above the main post and holds the upper pulley housing. This housing measures 6.5 cm in diameter and is 3 cm thick. The distance from the top of the lower housing to the pivot point is 47 cm. Under calm conditions the vane remains stationary without returning to a reference position.

All parts of the R. M. Young Gill Bivane appear to be well engineered and their function easily understood. If problems arise, they are easily diagnosed and their repair can usually be made in the field in minimum time.

1.1.2 Teledyne Geotech Multidirectional Bivane Model 1585

Teledyne Geotech of Garland, Texas engineered its Bivane Model 1585 (Figure 2) to be rugged for measuring atmospheric instability and estimating dispersion profiles (Teledyne Geotech, 1987). The design uses no contact transducers for a better transfer of mechanical movement of the vane assembly to an electrical signal.

The vane assembly is of aluminum construction with a flat plate fin in a cruciform orientation and rotated 45°. A flange, trimming the back edge of the fin sections by 0.4 cm, prevents boundary separations

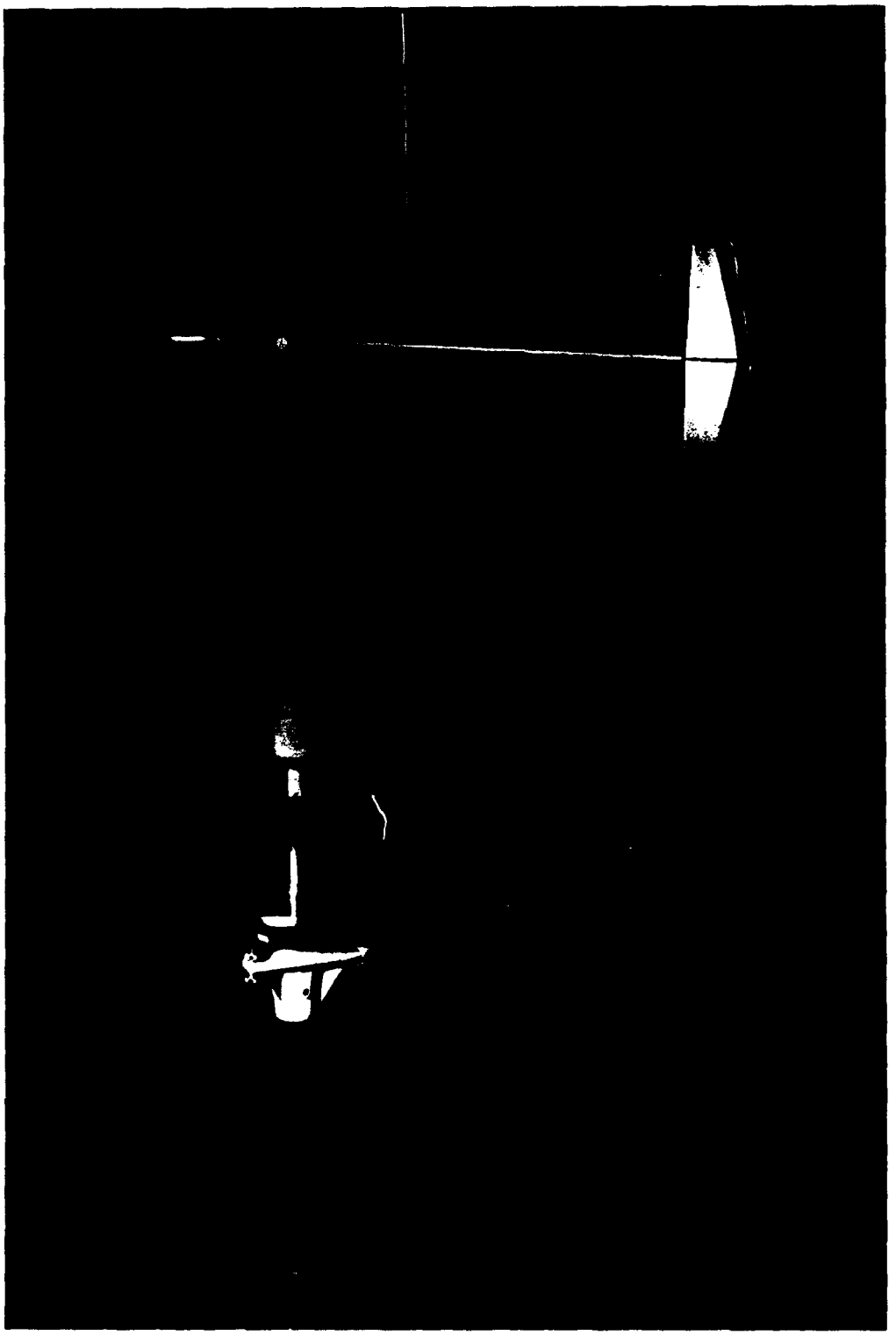

Figure 2. The Teledyne Geotech Multidirectional Bivane Model 1585.

due to the fin's thickness. The thickness of the fin is 0.5 cm, while the flange is 0.04 cm thick. Both plates of the cruciform are 30.5 cm in length and have a tapered width from 6.5 cm in the center to 4.0 cm at the ends.

Operating as a transformer, a resolver senses azimuthal angles. A shaft directly connected to the vane assembly rotates freely through a winding. Two secondary windings, at right angles to each other, are in phase with the primary winding, but differ in magnitude and sign according to the shaft angle. The outputs of the two secondary windings are added, producing a constant amplitude signal that varies in phase from 0 to 360 degrees, directly associated with the shaft angle. Subsequent conditioning circuitry produces an output voltage with the range of 0 to 5 volts DC.

An inductor transducer senses the elevation angles. Directly above a ferrite sensor are a pair of cams that are connected to the horizontal axis. As the vane pivots about the axis, the spacing between the cams and the ferrite sensor changes that in turn changes the current. The conditioned output signal ranges from 0 to 5 volts DC.

Dimensions of this bivane are 54 cm for the vane assembly of which 42.5 cm trail the pivot point. The entire vane assembly has a mass of 196.8 g. The fin dimensions are 30.5 x 30.5 cm. The post diameter is 4.5 cm that is considerably thicker than the other two bivanes. The post is 39.8 cm in length. There is no azimuthal reference angle, but the vane returns to a horizontal position under calm conditions for the elevation reference angle.

The Teledyne Geotech bivane uses advanced electronic technology to ensure the final signal output accurately represents the vane angle. Great care was used to eliminate frictional effects at the mechanical and electrical interfaces. The signal conditioning electronics also produces output as audio frequencies that allow the vane to transmit signal information up to 10 miles, giving it more remote capabilities than the other two bivanes.

1.1.3 Climatronics Dual Annulus Bivane

Climatronics Corporation of Bohemia, New York produces a bivane (Figure 3) with a dual annulus designed to be a rugged, highly responsive wind sensor to measure rapid fluctuations of wind direction

(Climatronic's Dual Annulus Bivane instruction manual, 1987). The work of Garbell (1947), Mazzarella (1952), Wierninga (1967), Baker and Sethu Raman (1987), and SethuRaman and Tuthill (1978) discuss the evolution of the annular type of biane. Tests by M. A. Garbell suggest that a cambered annular fin is an effective bivane fin design. D. A. Mazzarella determined that the annular bivane could resolve smaller eddies than those obtained from conventional flat-plate cruciform designs. Extensive studies of many types of bivane fin designs led J. Wierninga to discuss the practical utility of fins employing other than straight or flat designs. Additional structural characteristics on a fin causes more complex responses. Increasing the complexity also introduces additional problems and disadvantages that are more difficult to correct. It is more advantageous to use fins that respond to the air flow without altering the very air flow the bivane intends to measure. Climatronics doesn't employ an airfoil shape to its annuli. The annuli have straight, parallel sides minimizing alteration of air flow due to fin design. Thus, by avoiding the airfoil design, the Climatronics Dual Annulus bivane attempts to measure an unaltered wind flow.

The vane assembly consists of carbon fiber for the annuli and struts. The entire vane assembly weighs less than one ounce creating a very small moment of inertia. The larger annulus is behind the pivot point, while the smaller is found before the pivot point.

A synchro transducer senses azimuth wind direction via a shaft that is connected to the vane assembly. As the vane assembly turns horizontally, a printed circuit board located in the housing, conditions the synchro transducer output. Final sensor output for azimuth signal is from 0 to 1 volt DC.

A linear variable displacement transducer (LVDT) senses the elevation wind direction. Connected to the vane assembly is a pulley-dacron string system that travels through the LVDT and is held taught by a small weight. Inside the LVDT, the string holds a slug. The position of the slug corresponds to the vertical angle of the vane and the LVDT outputs the appropriate signal. Circuitry converts the LVDT signal to a 0 to 1 volt DC output representing -45° to +45°.

The vane assembly is 26 cm in length and is located 20.3 cm beyond the pivot point. Diameters of the annuli are 12.5 cm for the larger and 7 cm for the smaller. The post is 1.8 cm in diameter and 16.5 cm in

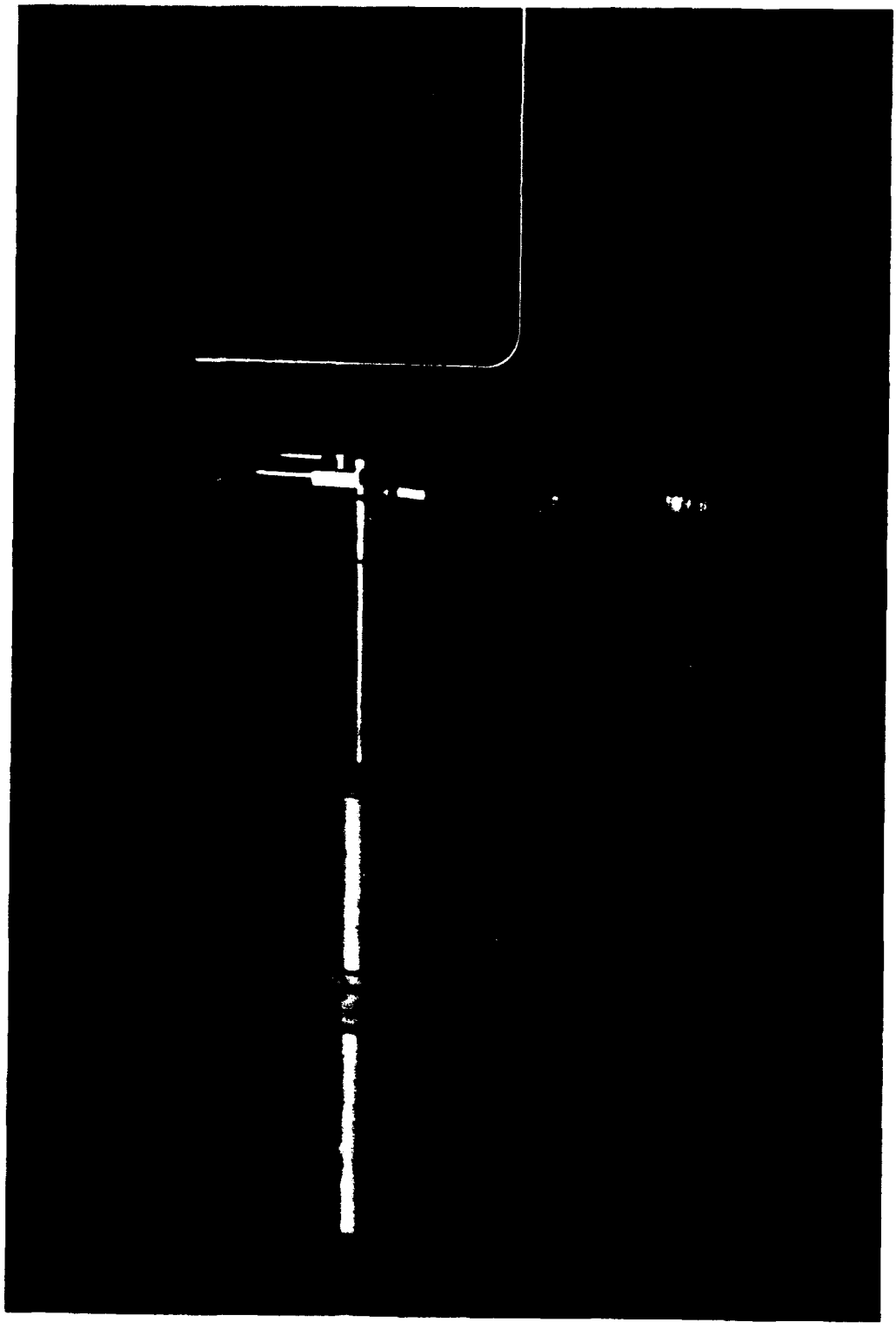

Figure 3. The Climatronics Dual Annulus Bivane.

length. The vane doesn't return to a reference azimuthal angle under calm conditions. For the elevation reference angle, it returns to an elevation of zero degrees or the horizontal position under calm conditions.

The design and materials of the Dual Annulus bivane show a priority at Climatronics to produce an environmentally tough, yet sensitive wind instrument. Its vane assembly was well thought out, with a documented research background. The conditioning electronics is theoretically sound and technologically advanced. Calibration and maintenance can't be performed by the user; the instrument must be returned to the manufacturer for these services.

1.2 Thesis Organization

Each of these bivanes is designed to measure changes in azimuthal and elevation wind directions using different vane assembly designs, transducers, and conditioning electronics. Designed to withstand harsh environmental conditions, all three bivanes can be used in the field over long periods of time. Assuming each has similar durability, this study focuses on the dynamic characteristics of each instrument. This paper discusses the performance properties or abilities of each bivane to measure wind directions accurately. First, the methodology used in this study for testing and calculation procedures to determine static and dynamic characteristics is described. This is followed by chapters on examination of calculated results with a discussion of observations, and a final chapter on summary and conclusions.

2. TEST PROCEDURES

According to the American Society for Testing and Materials (ASTM), the dynamic performance of wind vanes can be described using the parameters of damping ratio, ζ, and natural wavelength, λ_n. For bi-directional wind vanes, two sets of these parameters theoretically exist, one each for azimuth and elevation directions. This is true if the vane motion in the horizontal and vertical planes are independent. Static testing revealed the two axes were indeed independent. (See the section on Static Testing Procedures in this chapter.)

For both the static and dynamic tests, output voltages from the sensors were input into a data acquisition system consisting of an analog-to-digital converter aboard a computer with data acquisition software. The analog-to-digital converter was a Computer Boards, Inc. CIO-AD08 that allowed for up to eight synchronic analog input signals. Each analog signal was sampled sequentially and converted to a digital signal. The resolution of the analog-to-digital converter was 0.00244 vdc over a set 10 vdc range. This voltage resolution translated into a angle resolution of as little as 0.04° for the elevation angle on the R. M. Young bivane to as high as 0.88° for the azimuth angle on the Climatronics bivane. The difference in angle resolution is due to the R. M. Young bivane producing a voltage range of 12 volts, while the Climatronics bivane outputs a 1 volt range.

A CompuAdd 212 computer ingested the newly digitized voltage from the bivanes. Though slower than current state-of-the-art microprocessors used in many personal computers, the Intel 80286 microprocessor in the CompuAdd 212 performed the data management of each test quite well. Laboratory Technologies Corporation's Labtech Notebook Ver. 4.12 collected and filed the bivane data into ASCII format.

The setup was identical for both the static and dynamic tests. Static tests were performed on all three bivanes in the large section of the Civil Engineering wind tunnel at Purdue University (Figure 4). The dimensions of the large section are 1.83 m wide, 2.44 m long, and 1.83 m high. With the fan off, each bivane was attached to a three-screw, two-planar jig used to level the bivane. This leveling jig was fastened to a one inch pipe that was coupled to a solid steel rod that passed through a two inch diameter hole in the center of the tunnel floor. This rod was anchored to a heavy platform that rested on the concrete floor underneath the wind tunnel. With this setup, any movement inside the tunnel did not disturb the already leveled bivane. A rubber covering was placed around the rod where it passed through the tunnel floor preventing any exchange of air inside and outside the wind tunnel.

Wiring from the bivanes was taped to the tunnel floor and passed through a slot on a side wall to the signal conditioners or a circuit board.

2.1 Static Testing Procedures

Static testing the bivanes had a two-fold purpose: to determine if the motion about the two axes were in fact independent, and to measure the linearity of angle versus bivane output voltage. Concerning the latter, all transducers and conditioning electronics used in these bivanes theoretically produce output that are perfectly linear with respect to angle. Practically, no transducer/conditioning electronics can produce a perfectly linear output. Thus, the static test details the output versus true angle and reveals any asymmetry due to the transducers or assemblies. The difference between the actual voltage output and what would be the true linear output if the transducer was perfect can then be used to correct the bias.

To measure the voltage output versus known angles, a 3/8 inch thick aluminum disk had 36 slots milled 10° apart. For azimuth readings, the disk was clamped to the bivane post (Figure 5) and leveled. The vane assembly boom was placed in the 90° slot and the disk was rotated until the azimuthal voltage output was what the manufacturer specified as the 90° reading. Then the disk was adjusted vertically to where the elevation was at -25°. Output voltages were logged using Labtech Notebook starting with the boom in the 0° slot and then placed in each successive slot moving clockwise and counterclockwise three times. The

Figure 4. The wind tunnel in the Civil Engineering Hydraulics Laboratory at Purdue University used for this study.

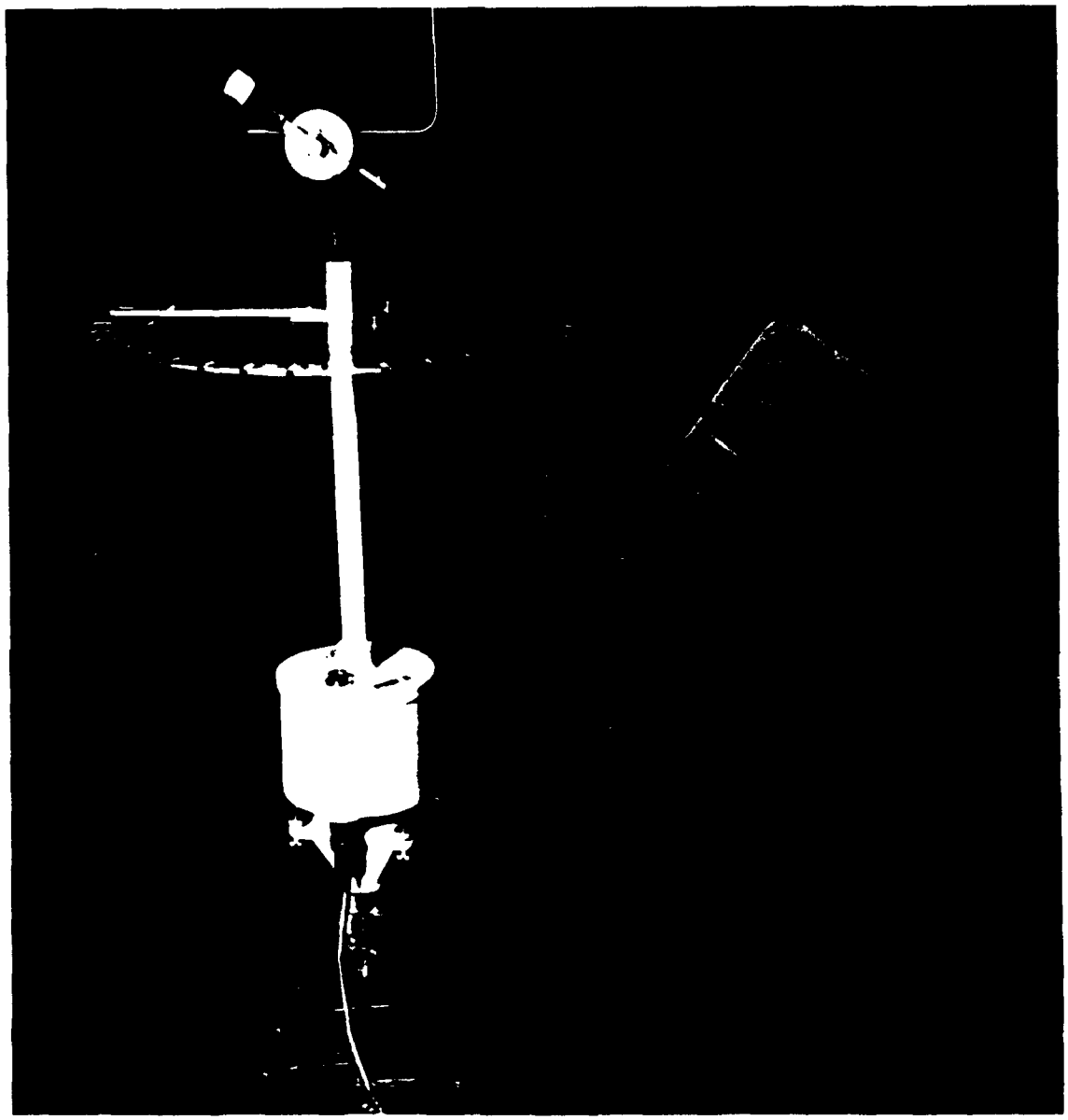

Figure 5. Static testing setup to record azimuth output voltages using the wheel with slots precisely machined at 10° intervals.

disk was rotated 90° azimuthally and the procedure repeated. Rotating the disk 90° isolated irregularities of the milled slots which were found to be undetectable or extremely small in comparison to vane output irregularities. The whole procedure was repeated at a 35° elevation angle.

Elevation static tests were performed with the disk clamped on the bivane post in a vertical fashion as seen in Figure 6. A rod was double bolted in the 0° slot and normal to the disk. The top surface of the rod was even with the lower edge of the slot. The boom rested on the slot between two additional bolts that positioned the boom parallel to the disk's surface. This arrangement allowed for the elevation static tests to measure an arc on a great circle about the bivane which kept azimuth output constant. If the boom was placed directly in the slots on the disk, azimuth angles would change as the elevation angle changed.

With the vane boom on the perpendicular rod in the 0° slot, the disk was rotated about the post to an azimuth angle of 90°. Beginning at the upper most slot, the rod and boom were moved down and up three times through each slot. Again, all data were recorded using Labtech Notebook. This procedure was repeated at an azimuth angle of 180°.

Static test data from ASCII files produced by Labtech Notebook were manipulated using Lotus 123 Release 3.0 and 3.1 spreadsheet of Lotus Development Corporation. Best-fit regressions of the data were used to determine the output linearity. The regressions were considered the ideal output signal and the actual data points described the systematic errors intrinsic to the bivane. An ASCII file was produced that contained the ideal voltage output and the error the bivane produces at that ideal voltage. Results for all three bivanes showed that azimuth and elevation voltage output were independent of each other.

2.2 Dynamic Testing Procedures

Dynamic tests of wind vanes must be performed in a wind tunnel with a cross-sectional area much larger than the cross-sectional area of the wind vane. The large section of the wind tunnel has a cross-sectional area of 4.46 m^2. The cross-sectional area of all three tails of the bivanes were less than 1.2% of the tunnel's cross-sectional area. Since the bivanes were placed in the center of the wind tunnel, blockage affects were negligible.

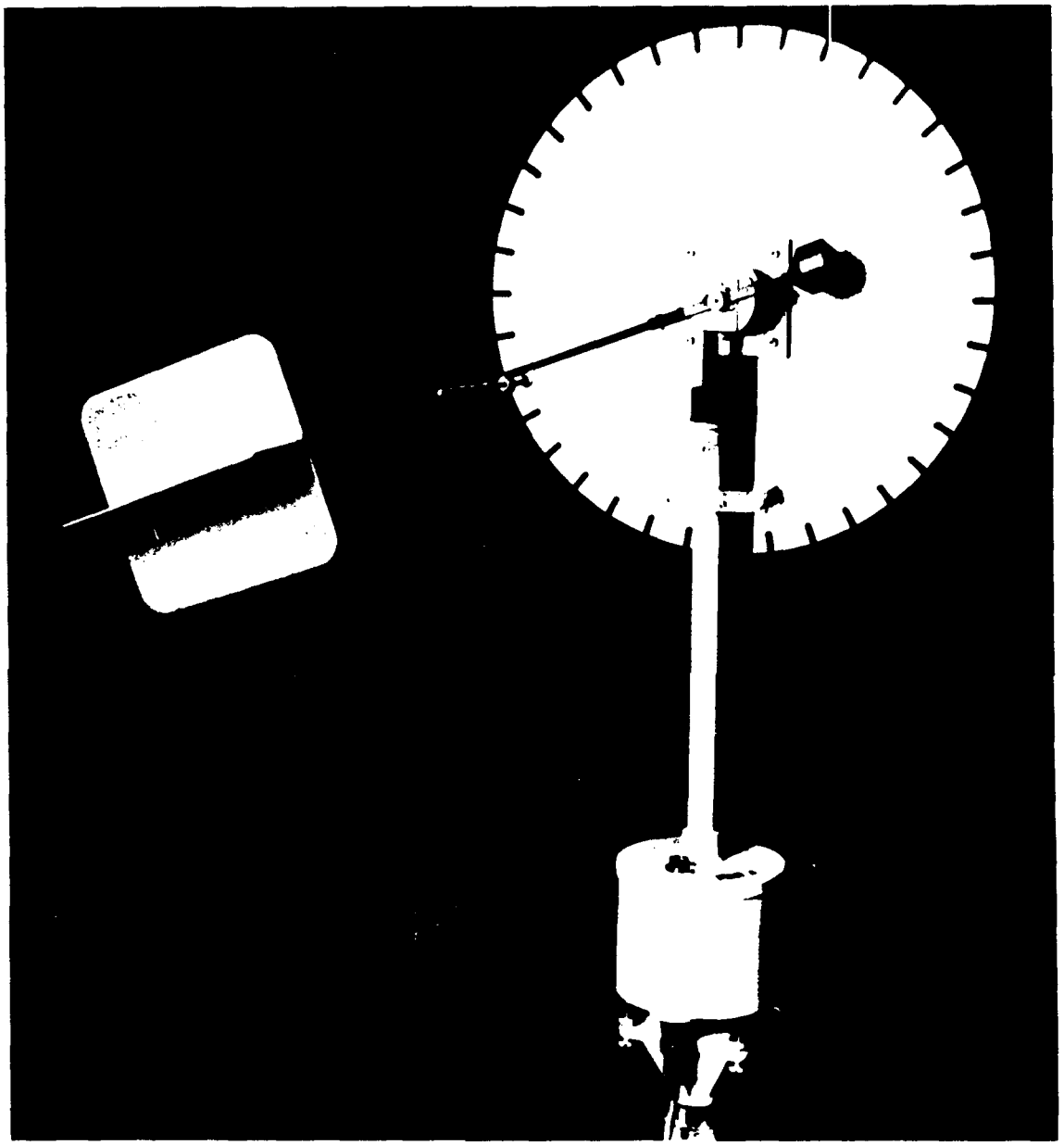

Figure 6. Static testing setup to record elevation output voltages where the wheel is centered on the same axis a the vane assembly's pivot point.

When facing the wind, a Pitot tube was placed 10 cm to the right of the vane. On top of the wind tunnel a stand held the Pitot tube which ran through a hole in the tunnel roof. Also on the roof was a transducer with a 0.5 pounds per square inch differential (PSID) diaphragm that translated differential pressures exhibited by the Pitot tube into voltages. A Validyne, Inc. calibrator provided a zero base and span for the voltages from the Pitot transducer. These voltages were converted into meaningful wind speeds using the relationship:

$$VDC = \frac{P}{TR}\left(\frac{V}{62.897}\right)^2 . \qquad (1)$$

where VDC is the voltage DC provided by the Pitot tube-transducer-calibrator system, P is the atmospheric pressure in mb, T is the temperature in K, R is the PSID value, and V is the wind speed in ms^{-1}. From (1) the tunnel operator can adjust the tunnel wind speed to obtain a voltage reading on a voltage meter corresponding to a desired wind speed.

For each test the tunnel was brought up to speeds of both 5 ms^{-1} and 10 ms^{-1} in accordance with ASTM procedures. The vane was displaced to an initial angular position and released using a release mechanism shown in Figure 7. The release mechanism has an arm attached to a spring. The arm is pulled 18 inches, extending the spring, and locked onto a relay lever. The bivane fin rests in a fork at the end of the arm (Figure 8). When the relay is activated via a remote button, the arm rapidly retracts producing a step function for the vane assembly to return to the equilibrium position, which is along the tunnel centerline. Due to the smooth, quick action of the release mechanism, starting effects are minimized . Since the location of the release mechanism needs to be adjusted only once, initial positions for a series of runs are nearly identical.

For each tunnel speed of 5 ms^{-1} and 10 ms^{-1}, the bivane tail was released 10 times at each of six initial angular positions. When facing into the wind, initial angular positions of the tail relative to the bivane's pivot point were at (A) upper center, (B) upper left, (C) left center, (D) lower left, (E) lower center,

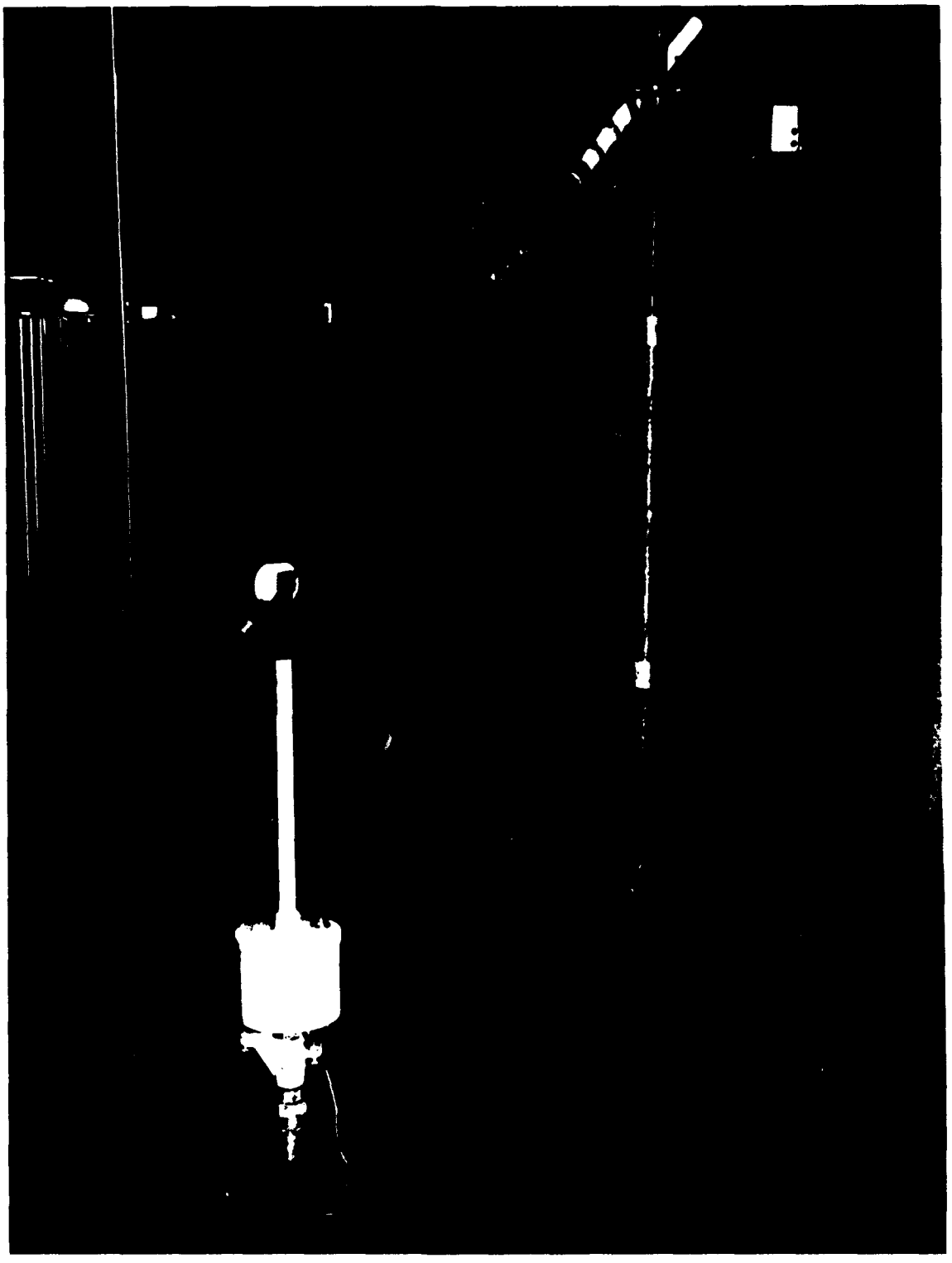

Figure 7. The electronically-controlled release mechanism used to release the tail of the vane assembly.

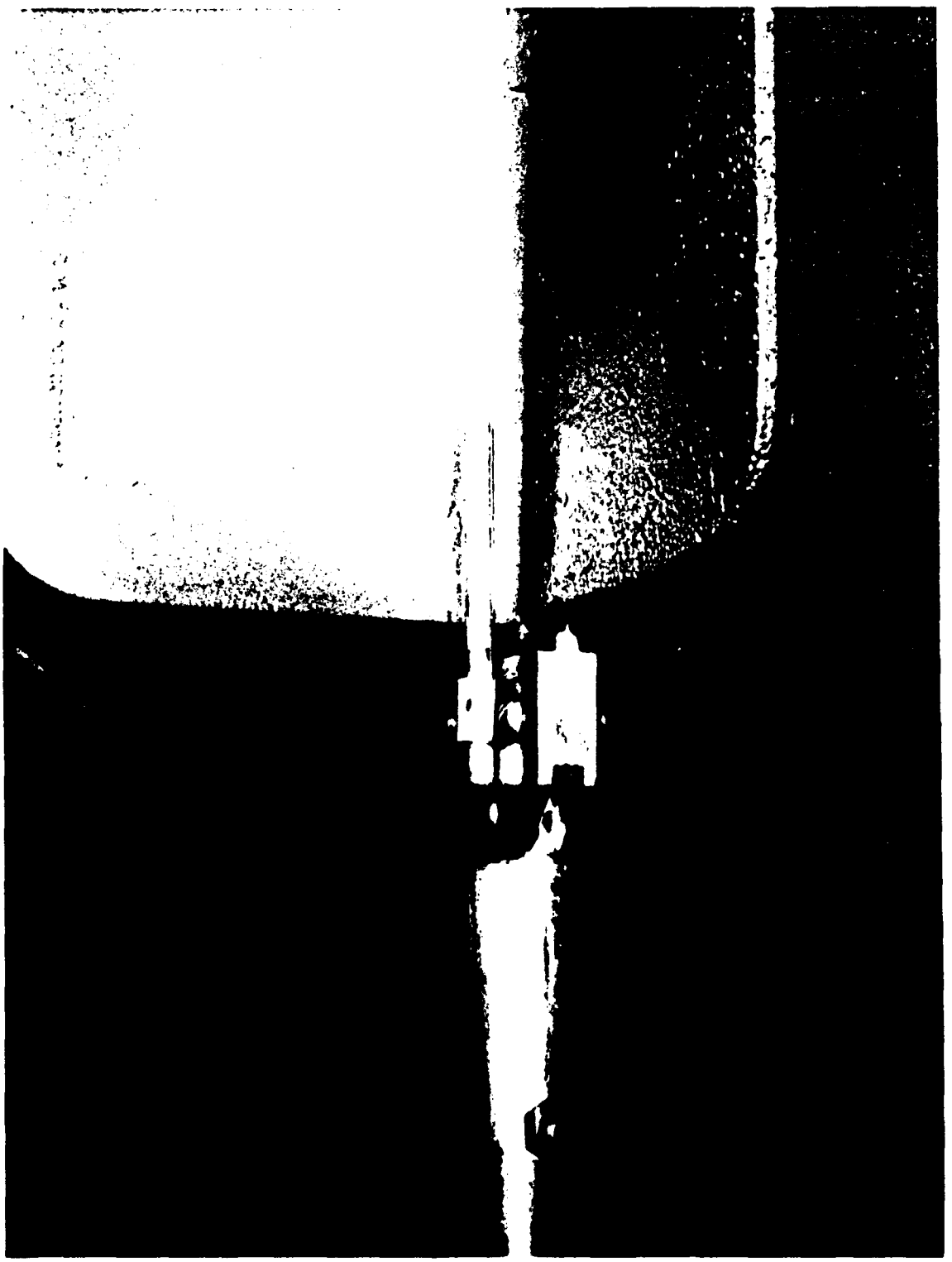

Figure 8. The fork of the release mechanism gently holds the bivane's fin.

and (F) lower right (Figure 9). Positions that would have been (G) right center and (H) upper right were not used due to the position of the Pitot tube. The initial angular position point and the equilibrium line define the plane of oscillation for the vane assembly. Thus, a release at position C allows the vane to oscillate in the horizontal plane. Releasing the vane at positions A and E allows the vane to oscillate in the vertical plane.

The dynamic response of wind vanes is best understood at small angles of deflection of $<15^{\circ}$ (Wang and Felton, 1983). This ensures all vane motion is within the envelope where aerodynamic affects are small and assumed negligible. Commonly, dynamic tests are performed using initial deflections of 10°. However, releasing the vane at 10° would include starting effects that may introduce unwanted motion into the data. In this study, vanes were released at large angles where the amplitude of the first peak was at or near 10°. All data prior to the first peak were not used since they included starting effects.

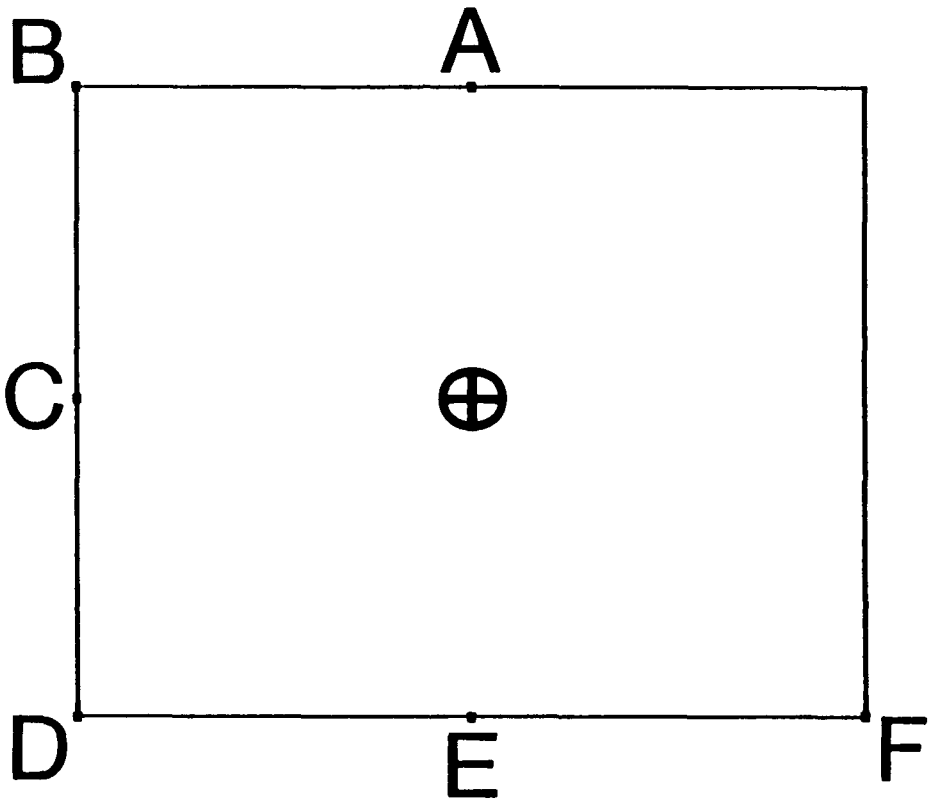

Figure 9. Schematic of the Test Geometry used in the wind tunnel. Facing into the wind, all positions are relative to the tail of the vane assembly.

3. PROCEDURES FOR CALCULATIONS

Linearity for each bivane was determined using the method described for static testing in Chapter 2 and the results applied to the actual dynamic output. Corrected dynamic data were used to calculate dynamic characteristics for each bivane.

3.1 Transfer Function

Every remote wind vane using electronic circuitry has a transfer function that relates the output voltage to the angle of the vane assembly. Bivanes have two transfer functions that translate azimuth and elevation output voltages to azimuth and elevation angles. Each of the three bivanes tested here have different transfer functions depending on the type of circuitry producing the output. The transfer functions for all three bivanes are theoretically linear. The tests determined the linearity of each bivane.

3.1.1 R. M. Young Static Test Results

According to the manufacturer's specifications, the R. M. Young bivane should have a regulated 12 volts DC input and outputs a maximum 12 vdc from both the azimuth and elevation circuitry. The ideal transfer functions are

$$\theta = 29.58\, V_{az} \tag{2}$$

$$\phi = 15\, V_{el} - 45, \tag{3}$$

where V_{az} is the azimuth voltage output and V_{el} is the elevation voltage output. Twelve volts range equally over a 355 degree spread (0° to 355°) for θ and 180 degrees (+90° to -90°) for ϕ. Thus, if the bivane behaved exactly like (2) and (3), all azimuth and elevation voltage output values lie exactly on the regression line with no error.

For this particular R. M. Young Gill Bivane, the static test results revealed the actual voltage output. Figure 10 is a plot of all azimuth point values taken in the static tests and averaged at each angle from 0° to 270° degrees. A best-fit regression line was calculated and plotted with the point values. Figure 11 is the same type of plot, but for elevation data from -30° to $+30^\circ$. These two plots show a strong linearity among the data points with very little error off the best-fit regression line. When the best-fit regression line is subtracted from the individual values, the error becomes more apparent (Figures 12, 13, and 14). From the ideal transfer equations, (2) and (3), all points have an error of less than 1° for both azimuth and elevation directions. This is well within the ASTM requirement of no more than a $\pm 3^\circ$ error for wind vanes.

Note that in Figures 12, 13, and 14, the points show a consistent pattern of error with each static test run. These systematic errors are useful to identify what the true output of the bivane is compared to the ideal output. By averaging all point values at each static test angle and removing the best-fit regression line, each angle has an associated error of voltage output specific to this particular bivane (Figures 15 and 16). These known systematic errors can be used to correct this bivane's output. For any set of output data, the originally measured voltage output is corrected to the best-fit linear output by adding the correction voltage (interpolated values included). All dynamic response data in this study were corrected using this procedure using the ASCII file BVY.COR listed in Table 1.

From the corrected data, the transfer equations particular to this R. M. Young bivane are

$$\theta = 30.18\, V_{az} \tag{4}$$

$$\phi = 8.36\, V_{el} - 48.92. \tag{5}$$

The coefficients and offset are similar to the ideal and reflect the linearity of this individual bivane.

Recall that the R. M. Young bivane uses two potentiometers for the azimuth and elevation transducers. Since potentiometers use a wiper as the electrical contact, some error must be introduced into the output due to the bending of this wiper. Bending of the wiper is necessary for a complete contact with the resistance element. The angle of the potentiometer shaft corresponding to the angle of the vane assembly is not exactly represented by the slightly bent wiper. For example, in Figure 17 the correct voltage

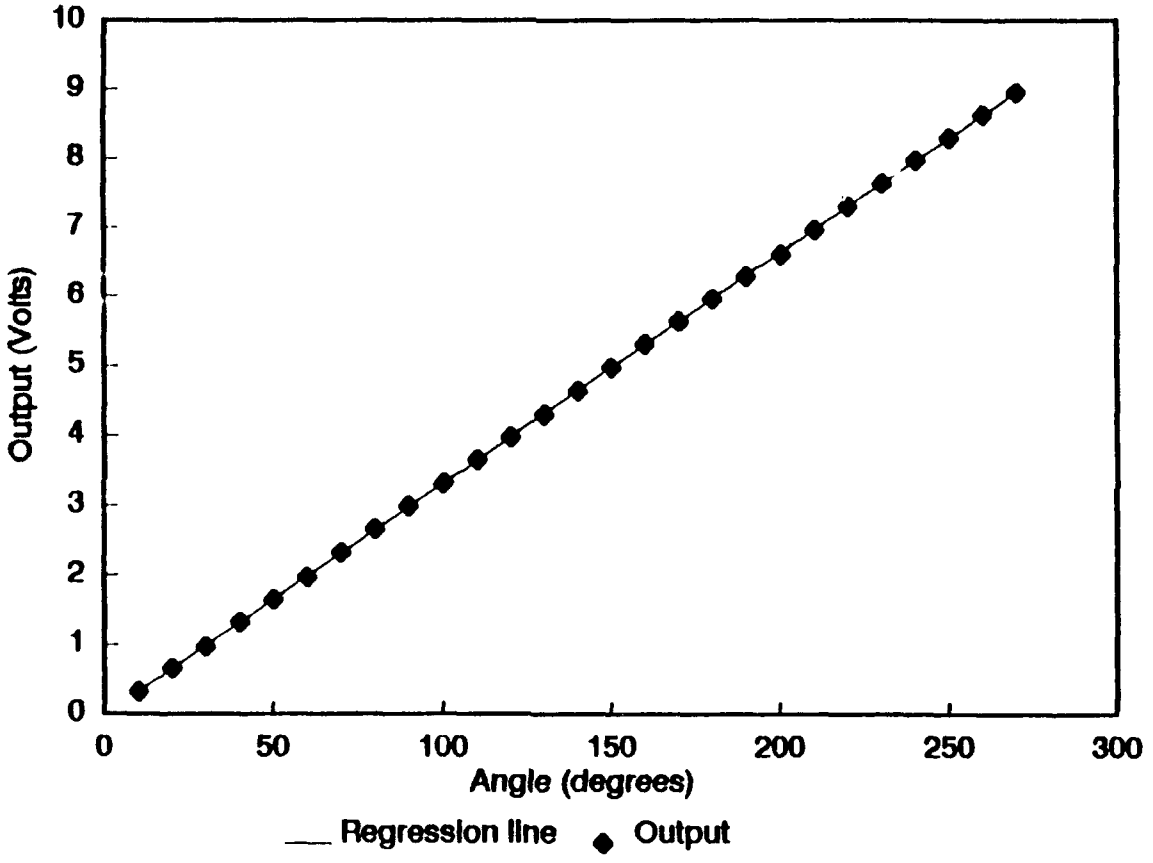

Figure 10. Consolidated output voltages from the R. M. Young bivane azimuth static test with a best-fit regression line.

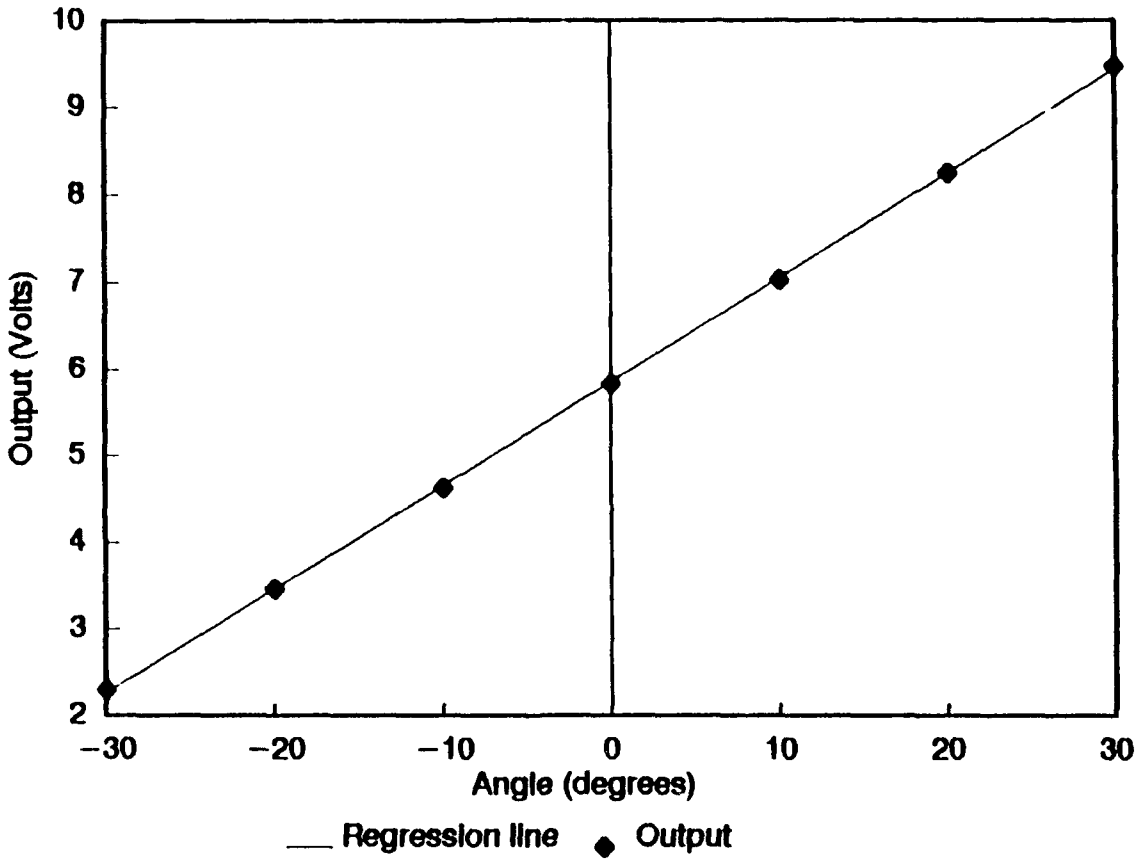

Figure 11. Consolidated output voltages from the R. M. Young bivane elevation static test with a best-fit regression line.

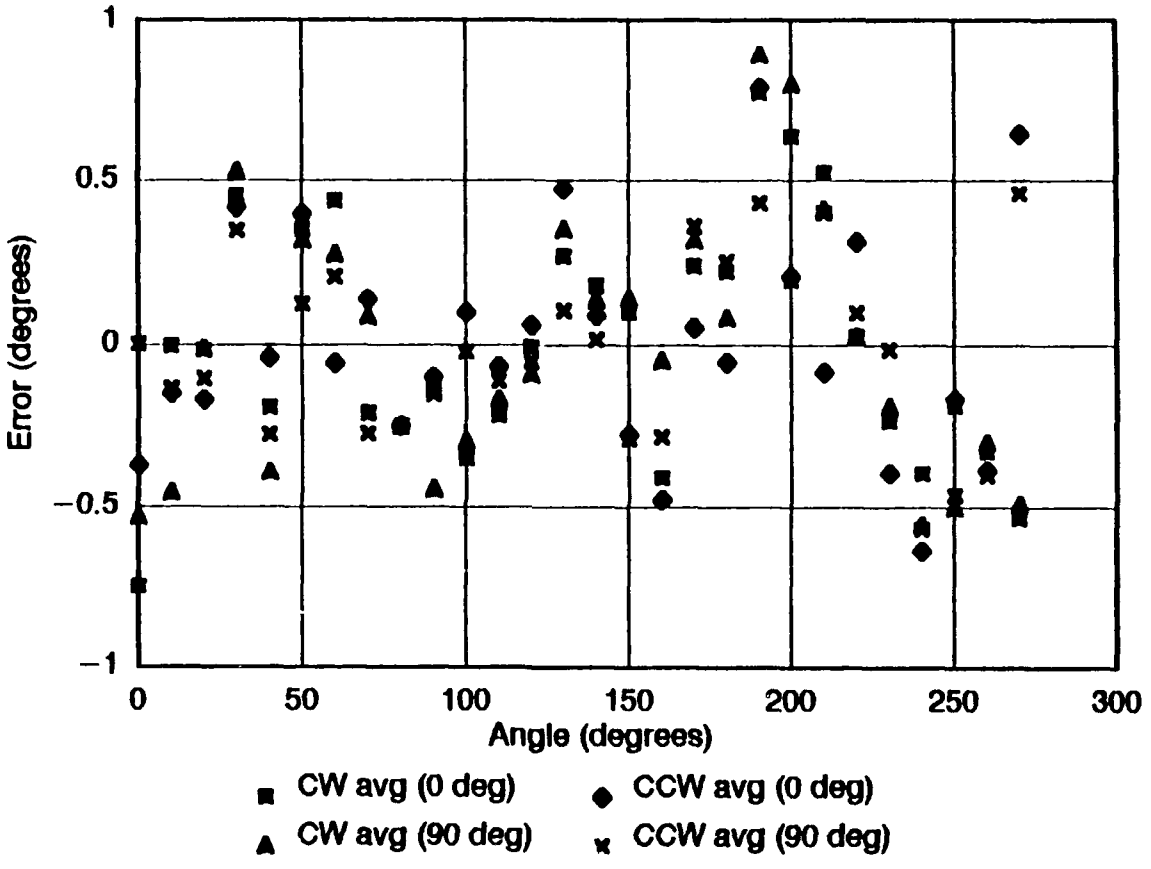

Figure 12. R. M. Young bivane azimuth static test at the 25° vertical position. Clockwise (CW) and counterclockwise (CCW) data from both horizontal positions (0° and 90°) of the machined static test wheel are shown with the best-fit regression subtracted from the individual voltage values.

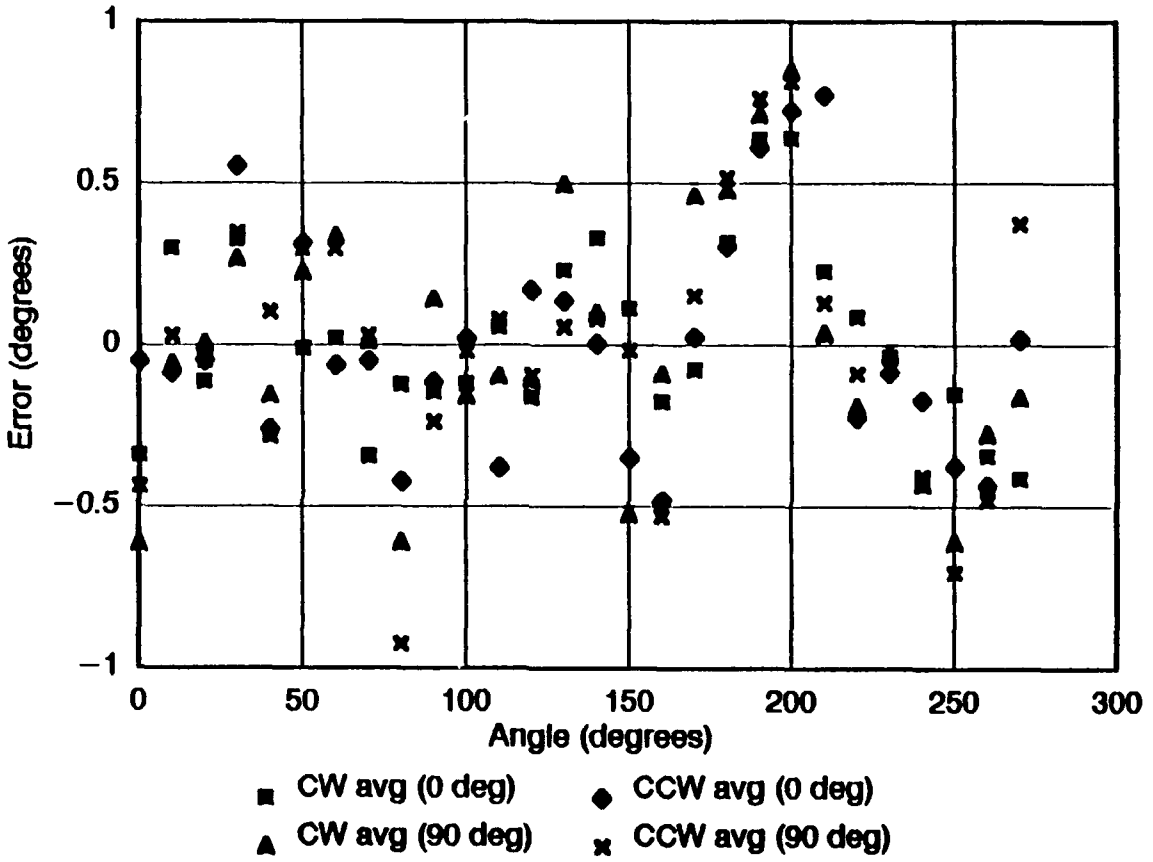

Figure 13. Same as Figure 12, but for the wheel lowered to the 35° vertical position.

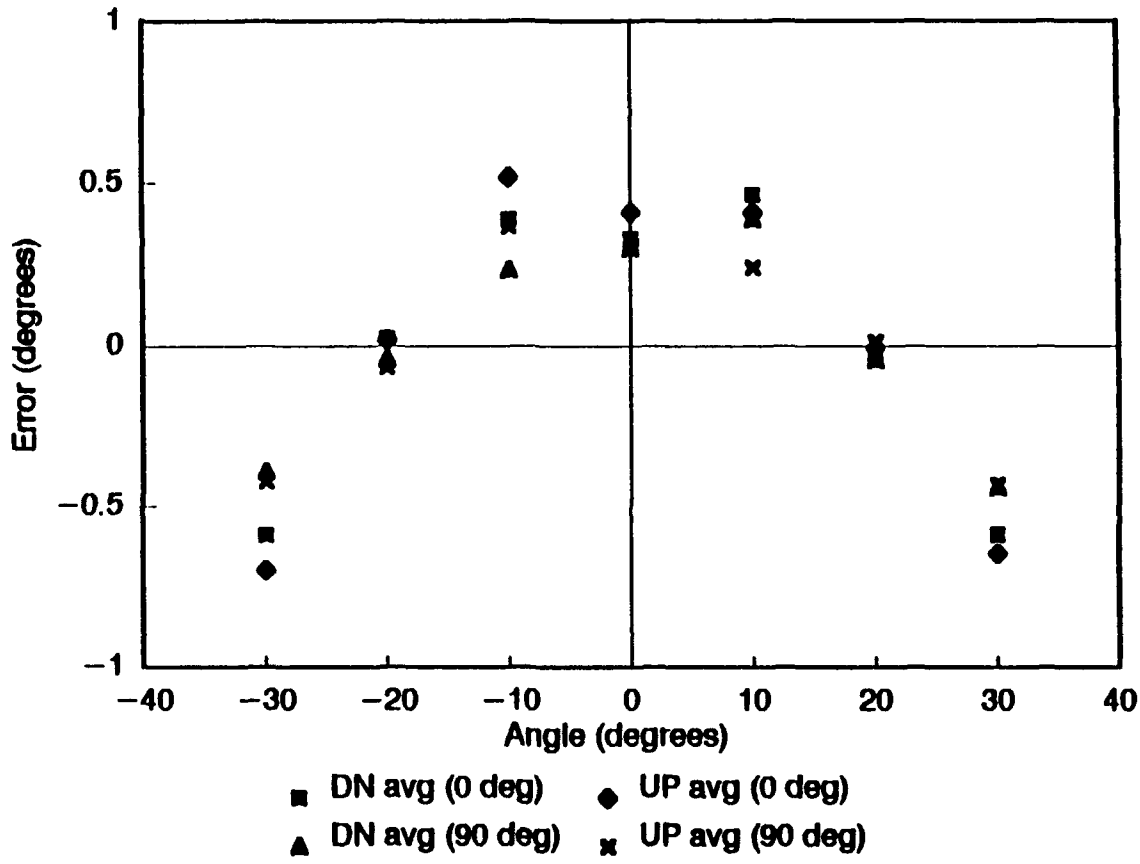

Figure 14. R. M. Young bivane elevation static test. Up and down data from both horizontal positions (0° and 90°) of the machined static test wheel are shown with the best-fit regression line subtracted from the individual voltage values.

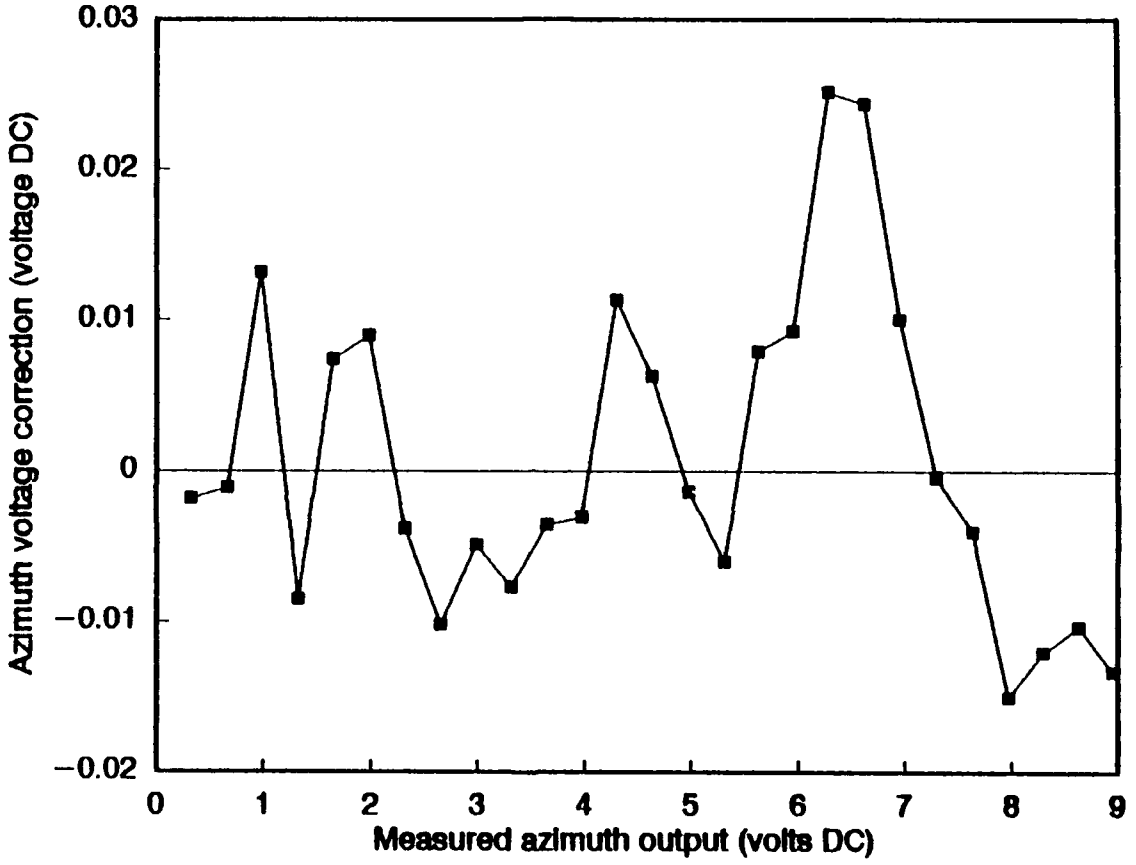

Figure 15. Azimuth correction values as a function of voltage output derived for this particular R. M. Young bivane.

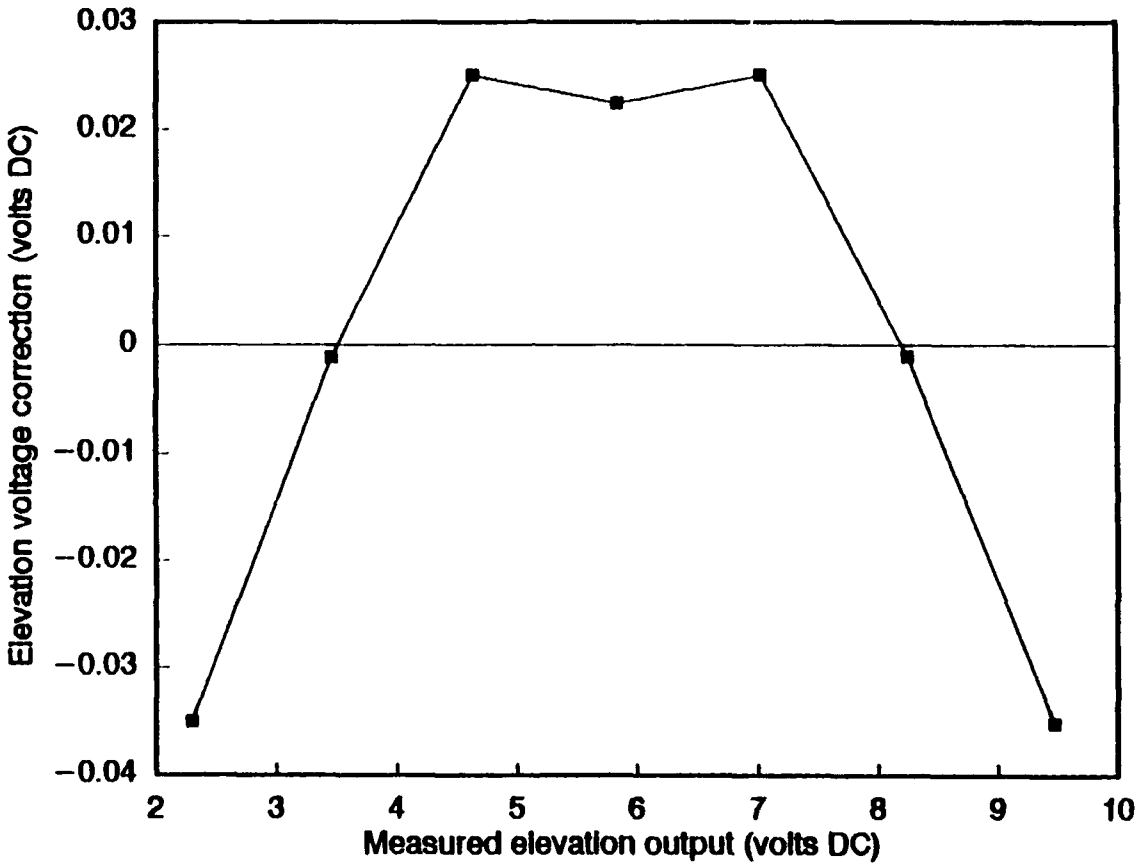

Figure 16. Same as Figure 15, but for elevation correction values.

Table 1. BVY.COR file used to add corrections to individual voltage data from dynamic tests.

```
Azimuth/Elevation
R.M.YOUNG
21/28 Jul 90
volts/error

28 Azimuth
 0.00588 -0.01859
 0.32999 -0.00184
 0.65797 -0.00115
 0.97249  0.01315
 1.32628 -0.00853
 1.64043  0.00740
 1.97487  0.00891
 2.31588 -0.00384
 2.64772 -0.01024
 2.98399 -0.00491
 3.31341 -0.00771
 3.64503 -0.00355
 3.97278 -0.00307
 4.29361  0.01126
 4.63175  0.00623
 4.96968 -0.00142
 5.30872 -0.00603
 5.62216  0.00787
 5.95770  0.00918
 6.26953  0.02512
 6.60991  0.02436
 6.94642  0.01001
 7.28473 -0.00049
 7.62716 -0.00408
 7.96977 -0.01501
 8.29447 -0.01209
 8.62691 -0.01037
 8.94613 -0.01335

7 Elevation
 9.47123 -0.03511
 8.24157 -0.00109
 7.01983  0.02501
 5.82683  0.02237
 4.62849  0.02507
 3.45908 -0.00116
 2.29737 -0.03509
```

representing the angle of the potentiometer shaft is V and ΔV is error introduced due to the bending of the wiper.

The potentiometer wiper bends opposite to the direction of motion of the potentiometer shaft. For azimuthal output, clockwise and counterclockwise motions favor opposing values of ΔV. The same applies to down versus up motion for elevation readings. Figures 18 and 19 show how the direction of motion of the potentiometer shaft produces a bias toward either side of the mean voltage. Clockwise motion consistently produces a $V - \Delta V$ output and counterclockwise motion produces $V + \Delta V$ voltages. The maximum difference between the two directions is approximately 3/4 of one degree occurring either side of the 200° azimuth angle, as is seen in Figures 18 and 19. Therefore, clockwise and counterclockwise azimuthal motions introduce a maximum error of 3/8 of one degree which is incorporated in the total error seen in Figure 14.

For the elevation potentiometer, Figures 20 and 21 again show a direction bias of the vane assembly motion. (Values at -30° elevation angle are not valid since the motion of the vane assembly changed at that point during static tests.) Note that at the angle of 10°, both up and down motions are very close to the mean. This may be due to the irregular shape of the resistance element (i.e., a bulging) allowing for less bending of the wiper. Maximum error of elevation angle due to the bending of the wiper is approximately 1/8 of one degree between down and up motions and 1/16 of one degree either side of the mean voltage. This maximum error occurs at -10°.

Additional error is introduced by differential bending of the wiper depending on which side is convex. Mean clockwise and counterclockwise values are not necessarily equal to the correct or true voltage, V, since clockwise values of ΔV are independent of counterclockwise values of ΔV and are dependent only on the properties of the wiper. The value of V is difficult to measure using static and dynamic test data. A physical measurement of ΔV must be made in order to arrive at a good estimate of V. However, the difference between the mean voltage and V is on the order of 10^{-3} or possibly 10^{-4} volts which corresponds to no more than a few hundredths of a degree and lies within the noise region of the A/D collection system.

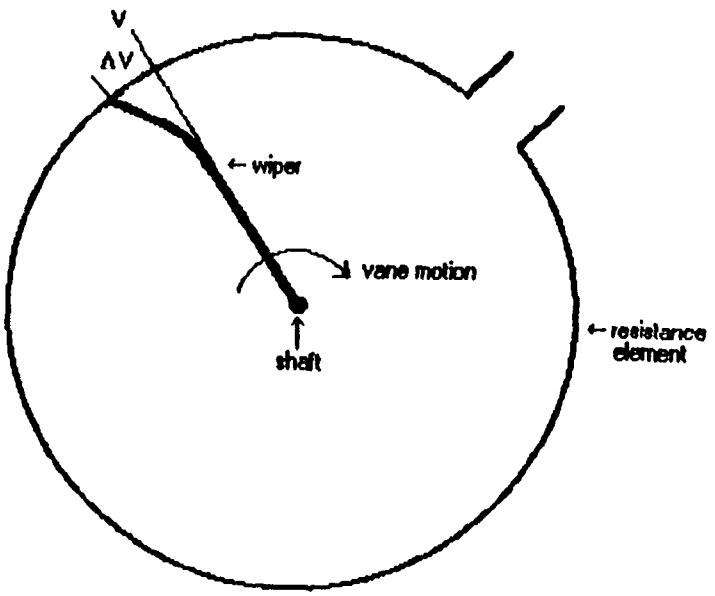

Figure 17. Schematic of a potentiometer with the wiper bent in the opposite direction of the shaft motion producing an output different from the true output by ΔV volts.

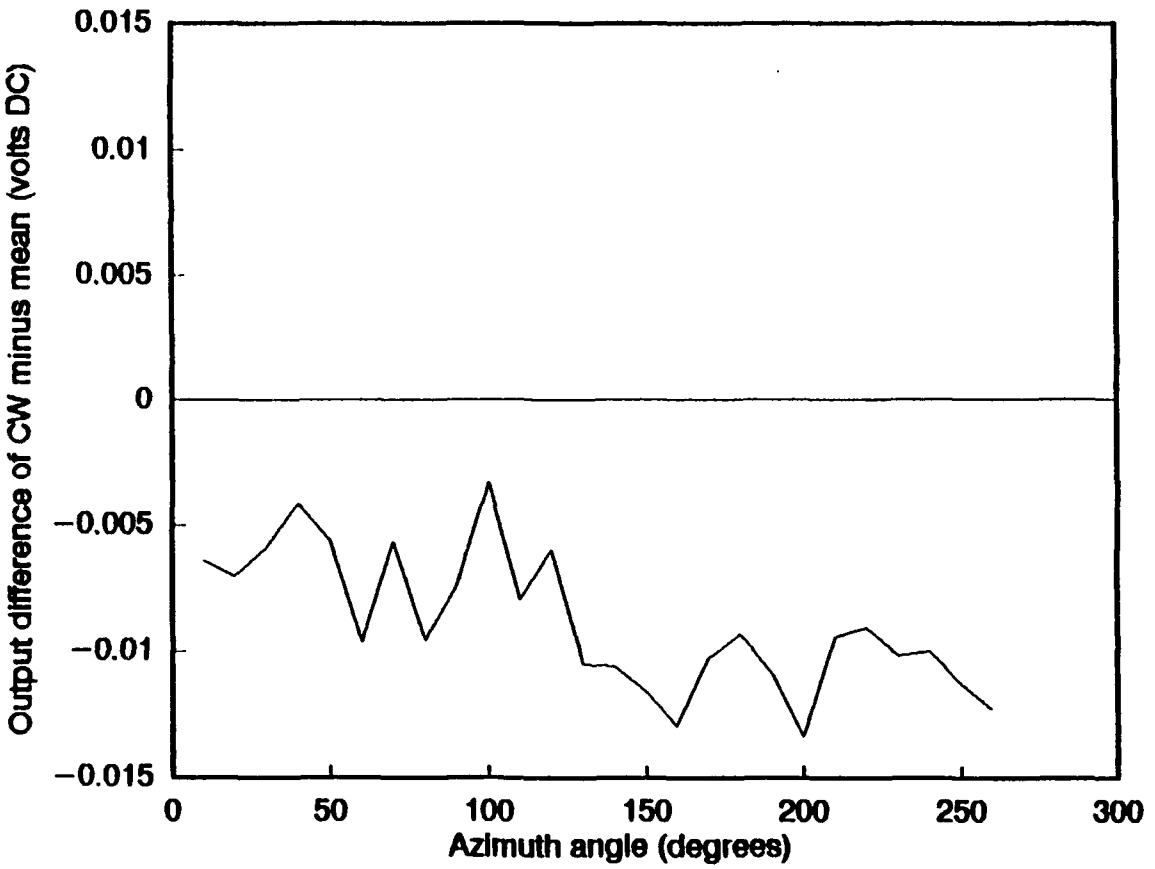

Figure 18. Effect of the bent wiper on the output of the R. M. Young azimuth potentiometer when the shaft (vane assembly) is rotated clockwise.

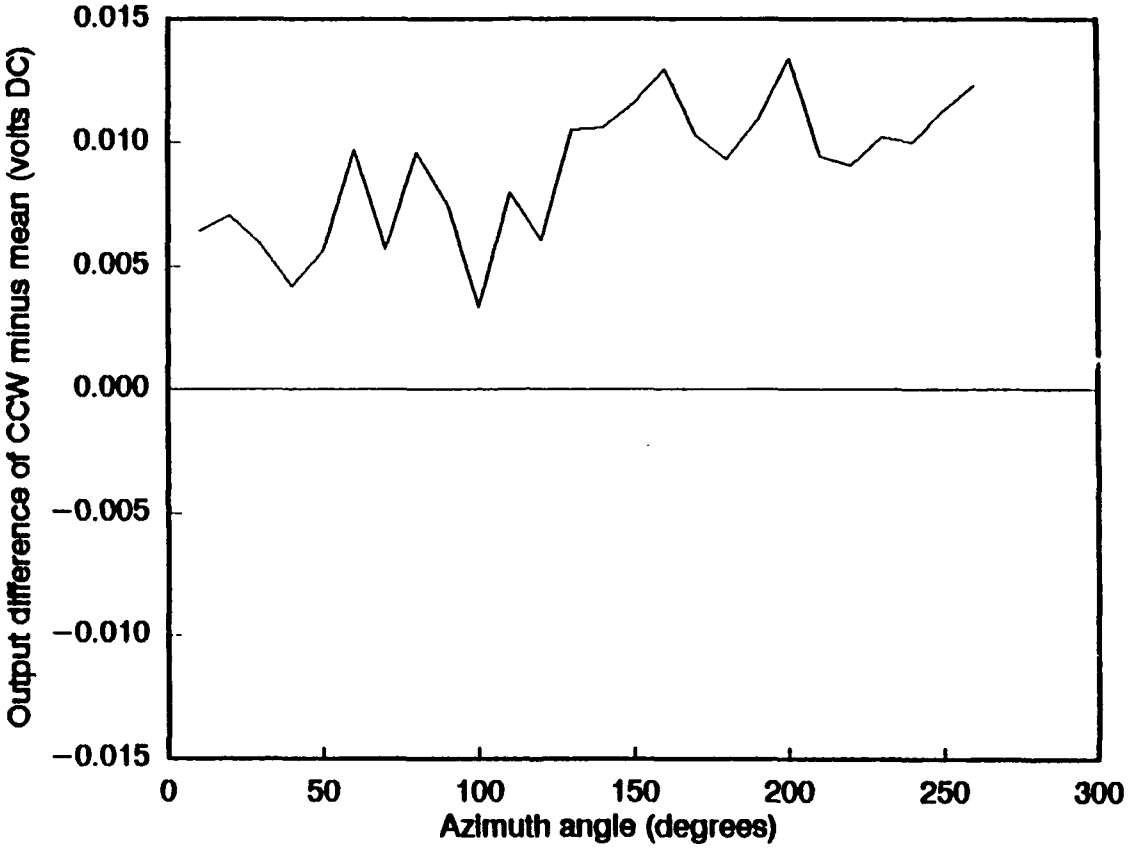

Figure 19. Same as Figure 18, but with the shaft rotated counterclockwise.

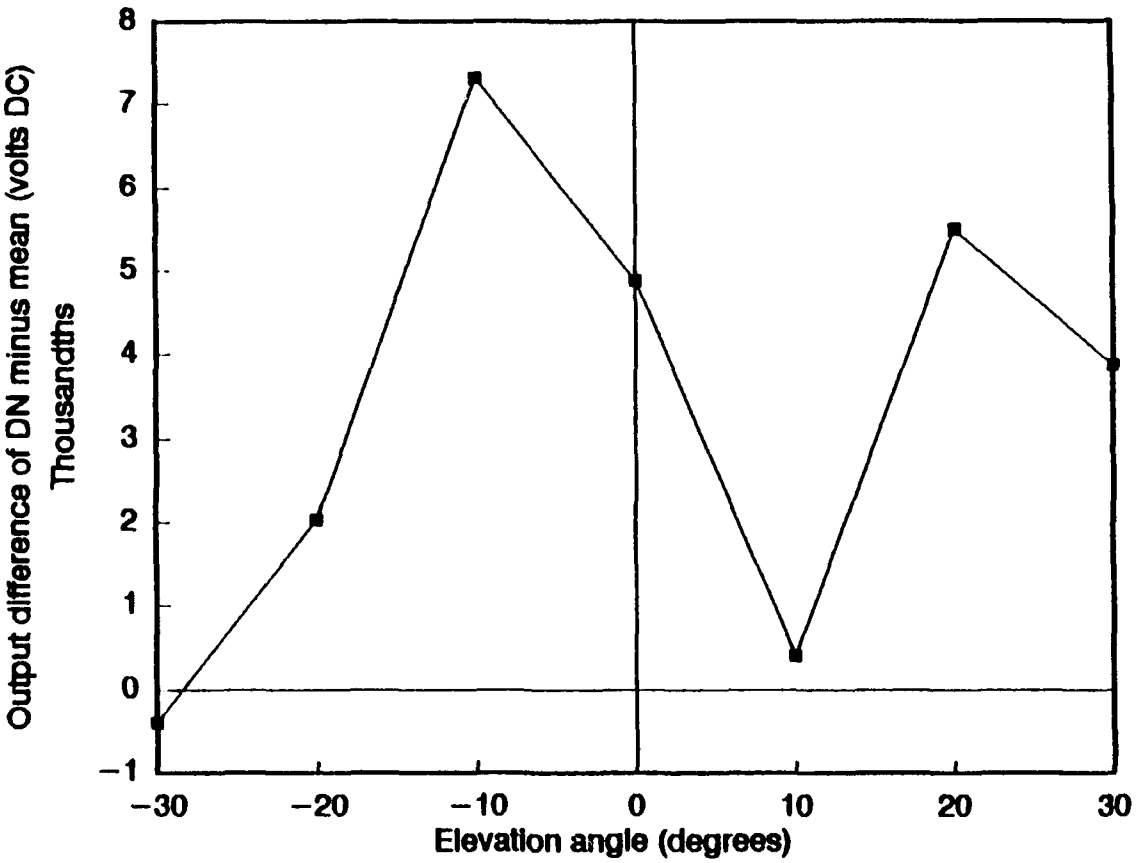

Figure 20. Same concept as in Figures 18 and 19, but for the elevation potentiometer with the vane assembly rotated down.

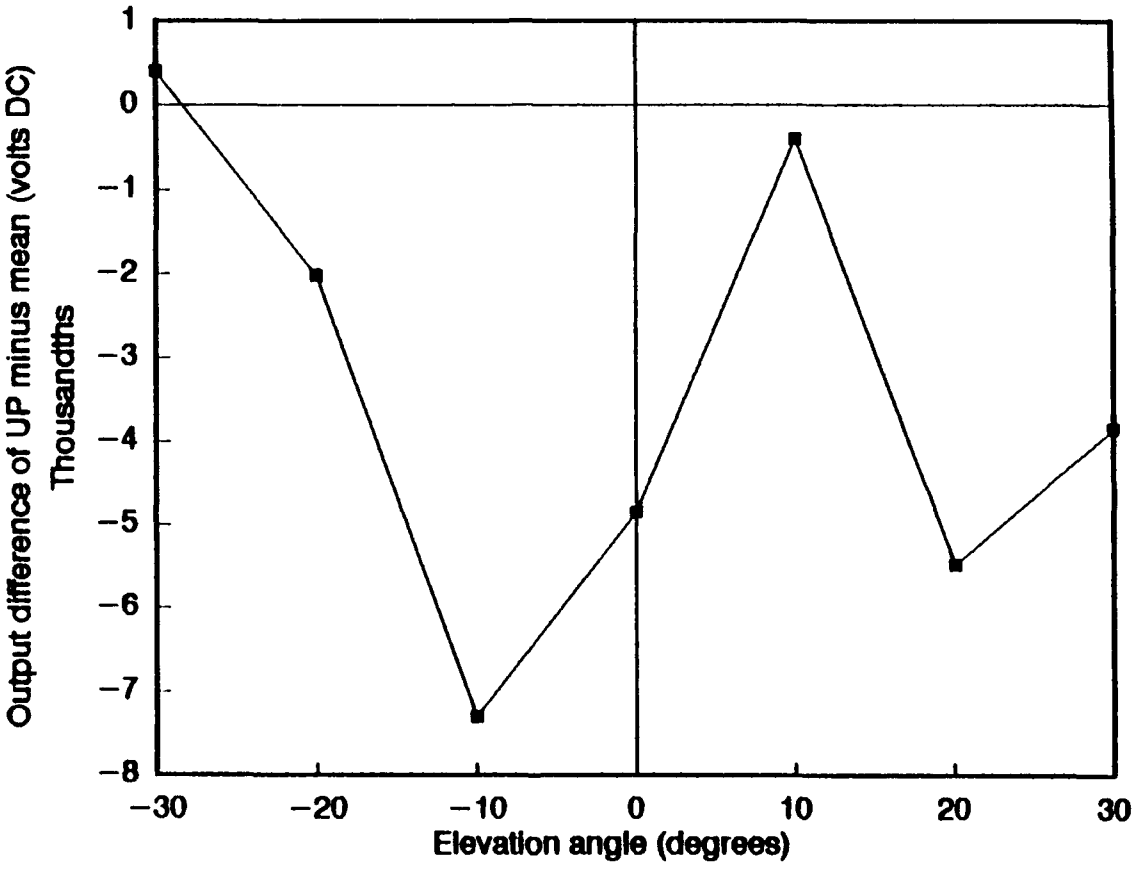

Figure 21. Same as in Figure 20, but for the vane assembly rotated up.

It should also be noted that ΔV changes with environmental factors, of which temperature is the most important. The metallic properties of the wiper are highly dependent on temperature which changes the amount it will bend. However, these errors are likely small.

3.1.2 Teledyne Geotech Static Test Results

The Teledyne Geotech bivane inputs 110 volts AC into its power supply and has the ideal transfer functions

$$\theta = 72\ V_{az} \tag{6}$$

$$\phi = 24\ V_{el} - 60. \tag{7}$$

This particular Teledyne Geotech bivane has azimuthal and elevation data that follow tightly with the appropriate best-fit regression lines (Figures 22 and 23). All azimuthal data points lie inside ± 0.5 degrees (Figures 24 and 25). Elevation data points lie within ± 0.018, degrees as seen in Figure 26. In this plot, the reason for the increased scatter at angles $\leq -40°$ and $\geq 20°$ is not known precisely, but may be due to the increased curvature of the cams at these angles.

From these data, the actual equations for this particular Teledyne Geotech bivane are

$$\theta = 72.14\ V_{az} \tag{8}$$

$$\phi = 26.57\ V_{el} - 62.45. \tag{9}$$

Figures 27 and 28 plot the error corrections used for correcting dynamic output test data. Table 2 details the correction values in the ASCII file BVT.COR.

The objective at Teledyne Geotech was to produce a bivane that avoids electrical contacts at the mechanical and electronic interface eliminating errors from the friction points (eg., where the wiper and resistance element meet in a potentiometer). Where the R. M. Young system produced a noticeable bias that was dependent on the direction of vane motion, the Teledyne Geotech showed no bias in either clockwise or counterclockwise directions, and all data appear random (Figures 29 and 30). At first glance, elevation data seen in Figures 31 and 32 indicate some bias especially at angles $\geq -10°$. With such a small sample population, plus the fact that values $\leq -10°$ are not consistent with the values at higher angles,

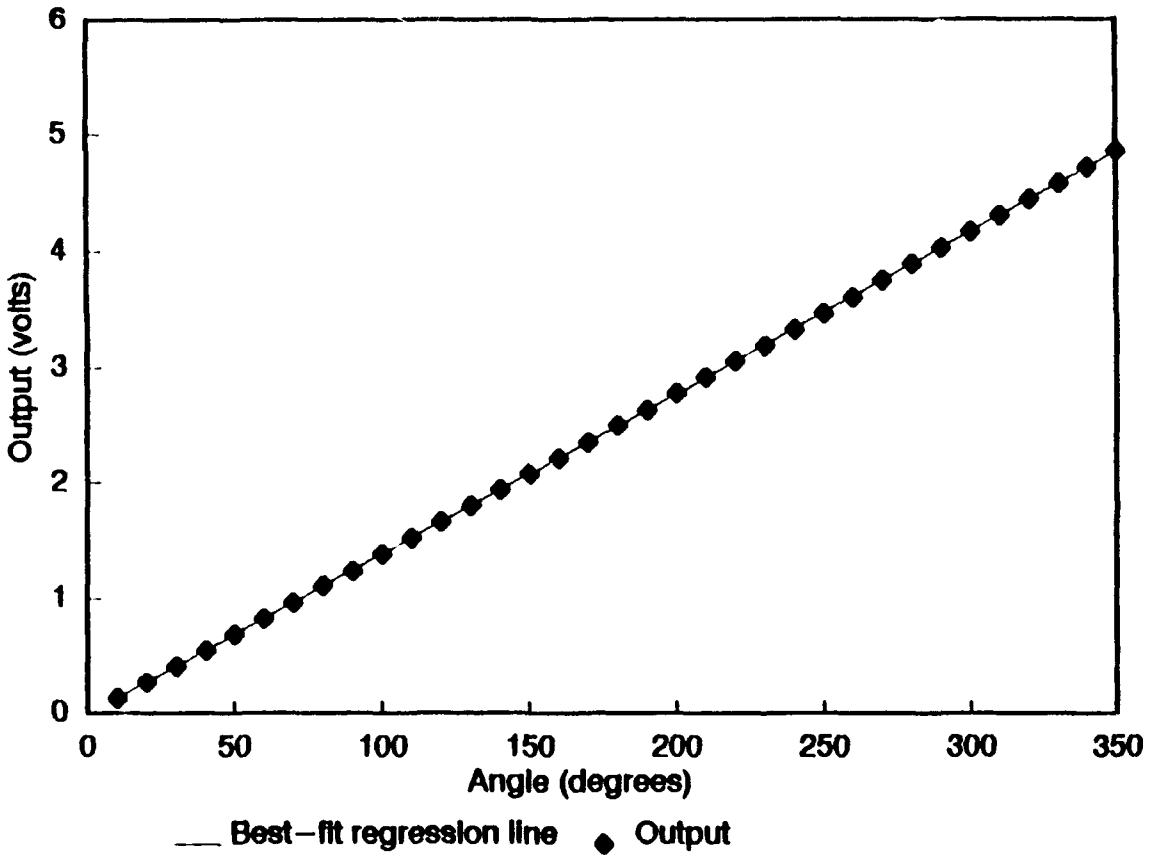

Figure 22. Consolidated output voltages from the Teledyne Geotech bivane azimuth static test with a best-fit regression line.

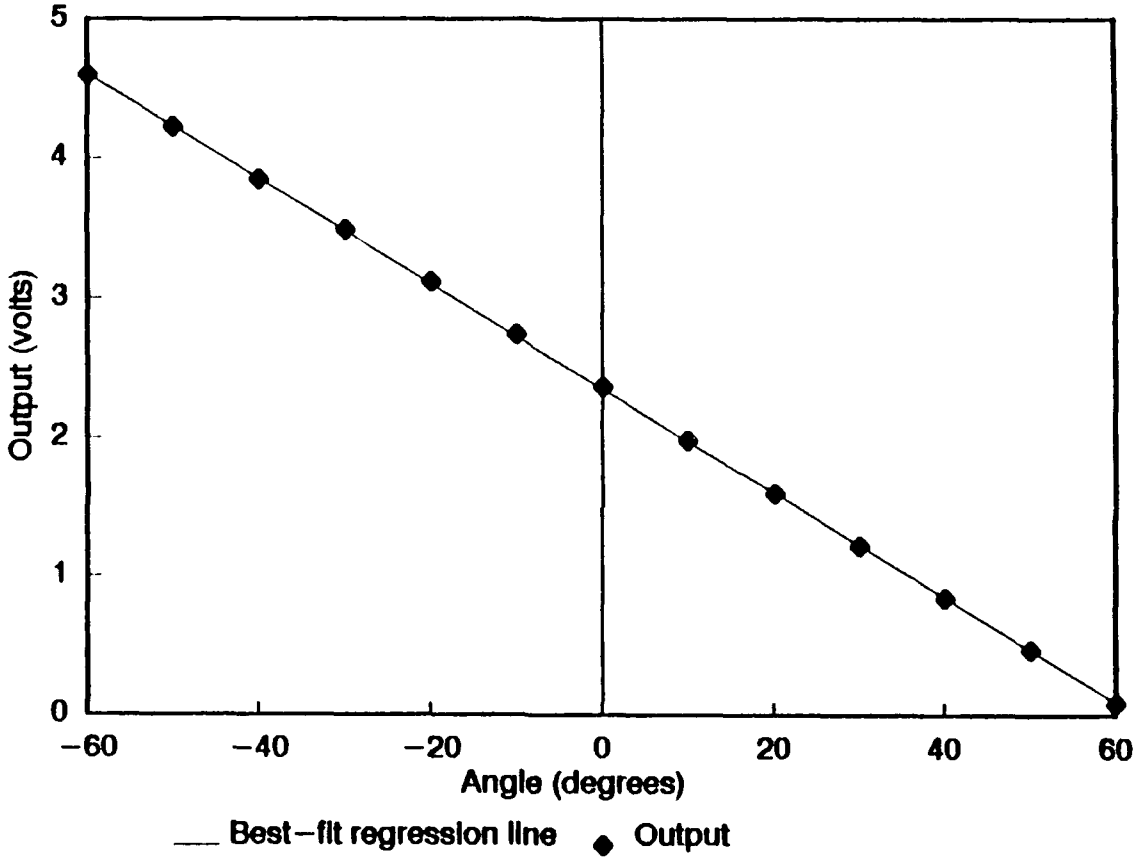

Figure 23. Consolidated output voltages from the Teledyne Geotech bivane elevation static test with a best-fit regression line.

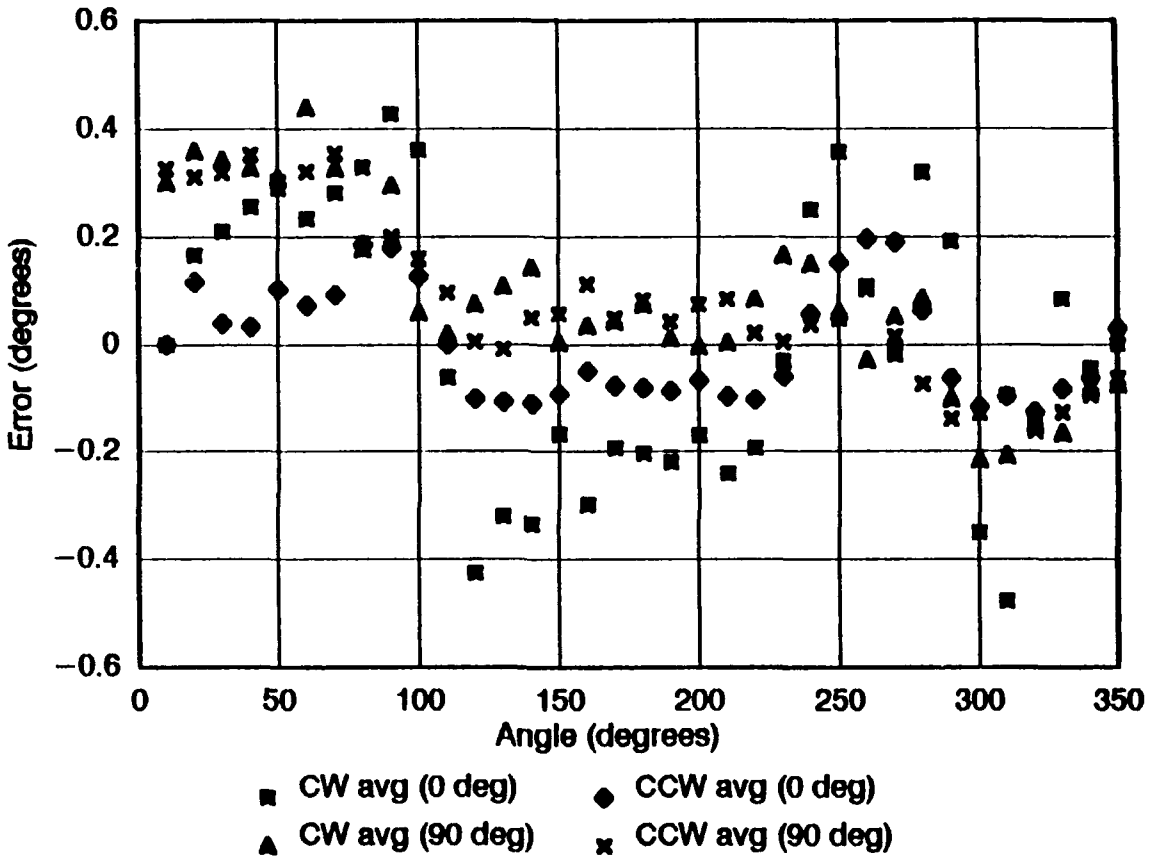

Figure 24. Teledyne Geotech bivane azimuth static test at the 25° vertical position. Clockwise (CW) and counterclockwise (CCW) data from both horizontal positions (0° and 90°) of the machined static test wheel are shown with the best-fit regression subtracted from the individual voltage values.

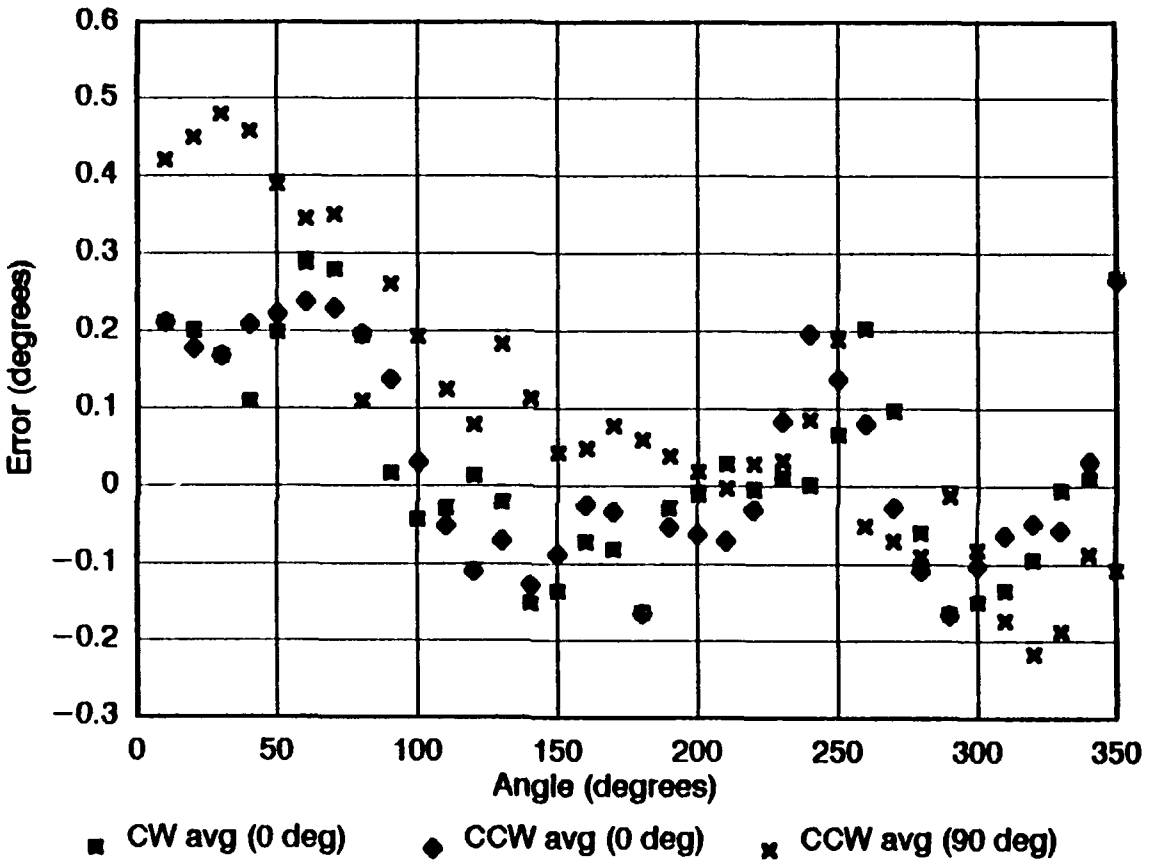

Figure 25. Same as Figure 24, but for the wheel lowered to the 35° vertical position.

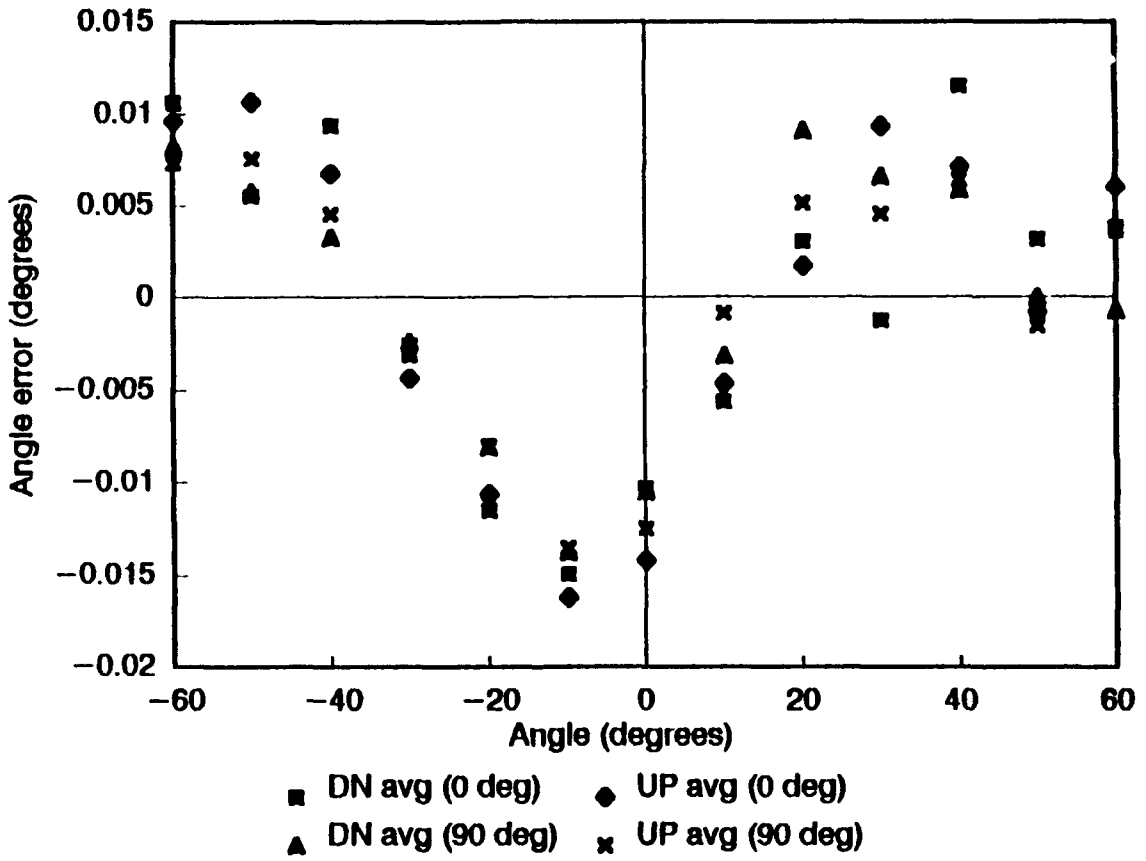

Figure 26. Teledyne Geotech bivane elevation static test. Up and down data from both horizontal positions (0° and 90°) of the machined static test wheel are shown with the best-fit regression line subtracted from the individual voltage values.

Table 2. BVT.COR file for correcting dynamic test data.

Azimuth/Elevation
TELEDYNE-GEOTECH
25 Oct 90
Volts Error

35 Azimuth
0.13000 0.00842
0.26896 0.00868
0.40791 0.00795
0.54678 0.00659
0.68513 0.00848
0.82286 0.01019
0.96181 0.00864
1.10518 0.00452
1.24237 0.00553
1.38560 -0.00072
1.52638 -0.00227
1.66515 -0.00078
1.80328 -0.00070
1.94264 -0.00164
2.08222 -0.00361
2.21986 -0.00233
2.35871 -0.00226
2.49818 -0.00280
2.63641 -0.00252
2.77558 -0.00325
2.91444 -0.00339
3.05205 -0.00168
3.18878 0.00040
3.32601 0.00088
3.46507 -0.00067
3.60495 -0.00101
3.74532 -0.00154
3.88651 -0.00391
4.02761 -0.00792
4.16667 -0.00885
4.30522 -0.00818
4.44397 -0.00790
4.58199 -0.00720
4.71873 -0.00593
4.85273 -0.00100

13 Elevation
0.08908 0.00316
0.46836 0.00021
0.83720 0.00769
1.21644 0.00477
1.59281 0.00473
1.97744 -0.00358
2.36208 -0.01189
2.74113 -0.01463
3.11240 -0.00957
3.48227 -0.00311
3.84951 0.00597
4.22446 0.00734
4.59922 0.00891

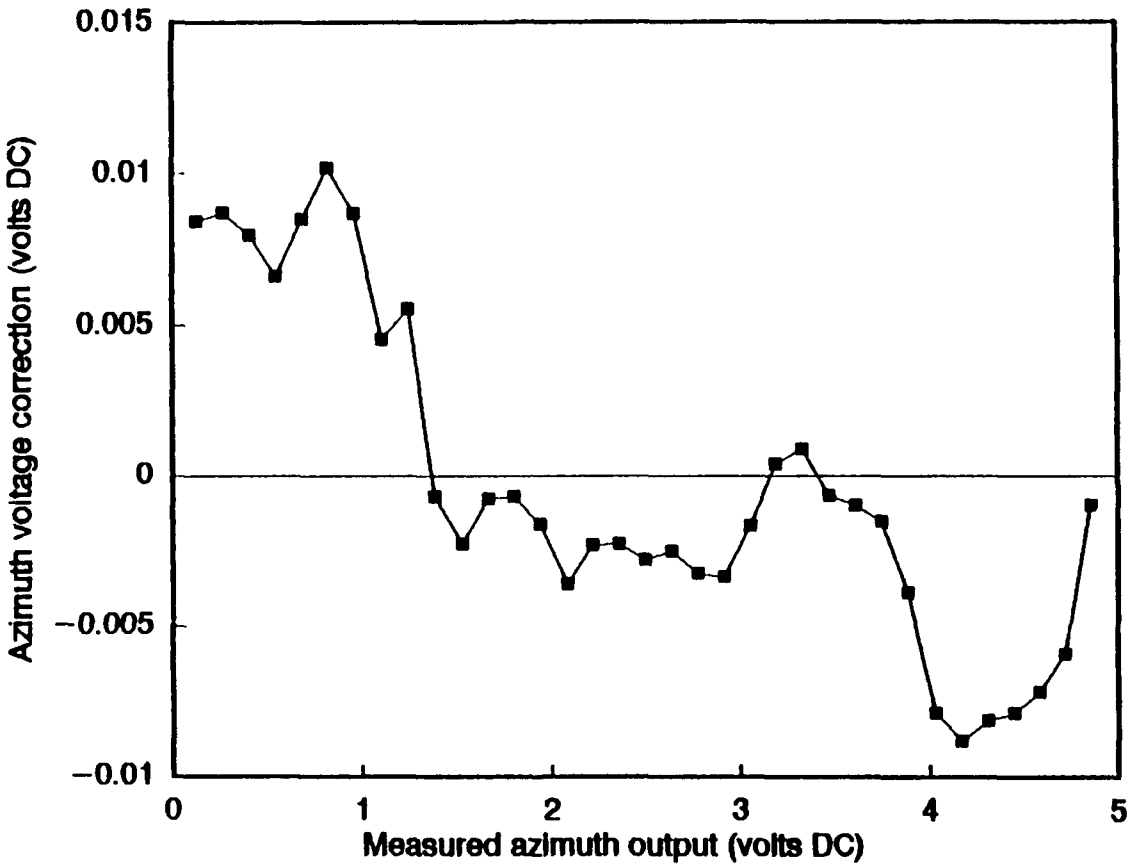

Figure 27. Azimuth correction values as a function of voltage output derived for this particular Teledyne Geotech bivane.

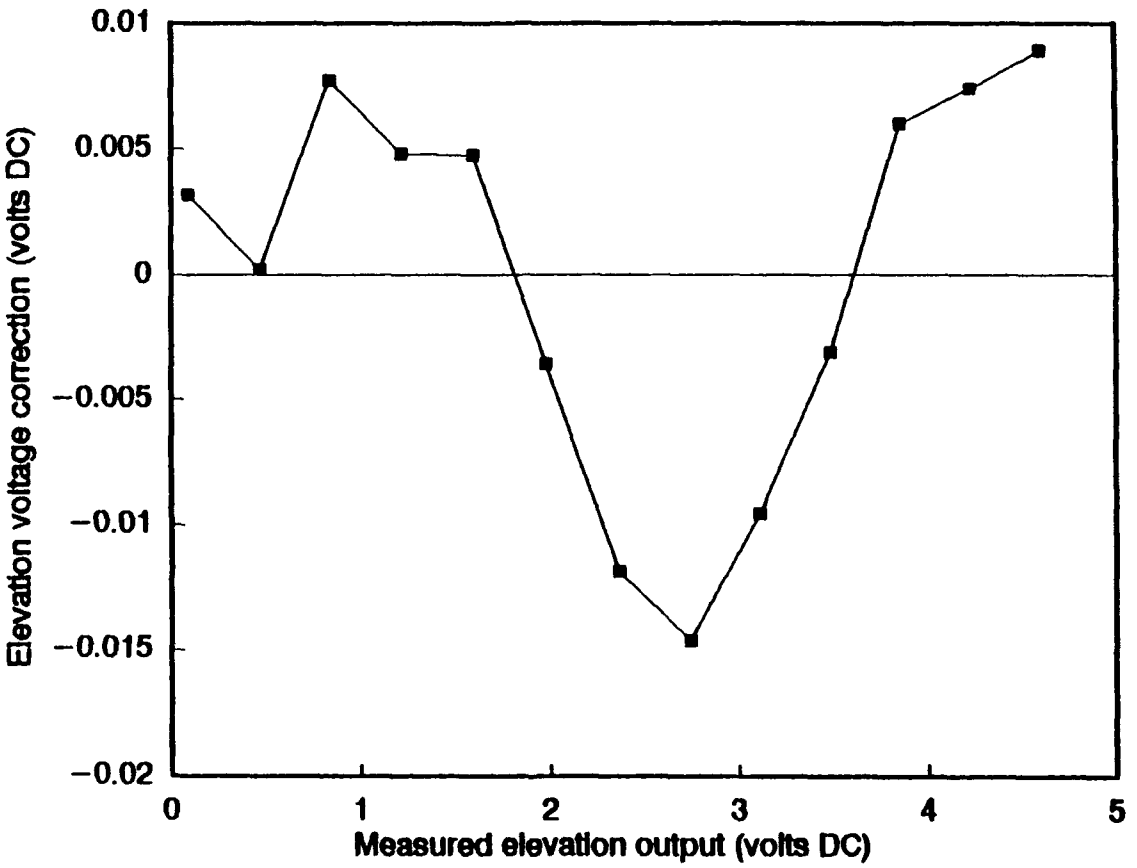

Figure 28. Same as Figure 27, but for elevation correction values.

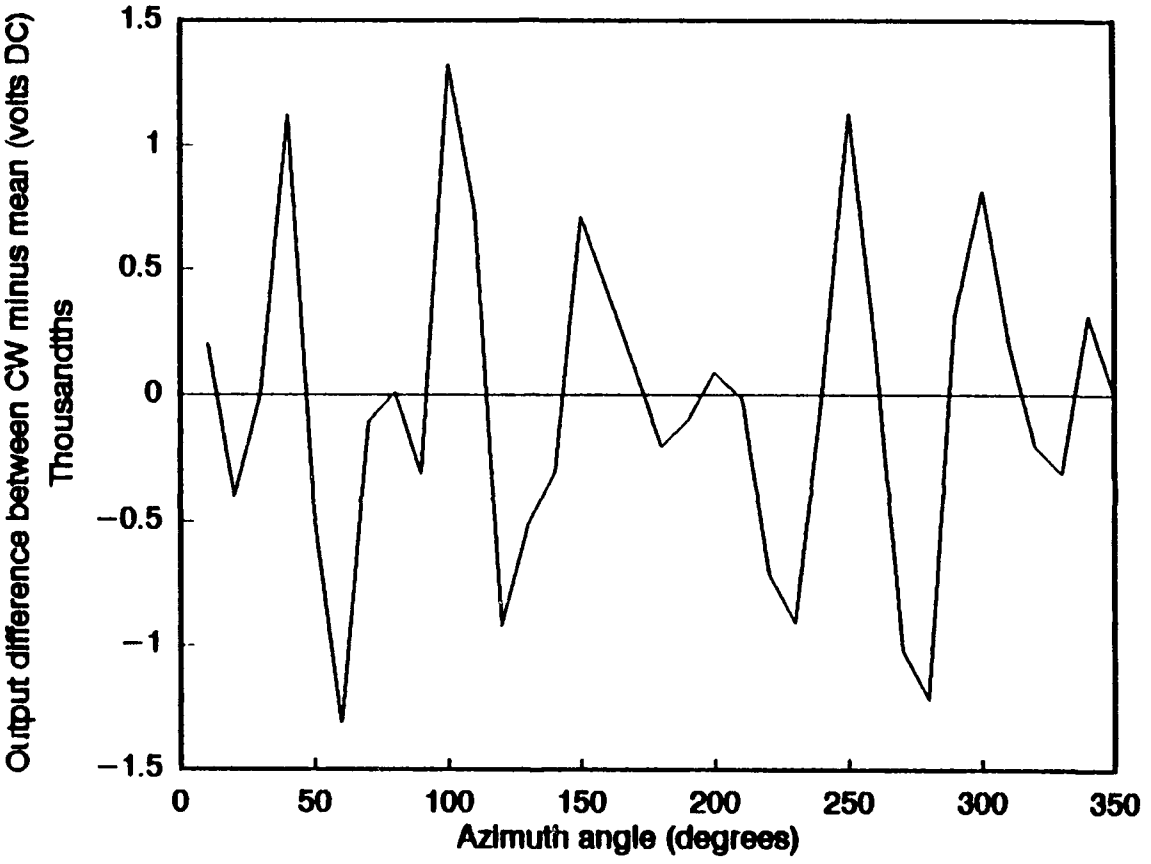

Figure 29. Same as in Figure 18 with CW motion, but for the Teledyne Geotech azimuth resolver that produces no ΔV.

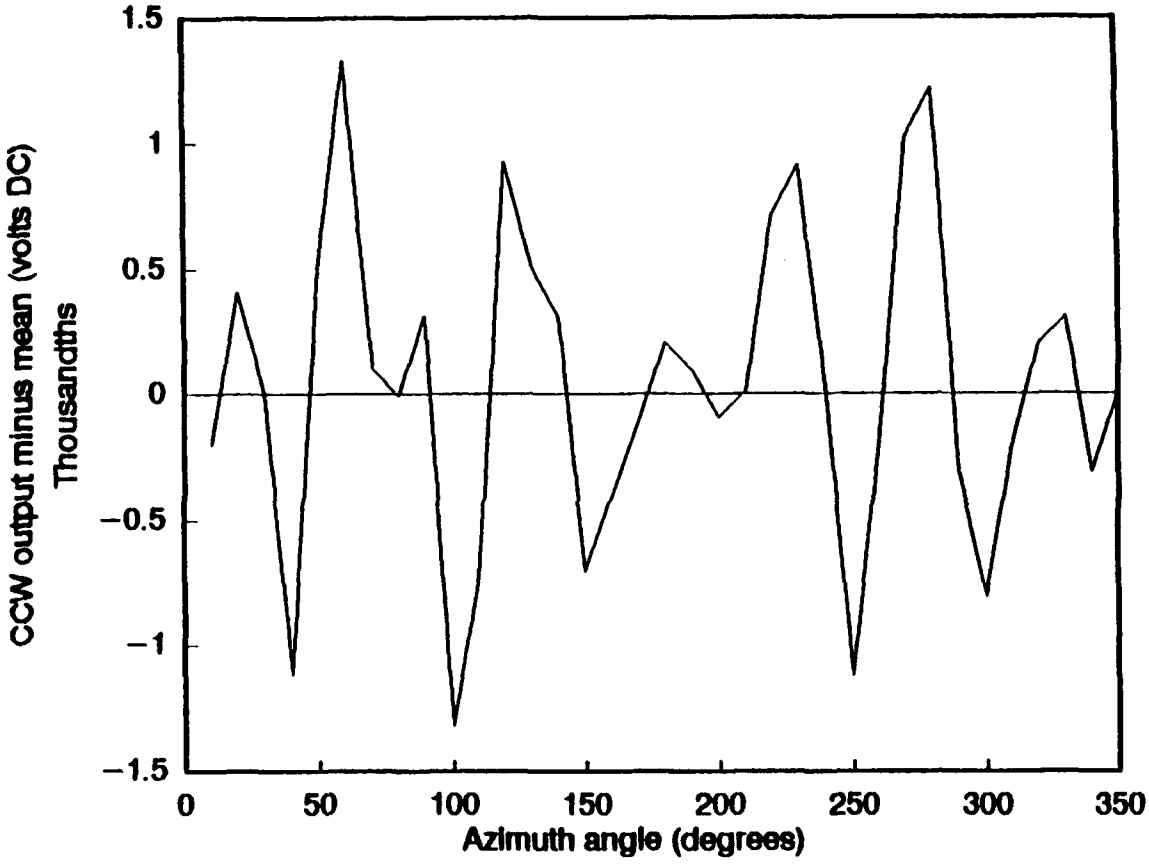

Figure 30. Same as in Figure 29, but for CCW motion.

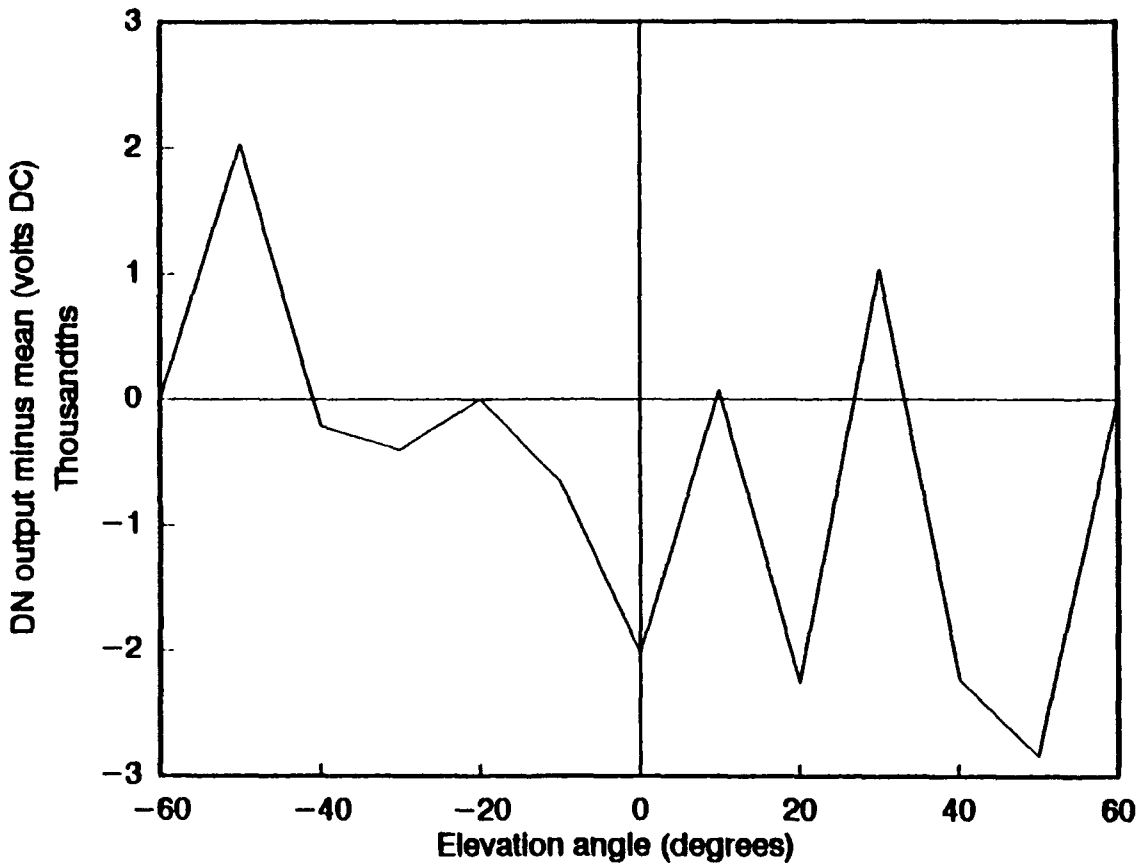

Figure 31. Same as in Figure 20 with down motion, but for the Teledyne Geotech elevation resolver that produces no ΔV.

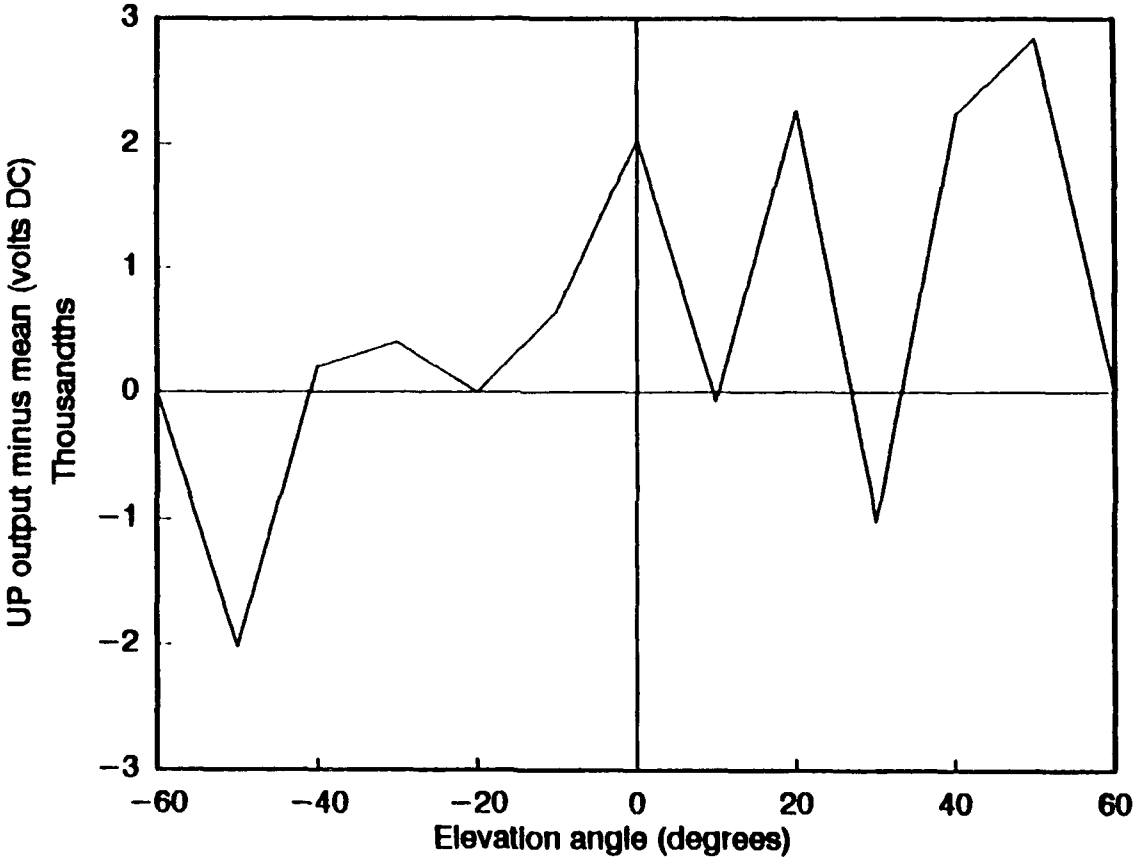

Figure 32. Same as in Figure 31, but for up motion.

these data may not reflect the true character of the elevation voltage output. Additional static tests are needed to obtain a satisfactory conclusion. Overall, it appears that Teledyne Geotech achieved its goal of eliminating errors that are dependent on the direction of vane motion.

3.1.3 Climatronics Static Test Results

Based on its theory of operation, the ideal linear transfer functions of the Climatronics bivane are

$$\theta = 360\ V_{az} \tag{10}$$

$$\phi = 90\ V_{el} - 45, \tag{11}$$

where both the azimuth and elevation output have a range of 0-1 volt DC.

Static tests of this particular Climatronics bivane revealed azimuth values that conformed to a linear regression, while the elevation test data tended to meander or even oscillate about a best-fit regression line (Figures 33 and 34). The manufacturer states that the elevation output should range from 0 to 1 volt DC corresponding to -45° and +45°. The LVDT is believed to be in need of calibration, since output values range from small negative values to slightly less than 0.8 volts DC. The instrument was sent to the factory for repair of the counterweight which is on the underside of the LVDT and for the LVDT to be calibrated. The counterweight was repaired, but apparently the LVDT was not calibrated. Lack of time prevented the bivane from being sent back to Climatronics. Since the output from the linearity of the LVDT output was within accepted standards, only the offset needed to be adjusted. In this study, the offset was corrected mathematically (see equation (13)).

Individual azimuth and elevation data points seen in Figures 35, 36, and 37 show that no values exceeded 2.5° off the best-fit regression line. These data fall within the manufacturer's specifications and ASTM requirements of ±3°. The striking oscillating pattern of the elevation error data may be due to a smooth variation of the interior wall of the LVDT. As the slug travels through the LVDT, variations in the wall thickness, diameter of the cavity, or other variables, can alter the resistance levels creating a less-than-linear response. The error, however, is still less than ASTM requirements.

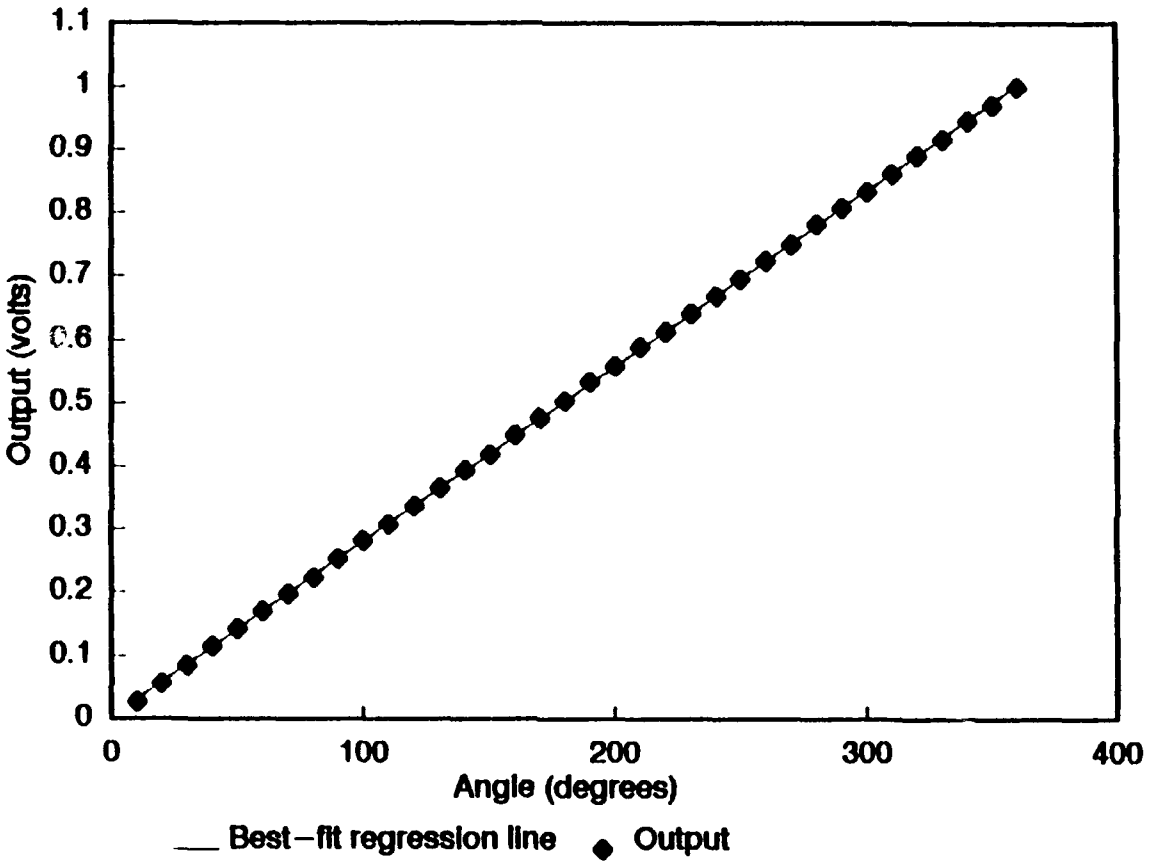

Figure 33. Consolidated output voltages from the Climatronics bivane azimuth static test with a best-fit regression line.

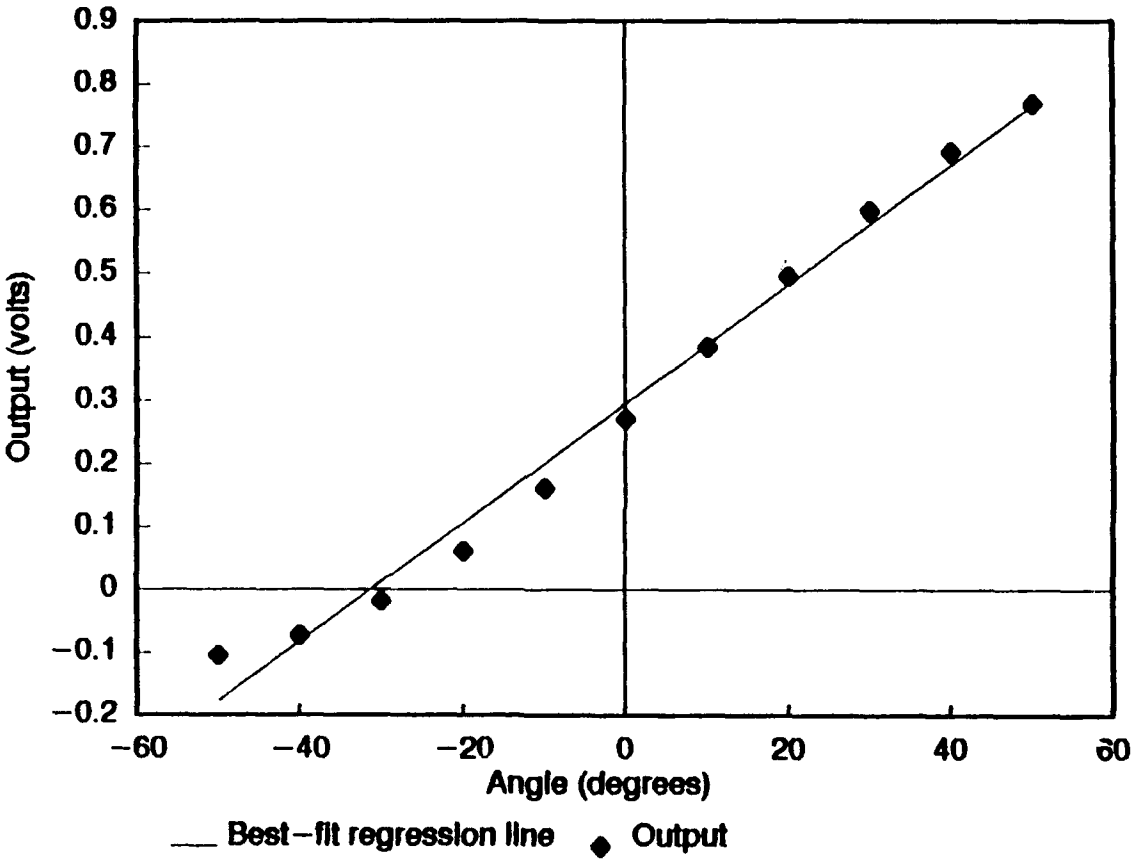

Figure 34. Consolidated output voltages from the Climatronics bivane elevation static test with a best-fit regression line.

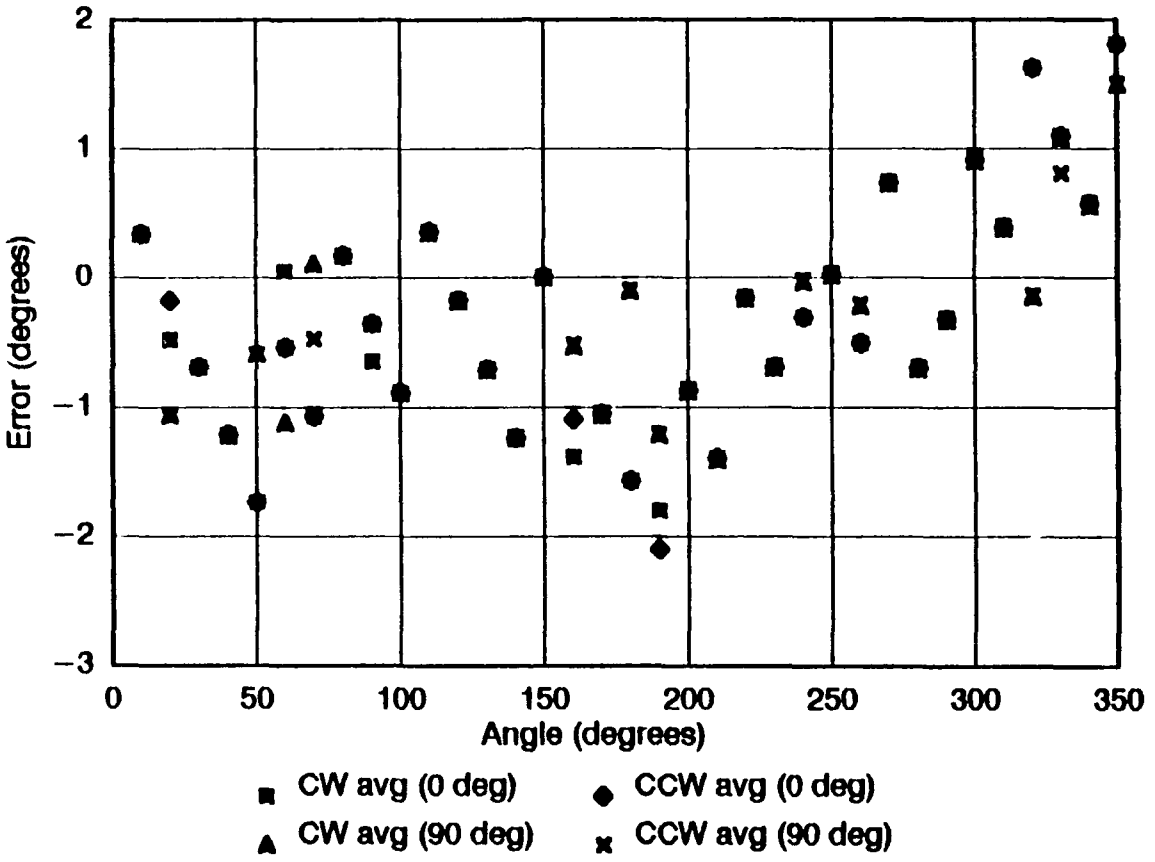

Figure 35. Climatronics bivane azimuth static test at the 25° vertical position. Clockwise (CW) and counterclockwise (CCW) data from both horizontal positions (0° and 90°) of the machined static test wheel are shown with the best-fit regression subtracted from the individual voltage values.

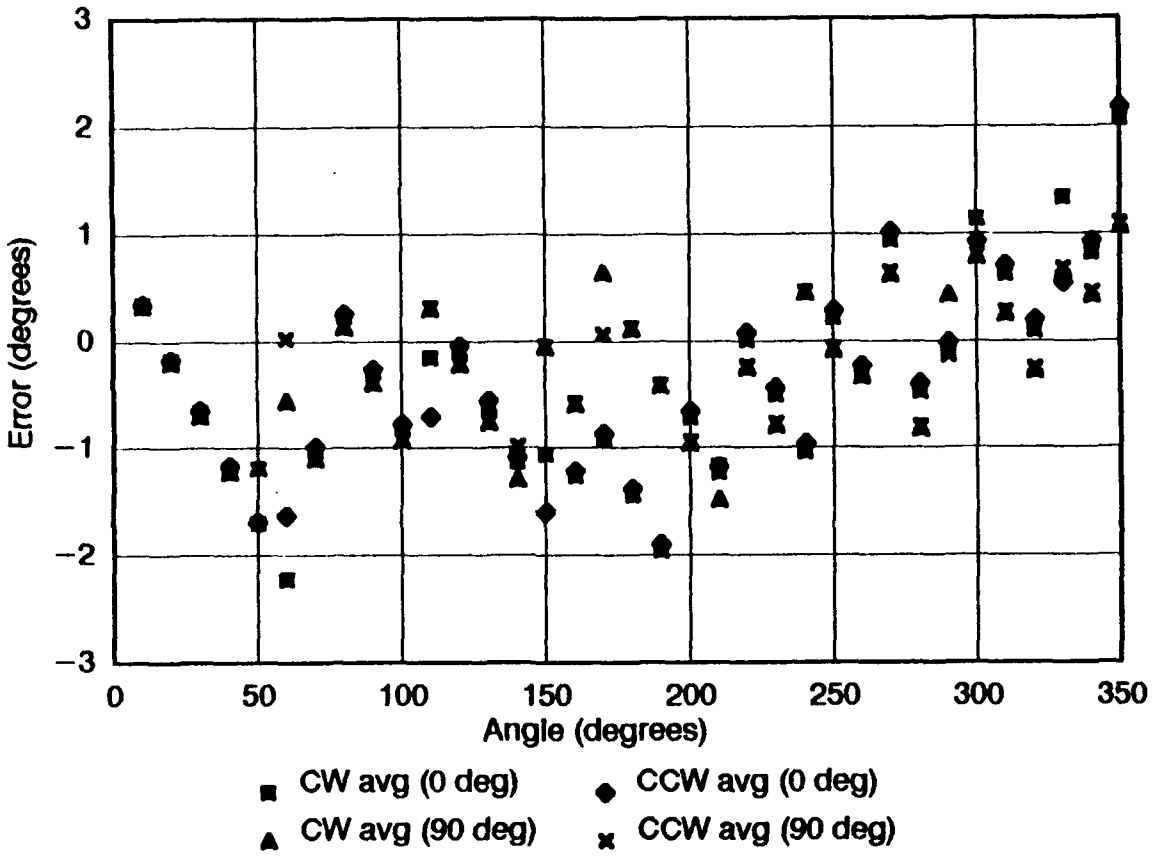

Figure 36. Same as Figure 35, but for the wheel lowered to the 35° vertical position.

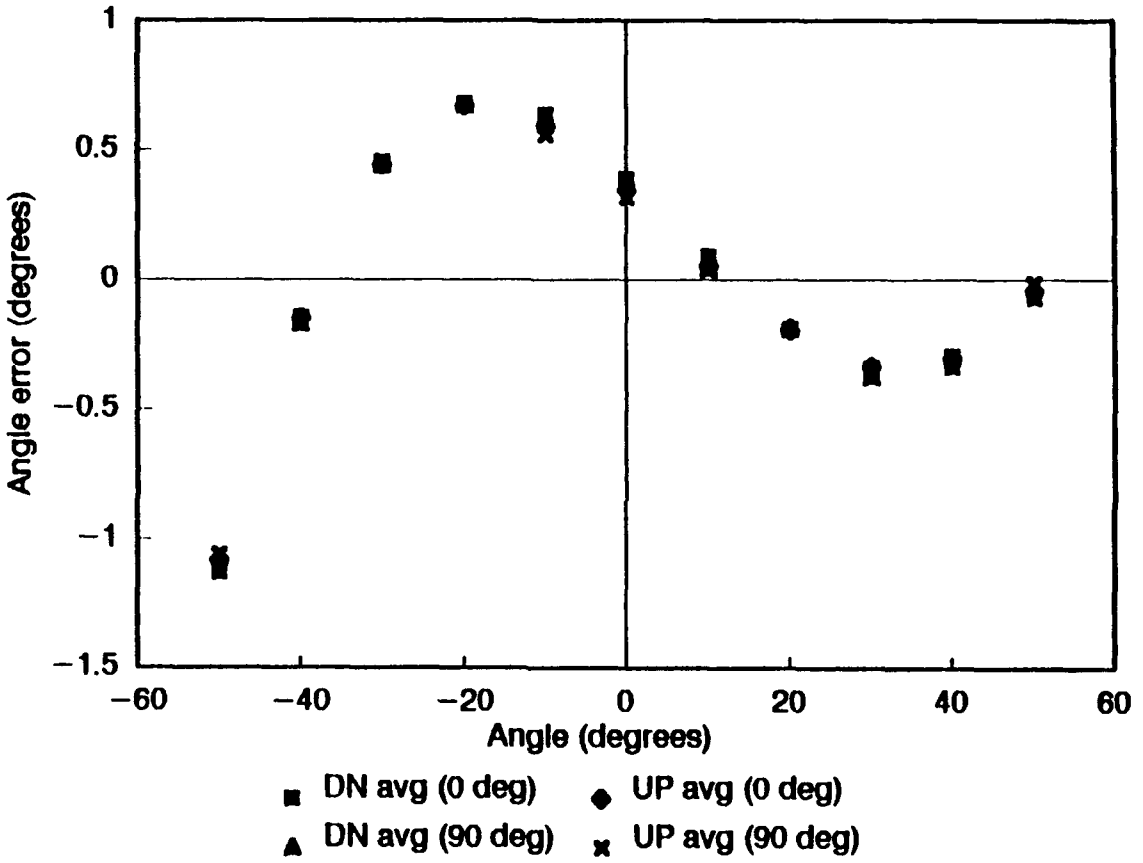

Figure 37. Climatronics bivane elevation static test. Up and down data from both horizontal positions (0° and 90°) of the machined static test wheel are shown with the best-fit regression line subtracted from the individual voltage values.

Static tests resulted in the following two transfer equations characterizing this particular bivane's output as a function of angle:

$$\theta = 359.24\ V_{az} \tag{12}$$

$$\phi = 106.15\ V_{el} - 31.19. \tag{13}$$

Large differences between ideal and actual offset in ϕ reflect the uncalibrated LVDT. The significant difference in the slope of ϕ may in part be related to the cause of the oscillation seen in Figure 34.

This strong systematic error in elevation data is clearly seen in Figure 38. Azimuth correction data are seen in Figure 39. The ASCII correction file, BVC.COR represented in Table 3, lists the correction values for each measured angle.

Bias due to the direction of vane motion is not apparent in the azimuth direction (Figures 40 and 41). Bias is evident between the up and down motions in the elevation data. Friction between the slug and LVDT wall probably cause the bias seen in Figures 42 and 43. The extra large bias at an elevation angle of 0° may be due to additional friction caused by a reduction of the cavity's diameter. Indeed, the trend toward larger error, while the slug approaches 0° from either the up or down direction, is the overwhelming characteristic of the data and is clearly seen in the figures. The maximum error introduced by this feature is approximately 1/2 of one degree, which is still within manufacturer's specifications and ASTM requirements.

3.2 Model for the Dynamic Response

In order to determine how well a bivane responds to changing wind directions, certain parameters of its response must be known. These parameters can be derived from a mathematical model that describes the vane response. This section of the chapter details the development of this model and the method used in locally-developed software to determine the parameters of each test run.

3.2.1 Theory

When wind acts on a wind vane, unequal forces are created on the two sides of the fin. The vane attempts to equalize these forces by turning into the wind. This motion by the vane closely resembles

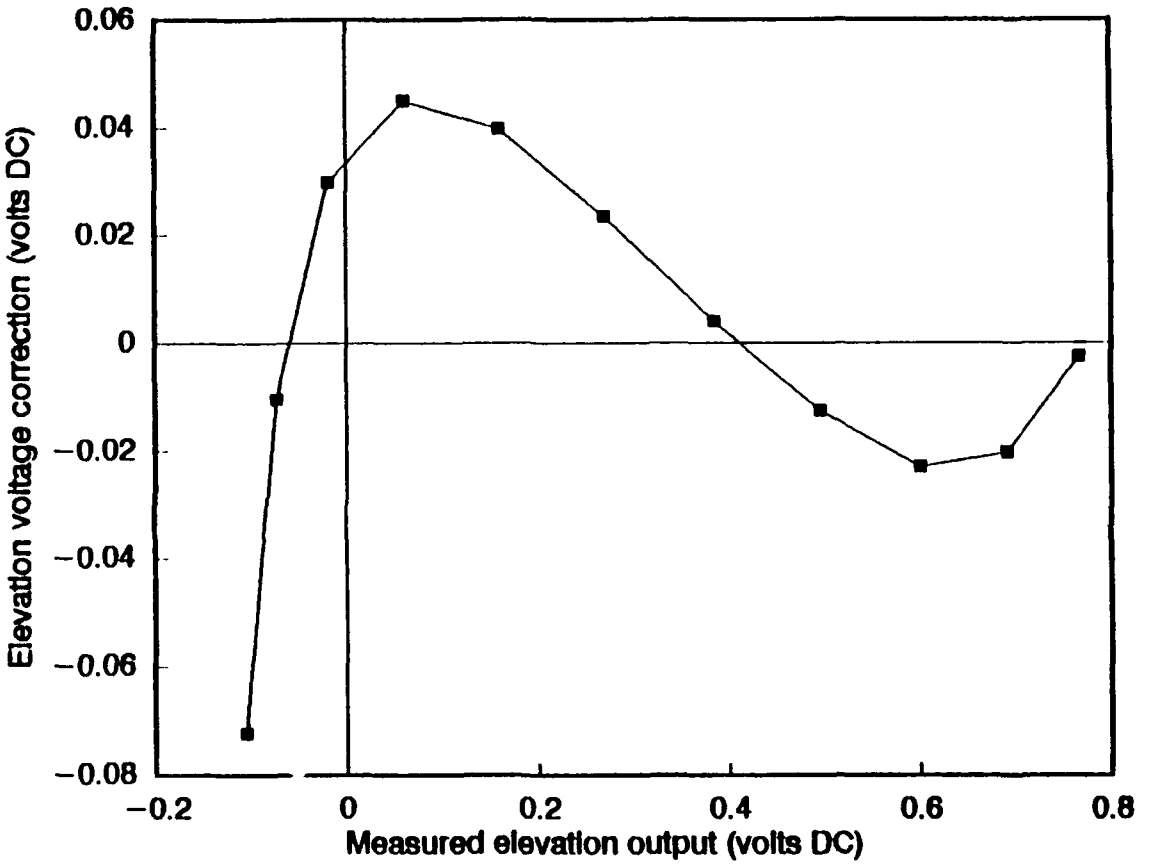

Figure 38. Elevation correction values as a function of voltage output derived for this particular Climatronics bivane.

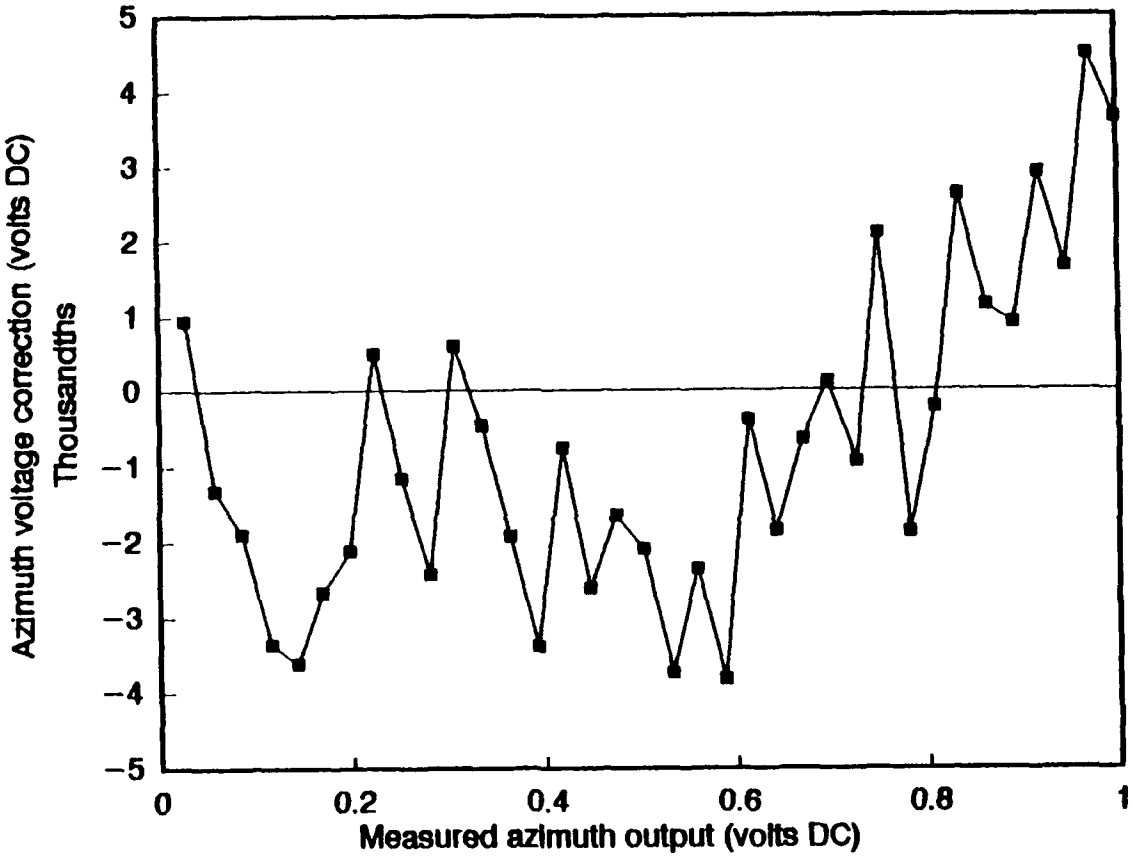

Figure 39. Same as Figure 38, but for azimuth correction values.

Table 3. BVC.COR file for correcting dynamic test data.

Azimuth/Elevation
CLIMATRONICS
14 Nov 90
Volts Error

27 Azimuth

0.02690	0.00094
0.05759	-0.00133
0.08540	-0.00189
0.11470	-0.00335
0.14240	-0.00362
0.16849	-0.00267
0.19658	-0.00213
0.22220	0.00050
0.25170	-0.00117
0.28080	-0.00243
0.30520	0.00060
0.33450	-0.00046
0.36380	-0.00192
0.39310	-0.00339
0.41750	-0.00077
0.44780	-0.00261
0.47610	-0.00165
0.50335	-0.00209
0.53324	-0.00374
0.55910	-0.00237
0.58840	-0.00383
0.61280	-0.00039
0.64210	-0.00186
0.66850	-0.00064
0.69580	0.00012
0.72470	-0.00094
0.74950	0.00209

7 Elevation

0.76740	-0.00253
0.69114	-0.02048
0.59955	-0.02309
0.49498	-0.01272
0.38413	0.00393
0.27039	0.02346
0.15991	0.03974
0.06063	0.04482
-0.01852	0.02976
-0.07242	-0.01054
-0.10479	-0.07237

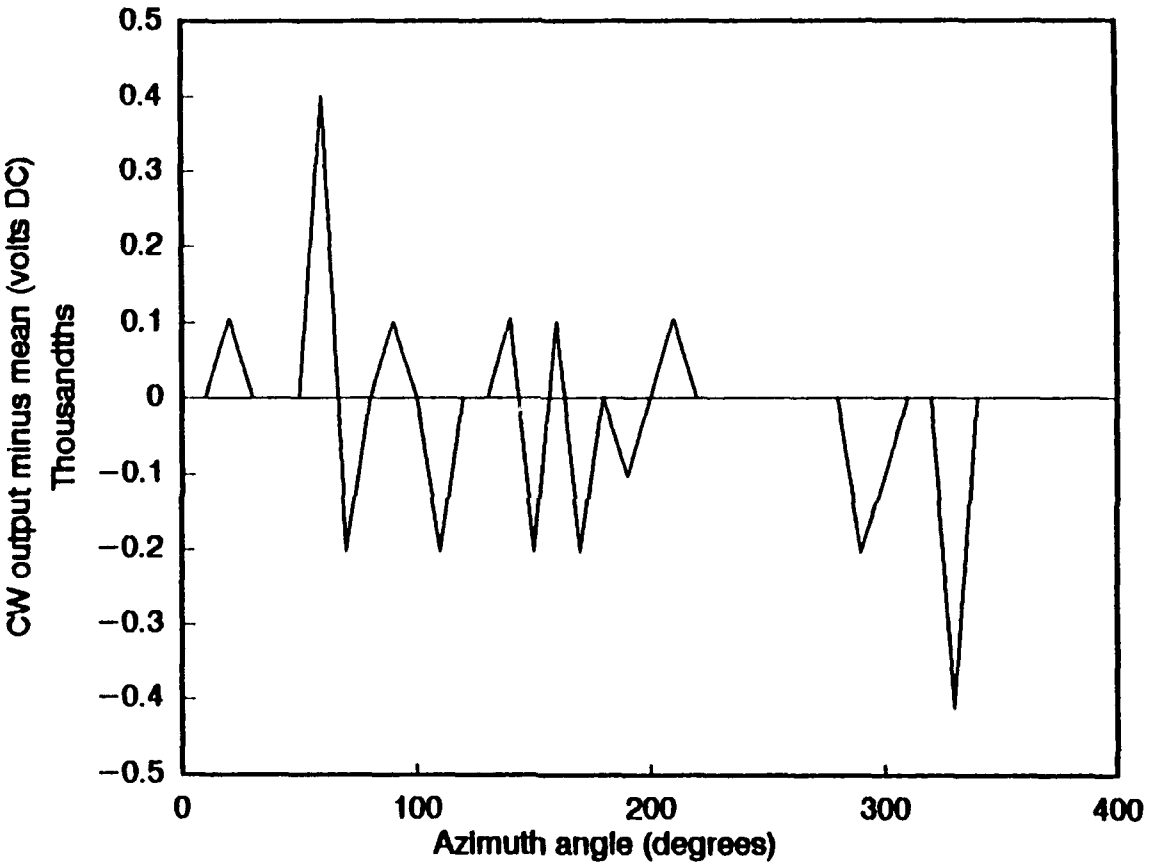

Figure 40. Same as in Figure 18 with CW motion, but for the Climatronics azimuth resolver that produces no ΔV.

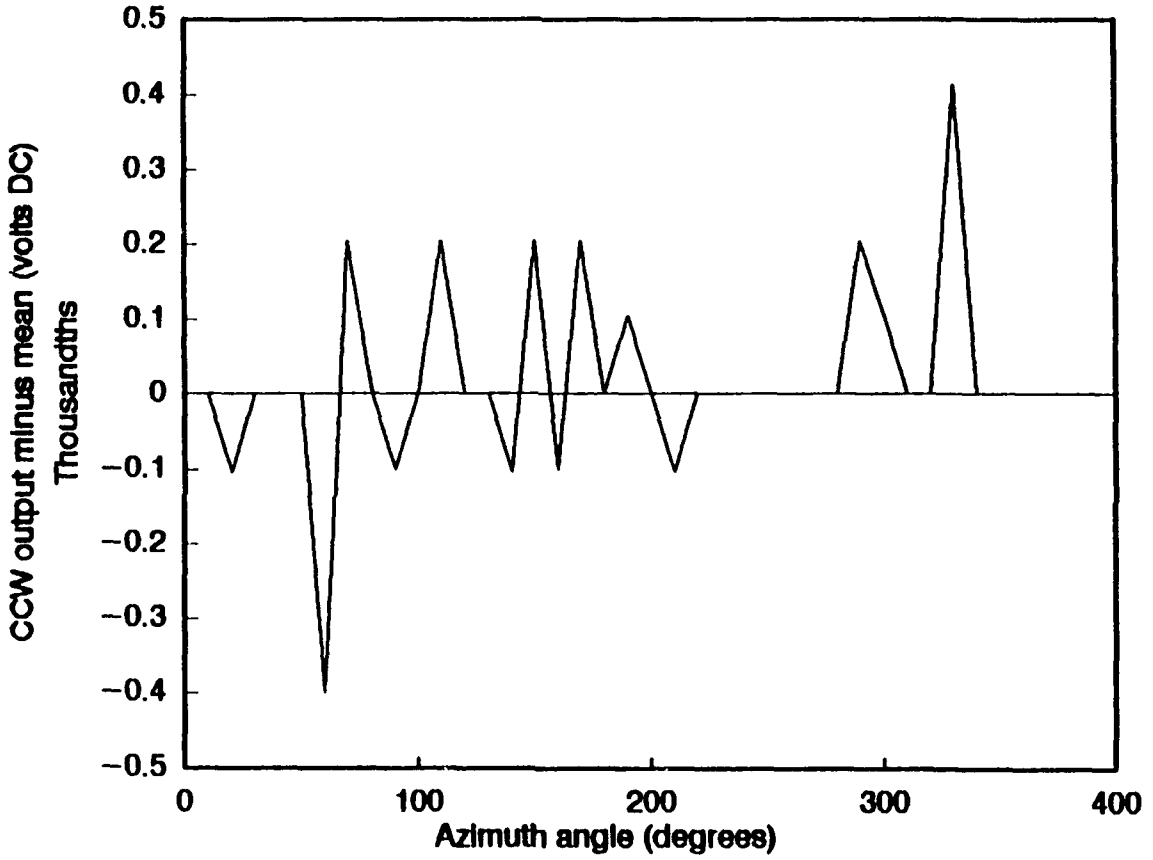

Figure 41. Same as in Figure 40, but for CCW motion.

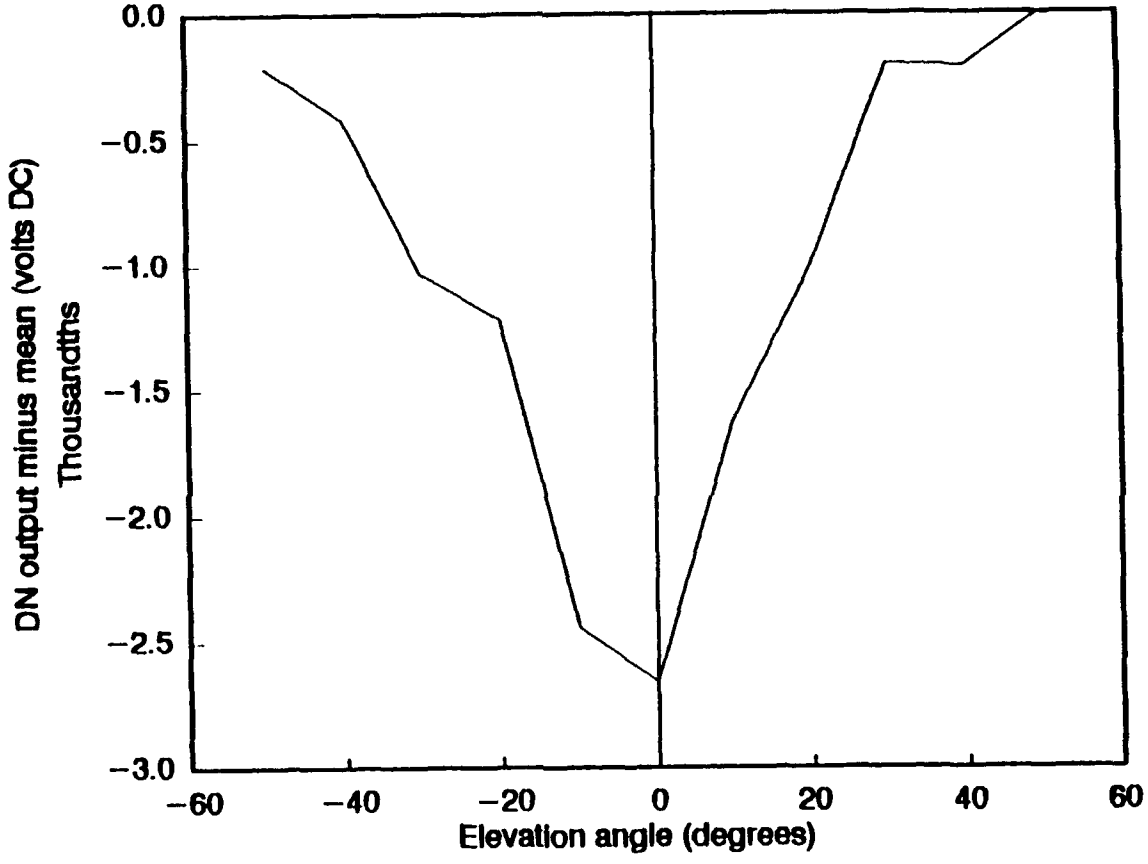

Figure 42. Same as in Figure 20 with down motion, but for the Climatronics elevation resolver that produces a distinct ΔV towards 0°.

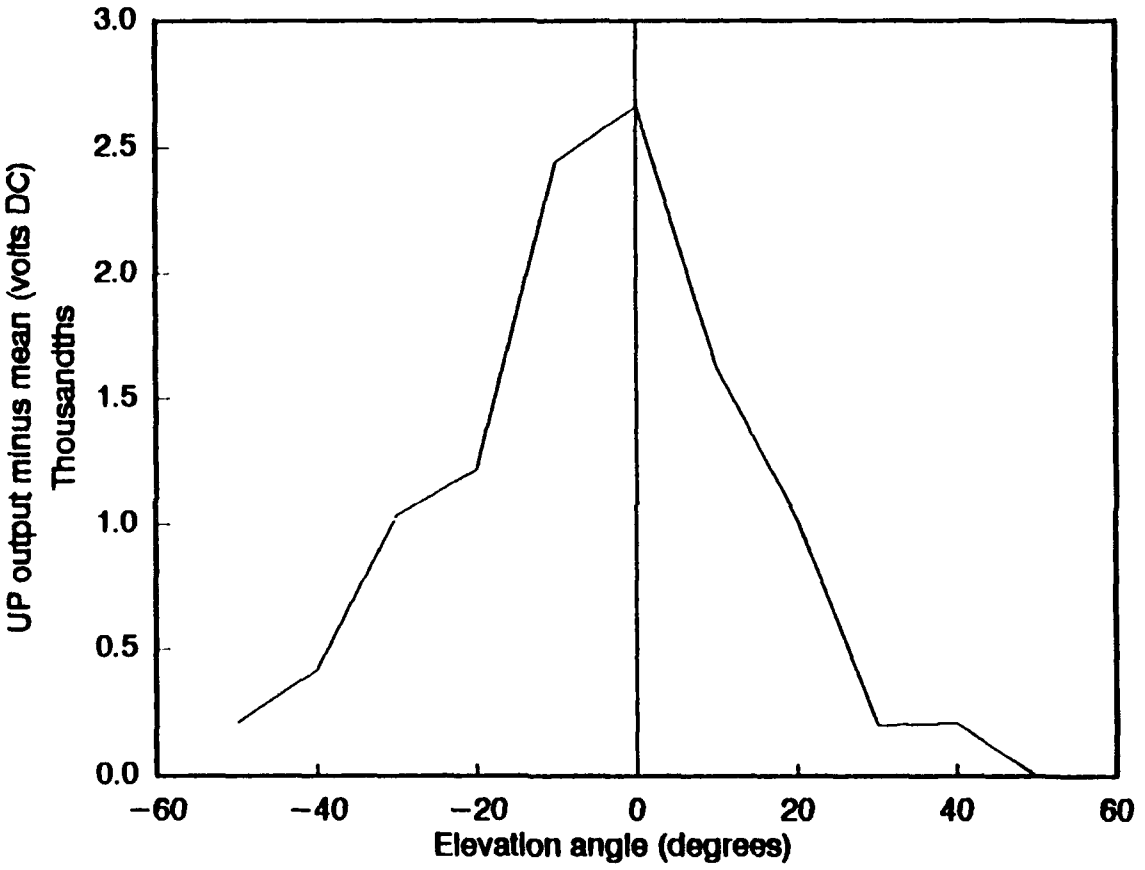

Figure 43. Same as in Figure 42, but for up motion.

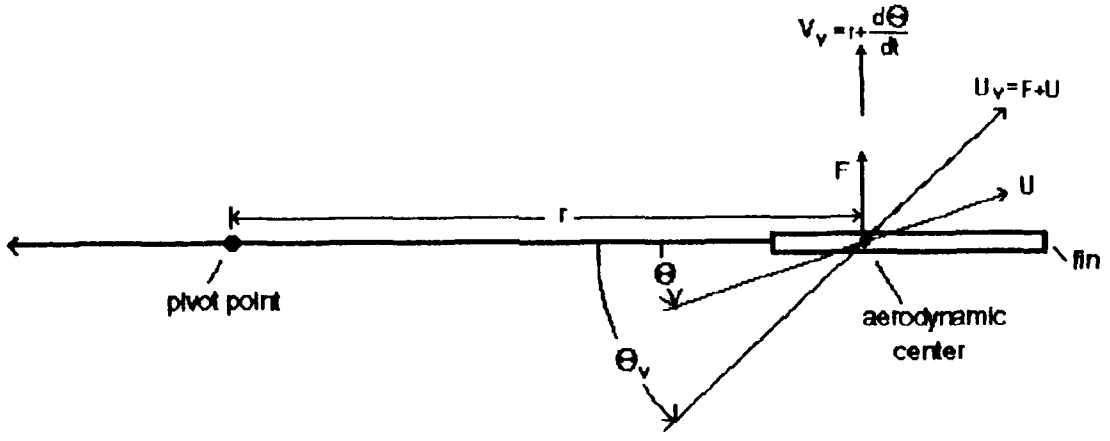

Figure 44. Schematic of the vane physics showing forces and movement about the vane assembly.

a second-order response. Figure 44 diagrams the angles and forces acting about the vane's center of dynamic pressure or aerodynamic center. The wind vector, U, intersects the aerodynamic center with an angle of attack of Θ. A force, F, created by U creates a torque that turns the vane.

As the vane moves about the pivot point, it moves with a speed of

$$V_v = r\frac{d\Theta}{dt} \quad , \tag{14}$$

where r is the boom length and t is time. With this motion, an effective wind, U_v, acts on the vane at an effective angle of attack, Θ_v. For small Θ of less than 15° (Wieringa, 1967, and Wang and Felton, 1983),

$$U_v \cong U, \text{ and} \tag{15}$$

$$\Theta_v \cong \Theta + \frac{r\,d\Theta}{U\,dt} \quad . \tag{16}$$

The aerodynamic force acting on the vane is

$$F = \rho\frac{U^2}{2}AC_L\cos(\Theta_v) \quad , \tag{17}$$

where ρ is the air density, C_L is the lift coefficient, and A is the projected area of the fin onto the zero plane of attack. Since, by definition, the torque (T) is

$$T = Fr \quad , \tag{18}$$

then,

$$T = r\rho\frac{U^2}{2}AC_L\cos(\Theta_v) \quad . \tag{19}$$

For $\Theta_v < 15°$,

$$\cos(\Theta_v) \cong 1 \tag{20}$$

$$C_L \cong \frac{\partial C_L}{\partial \Theta}\Big|_0 \Theta_v \quad . \tag{21}$$

Using equations (20) and (21), T is now

$$T = r\rho \frac{U^2}{2} A \frac{\partial C}{\partial \Theta}\Big|_0 \Theta_v \quad . \tag{22}$$

For a constant U, $r\rho \frac{U^2}{2} A \frac{\partial C_L}{\partial \Theta}\Big|_0 \Theta_v$ can be represented as a constant, K. Since the wind acts to decrease Θ_v, $\frac{\partial C_L}{\partial \Theta}$ becomes negative. Thus,

$$T = -K\Theta_v \quad . \tag{23}$$

T is also

$$T = I \frac{d^2\Theta}{dt^2} \tag{24}$$

where I is the moment oi inertia. Equations (23) and (24) yield,

$$I \frac{d^2\Theta}{dt^2} + K\Theta_v = 0 \quad . \tag{25}$$

Using (16) to substitute for Θ_v,

$$I\frac{d^2\Theta}{dt^2} + K\left(\Theta + \frac{r\,d\Theta}{U\,dt}\right) = 0 \tag{26}$$

where $K\left(\frac{r\,d\Theta}{U\,dt}\right)$ is called the damping torque and $K\frac{r}{U}$ is the damping factor, H (see Wang and Felton, 1983) which is

$$I\frac{d^2\Theta}{dt^2} + H\frac{d\Theta}{dt} + K\Theta = 0. \tag{27}$$

From Wyngaard (1981)

$$\omega_n^2 = \frac{K}{I} \tag{28}$$

$$\zeta = \frac{\omega_n H}{2} \tag{29}$$

where ω_n is the natural frequency and ζ is the damping ratio. Equation (27) now becomes

$$\frac{d^2\Theta}{dt^2} + 2\zeta\omega_n\frac{d\Theta}{dt} + \omega_n^2\Theta = 0. \tag{30}$$

This second order homogeneous linear differential equation (30) governs the vane response with a step change of Θ, since

$$\omega_n = \frac{2\pi U}{\lambda_n} \quad , \tag{31}$$

where λ_n is the natural wavelength. With λ_n independent of the wind speed, it is a good parameter to describe vane motion, along with ζ, which is also independent of wind speed. From (31), equation (30) becomes

$$\frac{d^2\Theta}{dt^2} + \frac{4\pi U\zeta}{\lambda_n}\frac{d\Theta}{dt} + \frac{4\pi^2U^2}{\lambda_n^2}\Theta = f(t) \tag{32}$$

where the wind direction varies with a forcing function, f(t). Here the wind speed, U, may also vary with time. This scenario where the wind speed and direction change in time severely complicates the solution. This being the case, (30) assumes no additional change in wind direction and a constant wind speed. It is generally used with the following relations

$$\frac{\omega_n}{\omega_d} = \frac{\lambda_d}{\lambda_n} \tag{33}$$

$$\lambda_n = \lambda_d\sqrt{1-\zeta^2} \tag{34}$$

where the subscript "d" stands for "damped" frequency and wavelength. Figure 45 shows the relationship between λ_n and λ_d.

Another method for calculating λ_n is by using the delay distance, D. The delay distance is the length of air that moves past the vane causing the vane assembly to travel half way between the peak and the equilibrium value from time T_0 to T_D (see Figure 46). T_D and D are related by

$$T_D = \frac{U}{D} \tag{35}$$

where D is independent of U. The delay distance is directly related to the design of the vane assembly as are λ and ω. An alternative to (34) that uses D is

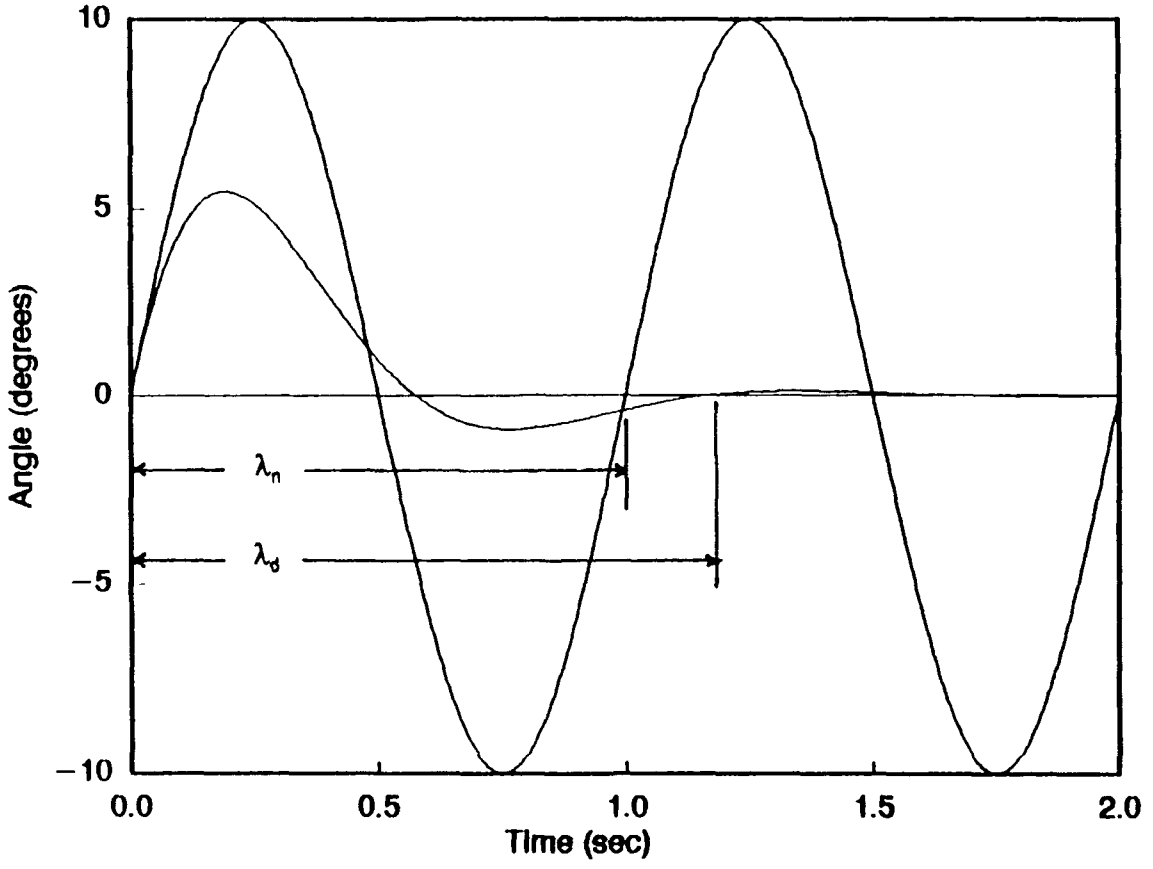

Figure 45. Schematic showing the difference between natural wavelength, λ_n, and damped wavelength, λ_d (from MacCready and Jex, 1964).

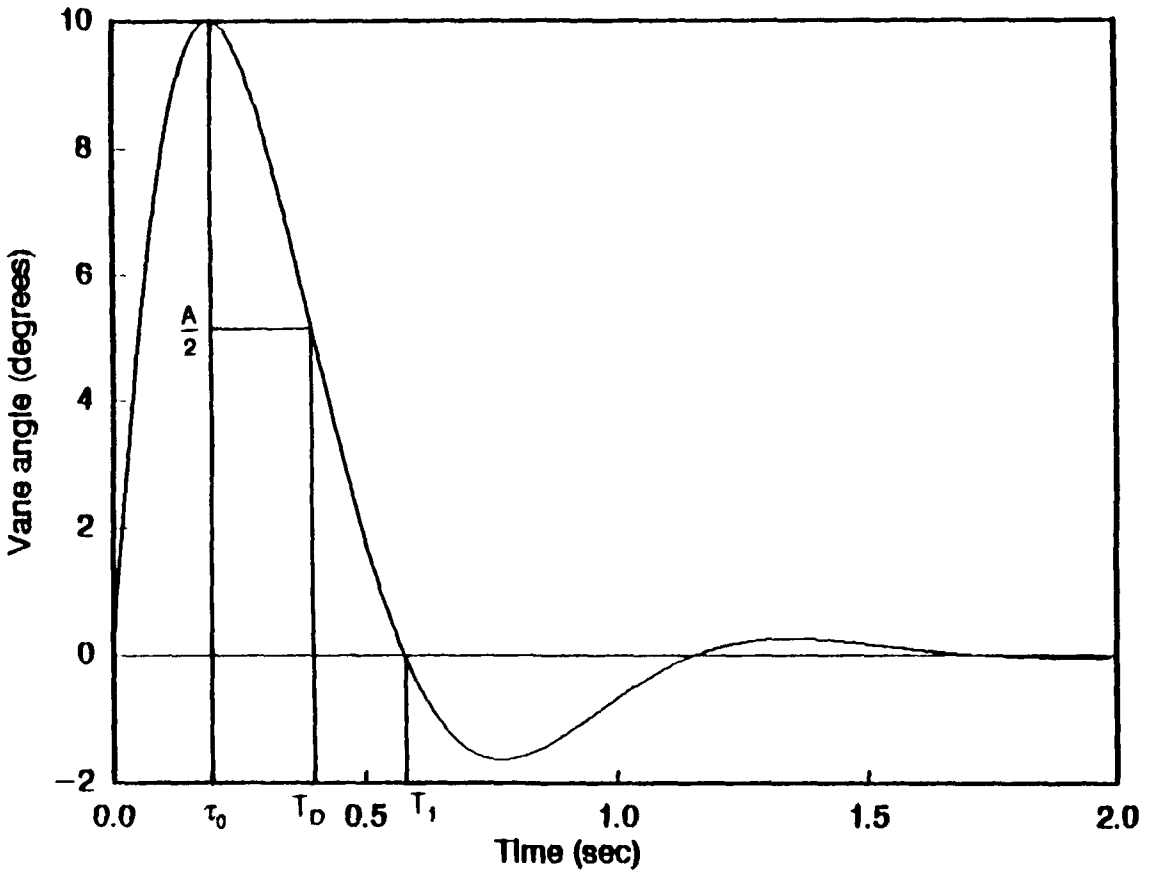

Figure 46. Locations of the time of the first peak, τ_0, time of the second zero-crossing T_1, and the time of the delay distance, T_D.

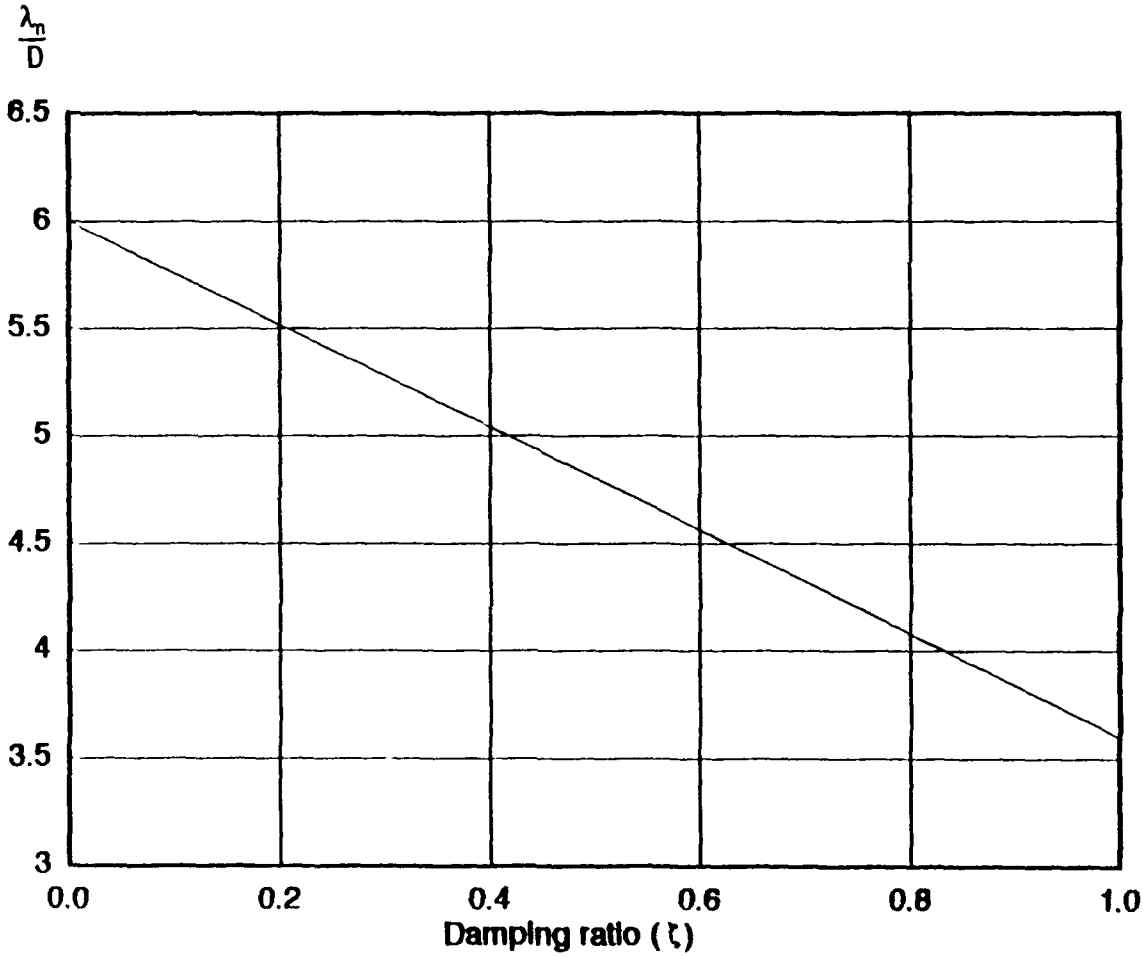

Figure 47. Relationship between ζ, D, and λ_n (from MacCready and Jex, 1964).

$$\lambda_n = D(6.0 - 2.4\zeta) \quad . \tag{36}$$

Figure 47 shows how ζ, D, and λ_n are related.

With a step change in Θ, the solution to (30) depends on the coefficients $\zeta\omega_n$ and ω_n^2. The governing equation has the roots

$$r = -\zeta\omega_n \pm \omega_n\sqrt{\zeta^2-1} \quad . \tag{37}$$

Three forms of the solution depend on the nature of the discriminate ζ^2-1. If the damping ratio is:

$\zeta > 1$, the vane motion is overdamped with real and unequal roots (Figure 48);

$\zeta = 1$, the vane motion is critically damped with real and equal roots (Figure 49);

$\zeta < 1$, the vane motion is underdamped with imaginary roots (Figure 50).

Practical vanes require some overshoot to quickly return to equilibrium and employ the $\zeta < 1$ case. The general solution uses the roots $\alpha \pm i\beta$ where $\alpha = -\zeta\omega_n$ and $\beta = \omega_n\sqrt{1-\zeta^2}$. Thus, the general form is

$$\Theta(t) = C_1 e^{-\zeta\omega_n t}\cos(\omega_n\sqrt{1-\zeta^2})t + C_2 e^{-\zeta\omega_n t}\sin(\omega_n\sqrt{1-\zeta^2})t \quad , \tag{38}$$

where C_1 and C_2 are constants. Equations (33) and (34) substituted into (38) give

$$\Theta(t) = C_1 e^{-\zeta\omega_n t}\cos(\omega_d)t + C_2 e^{-\zeta\omega_n t}\sin(\omega_d)t.$$

For the case where the vane is aligned with the applied wind and has a non-zero speed, the initial conditions are

$$\Theta(0) = \Theta_0 \tag{39}$$

$$\left.\frac{d\Theta}{dt}\right|_0 = \Lambda_0 \quad . \tag{40}$$

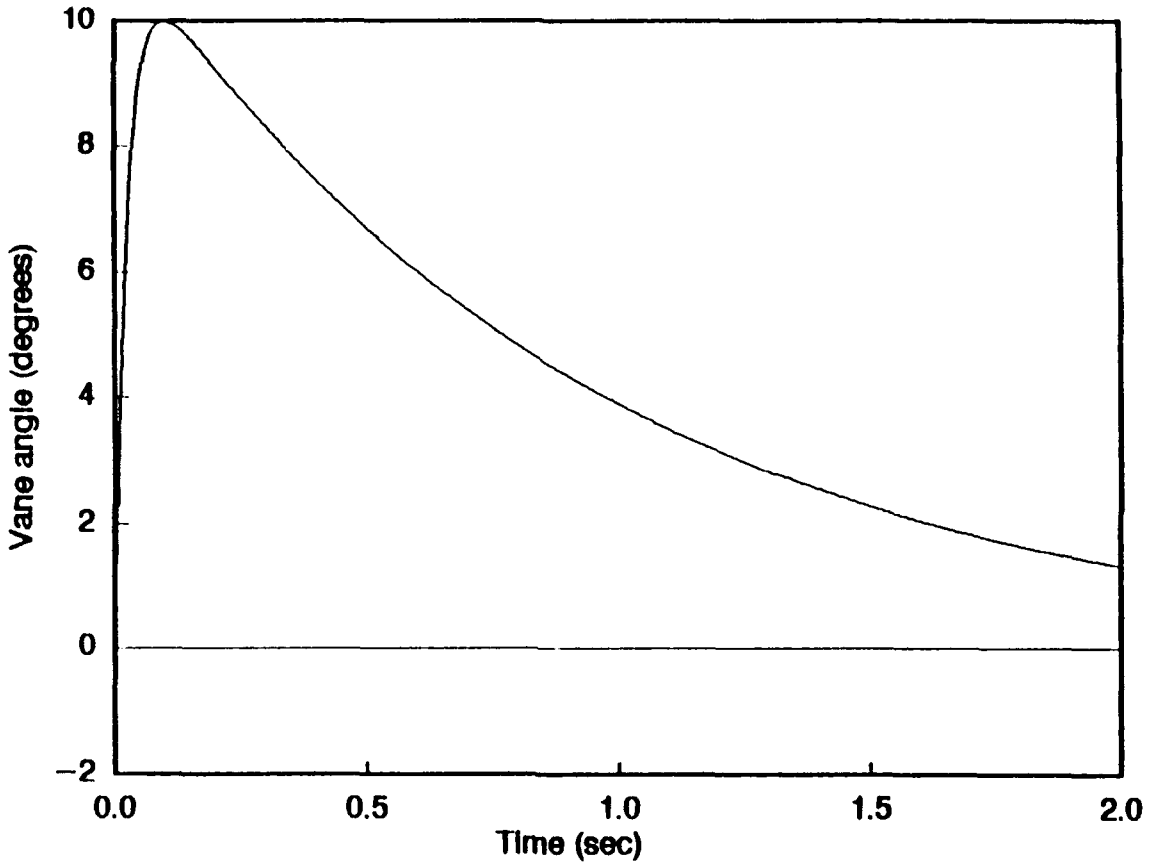

Figure 48. Overdamped curve with $\zeta = 3.0$.

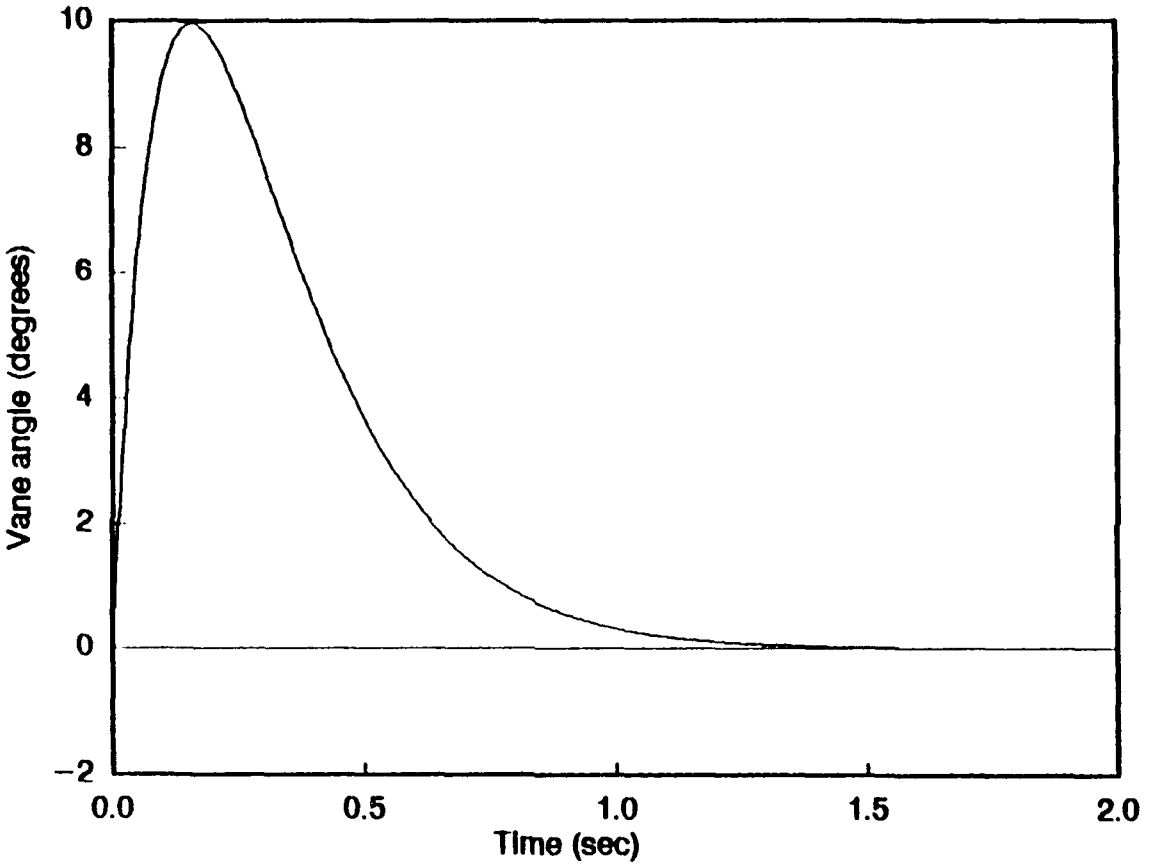

Figure 49. Critically damped curve with $\zeta = 1.0$ by definition.

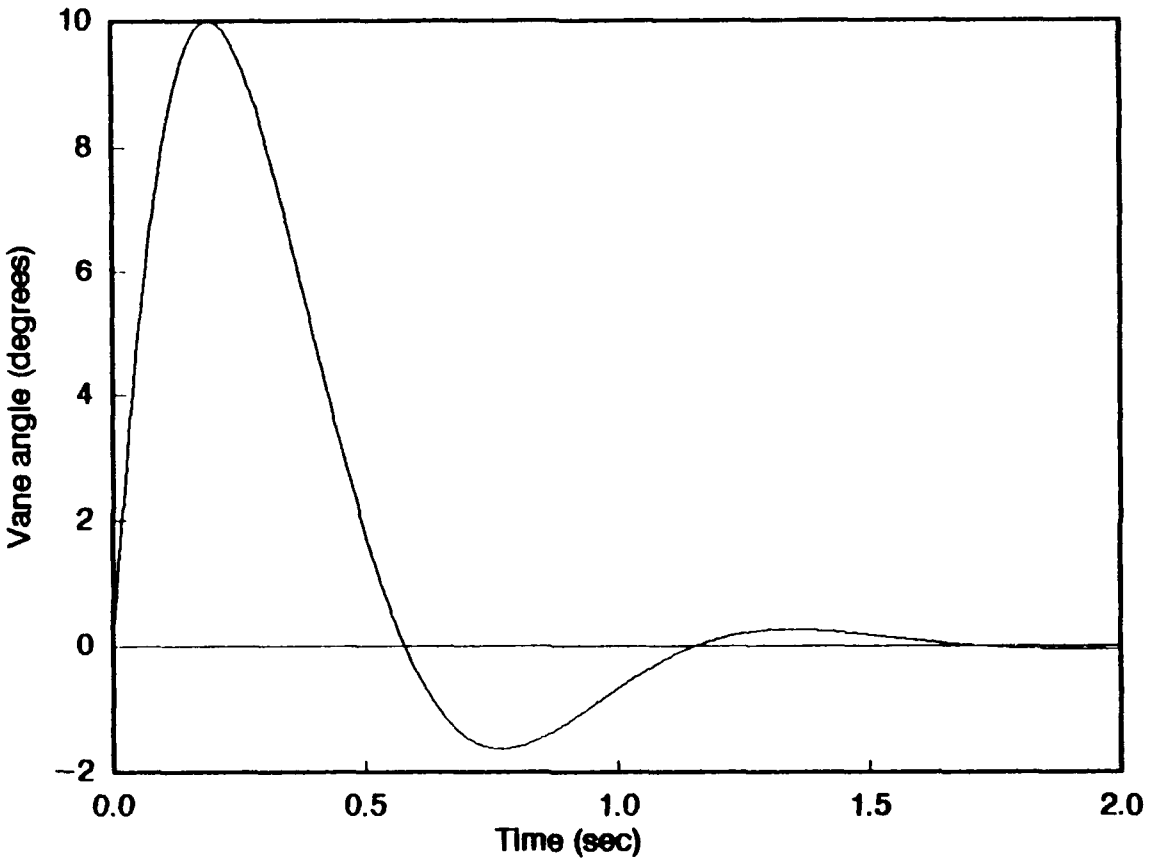

Figure 50. Underdamped curve with $\zeta = 0.5$.

Then,

$$C_1 = \Theta_0 \tag{41}$$

$$C_2 = \frac{\Lambda_0 + C_1}{\omega_d} \quad . \tag{42}$$

The objective for analyzing each of the bivane's responses is to calculate the damping ratio, ζ, and natural wavelength, λ_n. A common approach to calculating ζ uses the ratio of the amplitudes of consecutive peaks. Times when the response curve touches the exponential curves are

$$B = \pm A\, e^{-\zeta\omega_n t} \quad , \tag{43}$$

where B is the distance from the envelope to the equilibrium value and A is the amplitude (see Figure 51). The quasi-period is

$$P_q = \frac{2T_q}{i} \quad , \tag{44}$$

where T_q is the time when the curve touches the exponential curve and

$$P_q = \frac{2\pi}{\omega_n\sqrt{1-\zeta^2}} \quad . \tag{45}$$

The exponential curve can be modified to (46) by using (44) and (45) in (43)

$$B = A \exp\left[\frac{-\zeta\pi}{\sqrt{1-\zeta^2}}\right] \quad . \tag{46}$$

From Wieringa (1967), the ratio, r, of the second peak to the first peak is

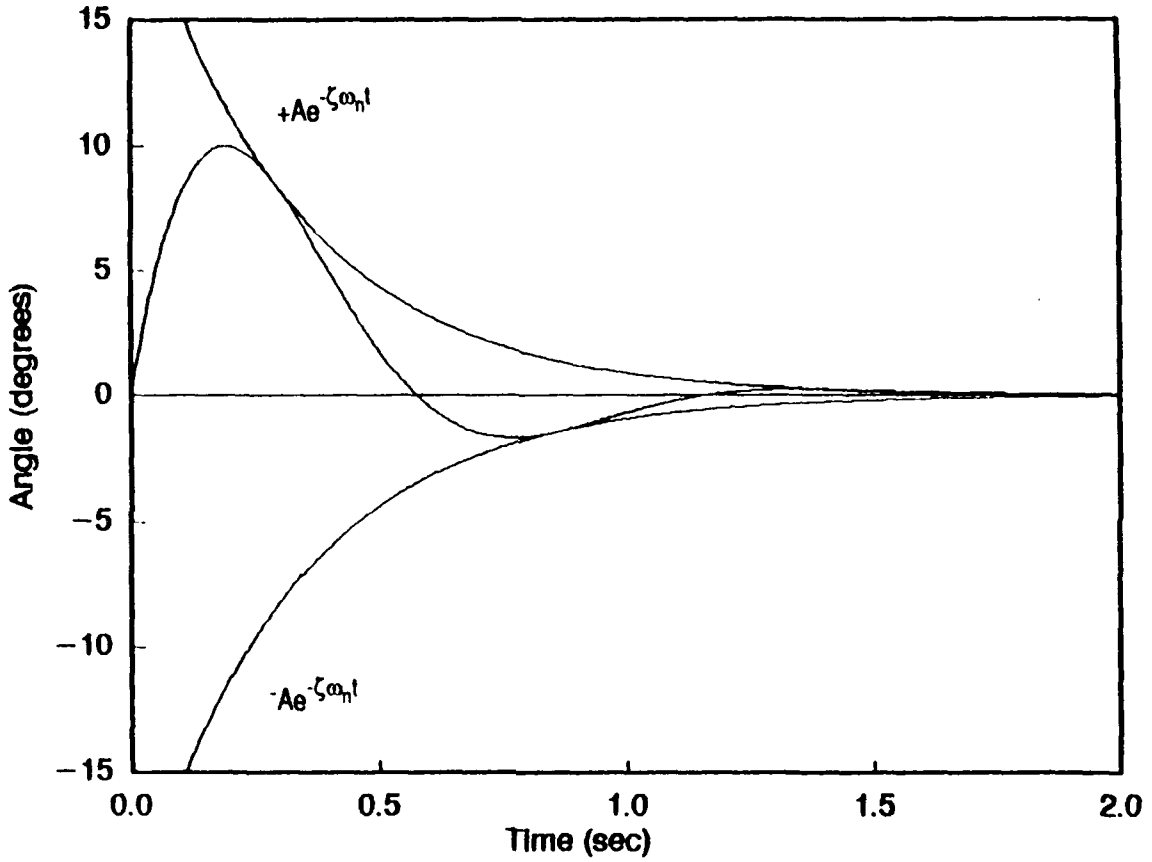

Figure 51. Underdamped curve within $\pm Ae^{-\zeta\omega_n t}$ envelope.

$$r = \frac{B_{i+1}}{B_i} = \frac{A \exp\left(\frac{-(i+1)\zeta\pi}{\sqrt{1-\zeta^2}}\right)}{A \exp\left(\frac{-i\zeta\pi}{\sqrt{1-\zeta^2}}\right)}$$

which reduces to

$$r = \exp\left(\frac{-\zeta\pi}{\sqrt{1-\zeta^2}}\right). \tag{47}$$

From (47), ζ can be isolated via

$$\ln\left(\exp\left(\frac{\zeta\pi}{\sqrt{1-\zeta^2}}\right) = \frac{1}{r}\right)$$

$$\zeta^2\pi^2 = \left(\ln\frac{1}{r}\right)^2 (1-\zeta^2)$$

$$\zeta^2\left(\pi^2 + \left(\ln\frac{1}{r}\right)^2\right) = \left(\ln\frac{1}{r}\right)^2$$

leading to the damping ratio as a function of the ratio of the peaks in

$$\zeta = \frac{\left(\ln\frac{1}{r}\right)}{\sqrt{\pi^2 + \left(\ln\frac{1}{r}\right)^2}}. \tag{48}$$

This relation assumes that at least two successive peaks are evident and their amplitudes are confidently measured. The response traces of the bivanes tested had small amplitudes of the second peaks that were usually difficult to measure. First peaks and first and second times, when the vane oscillated through the

applied wind direction (called zero-crossings), were easily identifiable. Consequently, a method to determine ζ that employs the times of the first peak and second zero-crossing was developed.

When the vane oscillates, it periodically aligns itself with the applied wind with a non-zero Λ_0. At the zero-crossings, T_i (where i = 0, 1, 2, and so forth), the initial condition is $\Theta(T_i) = \Theta_0$. Each T_i is a multiple of one-half of the period of damped oscillations in that

$$T_i = \frac{iP_d}{2} \tag{49}$$

and

$$P_d = \frac{2\pi}{\omega_d} \quad , \tag{50}$$

where P_d is the damped period. Then T_i are related to ω_d by

$$T_i = \frac{i\pi}{\omega_d}. \tag{51}$$

Extremes or peaks occur at times

$$\tau_j = \frac{j\pi + \cos^{-1}(\zeta)}{\omega_d} \quad j = 0, 1, 2, ..., \tag{52}$$

and have amplitudes of $\Theta(\tau_j)$.

Using the difference between the time of the first peak, τ_0 (j=0), and the second zero-crossing, T_1 (i=1), equations (51) and (52) become

$$\tau_j = \frac{\cos^{-1}(\zeta)}{\omega_d}$$

$$\omega_d = \frac{\pi}{T_1}$$

and together give

$$\zeta = \cos\left[\frac{\pi\tau_0}{T_1}\right]. \tag{53}$$

Equation (53) was found to be a reliable method to determine the damping ratio when the amplitude of the second peak is not available.

Calculations of the natural wavelength, λ_n, also uses the time of the second zero-crossing, T_1. Equations (33), (34), (51), and the relation

$$\omega_n = \frac{2\pi U}{\lambda_n} \tag{54}$$

produce

$$\lambda_n = 2T_1 U\sqrt{1-\zeta^2} \tag{55}$$

which uses the time of the second zero-crossing. For calculating the natural wavelength, Approach 1 uses (55) and Approach 2 uses (36) which is based on the delay distance, D.

3.2.2 Applications

Dynamic data were collected by Labtech Notebook software and processed by two C language programs that were compiled using Microsoft Corporation's Quick C version 2.0. The first (or conversion) program converts the data by adding the voltage correction information via the ASCII correction file for that particular bivane, and determines the equilibrium values, times of zero-crossings, and times of the peaks. The program also allows the user to place a user-defined running average on the data. The second (or calculation) program calculates the parameters ζ and λ_n using equations (36), (53), and (55) discussed in the previous section. Since the reader may wish to consider the methods used to determine the important values of the response in the first program and the parameters calculated in the second program, this section describes the software procedures used for these purposes.

The conversion program first applies a voltage correction for every azimuth and elevation voltage in accordance with the correction values in the ASCII correction file specific for this bivane. Correction values are interpolated using a simple distance routine.

Pitot tube output voltages are corrected using an empircally derived analog-to-digital board input conversion factor. A linearity test was applied to the wind measuring system using voltages at ten different wind speeds. A coefficient and offset were calculated giving

$$\text{corrected } V_w = (0.9712 * V_w) + 0.00244 \tag{56}$$

where V_w is the voltage produced by the wind speed sensing system. Each voltage corresponding to the wind speed was corrected using equation (56) as the conversion factor.

Additionally, in the beginning of the program, a running average is calculated using a user-defined point average. Next, the equilibrium value is calculated by averaging the last several seconds of voltage data.

Times of zero-crossings are found by sequentially searching the data for values within a ±2% envelope of the equilibrium value for that test run. All data within this envelope are held in an array. The time of the occurrence of the data point closest to the equilibrium value is the zero-crossing or T_i. If the times of two or more data points qualify as the T_i, then the T_i is the average of these times. Ten zero-crossing are identified using this method. Normally, only the first two zero-crossings, T_0 and T_1, are reliable. The other eight zero-crossings have random values and are overwhelmed by system noise.

Times-of-peaks (τ_i) are determined by searching for the minimum or maximum voltage value (depending on which side of the equilibrium line the vane is oscillating) between two successive T_i. The first peak was always found reliable, while the second peak was usually dectectable, but τ_1 was not reliable. Times τ_2 through τ_9 were usually undetectable.

All zero-crossings and times-of-peaks are printed to an output file. The converted data are listed in the same output file following the crossing and peak data. Thus, there is one converted data file per test run.

The calculation program first calculates two damping ratios for a single test run using equations (48) and (53). Results from (48) were widely variable due to an unreliable τ_1. The natural and damped wavelengths are calculated by using the tunnel equation (1) for wind speed, U, and equation (35) for the delay distance, D. Both approaches to calculate λ_n, (36) and (55), were used. The damped wavelength, λ_d, was calculated using (34) with its λ_n from (36).

The average U, D, τ_0, and T_i with their standard deviations were calculated for all ten runs of each position, per wind speed, for both azimuth and elevation directions. The average of the ratio τ_0/T_i was used to calculate azimuth and elevation damping ratios for the position. Similarly, the average D was used to calculate the final azimuth and elevation natural wavelengths.

4. RESULTS AND DISCUSSION

The software mentioned in Chapter 3 calculated the damping ratio and natural wavelength data for each test run of the three bivanes. At each of the six starting positions, ten runs were executed for wind tunnel speeds of 5 and 10 m s^{-1}. The averages of ζ and λ_n at each starting position showed how these dynamic characteristics varied depending on the primary plane of oscillation. At starting positions A and E, the dynamic characteristics associated with azimuth data were meaningless since the vane only oscillated in the vertical plane. At position C, the vane oscillated in the horizontal plane and only azimuth dynamic characteristics were considered.

For all three bivanes, the vertical plane of oscillation included the staff supporting the vane assembly. Owing to this fact, it is possible that the fin of the vane assembly is affected by the wake produced by the staff. Data from both the R. M. Young and Climatronics bivanes did show discrepancies at starting positions A and E. Elevation data at these two starting positions from the Teledyne Geotech bivane could not be interpreted for reasons to be discussed later. Though data originating from position C didn't include elevation dynamic characteristics, the azimuth data were good.

Best values of ζ and λ_n for each bivane were calculated using the averages of these dynamic characteristics at positions B, C, D, and F. One set of best values represented responses occurring at 5 m s^{-1} and a second set for data at 10 m s^{-1}. Each set of best values includes azimuth and elevation damping ratios (ζ_{az} and ζ_{el}), and azimuth and elevation natural wavelengths ($\lambda_{n\text{-}az}$ and $\lambda_{n\text{-}el}$) for both Approach 1 and Approach 2.

Again, the equations used to calculate ζ and λ_n assume that the bivane is a second-order system with an oscillatory response (i.e., $\zeta < 1$). The response of a model second-order wind vane system seen in Figure 52 holds true to equation (38). The traces have a damping ratio of 0.5 and a natural wavelength of

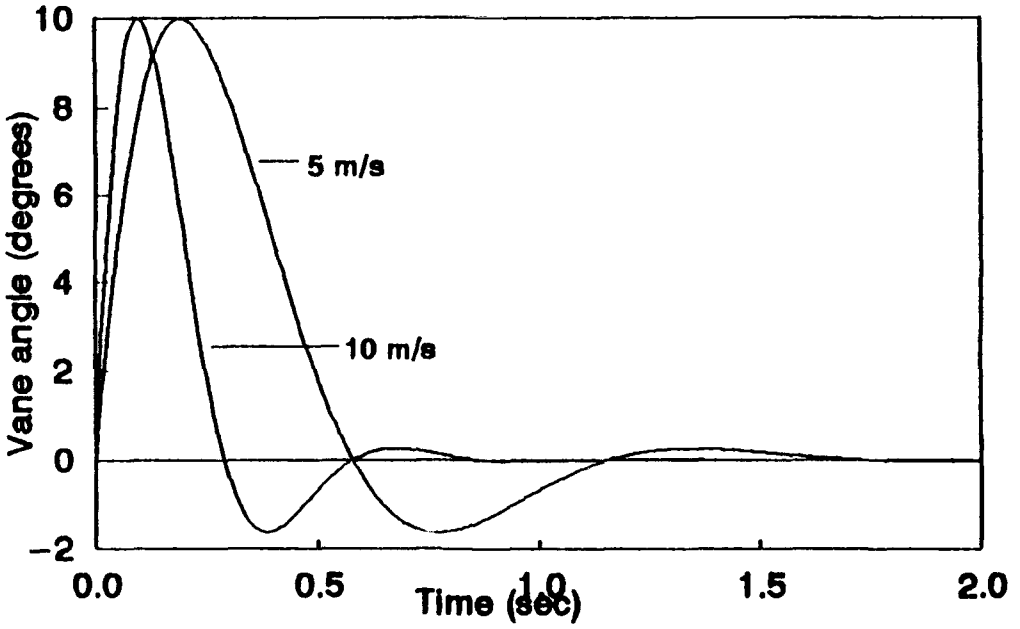

Figure 52. Ideal curves from equation (38) at two wind speeds. Both curves use the same dynamic characteristics of $\zeta = 0.5$ and $\lambda_n = 5.0$ m. The velocity at the equilibrium angle (Λ_0) is 115 deg s^{-1} for U = 5 m s^{-1} and 230 deg s^{-1} for U = 10 m s^{-1}.

5.0 m, and Λ_0 is 115 deg/sec for 5 m s^{-1} and 230 deg/sec for 10 m s^{-1}. The time of each peak is between two zero-crossings. Without damping, the times of the peaks would be at the midpoint between the two neighboring zero-crossings (see Figure 45). Notice that the times of the peaks are closer to the earlier zero-crossing than the later zero-crossings. This feature is due to energy being extracted from the system during oscillation and attempts to achieve an equilibrium of forces about its fin. If the times of the peaks were closer to the second or later zero-crossing, then energy would have to be introduced into the system and the forcing function, f(t), is non-zero. For critically or overdamped systems, an introduction of additional energy causes the vane to take longer to return to equilibrium.

For underdamped or oscillatory systems, the vane never achieves the stable equilibrium position if f(t) is non-zero. If the governing equation (30) is used where f(t) is assumed to be zero, the damping ratio from (48) and ζ from (53) is always positive. However, if equation (30) is used and f(t) is non-zero, then (48) and (53) yield negative damping ratio values. Where positive damping extracts energy from the vane motion, negative damping injects energy into the vane motion. An example of negative damping is discussed later in this chapter with respect to the Teledyne Geotech bivane.

In this chapter, test results for each bivane are presented and compared with the model governing equation and manufacturer's specifications. Discussion of these results leads to a final conclusion given in the next chapter.

4.1 R. M. Young

Table 4 gives the damping ratio and natural wavelength results for each position. Again, there are no ζ_{az} and $\lambda_{n\text{-}az}$ data for positions A and E since the vane oscillated only in the vertical plane and no ζ_{el} and $\lambda_{n\text{-}el}$ data exists for position C since the vane stayed in the horizontal plane. Figures 53 (5 m s^{-1}) and 54 (10 m s^{-1}) show a plot of the damping ratio values for each position from Table 4 against the manufacturer's published values (ζ=0.53, λ=4.4m). Figures 55 and 56 show λ_n for both approaches and speeds.

Ideally, both ζ and λ_n are independent of wind speed and initial angular position. Data from azimuthal motion does not appear to have any systematic variation. However, elevation data show a

Table 4. Results of dynamic testing of the R. M. Young Gill Bivane model 17003.

Air Speed: 5 m s^{-1}

Position	ζ_{az}	$\lambda_{n\text{-}az}$ Approach 1 Approach 2	ζ_{el}	$\lambda_{n\text{-}el}$ Approach 1 Approach 2
A	----	----	0.44±0.02	5.37±0.04
				5.34±0.13
B	0.48±0.13	5.24±0.35	0.49±0.04	5.08±0.15
		5.57±0.35		5.28±0.10
C	0.52±0.06	5.09±0.17	----	----
		5.65±0.17		
D	0.54±0.05	4.86±0.16	0.50±0.03	5.02±0.12
		5.50±0.15		5.15±0.12
E	----	----	0.49±0.02	4.94±0.07
				5.03±0.06
F	0.49±0.08	4.62±0.33	0.50±0.04	4.69±0.24
		4.95±0.22		4.72±0.26

Air Speed: 10 m s^{-1}

Position	ζ_{az}	$\lambda_{n\text{-}az}$ Approach 1 Approach 2	ζ_{el}	$\lambda_{n\text{-}el}$ Approach 1 Approach 2
A	----	----	0.58±0.03	4.35±0.15
				5.13±0.06
B	0.53±0.04	4.80±0.20	0.48±0.04	4.75±0.13
		5.36±0.12		4.82±0.11
C	0.54±0.07	4.55±0.26	----	----
		4.99±0.20		
D	0.54±0.03	4.58±0.16	0.54±0.05	4.73±0.20
		5.22±0.09		5.08±0.20
E	----	----	0.42±0.02	5.14±0.09
				4.82±0.13
F	0.54±0.06	4.49±0.20	0.51±0.06	4.62±0.21
		4.99±0.21		4.72±0.10

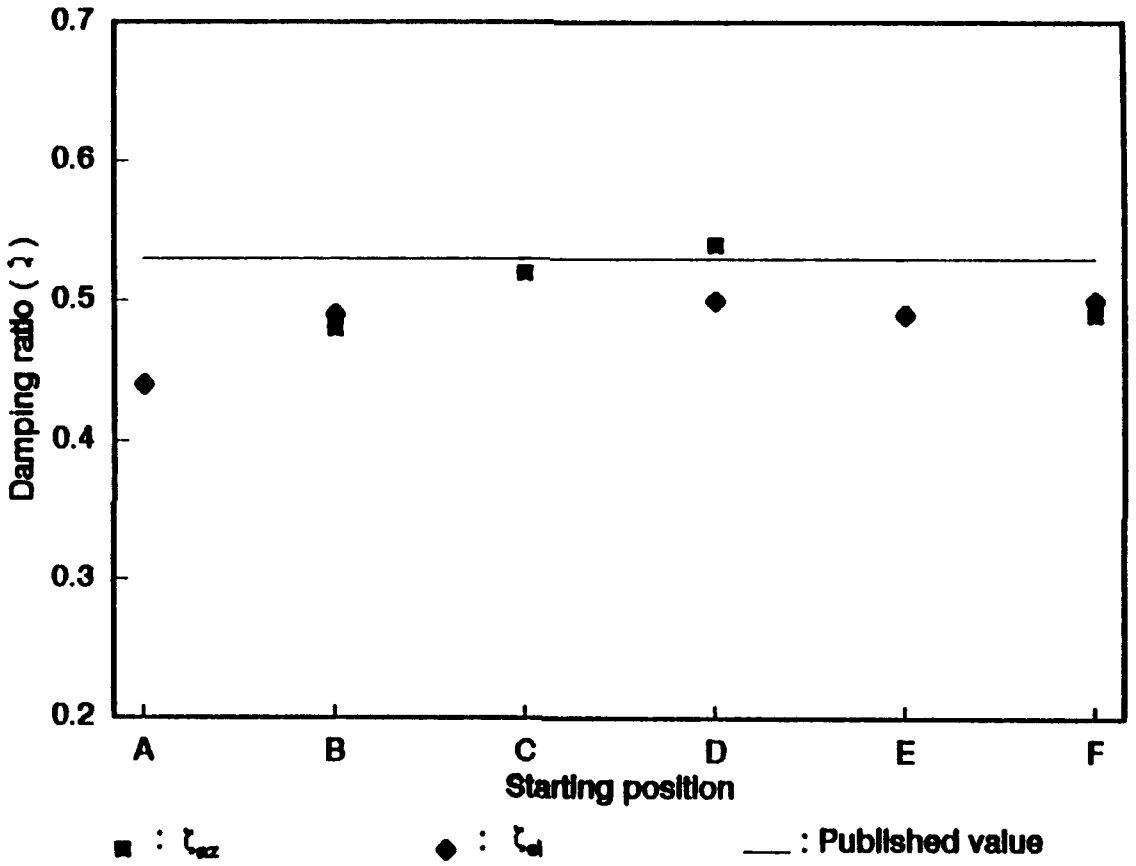

Figure 53. Damping ratio results, by position, of the R. M. Young dynamic tests at 5 m s^{-1}.

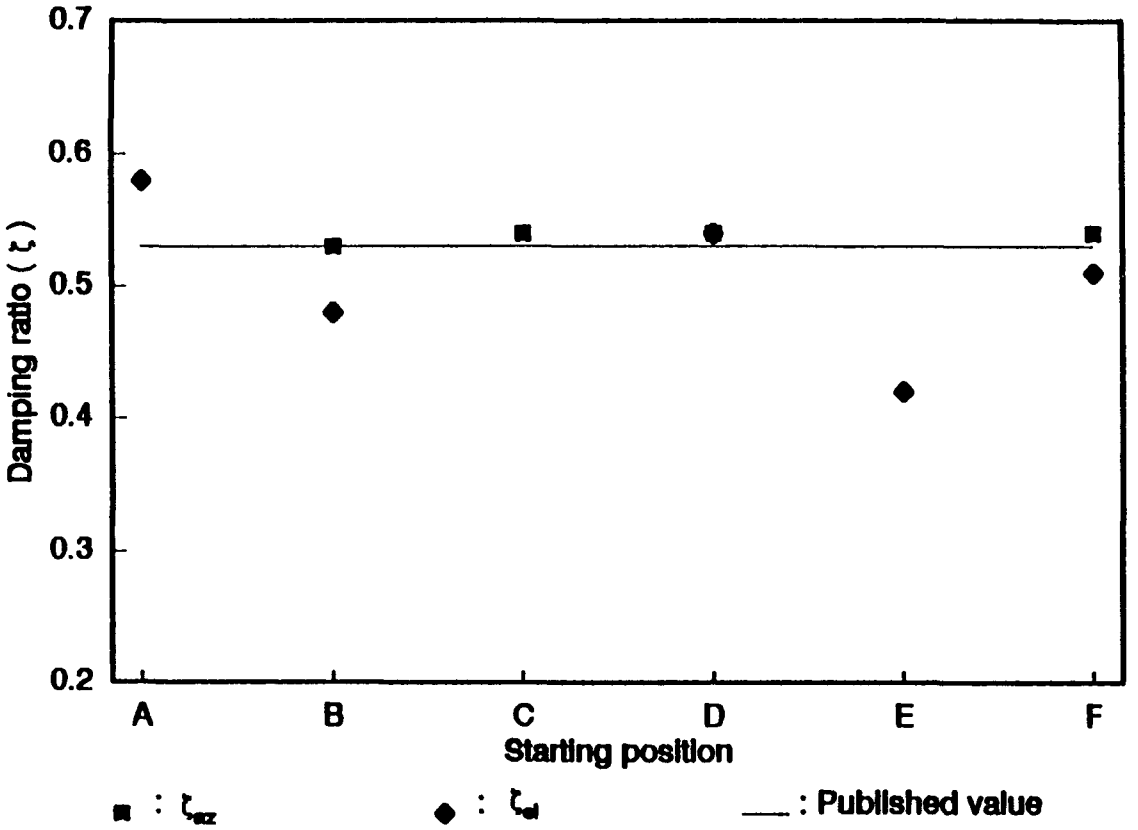

Figure 54. Same as Figure 53, but for U = 10 m s^{-1}.

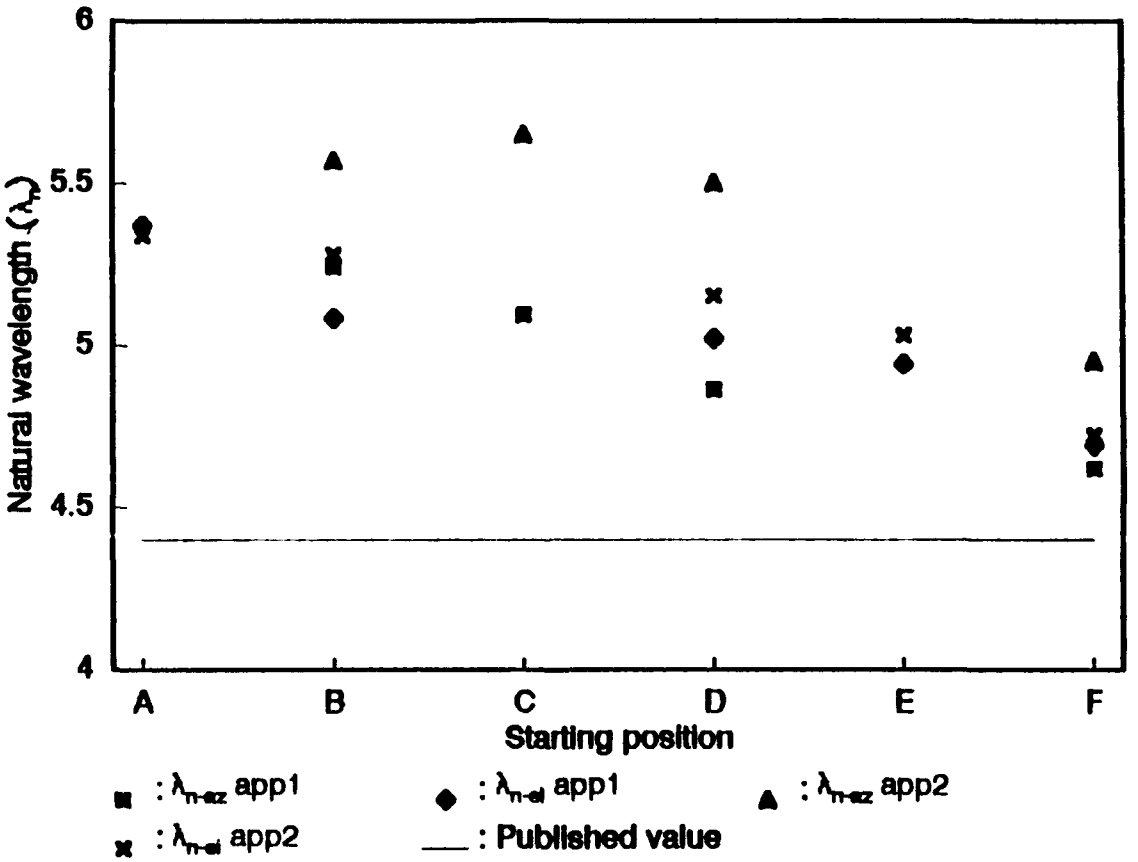

Figure 55. Same as Figure 53, but for natural wavelength results.

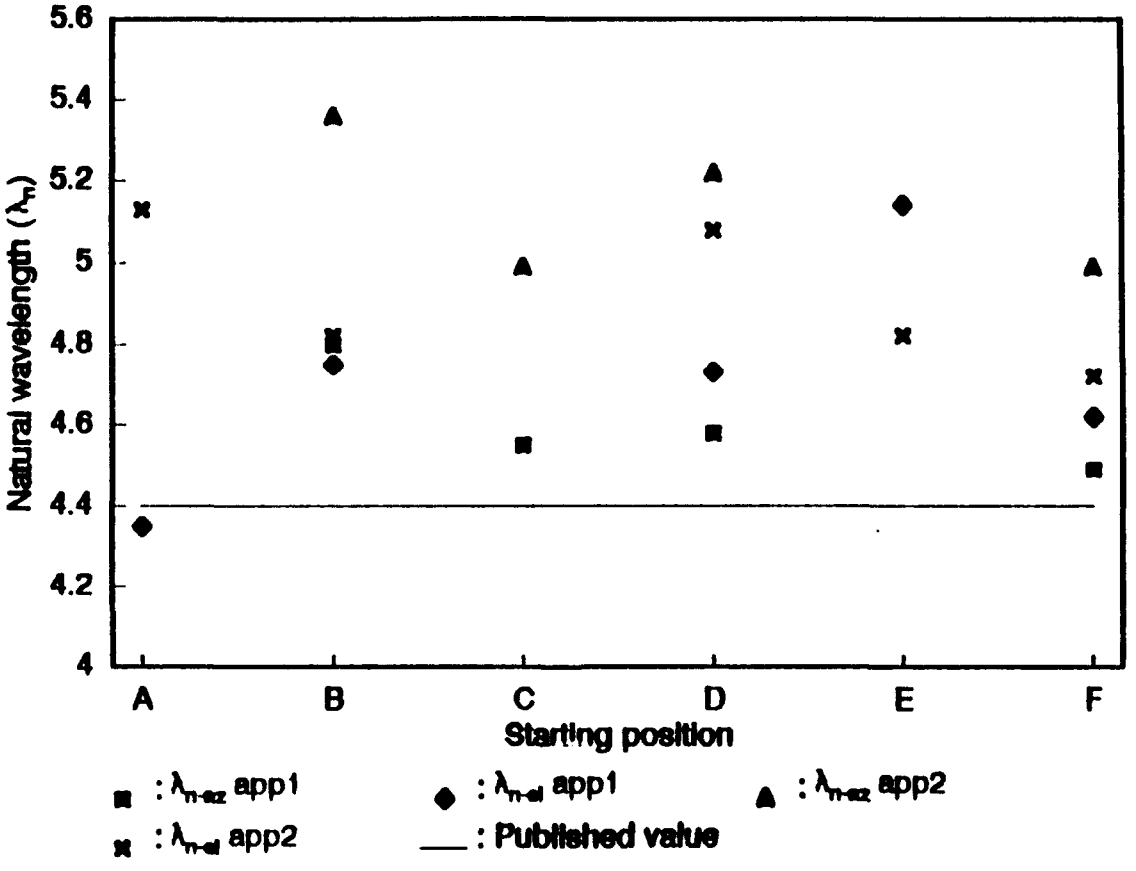

Figure 56. Same as Figure 55, but for U = 10 m s^{-1}.

possible relationship between ζ_{el} and wind speed at positions A and E. Recall that when the vane is released from position A, the vane tail is in the wake of the housing between the times of the first- and second-zero crossings, T_0 and T_1. Both ζ and λ_n are calculated using data between these two times. For speeds of 5 m s^{-1}, ζ_{el} at position A is significantly lower than ζ_{el} for speeds of 10 m s^{-1}.

When the vane is released from position E, the tail is outside the wake between T_0 and T_1 but is in the wake from the vane's release to T_0. Thus, significant starting effects from the housing wake may affect the response between these two zero-crossings. The data show that ζ_{el} is higher at 5 m s^{-1} than at 10 m s^{-1}. The damping ratio tendencies for releases at position E are opposite to those tendencies when the vane is released from position A. Since the response curves of runs released from these two positions are also opposite, the change in wind speed seems to directly affect the damping capabilities when the vane oscillates in the vertical plane.

Changes in ζ and λ_n correlate well with changes in wind speed. The ζ values tend to increase and values of λ_n tend to decrease from the lower to the higher wind speed for nearly all positions. The original assumption is that aerodynamic affects are small and can be ignored. The change in force due to the lift of the fin (ΔF_L) over small angles is considered essentially constant (see equation (21)) and introduces negligible error. For a constant U, changes in the lift coefficient C_L, and projected area of the fin *A*, are considered insignificant with respect to wind speed and are expressed by the constant K in equation (23). However, ΔF_L about the fin increases with an increase in wind speed and the errors become more significant even though the range of Θ is narrow. Small increases in ζ and reductions of λ_n are possibly due to a larger ΔF_L at 10 m s^{-1} than at 5 m s^{-1}.

Table 5 lists the final results per speed for the R. M. Young bivane. Again, these numbers are an average of the values at positions B, C, D, and F. The values from positions A and E were not included since the vane response is believed to be considerably affected by the wake off the vane housing. The evidence of a wind speed dependence can be seen in the final results and Figure 57. In Figure 57, both dynamic characteristics of the azimuth final results are used in equation (38) and the curve was generated using MathCad, version 2.0 by MathSoft, Inc. and plotted using Lotus 123. (Thus, these curves represent

Table 5. Final results for R. M. Young Gill Bivane Model 17003. These results are a mathematical average of values from positions B, C, D, and F.

Air Speed: 5 m s^{-1}

ζ_{az} = 0.51±0.08	$\lambda_{n\text{-}az}$:	Approach 1 = 4.95±0.25 Approach 2 = 5.42±0.22
ζ_{el} = 0.50±0.04	$\lambda_{n\text{-}el}$:	Approach 1 = 4.93±0.17 Approach 2 = 5.05±0.16

Air Speed: 10 m s^{-1}

ζ_{az} = 0.54±0.05	$\lambda_{n\text{-}az}$:	Approach 1 = 4.60±0.20 Approach 2 = 5.14±0.16
ζ_{el} = 0.51±0.05	$\lambda_{n\text{-}el}$:	Approach 1 = 4.70±0.18 Approach 2 = 4.87±0.14

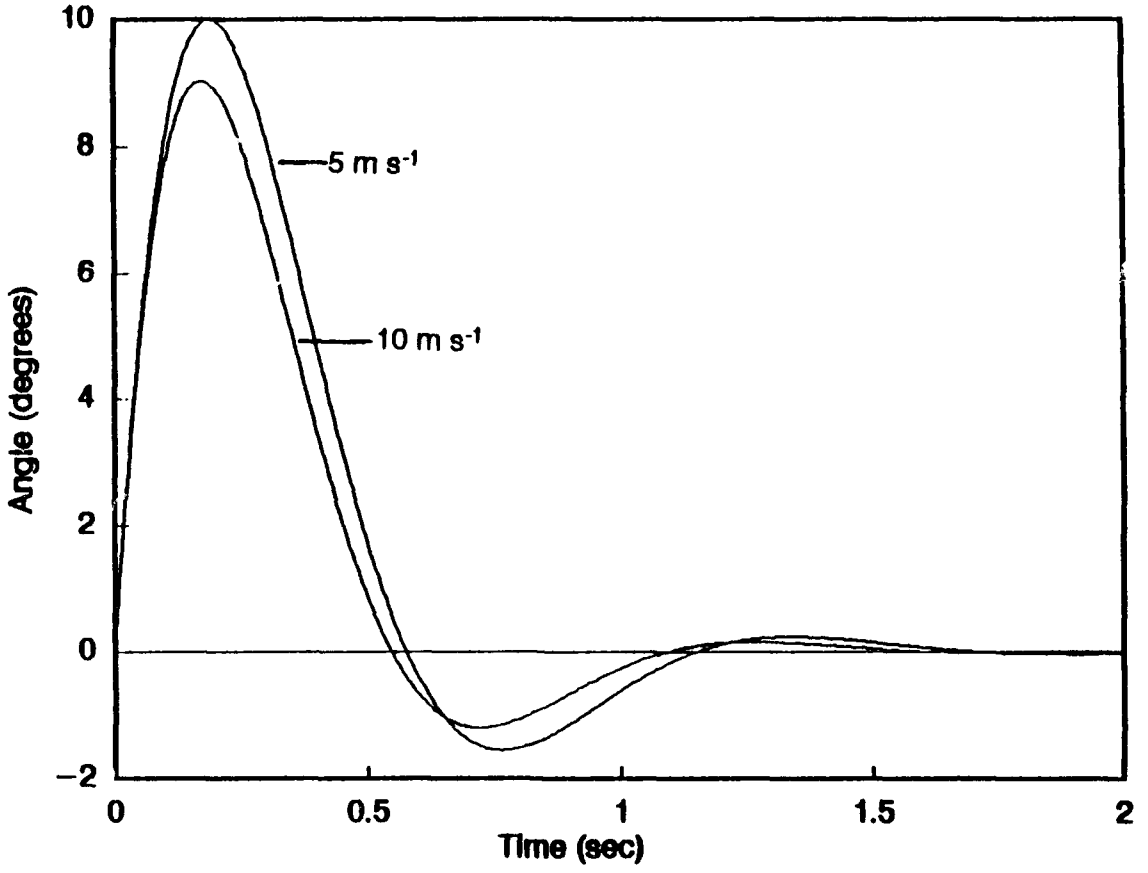

Figure 57. Traces of the 5 and 10 m s^{-1} final results using model equation (38). The times of the 10 m s^{-1} are expanded twice their original values for comparing with the 5 m s^{-1} trace. The 10 m s^{-1} trace has a smaller overshoot and a shorter damped wavelength. Both traces use the same Λ_0.

model responses versus actual data runs.) The curve for 5 m s^{-1} is forced to a peak of 10° by adjusting its $\Lambda_{0(5m/s)}$ and was 117.25 deg s^{-1}. In the same figure, the curve using dynamic characteristics for 10 m s^{-1} and the same $\Lambda_{0(5m/s)}$ is plotted with the wind speed at 5 m s^{-1} so that both curves can be compared. The curve at 10 m s^{-1} shows a smaller first peak or overshoot and a shorter wavelength corresponding to the higher ζ and smaller λ_n than over the dynamic characteristics calculated using 5 m s^{-1} data. Approach 1 was used for the λ_n in both response curves representing both speeds. Figure 58 shows this same 10 m s^{-1} curve forced to to a peak of 10° using $\Lambda_{0(10m/s)}$ as 129.75 deg s^{-1}. Since $\Lambda_{0(10m/s)} > \Lambda_{0(5m/s)}$, a greater force is needed to act on this particular R. M. Young bivane for the 10 m s^{-1} response to achieve the same amplitude of the first peak as for the 5 m s^{-1} response. Knowledge of the additional energy required for the 10 m s^{-1} response to reach 10° allows for a comparison of the bivane's response characteristics as a function of wind speed.

If the second derivative of equation (38) is referenced to $\Theta_0 = 0°$, then the acceleration at 0° and t=0 (i.e., T_0) is

$$\left.\frac{d^2\Theta}{dt^2}\right|_0 = -4\pi \frac{U\zeta}{\lambda_n}\Lambda_0. \qquad (57)$$

Theoretically, it is possible that the acceleration can be used to determine the forces or torques about the vane. The comparisons of the forces and torques at various wind speeds can describe how the vane responds as a function of U. If the vane responds significantly different at different wind speeds, then the instrument may not "faithfully" respond to the fluctuations in the Reynolds stresses required in the Chimonas technique (Chimonas, 1980). Therefore, it should be determined how much the bivane's azimuth and elevation responses are a function of wind speed. A greater sensitivity to wind fluctuations requires the vane response to be less dependent on U. Since ζ, λ_n, and Λ_0 are related in equation (57), further study of this relationship may prove valuable in assessing a vane's dependence on U and how fin designs affect the assumption that all aerodynamic affects are constant at these small angles.

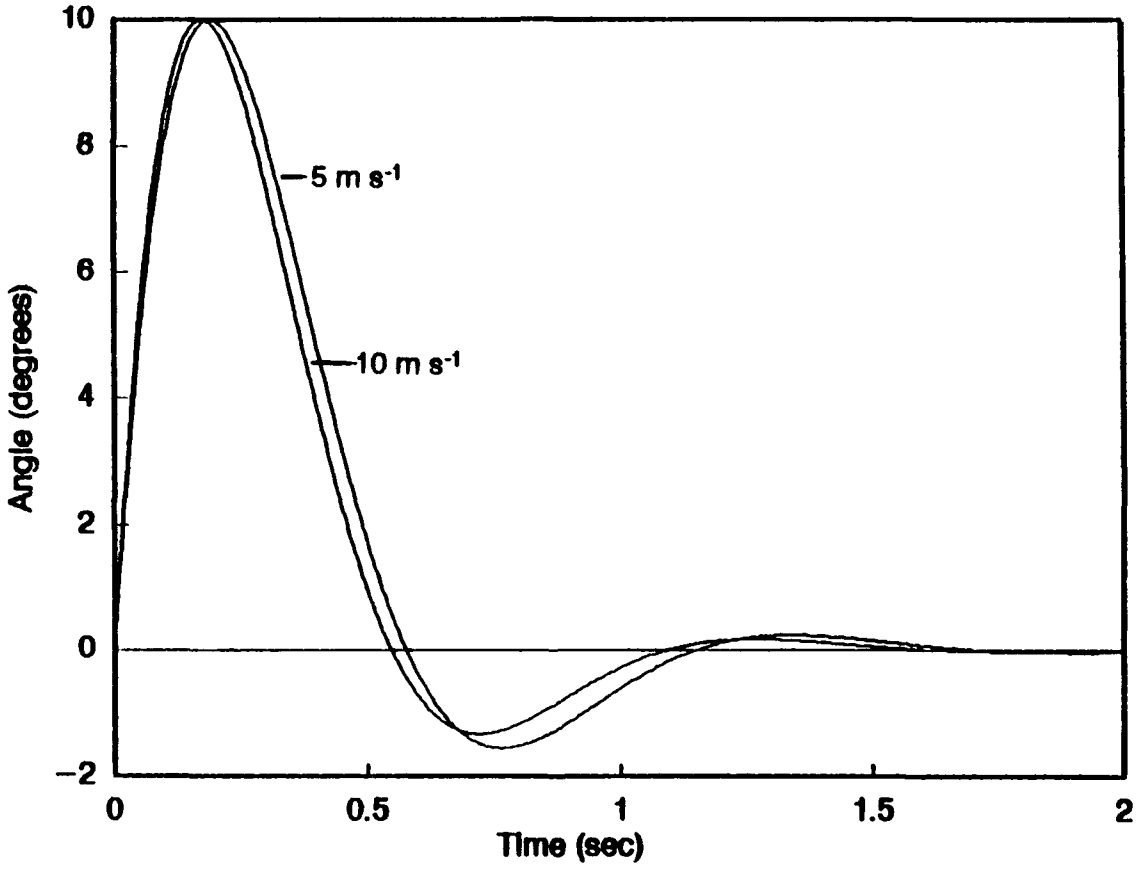

Figure 58. Same as Figure 57, but with the 10 m s^{-1} trace forced to a first peak of 10° by increasing Λ_0.

Figures 59 and 60 are similar to Figures 57 and 58, but represent the bivane's elevation response. The velocities were $\Lambda_{0(5m/s)}$ = 116.75 deg s^{-1} and $\Lambda_{0(10m/s)}$ = 123.52 deg s^{-1} and very nearly the same as those for the azimuth response. This is no surprise since the tail of the R. M. Young bivane is a cruciform with identical plates at right angles generating nearly the same aerodynamic flow. It is suspected that aerodynamic affects are contributing to the different values of the dynamic characteristics at the two speeds. Additional tests must be done at several more wind speeds before a conclusion can be reached regarding aerodynamic affects.

Ideally, the vane oscillates in a plane containing the release point and the boom's equilibrium position. This is true only if the azimuth and elevation response characteristics are identical. For example, Figure 61 shows run number YABC (R. M. Young, speed A of 5 m s^{-1}, position B, test run C) with the azimuth and elevation response data plotted against one another. Angles in the figure are referenced to the equilibrium value of 0°. Azimuth dynamic characteristics were 0.54 for ζ and 5.06 m for λ_n. Elevation dynamic characteristics were 0.52 for ζ and 4.72 m for λ_n. The difference between the azimuth and elevation dynamic characteristics help produce this spiraling affect away from the plane of oscillation. The trace begins at T_0 for the elevation data and at T_0 - 0.030 sec for the azimuth data. In all test runs there was a small delay or shift to the right in the azimuth response from the elevation response (see Figure 62). Using the model equation (38), the azimuth and elevation dynamic characteristics of run YABC were plotted in Figure 63 and include the 0.030 second delay of the azimuth data. The model response shows the same spiraling feature as the raw data in Figure 61.

To isolate the cause of this spiraling affect, the 0.030 second offset was eliminated. Figure 64 shows the trace beginning at T_0 for both directions but the spiral is still evident. In Figure 65 the elevation λ_n was adjusted to the azimuth value of 5.06 m while the damping ratio was fixed. The spiral disappears, isolating the difference of azimuth and elevation natural wavelengths as the cause for the vane to oscillate outside the ideal plane of oscillation.

Reasons for the differences in azimuth and elevation natural wavelengths are varied. Design considerations of the vane assembly dominate the list. Circuitry and even conditioning electronics may be

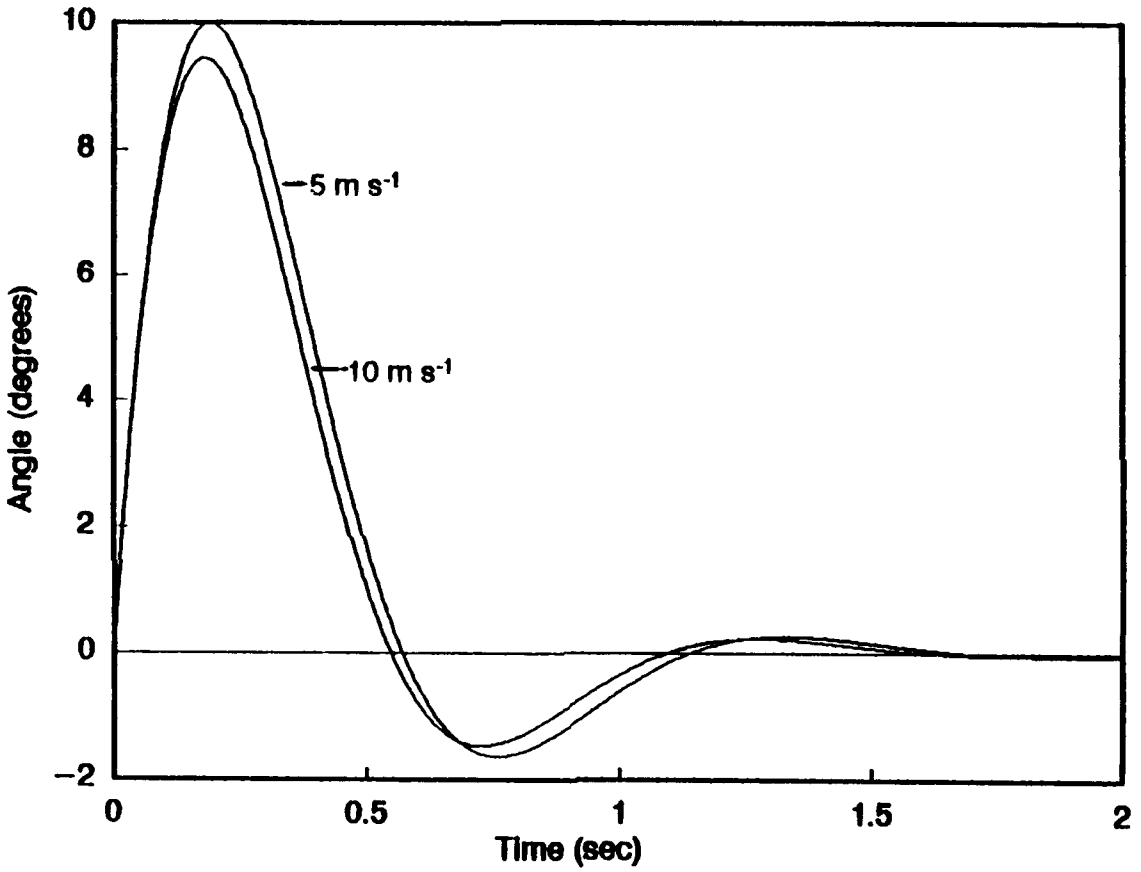

Figure 59. Same as Figure 57, but for elevation final results.

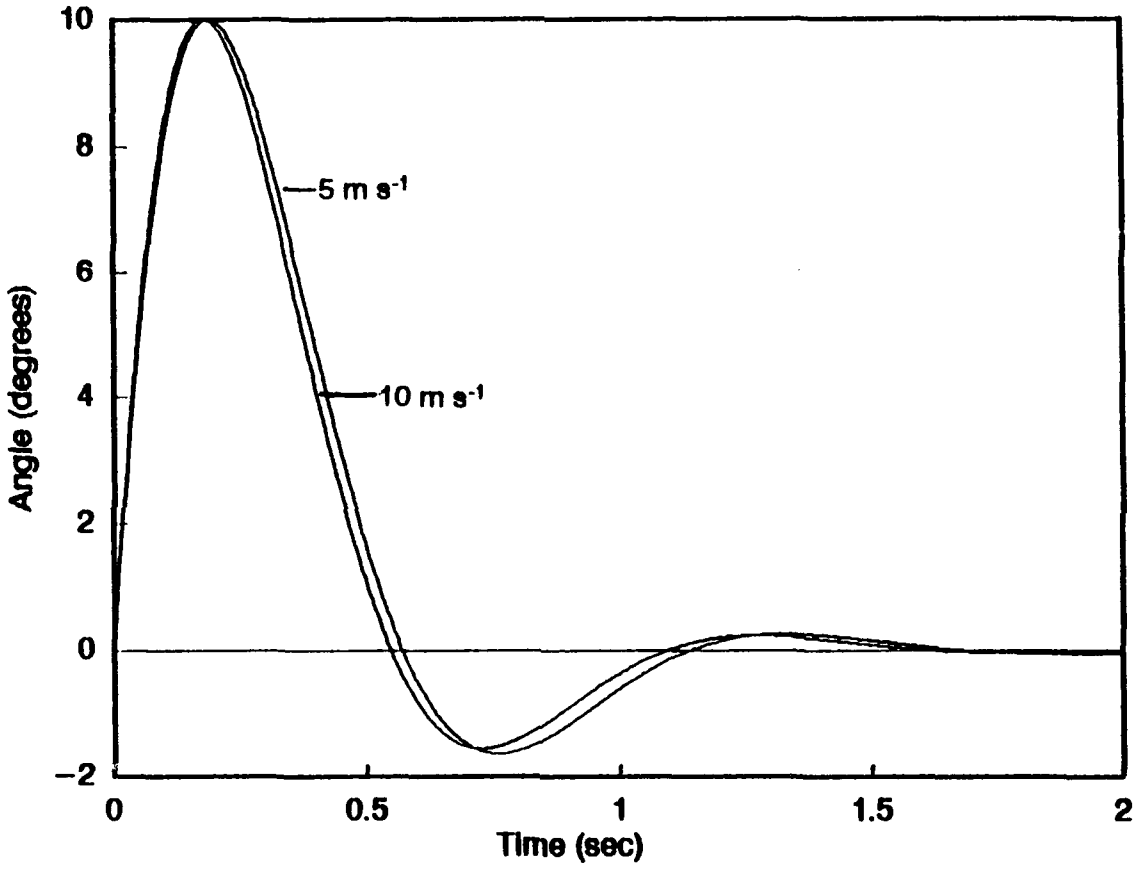

Figure 60. Same as Figure 58, but for elevation final results.

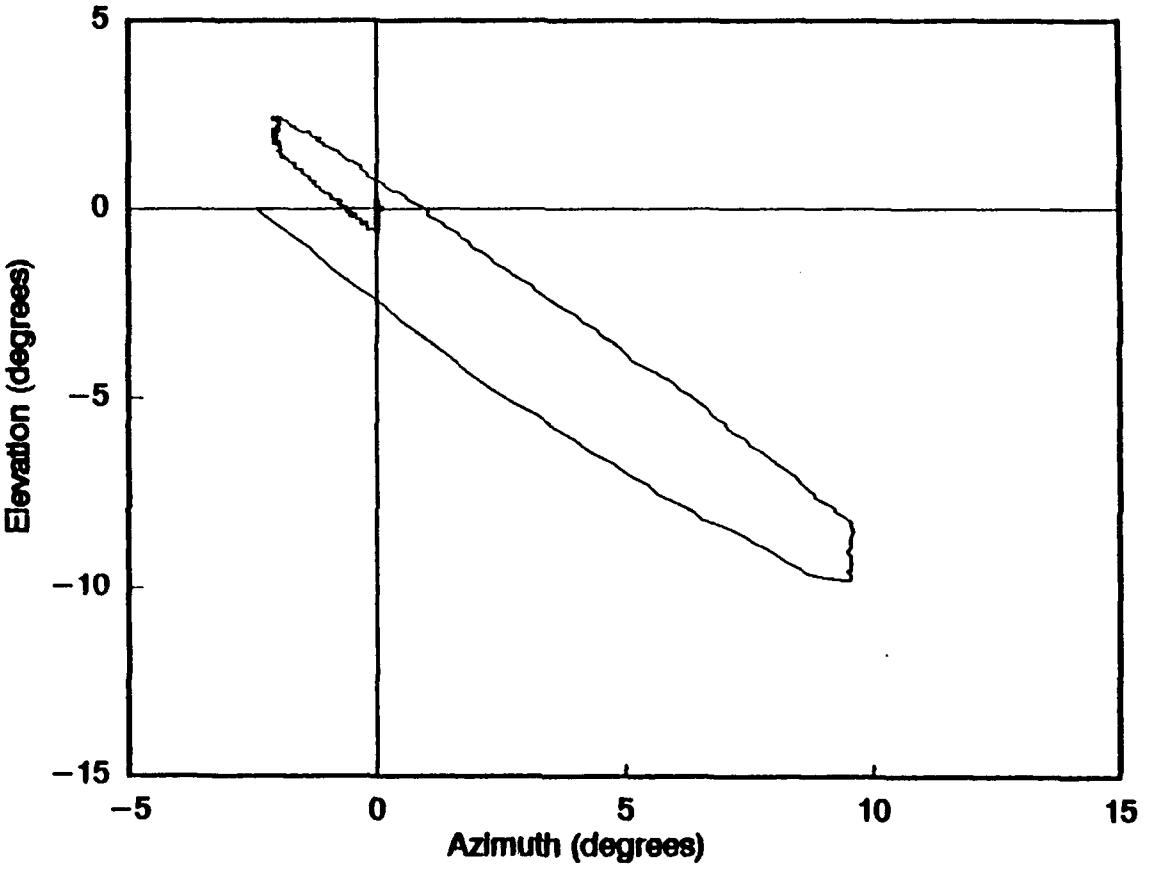

Figure 61. Plot showing the spiral into the equilibrium position resulting from a mismatch in the azimuth and elevation dynamic characteristics (from run YABC). The trace begins at the first zero-crossing.

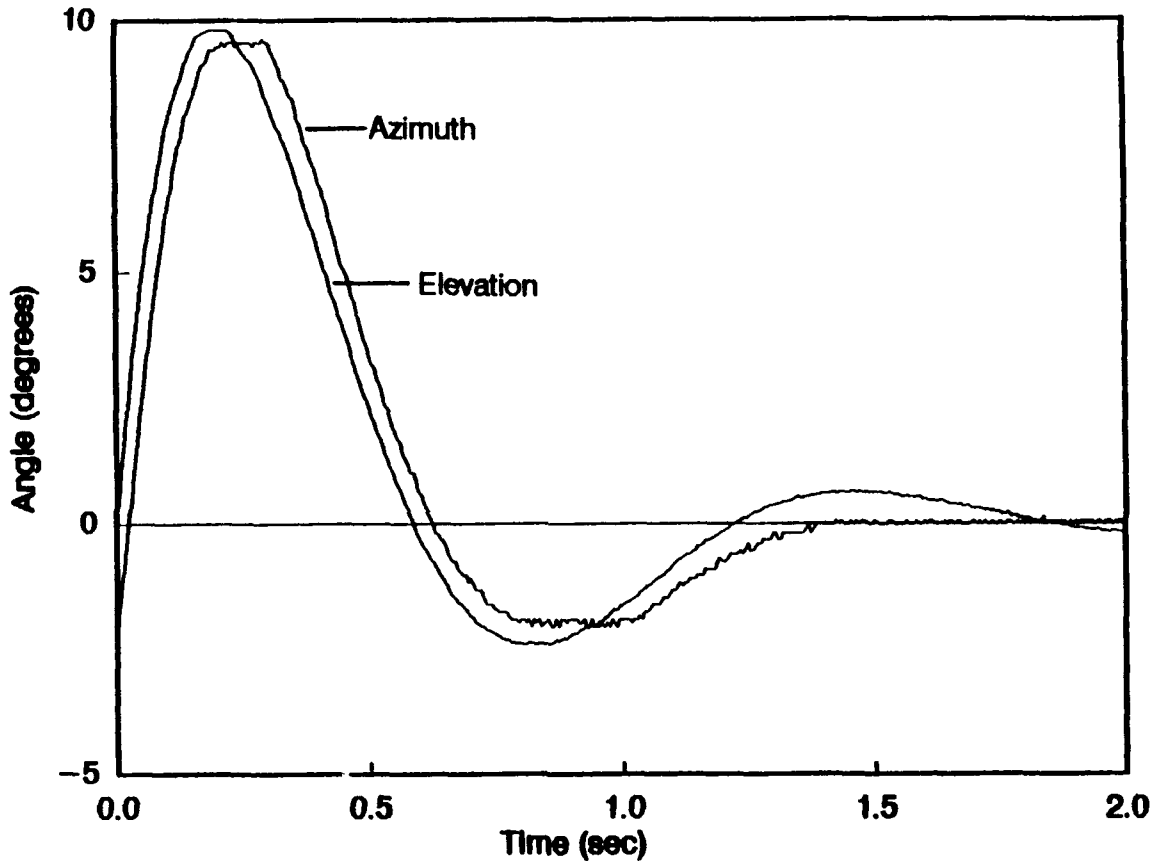

Figure 62. Traces of the YABC azimuth and elevation data that produced the spiralled plot in Figure 61.

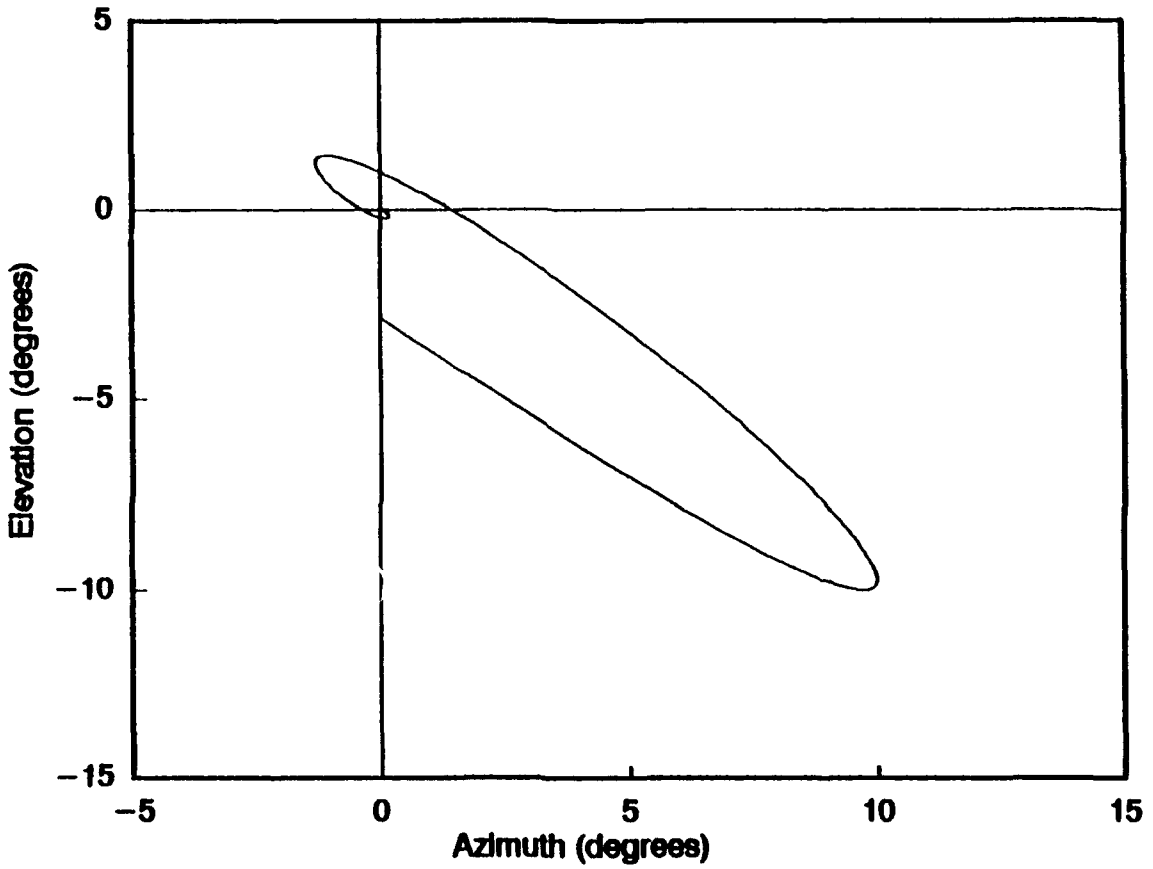

Figure 63. Model plot using the azimuth and elevation dynamic characteristics from run YABC. Spiral includes the difference in the times of the first zero-crossings between the azimuth and elevation data.

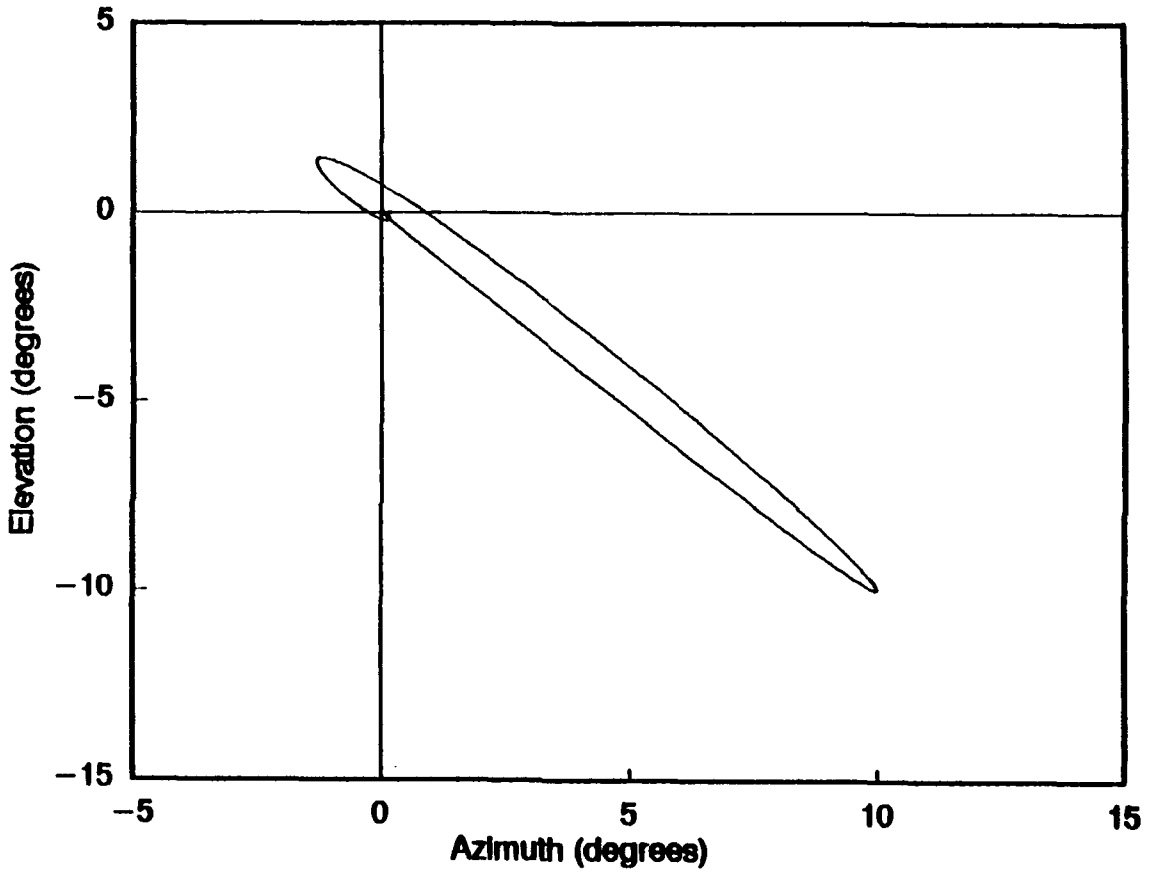

Figure 64. Same as Figure 63, but without the difference in the times of the first zero-crossings.

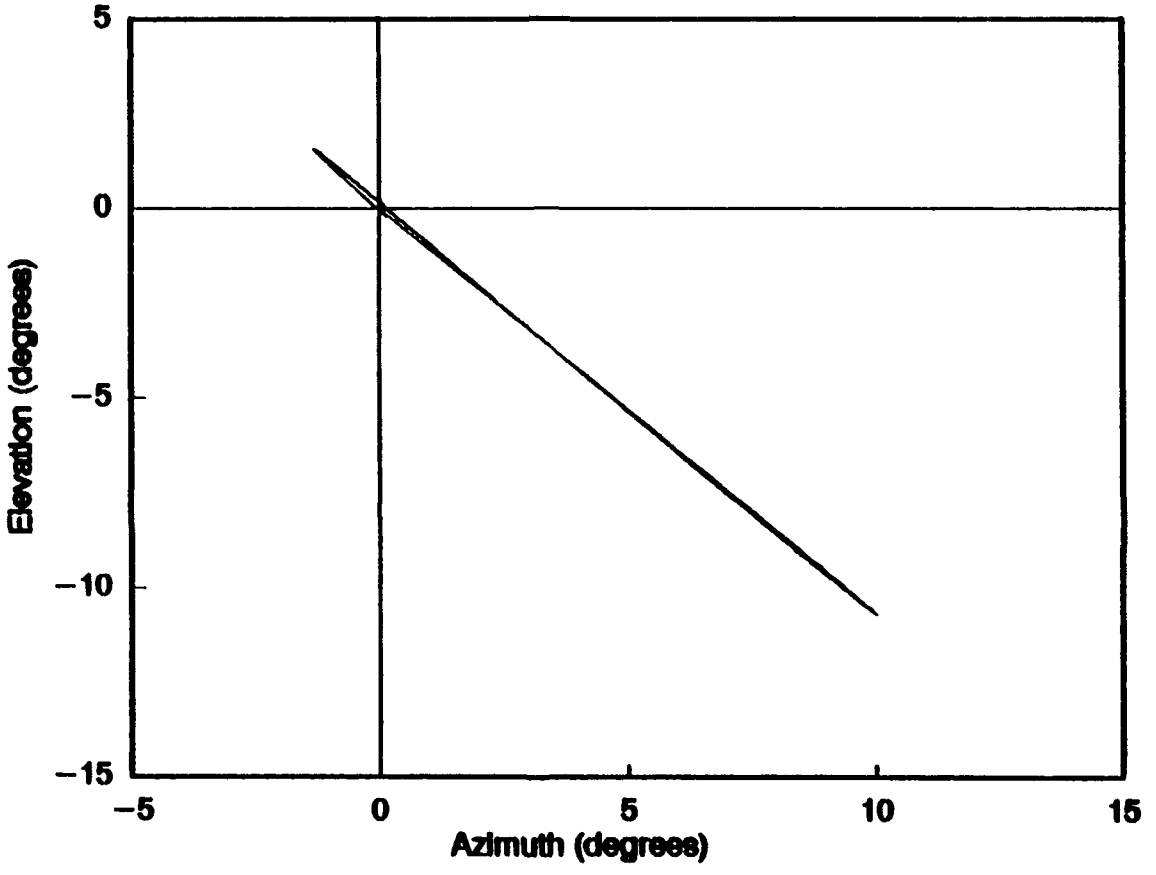

Figure 65. Same as Figure 64, but the elevation natural wavelength was adjusted to the azimuth value, while the damping ratios were held at their original values. The vane now oscillates in one plane. Thus, the natural wavelength is isolated as the cause of the spiral.

the culprit. However, the more probable reason for the spiral is asymmetries in the gimbal hardware. Thus, the moments of inertia about the azimuth and elevation axes are slightly different creating different values of natural wavelength. Manufacturing perfectly symmetrical gimbal hardware is not possible. Therefore, the spiral is unavoidable, but can be reduced if the asymmetry is minimized.

The manufacturer's specifications of a damping ratio of 0.53 and natural wavelength of 4.4 m for both azimuth and elevation responses are compared with individual real data and model traces in Figures 66 through 69. The calculated ζ and λ_n for the real data and the manufacturer's specifications are input into the model equation (38) producing the two smooth traces seen in the figures. The amplitudes of the first peaks are forced to the same amplitude as the real data. With a 4.4 m natural wavelength, the curve representing the manufacturer's specifications shows a faster response.

When the model response using the dynamic characteristics of the real data is forced to the amplitude of the first peak by adjusting Λ_0, the model and real data traces closely agree in the first quarter cycle. Thereafter, the zero-crossings and peak amplitudes do not agree while the times of the peaks continue to agree. All data runs show this feature where the actual amplitudes are more extreme than the model predicts. This is due to the second-order model not exactly representing the vane response.

The technique of forcing the model trace to fit the real data curve can be used to determine ζ and λ_n of the real data. If the real data of a test run has noise that cannot be smoothed without damaging the data's integrity, a common method of estimating ζ and λ_n can be applied by physically drawing a smooth curve through the plotted test run data and extracting the necessary amplitudes and times for calculation. Another method is to use software such as MathCad to force the model to the amplitude and timing of the first peak by adjusting Λ_0, ζ, and λ_n which in turn are the estimates of the dynamic characteristics, ζ and λ_n. All the test data for the R. M. Young bivane were good and there was no need to estimate ζ, and λ_n using the above technique.

When the model response using the dynamic characteristics of the real data is forced to the amplitude of the first peak by adjusting Λ_0, the model and real data traces closely agree in the first quarter

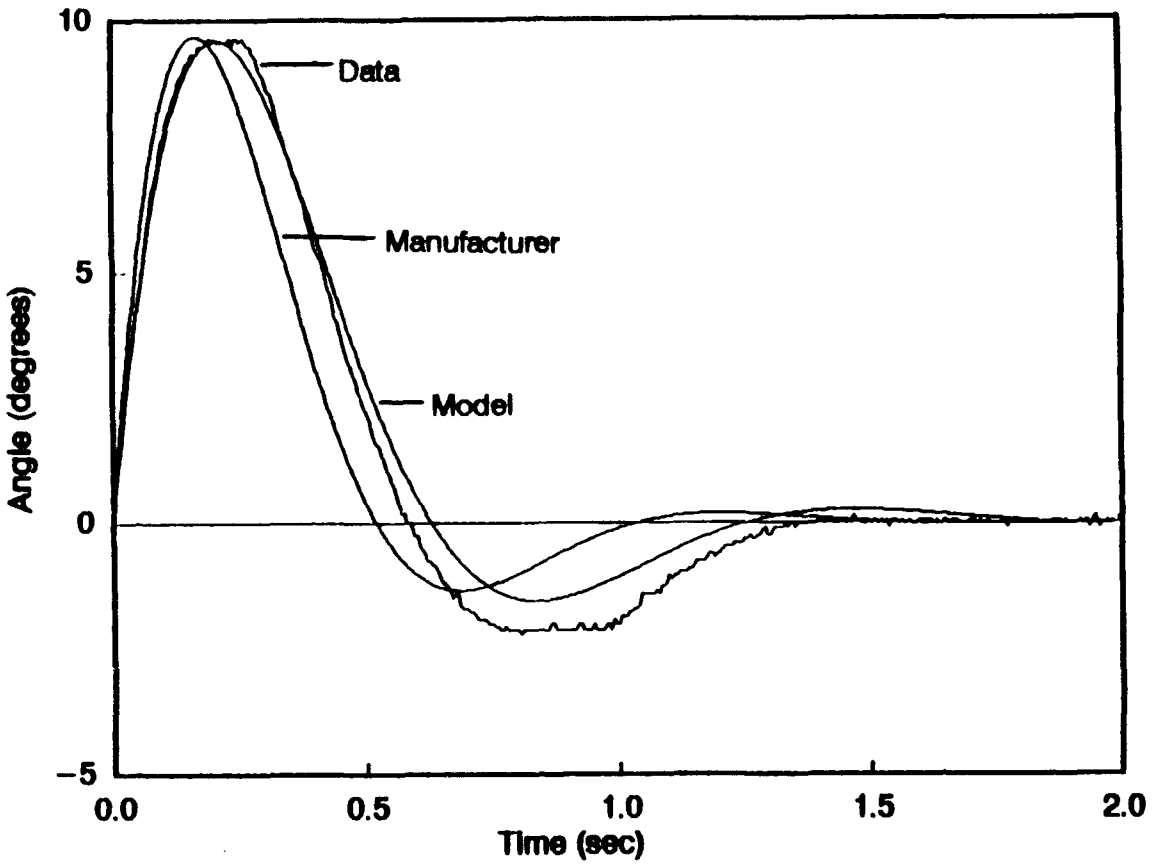

Figure 66. Azimuth data trace in the 5 m s^{-1} run YABC compared with the model traces of the dynamic characteristics of the run (ζ=0.54, λ_n=5.06m) and the manufacturer's published values (ζ=0.53, λ_n=5.2m). Both model traces were forced to the same amplitude of the first peak of the azimuth data in run YABC.

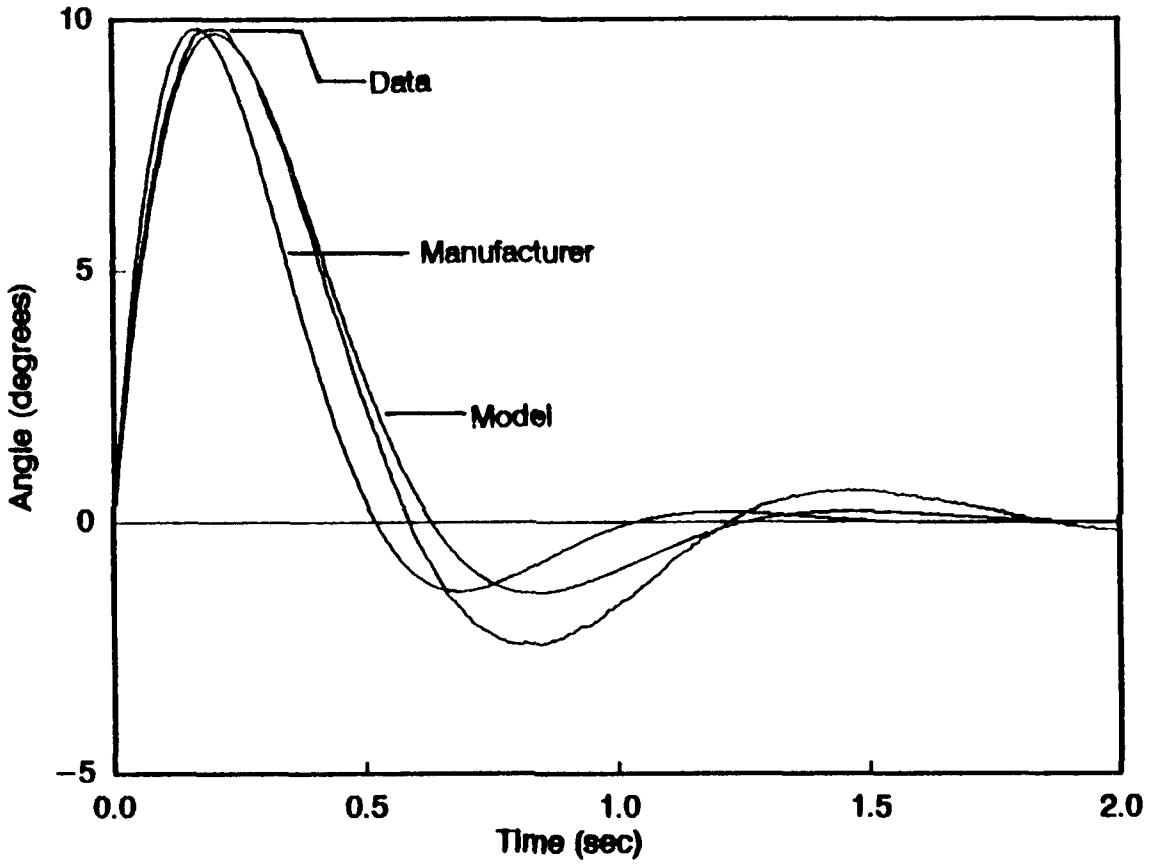

Figure 67. Same as in Figure 66, but for the elevation data in the 5 m s^{-1} run YABG (ζ=0.50, λ_n=5.44m).

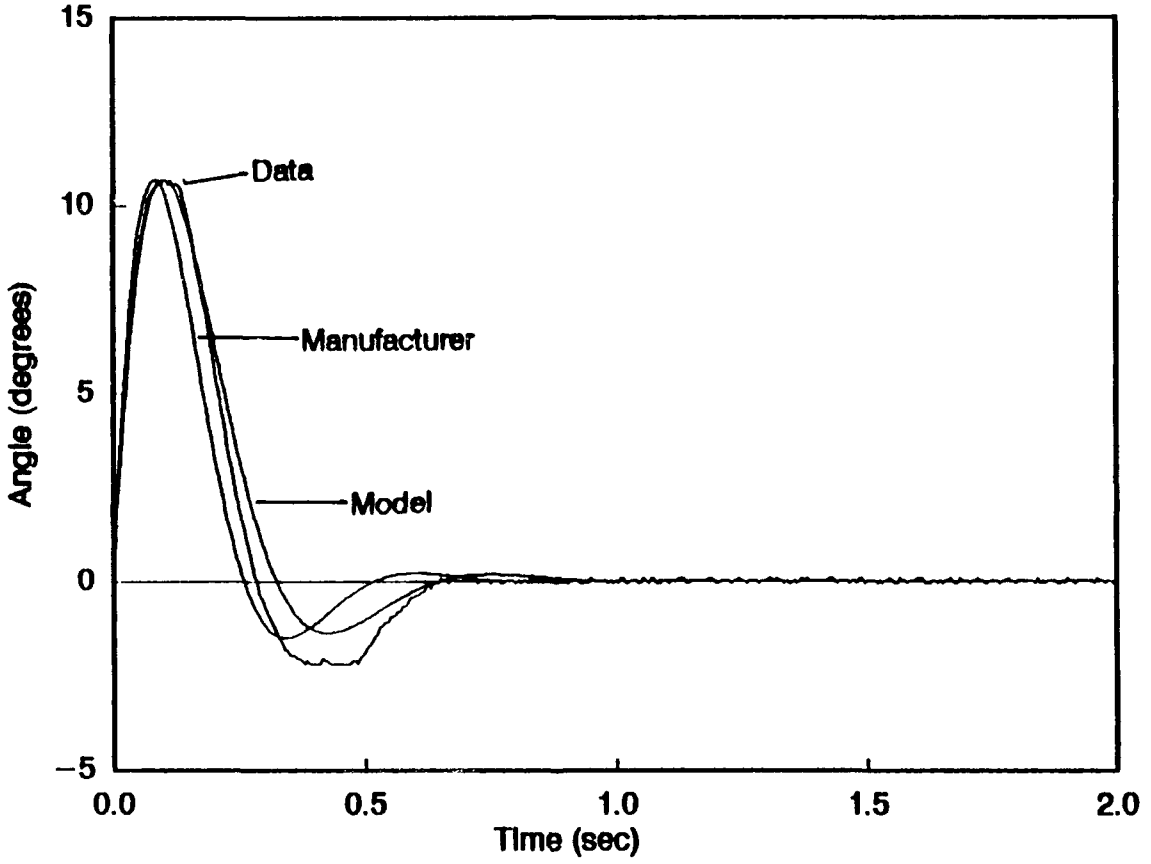

Figure 68. Same as in Figure 66, but for the azimuth data in the 10 m s^{-1} run YBBG (ζ=0.55, λ_n=5.42m).

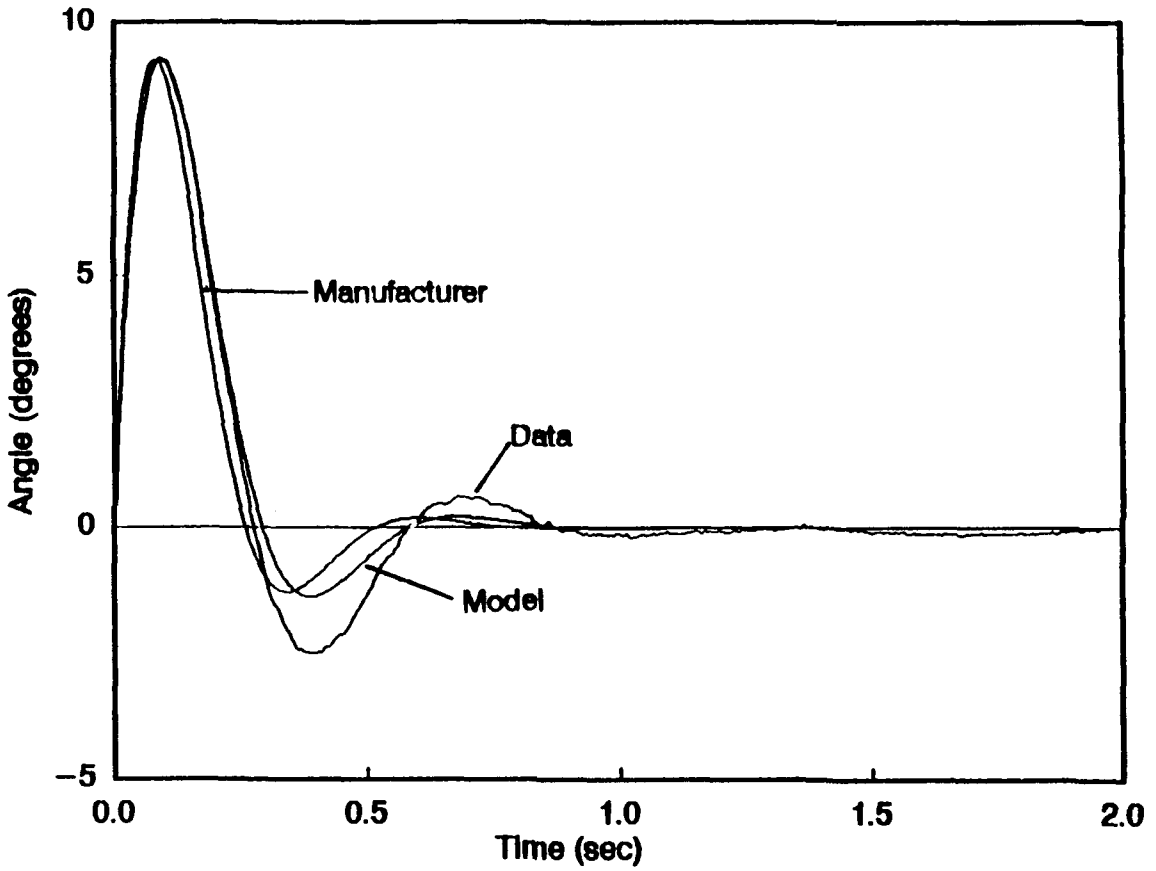

Figure 69. Same as in Figure 66, but for the elevation data in the 10 m s^{-1} run YBBB (ζ=0.52, λ_n=5.02m).

cycle. Thereafter, the zero-crossings and peak amplitudes do not agree while the times of the peaks continue to agree. All data runs show this feature where the actual amplitudes are more extreme than the model predicts. This is due to the second-order model not exactly representing the vane response.

4.2 Teledyne Geotech

Table 6 details the results of the Teledyne Geotech bivane by position and wind speed. Table 7 lists the final results by wind speed. Recall that Teledyne Geotech published damping ratio is 0.4. The published delay distance is 1.0 m that corresponds to a natural wavelength of 5.04 m, using relation (36). The results by position vary widely and the final results are considerably different from the manufacturer's published results.

Figures 70 through 73 show a plot of the data points from Table 6. In the damping ratio figures, all data values are consistent and below the manufacturer's stated damping ratio of 0.4, except for the value at position D in Figure 70. There doesn't appear to be a systematic variation in damping ratio values from position to position and between wind speeds.

On the other hand, the natural wavelength values do show a significant systematic variation between positions. Natural wavelength values at positions A, C, and E are smaller than values at positions B, D, and F. The former positions are associated with only the elevation or azimuth planes of oscillation. The reason for the shorter lengths at positions A, C, and E could be related or the phenomena at positions A and E could be attributed to wake effects from the housing or the fact that the vane is forced to the zero elevation reference point and the phenomena at position C could be related to some other reason. All positions show smaller λ_n at 10 m s^{-1} than at 5 m s^{-1}.

From the results in Table 7, this particular Teledyne Geotech bivane should exhibit a greater overshoot and a longer damped wavelength compared to a response with the published dynamic characteristics if both use the same value of Λ_0. Using the model equation (38) and forcing the first peak of the published dynamic characteristic's curve to 10°, Figures 74 through 77 show the result's curves

Table 6. Results of dynamic testing of the Teledyne Geotech Multidirectional Bivane Model 1585.

Air Speed: 5 m s^{-1}

Position	ζ_{az}	$\lambda_{n\text{-}az}$ Approach 1 Approach 2	ζ_{el}	$\lambda_{n\text{-}el}$ Approach 1 Approach 2
A	----	----	0.24±0.05	5.19±0.12
				5.46±0.10
B	0.35±0.23	5.78±0.48	0.26±0.08	6.17±0.18
		6.61±0.70		6.68±0.26
C	0.34±0.21	4.29±0.30	----	----
		4.57±0.60		
D	0.49±0.15	5.04±0.69	0.03±0.10	5.70±0.22
		6.57±0.28		5.78±0.43
E	----	----	0.28±0.07	4.42±0.16
				4.80±0.09
F	0.16±0.11	6.33±0.26	0.28±0.05	6.45±0.18
		7.00±0.37		7.20±0.24

Air Speed: 10 m s^{-1}

Position	ζ_{az}	$\lambda_{n\text{-}az}$ Approach 1 Approach 2	ζ_{el}	$\lambda_{n\text{-}el}$ Approach 1 Approach 2
A	----	----	0.27±0.08	4.23±0.85
				4.44±1.02
B	0.29±0.17	5.73±0.39	0.18±0.12	5.77±0.18
		6.34±0.44		6.08±0.44
C	0.37±0.18	4.17±0.27	----	----
		4.60±0.55		
D	0.30±0.18	4.89±0.38	0.23±0.31	4.78±1.22
		5.21±0.71		5.70±0.74
E	----	----	0.19±0.09	4.22±0.09
				4.26±0.27
F	0.20±0.13	5.80±0.28	0.20±0.09	5.96±0.25
		6.35±0.27		6.29±0.35

Table 7. Final results for Teledyne Geotech Multidirectional Bivane Model 1585. These results are a mathematical average of values from positions B, C, D, and F.

Air Speed: 5 m s^{-1}

$\zeta_{az} = 0.34 \pm 0.18$	$\lambda_{n\text{-}az}$:	Approach 1 = 5.36±0.43 Approach 2 = 6.19±0.49
$\zeta_{el} = 0.19 \pm 0.08$	$\lambda_{n\text{-}el}$:	Approach 1 = 6.11±0.19 Approach 2 = 6.55±0.31

Air Speed: 10 m s^{-1}

$\zeta_{az} = 0.29 \pm 0.16$	$\lambda_{n\text{-}az}$:	Approach 1 = 5.62±0.49 Approach 2 = 5.15±0.33
$\zeta_{el} = 0.20 \pm 0.17$	$\lambda_{n\text{-}el}$:	Approach 1 = 6.02±0.51 Approach 2 = 5.50±0.55

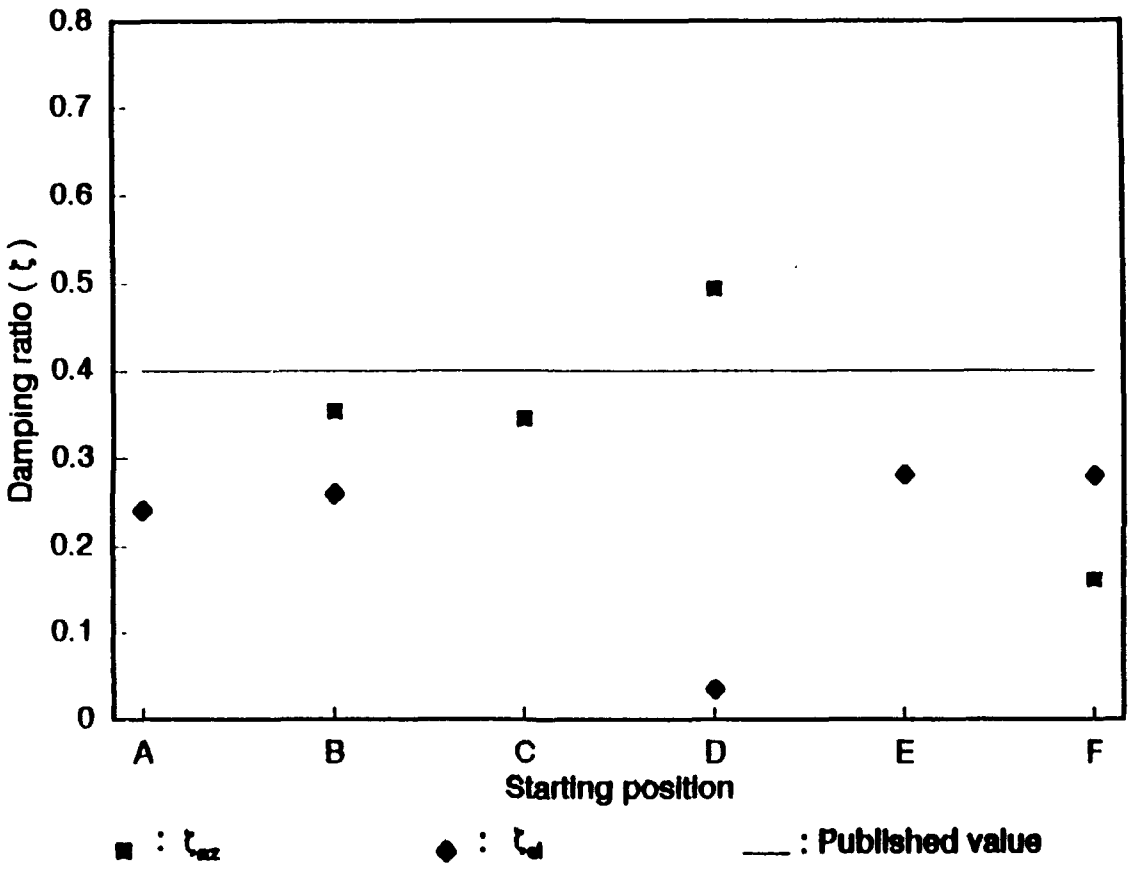

Figure 70. Damping ratio results, by position, of the Teledyne Geotech dynamic tests at 5 m s^{-1}.

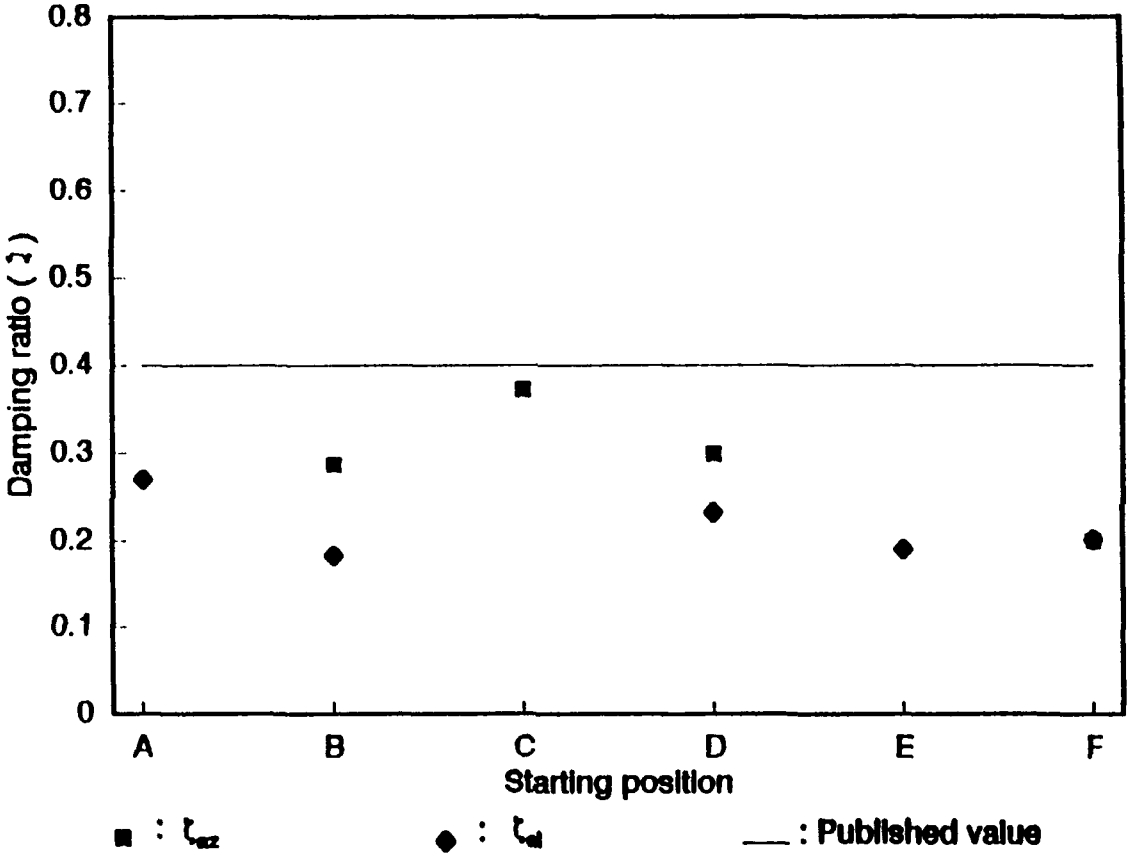

Figure 71. Same as Figure 70, but for U = 10 m s^{-1}.

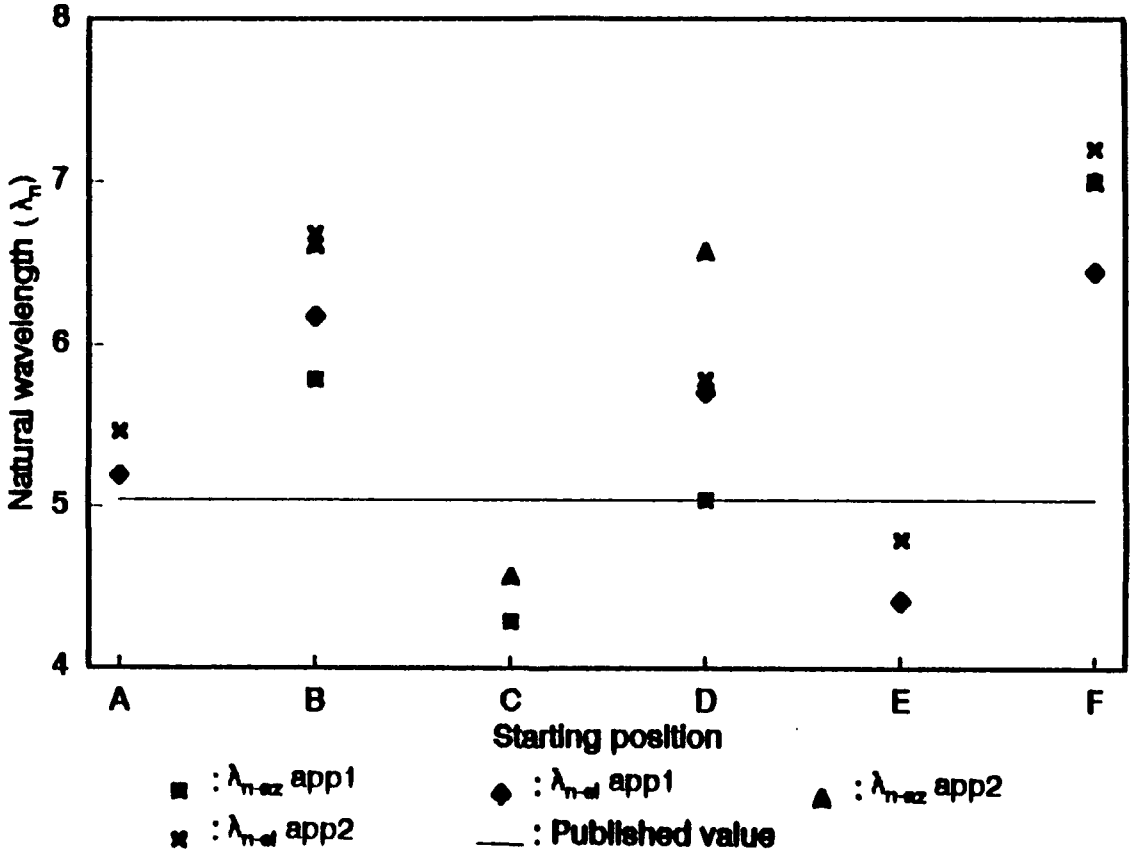

Figure 72. Same as Figure 71, but for natural wavelength results.

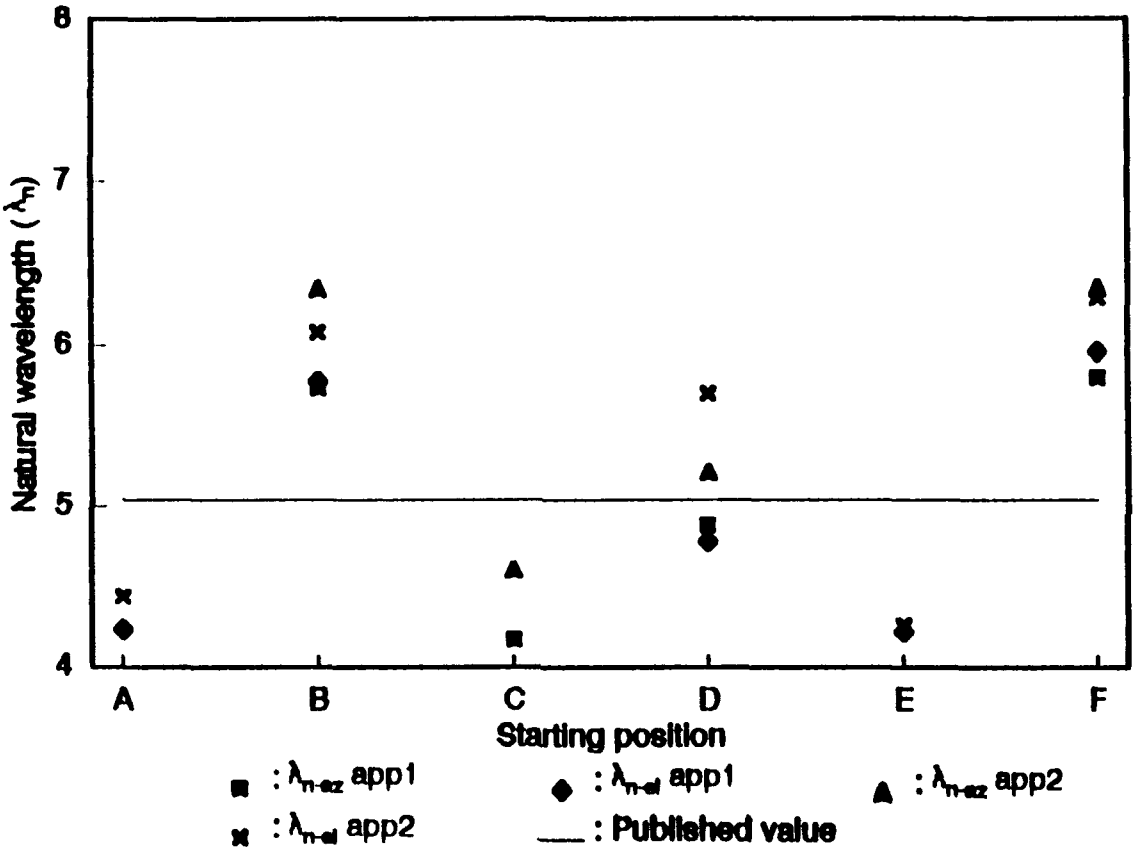

Figure 73. Same as Figure 72, but for U = 10 m s^{-1}.

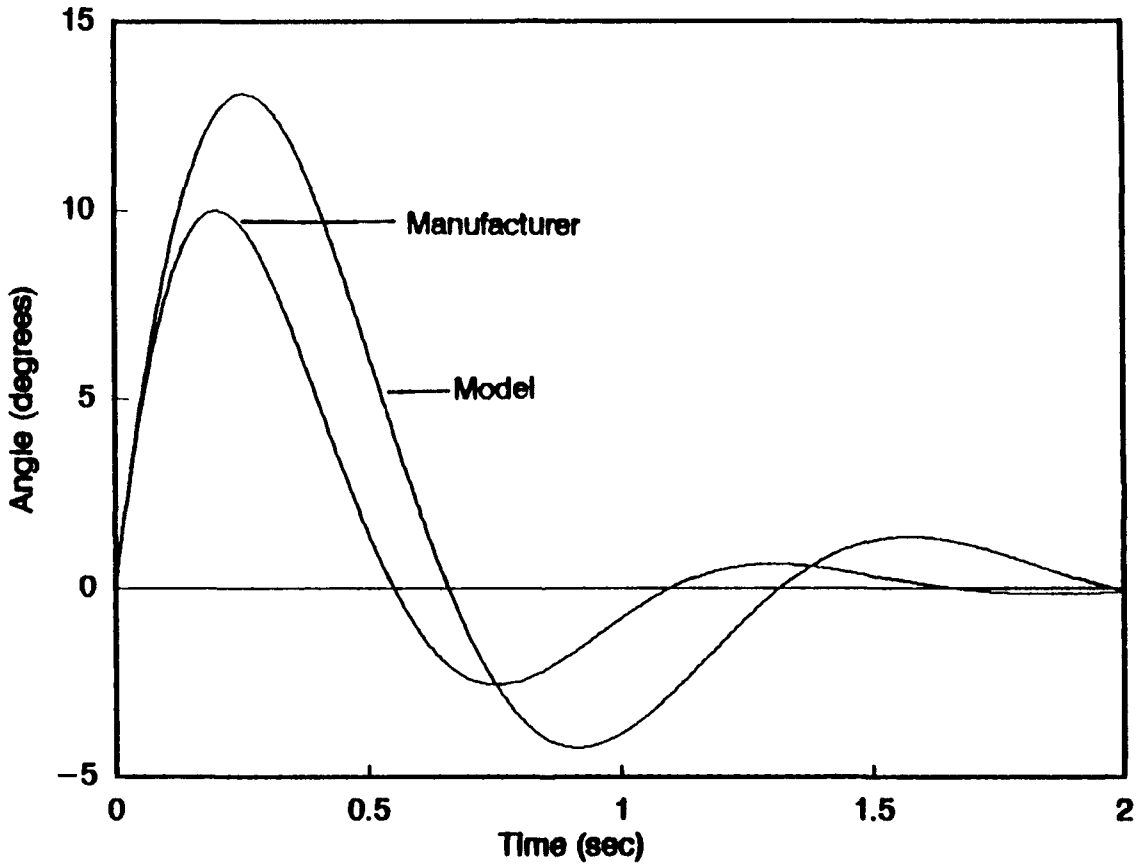

Figure 74. Comparison of model traces using the final results and the manufacturer's published dynamic characteristics for the azimuth response at 5 m s^{-1} using a Λ_0 of 103.39 deg s^{-1}.

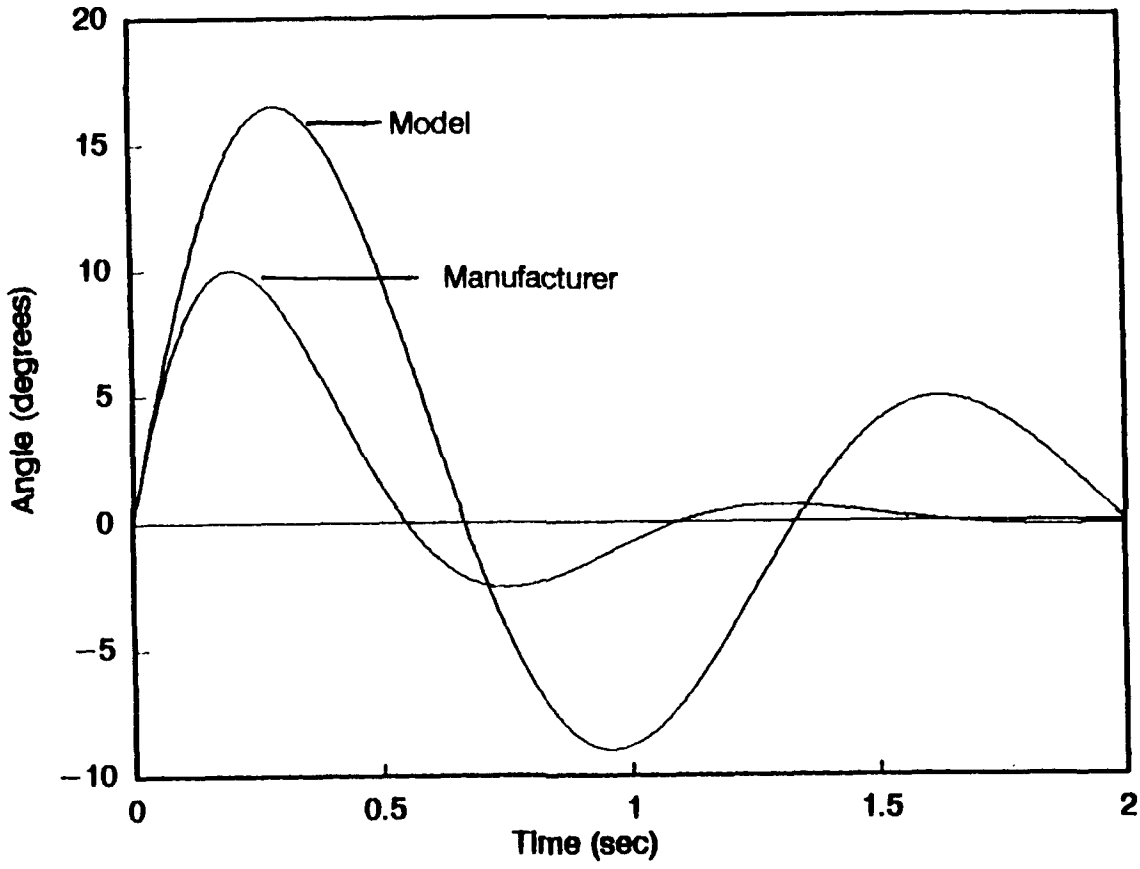

Figure 75. Same as in Figure 74, but for the elevation response.

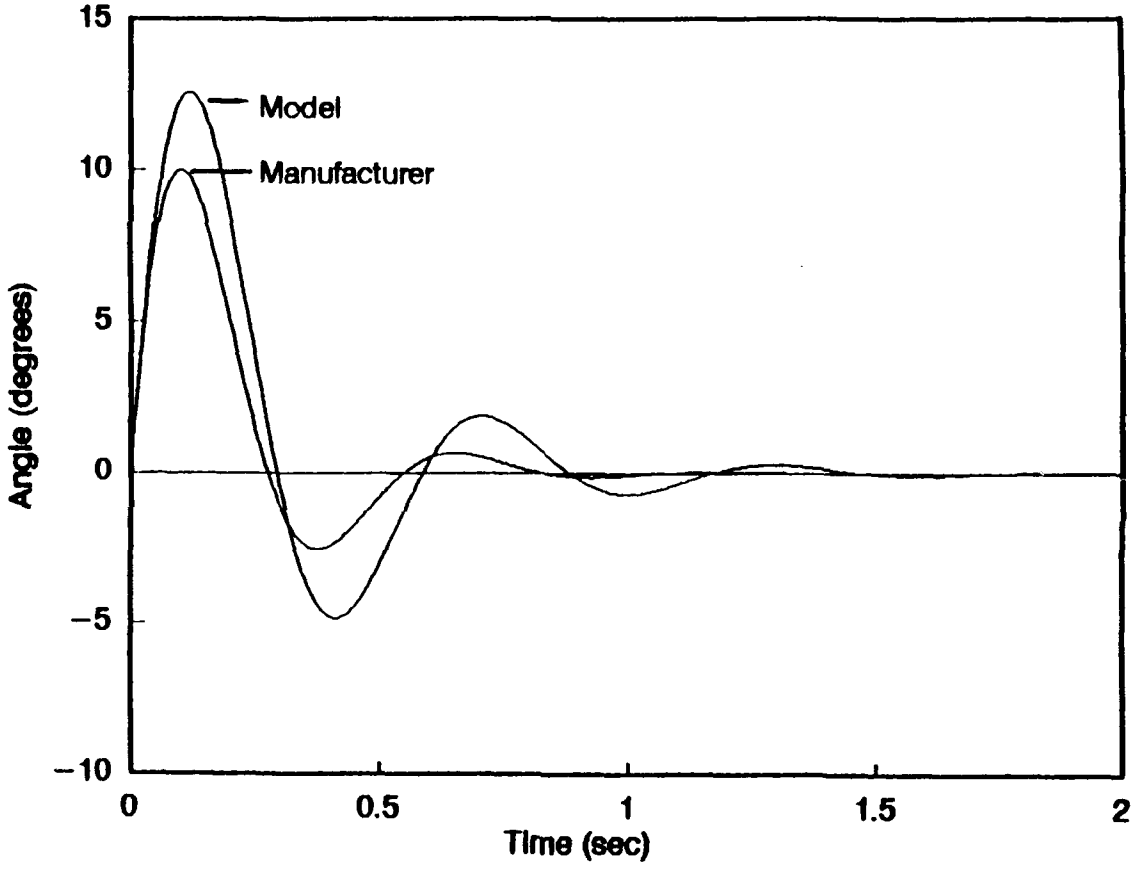

Figure 76. Same as in Figure 74, but for U = 10 m s^{-1} using a Λ_0 of 206.40 deg s^{-1}.

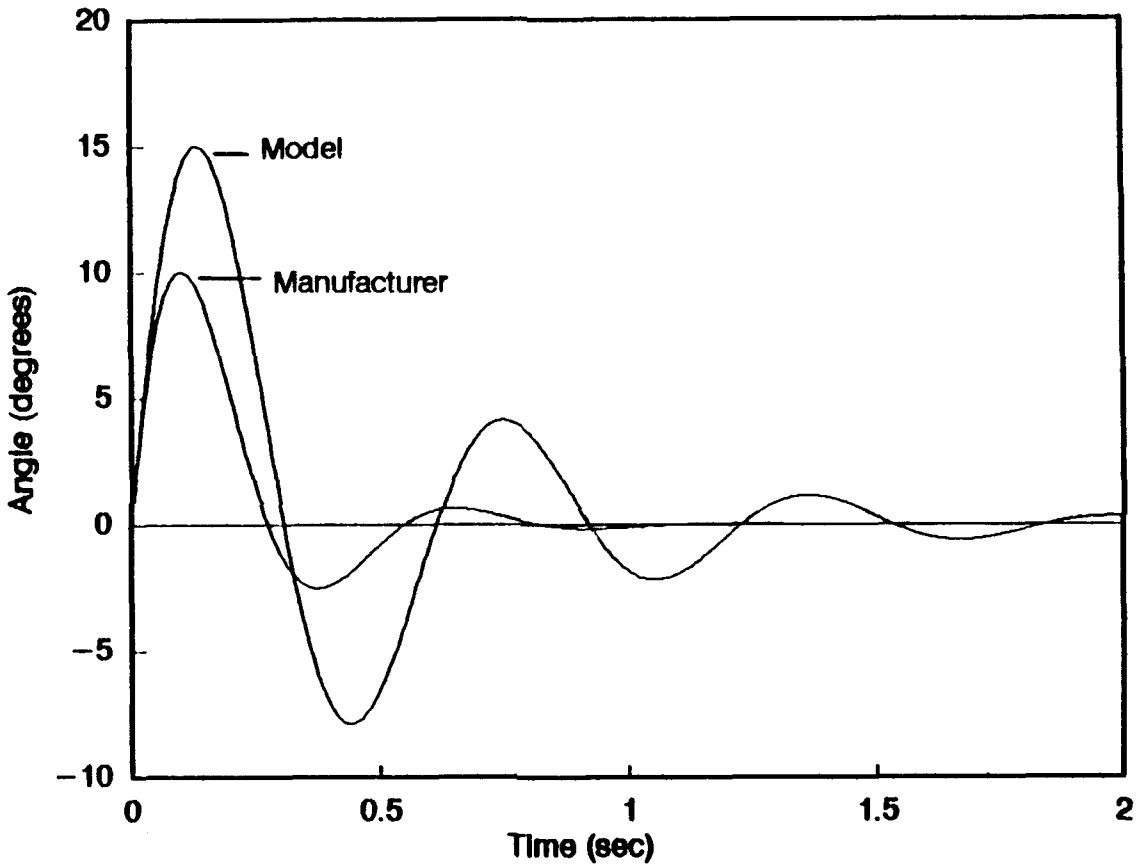

Figure 77. Same as in Figure 76, but for the elevation response.

having larger overshoots and longer damped wavelengths when using the same value of Λ_0 that the curve from the published characteristics uses.

However, the model response curves that use ζ and λ_n from individual test runs do not accurately represent the actual response of the bivane. Figures 78 through 81 compare data from individual test runs and model response traces calculated using equation (38). In all the figures, the first peaks of the model traces were forced to the same amplitude of the first peak of the actual response data. Figure 78 shows the azimuth data and model traces of test run TADE. The model trace having a Λ_0 of 94.66 deg s^{-1}, shows an overall longer damped wavelength than what the actual data indicate. However, the τ and T of the model and real data correspond well within the first half-period. Subsequent τ and T do not correspond well and the full-period λ_d of the model is longer than the real data indicate. The length of time of the second half-period of the real data is shorter than the first half-period. Under normal conditions, λ_d should remain constant, as the model predicts. The damped wavelength is a function of T_1, U, and ζ. By directly measuring the actual response data of the trace, λ_d is

$$\lambda_d = 2UT_1 \tag{58}$$

where T_1 is the second zero-crossing and is directly measured from the test data. Additionally, T_1 is fixed by the nature of the test data. From (60), since T_1 is fixed, then the wind speed must vary for a change in λ_d. Figure 82 shows the wind speed for the first two seconds of test run TADE. With a standard deviation of 0.32 m s^{-1}, only minimal turbulence and system noise is noted indicating an absence of a varying U. From (34), (35), and (36),

$$\lambda_d = \frac{U}{T_D}\frac{(6.0 - 2.4\zeta)}{\sqrt{1 - \zeta^2}} \tag{59}$$

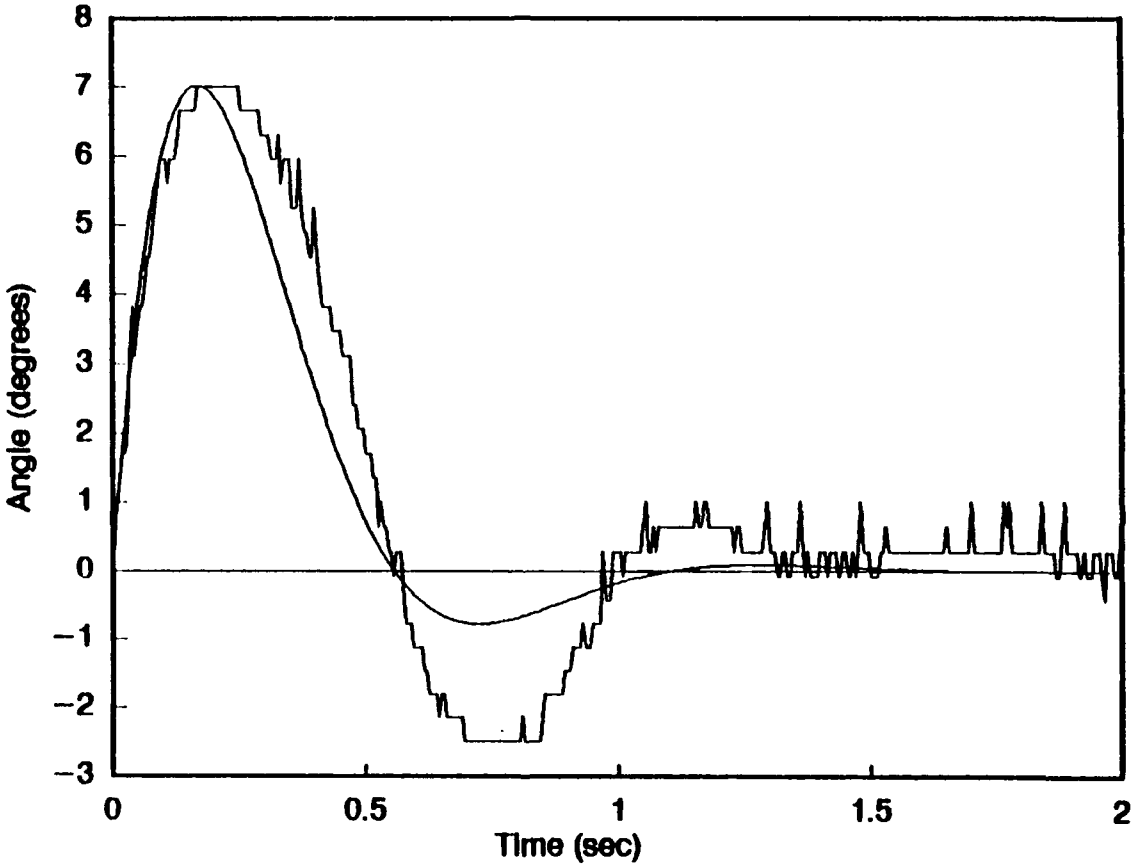

Figure 78. Comparison of the azimuth tr[illegible]nd the model using ζ=0.57 and λ_n=4.83 m from the 5 m s^{-1} run TADE where Λ_0 was found to be 94.66 deg s^{-1}.

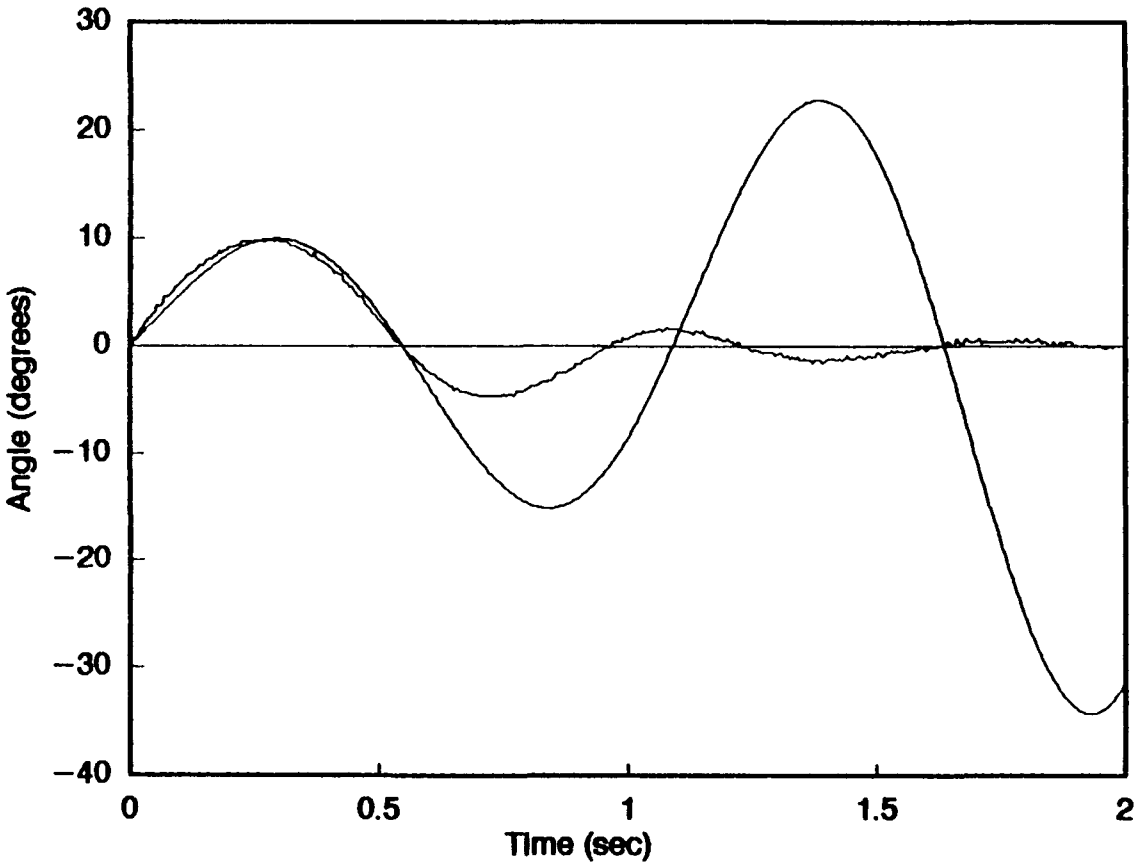

Figure 79. Same as in Figure 78, but for the elevation data ζ=-0.13 and λ_η=5.73 m where Λ_0 was found to be 46.58 deg s^{-1}.

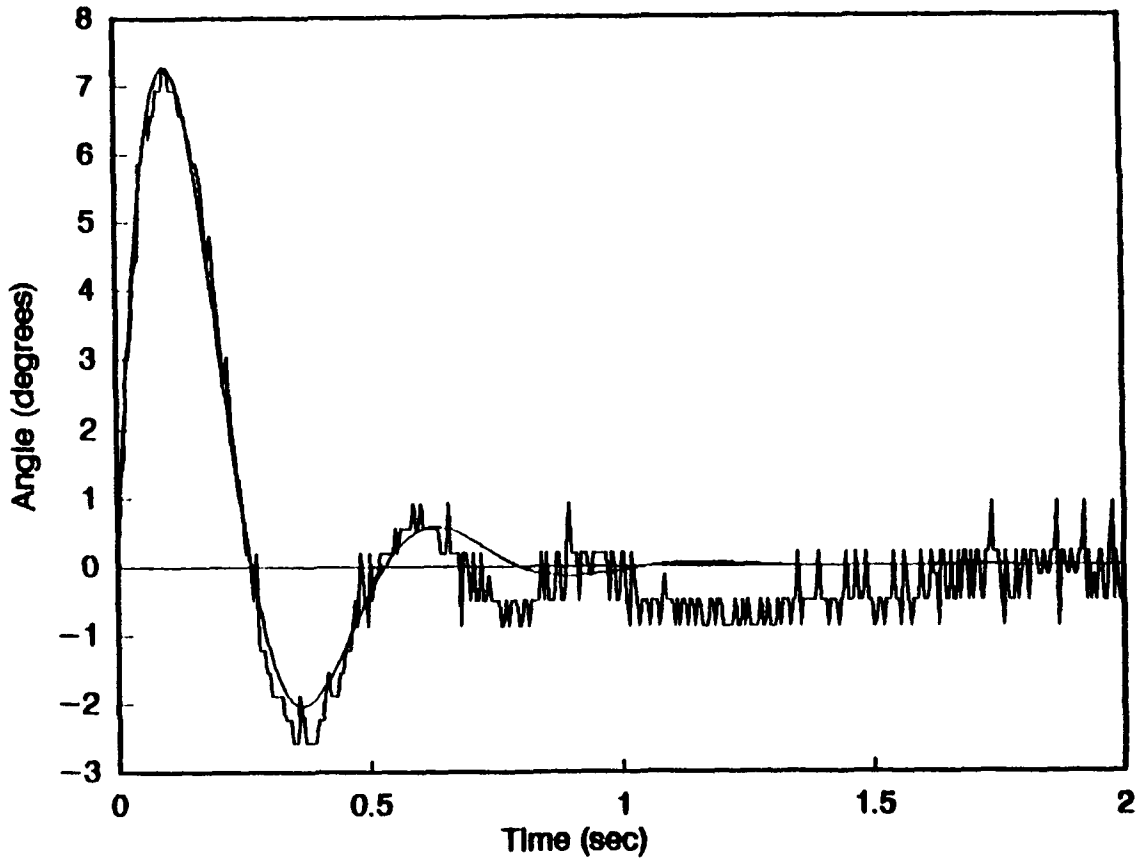

Figure 80. Same as in Figure 78, but for the 10 m s^{-1} run TBDH where ζ_s=0.38, λ_n=5.00 m, and Λ_0 was found to be 150.75 deg s^{-1}.

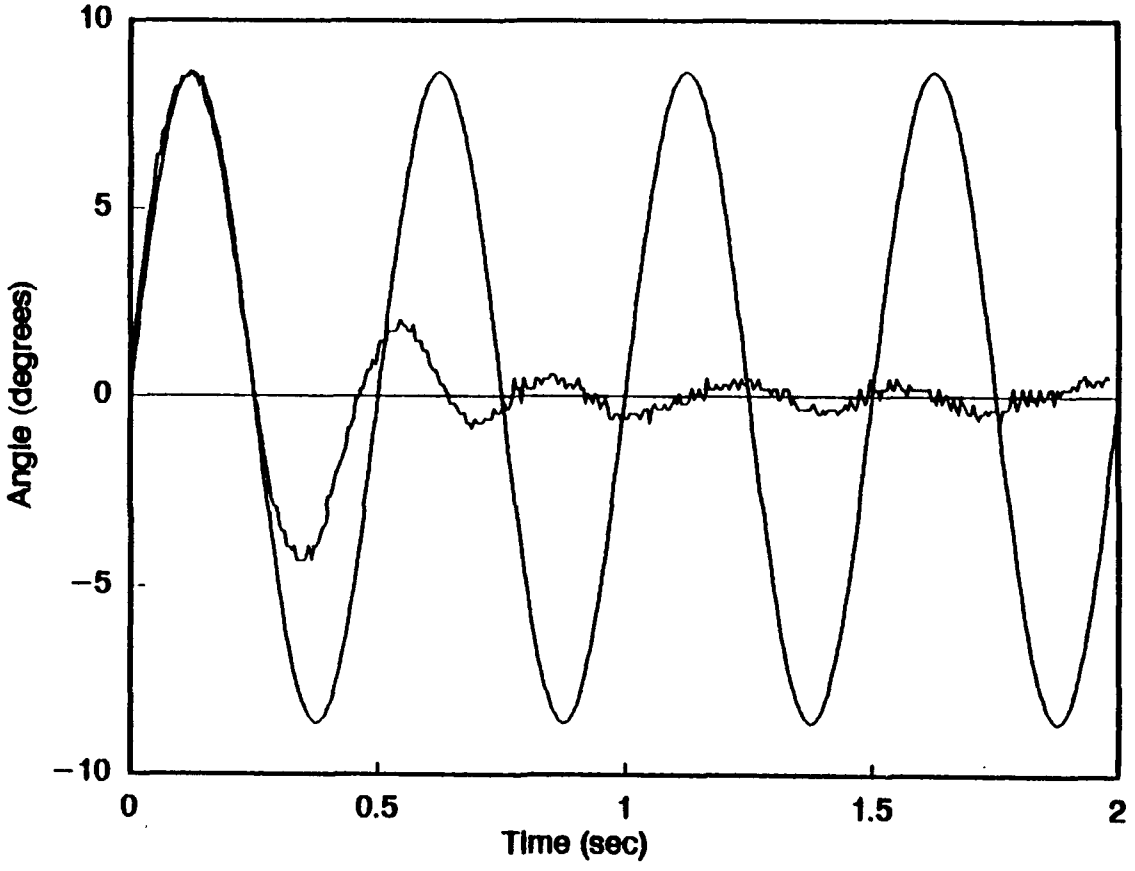

Figure 81. Same as in Figure 80, but for elevation data ζ= 0.00 and λ_n=5.09 m where Λ_0 was found to be 108.45 deg s^{-1}.

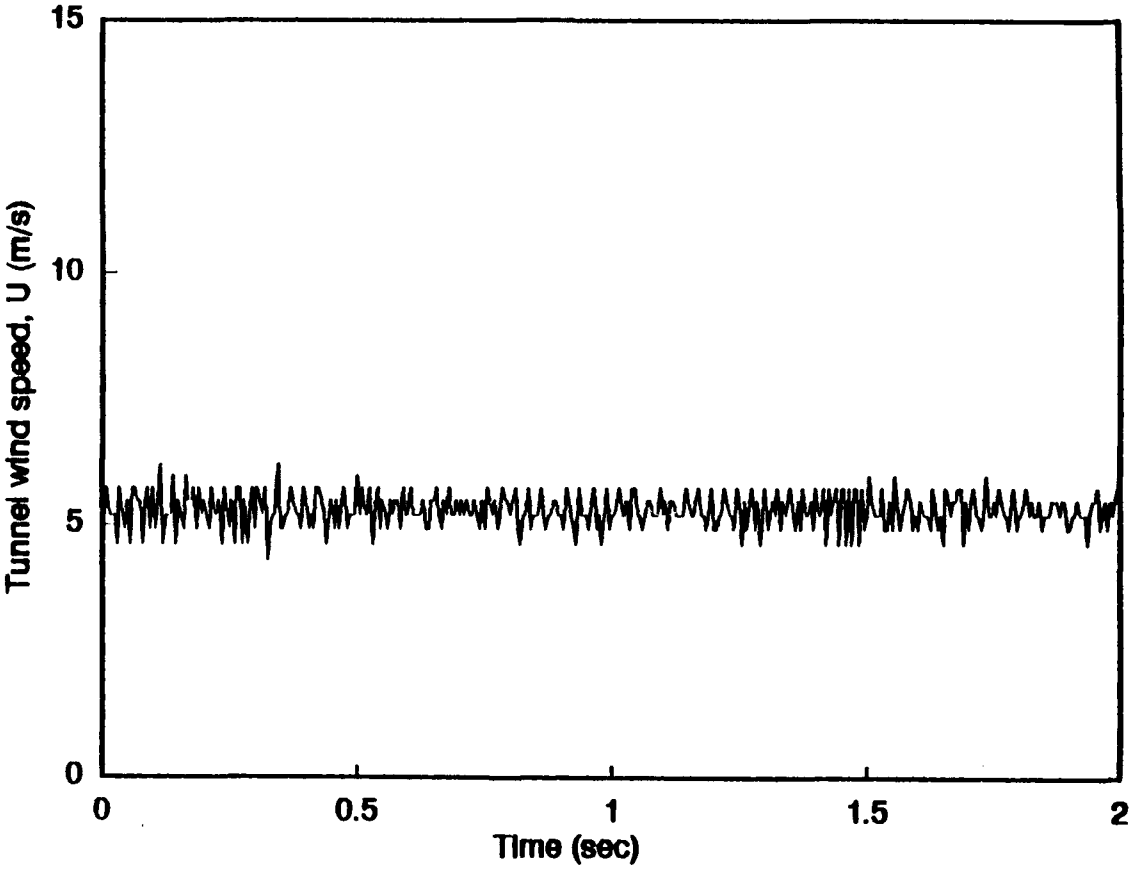

Figure 82. Plot of wind tunnel speed for run TADE where the standard deviation, σ, was found to be nominal at 0.32 m s^{-1}. The wind speed trace shows no systematic trend.

given that U is constant and T_D is fixed by the nature of the test data, then changes of λ_d depend on changes in ζ.

To test whether ζ changes with time, the generic equation to calculate ζ for all times is

$$\zeta = \cos\left[\frac{2\pi}{T_{i+1}}(\tau_i - T_{i+1})\right] \tag{60}$$

and is derived from (51) and (52). For test run TADE, the damping ratio, ζ_0 for times of the first half-period, is 0.57. If T_{i+1} are exactly multiples of T_i and $\tau_i = \tau_{i-1} + T_i$ (as in the normal response case), then using (62) gives a constant ζ for all times. However, for run TADE, τ_0 is 0.1700 s, T_1 is 0.5549 s while τ_1 and T_2 are 0.7686 s and 1.0098 s respectively. Both τ_1 and T_2 are not consistent with the normal case. Using the times of the second peak and the third zero-crossing and (62), ζ_1 is 0.24.

If ζ_1 was greater than ζ_0, then energy would be extracted from the system at an accelerated rate. For TADE data, $\zeta_1 < \zeta_0$ and energy is being extracted from the system at a decreasing rate. If in this case ζ_1 was negative, then, theoretically, energy is actually added to the system. In Figure 80, the elevation data for run TADE has a damping ratio from the first half-period of -0.13 and a natural wavelength, λ_{n0}, of 4.83 meters. When the ζ_0 and λ_{n0} from this data are used in (38), the amplitudes of the model curve continually increase suggesting continual input of energy into the system, within the first half-period. In the data from the second half-period, ζ increases to 0.36 meaning that energy is now being extracted from the system rather than injected into the system as is seen in the first half-period. Thus, the real data trace dampens as ζ increases from the first half-period to the second half-period, while the model trace shows a negative damping using ζ and λ_n from only the first half-period. Figures 80 and 81 from test run TBDH are similar examples where the azimuth ζ_0 is 0.38 and the elevation ζ_0 is zero.

Note that in Figure 81 the test data trace never actually dampens out, but continues to oscillate. Continuing the trace beyond two seconds, as seen in Figure 83, the elevation data of test TBDH show a regular oscillation that never dampens to equilibrium. The frequency of these oscillations are roughly 3.0 Hz

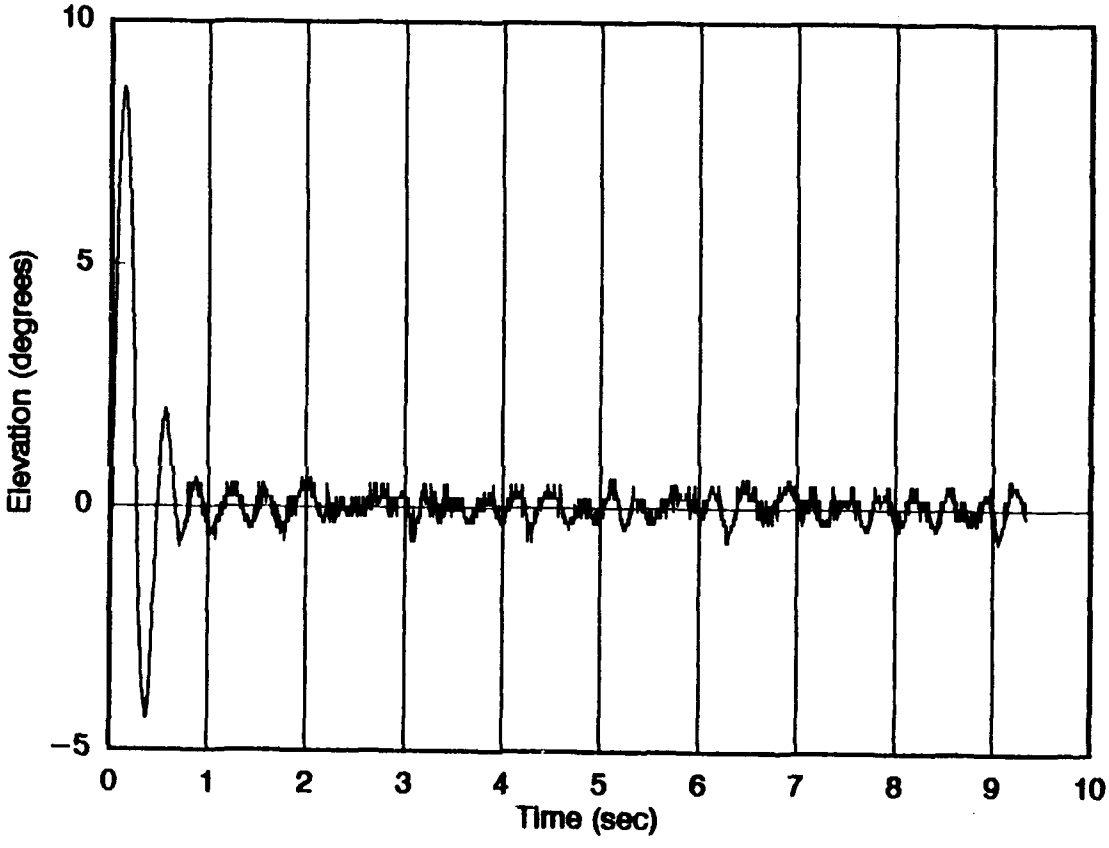

Figure 83. Full time response of the elevation data from run TBDH showing trailing oscillations occurring with an approximate frequency of 3.0 Hz.

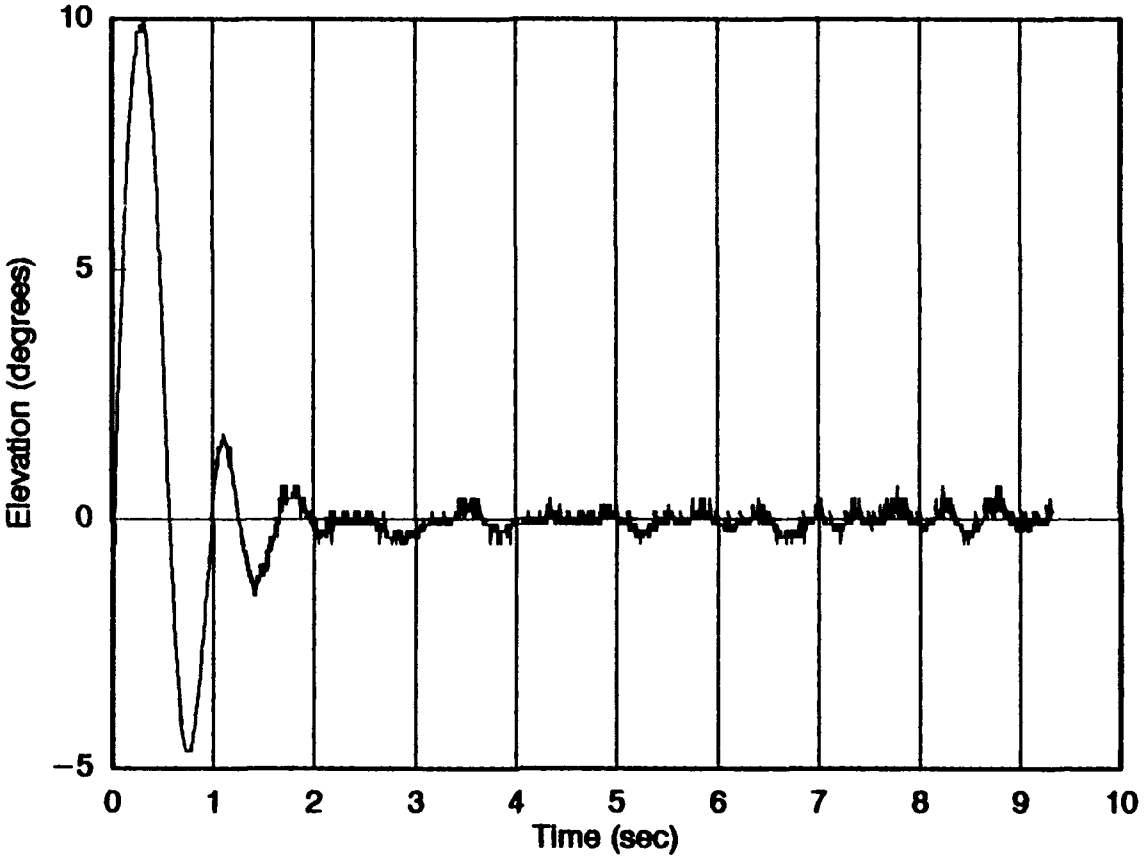

Figure 84. Same as in Figure 83, but for run TADE with trailing oscillations at approximately 1.5 Hz.

at a tunnel speed of 10 m s^{-1}. Again from position D, Figure 84 shows the elevation trace from test TADE taken at a tunnel speed of 5 m s^{-1}. The amplitudes of the peaks after two seconds in Figure 84 are not as great as the amplitudes in Figure 83, and have one-half the frequency. Note however, that in Figures 85 and 86 the frequency of the trailing oscillations in the azimuth data is constant at approximately 0.4 Hz at both wind speeds. Oscillations in the azimuth data do not appear to be a function of wind speed, while oscillations in the elevation data do appear to be directly related to wind speed.

Since the trailing oscillations seen in the azimuth motion are not associated with changes in wind speed, other factors are the cause. Mechanical irregularities, particularly in the resolver, are directly related to the motion of the vane assembly and can be ruled out. The data-logging system does not show this phenomena in the other two bivanes. Thus, a problem in the conditioning electronics is likely the cause of these oscillations of the azimuth data. Isolating this problem is beyond the scope of this study.

A phenomena related to Karman vorticies shedding off the bivane staff and affecting the tail is one possible explanation of the vertical oscillations. For an infinitely long cylinder, the air flow past the cylinder can be distorted producing vortex sheets that shed off the cylinder and move through the flow at less than the wind speed. A schematic of Karman vorticies or streets is shown in Figure 87 where the frequency, f is the number of vorticies that pass a stationary point in time. In the bivane case, the stationary point is the tail of the vane assembly. As the vorticies pass the vane's tail, the fins may be pulled downward into the distorted flow with a frequency corresponding to the frequency of the vorticies. The frequency can be calculated by combining the equations

$$S = \frac{f D}{U} \tag{61}$$

$$Re = \frac{UD}{\nu} \tag{62}$$

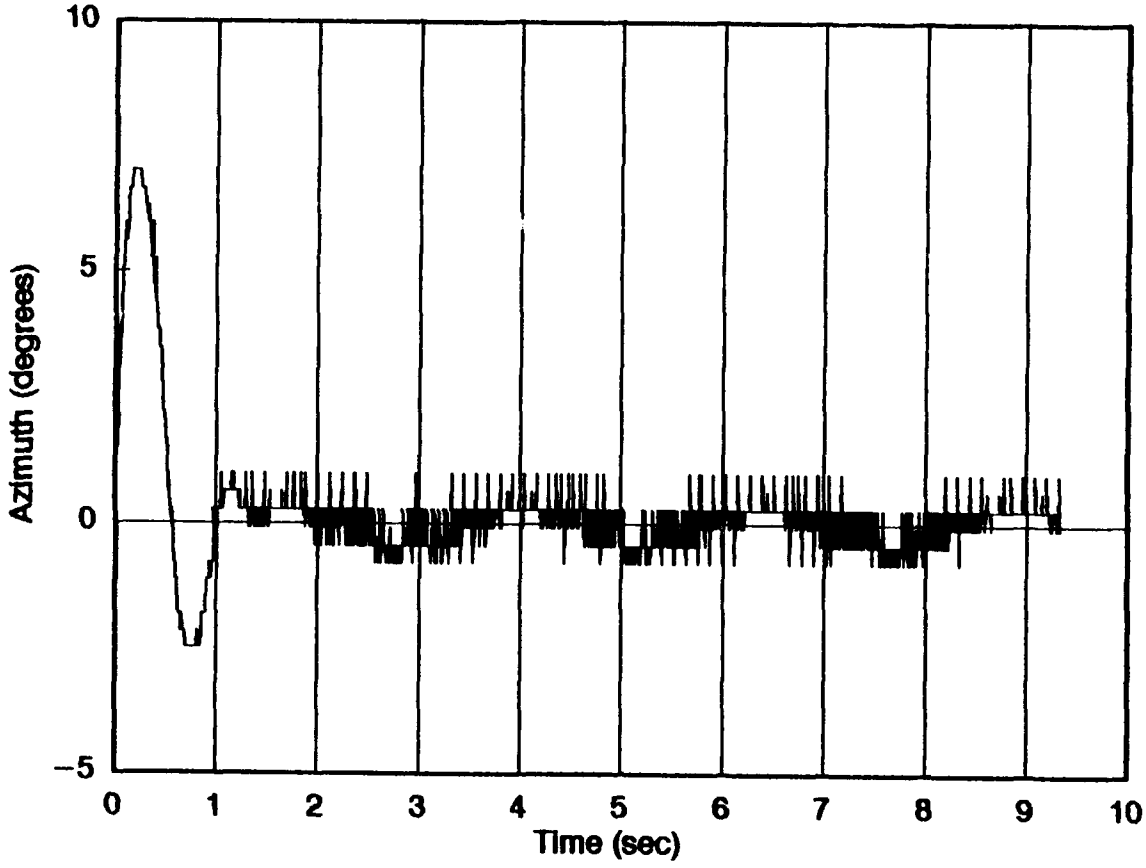

Figure 85. Same as in Figure 83, but for azimuth data. The trailing oscillations occur at 0.4 Hz.

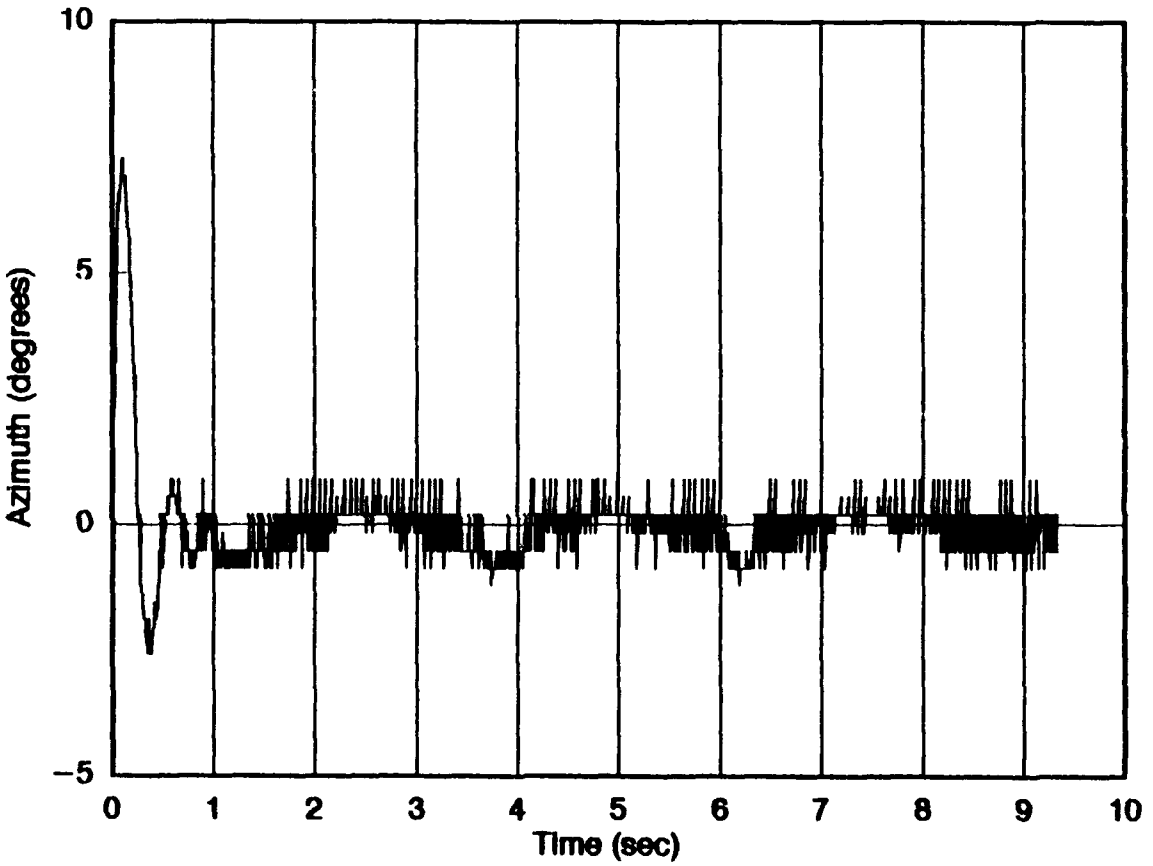

Figure 86. Same as in Figure 85, but for run TBDH where the trailing oscillations are at 0.4 Hz.

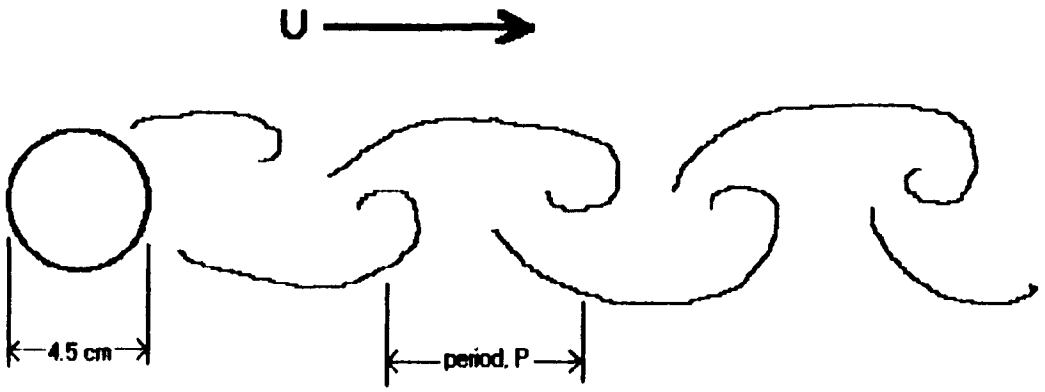

Figure 87. Schematic of Karman vorticies shedding from an infinite cylinder with a diameter of 4.5 cm.

into

$$f = \frac{SU}{D} \tag{63}$$

where S is the Strouhal number (by definition is 0.21), D is the diameter of the cylinder, Re is the Reynolds number, and v is the viscosity of air. With the cylinder having diameter of 4.5 cm and the wind speed at 5.30 m s^{-1} (for test run TADE), the frequency is 24.7 Hz and the Reynolds number is 16,476. From Schlichting (1968) regular Karman streets are observed only in the range of Reynolds numbers of 60 to 5000, well below what is observed for this bivane. The calculated frequency is also much greater than that observed.

These numbers are for an infinitely long cylinder while the oscillations seen in the bivane trace are near the top of the cylinder. Air flowing over, as well as around, the bivane housing complicates the situation beyond a smooth, understandable flow. Additionally, wind speeds used in these tunnel tests should distort the flow into random turbulent motions rather than create a regular pattern.

The more probable reason for the trailing oscillations in the elevation data concerns the elevation reference point. Recall that the Teledyne Geotech bivane is balanced in the vertical such that the vane assembly will always return to the horizontal or zero angle position in very light or calm winds. The forcing on the vane assembly is due to the design of the cams in the elevation resolver. This feature adds additional forcing to the vane assembly, requiring another term in (17). Since the additional force is incorporated in the vane assembly, the response of the vane to deflection intrinsically includes this additional force. Therefore, the natural response and the additional forcing are nearly in phase, and simple addition of this additional forcing cannot be added to model equation (38). However, the adjusted form of equation (38) should include a non-damped (without an exponent) term, derived from the knowledge of the forces produced by the cams.

Much study can be done on the effects of the additional forcing produced by the vane forcing itself to equilibrium. However, wind vanes and bivanes should not include an additional force that attempts to

restore the vane assembly to a predetermined reference point. Vane assemblies should be balanced so that no particular position is preferred (Wang and Felton, 1983; Lockhart, 1989).

4.3 Climatronics

The voltage range for the Climatronics bivane is one volt dc for both the azimuth and elevation angles. This equates to an ideal resolution of 360° per volt for the azimuth and 90° per volt for the elevation angles. For this particular bivane, the resolution is 359.24° per volt for azimuth and 106.15° per volt for elevation angles. Since the CIO-AD08 has a resolution of 0.00244 volts, the azimuth data have a minimum resolution of 0.88° that is more coarse than 0.26° for elevation data. Figures 88 and 89 show the difference in resolutions between the azimuth and elevation data from the typical run of CABB with no smoothing of the data. From the last seven seconds of the run, the elevation data have a standard deviation of 0.16°, while the azimuth data have a standard deviation of 1.29°. The azimuth standard deviation is well above the minimum resolution and suggests additional noise in the data.

Due to the coarse and noisy azimuth data trace in Figure 88, analytical techniques used in the software cannot retrieve the appropriate peaks and zero-crossings for calculating the damping ratio and natural wavelength. The common approach to retrieving the dynamic characteristics is by hand-drawing a smooth curve through the data. Each run must be laboriously hand-drawn in the same way, and the results are affected by human subjectivity. A more objective method is to average each data point of all the runs to produce a curve representing the average response. For example, the azimuth values from all the runs at the time of the first zero-crossing (t=0 sec) are averaged and the values at the next time point (t=0.005 sec) are averaged, and so forth. Figures 90 to 93 show the averaged azimuth and elevation data for position D at 5 and 10 m s^{-1}.

Tables 8 and 9 are the results, by position, of the dynamic characteristic averaging method (Table 8) and the data point averaging method (Table 9). Figures 94 to 97 show plots of the ζ and λ_n results against the manufacturer's published values of ζ=0.45 and λ_n=2.85m. The azimuth data improve significantly, especially for position F. Figures 98 to 101 compare the elevation dynamic characteristics

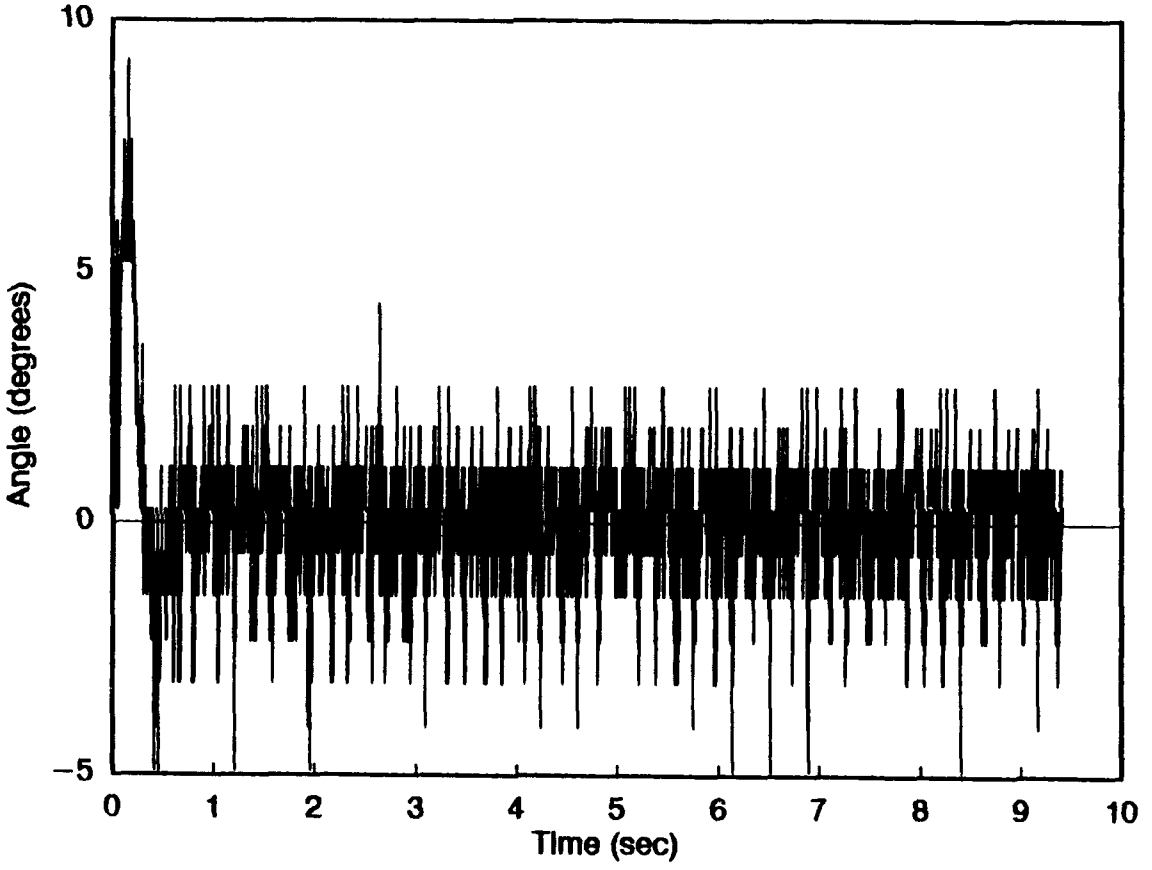

Figure 88. Plot of the full time response of the Climatronics azimuth data from the 5 m s^{-1} run CABB where σ = 1.29° from the last seven seconds of the trace.

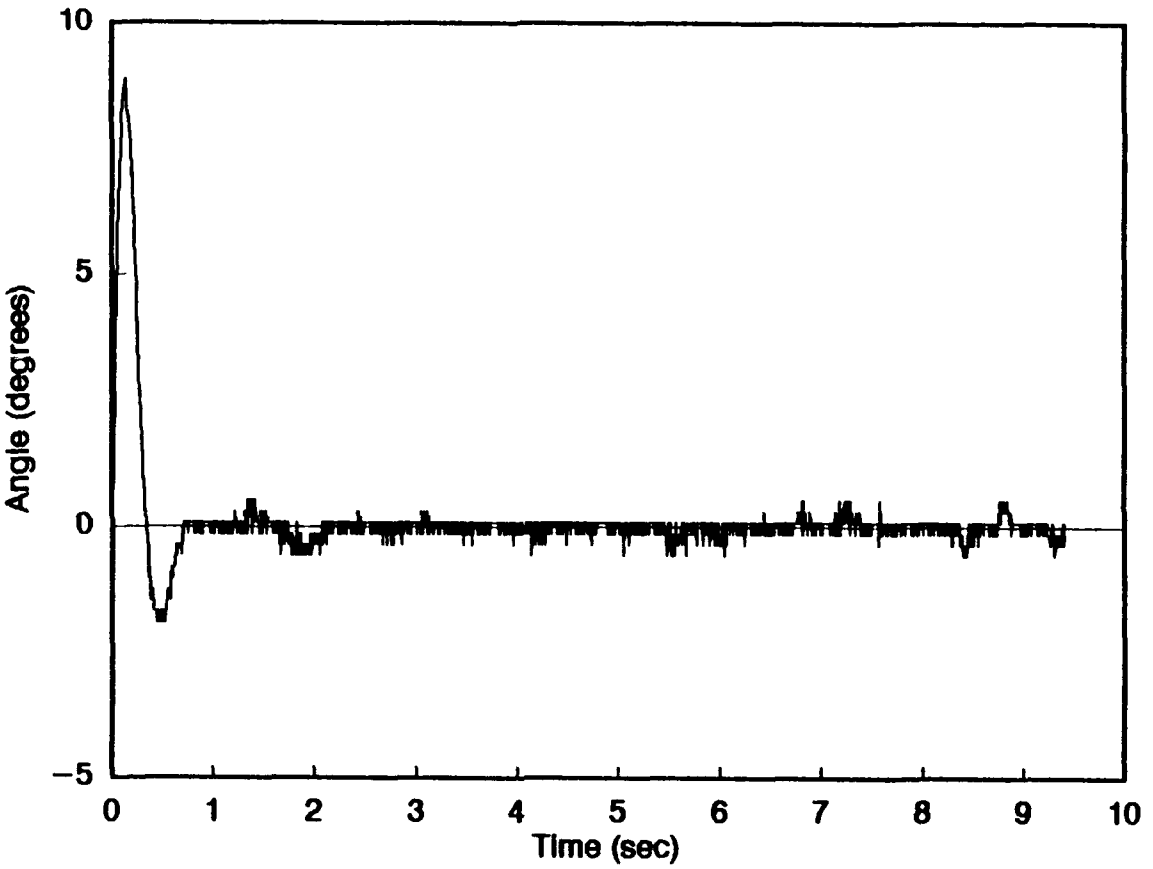

Figure 89. Same as in Figure 88, but for elevation data where $\sigma = 0.16°$ from the last seven seconds of the trace.

Table 8. Results of dynamic testing of the Climatronics Dual Annulus Bivane using seven-point running averages and averaging the dynamic characteristics of each run.

Air Speed: 5 m s^{-1}

Position	ζ_{az}	$\lambda_{n\text{-}az}$ Approach 1 Approach 2	ζ_{el}	$\lambda_{n\text{-}el}$ Approach 1 Approach 2
A	----	----	0.44±0.05	2.64±0.11
				2.61±0.12
B	0.25±0.20	2.55±0.69	0.42±0.04	2.82±0.06
		2.54±0.84		2.83±0.08
C	0.27±0.12	2.81±0.12	----	----
		2.76±0.30		
D	0.41±0.12	2.66±0.17	0.45±0.05	3.04±0.09
		2.55±0.22		3.01±0.13
E	----	----	0.52±0.03	2.71±0.09
				2.72±0.08
F	0.35±0.66	8.75±3.31	0.41±0.03	2.95±0.09
		46.79±0.14		3.00±0.07

Air Speed: 10 m s^{-1}

Position	ζ_{az}	$\lambda_{n\text{-}az}$ Approach 1 Approach 2	ζ_{el}	$\lambda_{n\text{-}el}$ Approach 1 Approach 2
A	----	----	0.47±0.04	2.74±0.08
				2.76±0.08
B	0.48±0.12	2.54±0.23	0.47±0.04	2.83±0.08
		2.96±0.13		2.92±0.11
C	0.30±0.16	2.33±0.24	----	----
		2.13±0.31		
D	0.30±0.28	2.50±0.20	0.47±0.04	2.86±0.12
		2.48±0.65		2.91±0.11
E	----	----	0.51±0.01	2.64±0.02
				2.81±0.18
F	-0.44±0.36	3.28±3.36	0.44±0.03	2.91±0.09
		16.20±3.07		3.03±0.31

Table 9. Results of dynamic testing of the Climatronics Dual Annulus Bivane using seven-point running averages and averaging the data points of each run.

Air Speed: 5 m s^{-1}

Position	ζ_{az}	$\lambda_{n\text{-}az}$ Approach 1 Approach 2	ζ_{el}	$\lambda_{n\text{-}el}$ Approach 1 Approach 2
A	----	----	0.44	2.70
				2.65
B	0.36	2.86	0.41	2.86
		3.24		2.76
C	0.31	2.73	----	----
		2.20		
D	0.47	2.63	0.37	3.15
		2.63		2.89
E	----	----	0.53	2.72
				2.69
F	0.42	2.59	0.41	3.00
		2.59		2.88

Air Speed: 10 m s^{-1}

Position	ζ_{az}	$\lambda_{n\text{-}az}$ Approach 1 Approach 2	ζ_{el}	$\lambda_{n\text{-}el}$ Approach 1 Approach 2
A	----	----	0.44	2.80
				2.73
B	0.31	2.85	0.50	2.85
		2.36		2.87
C	0.46	2.29	----	----
		2.19		
D	0.40	2.50	0.50	2.88
		2.29		2.90
E	----	----	0.60	2.75
				2.76
F	0.35	2.46	0.41	3.03
		2.34		2.78

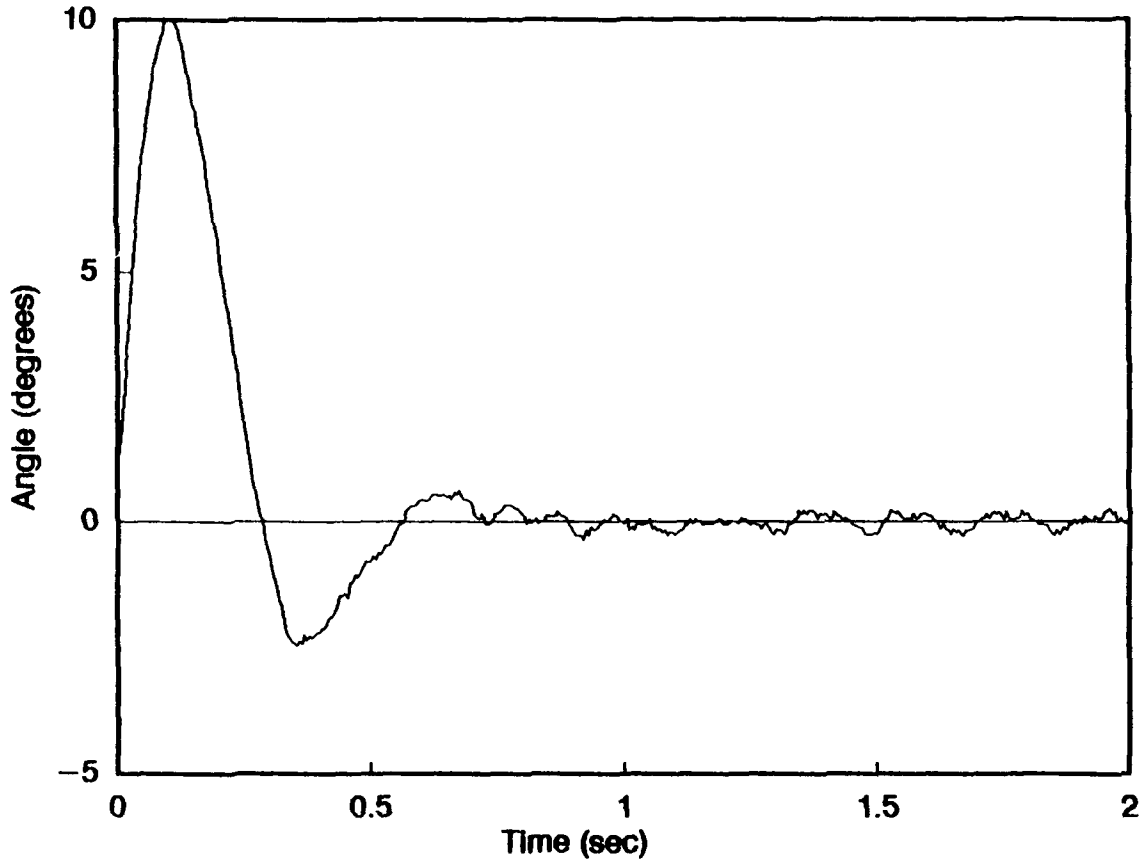

Figure 90. Azimuth trace computed from the average of all test runs taken at position D with U = 5 m s^{-1}. This computed trace unmasks trailing oscillations not detectable in individual azimuth response traces (see Figure 89).

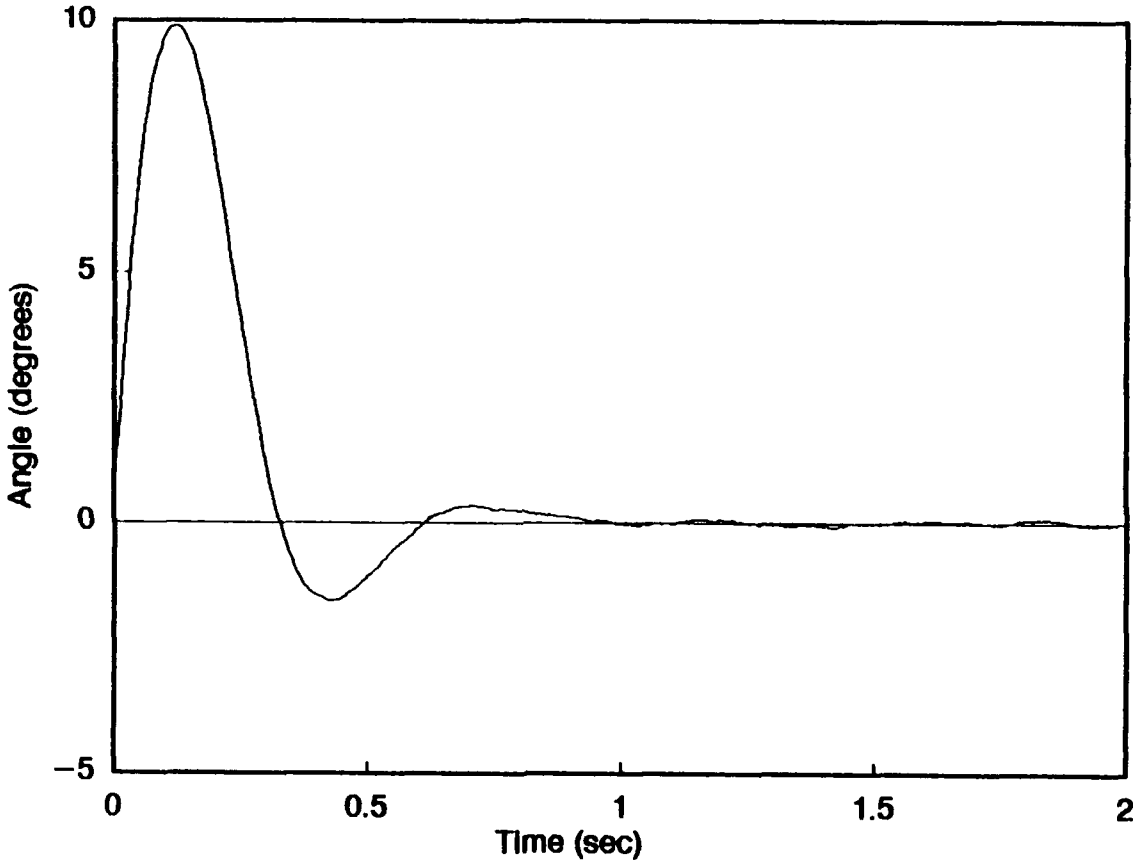

Figure 91. Same as in Figure 90, but for elevation data with no trailing oscillations.

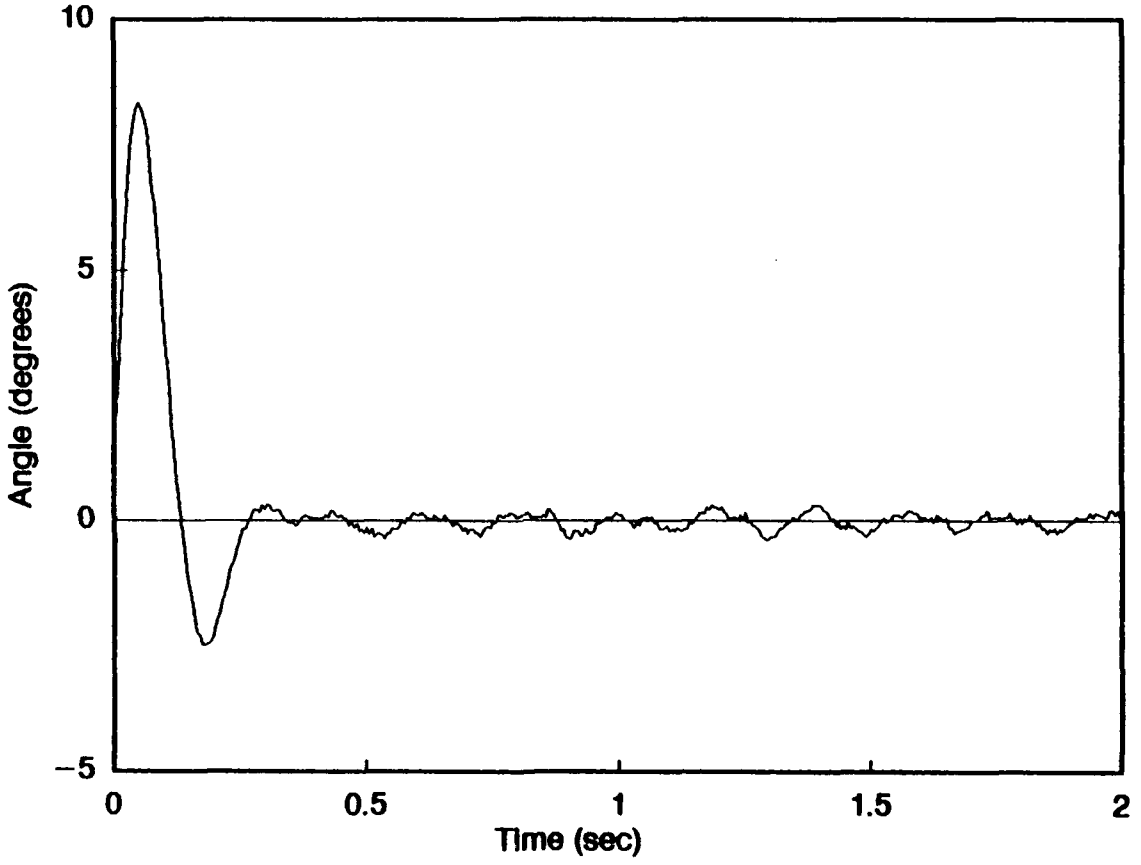

Figure 92. Same as in Figure 90, but for U = 10 m s^{-1}.

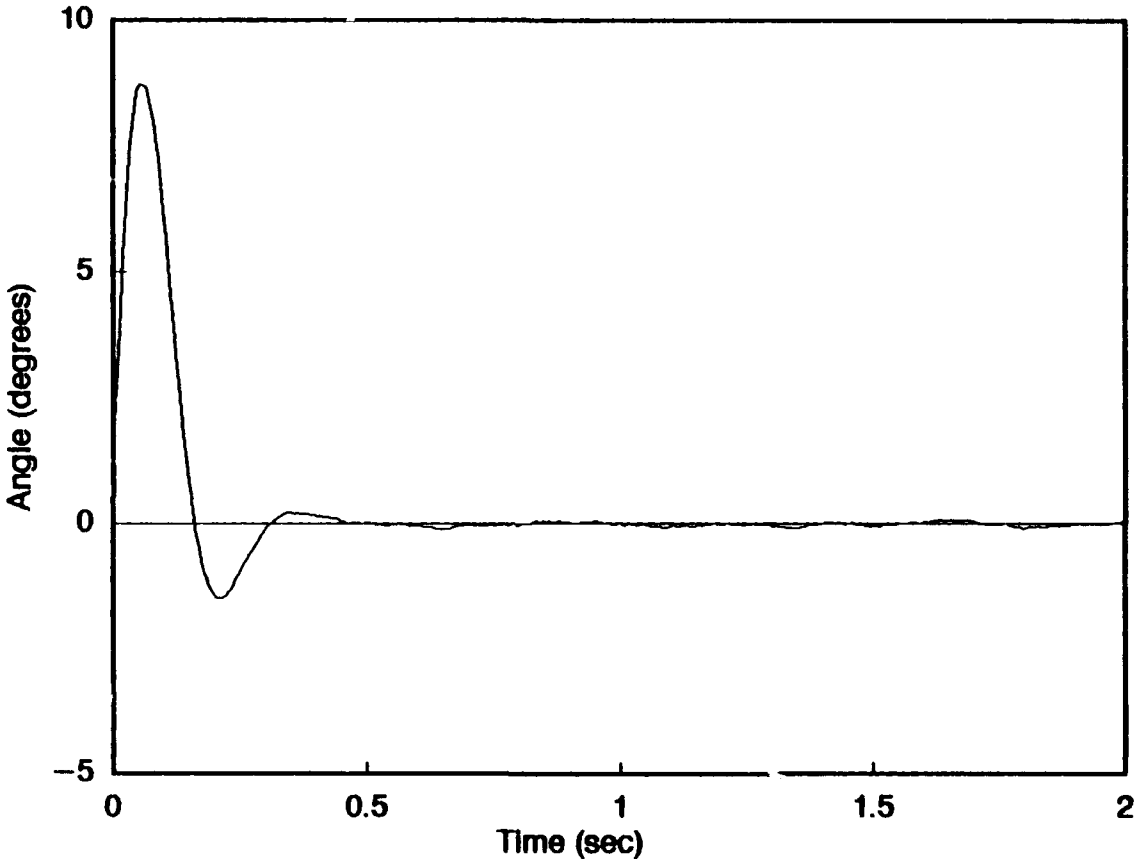

Figure 93. Same as in Figure 92, but for elevation data with no trailing oscillations.

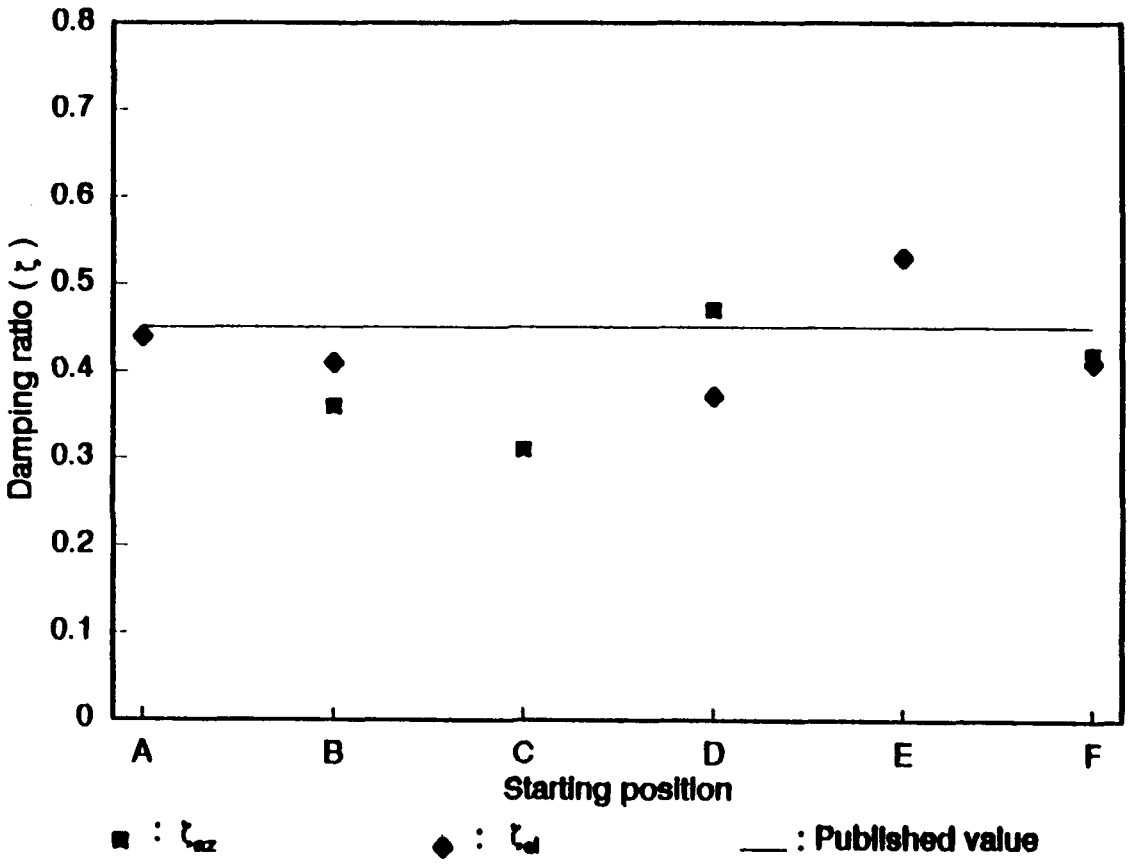

Figure 94. Plots, of the damping ratio, by position, for U = 5 m s^{-1} using the dynamic characteristic averaging procedure.

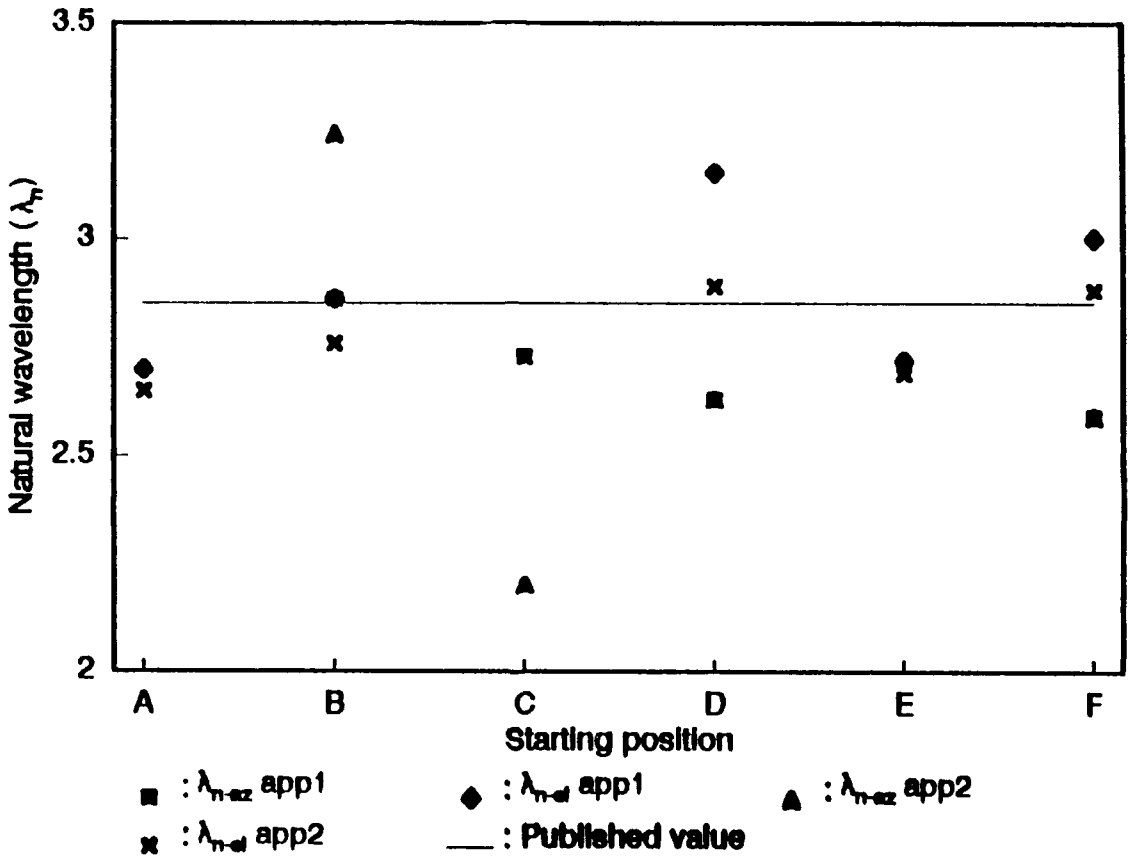

Figure 95. Same as in Figure 94, but for natural wavelength data.

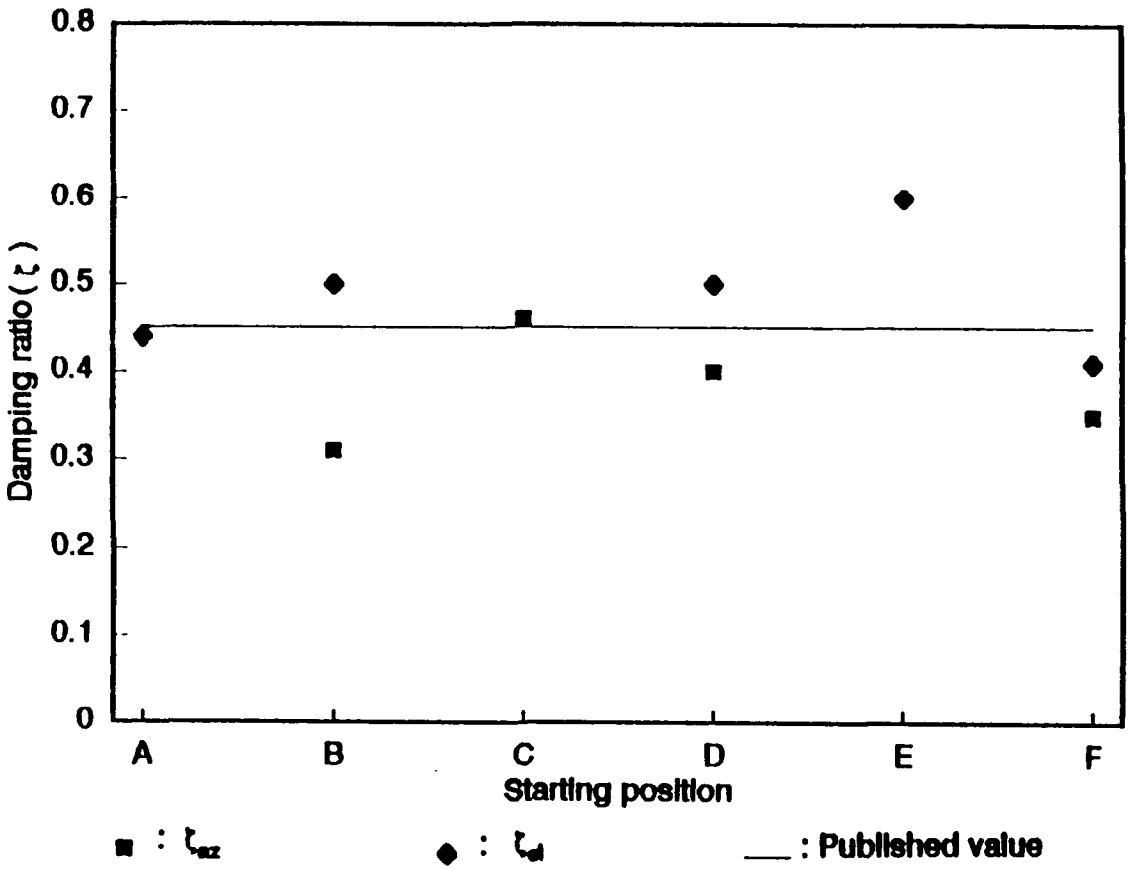

Figure 96. Same as in Figure 94, but for U = 10 m s^{-1}.

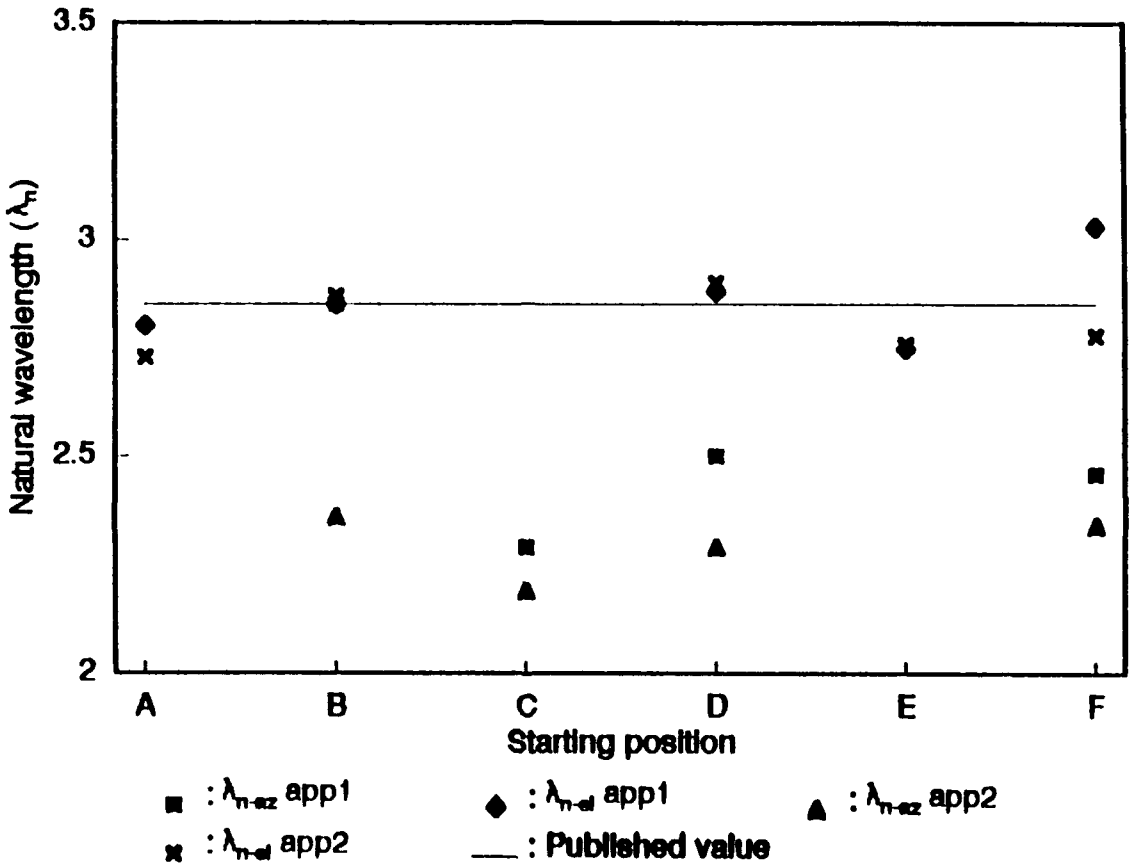

Figure 97. Same as in Figure 95, but for U = 10 m s^{-1}.

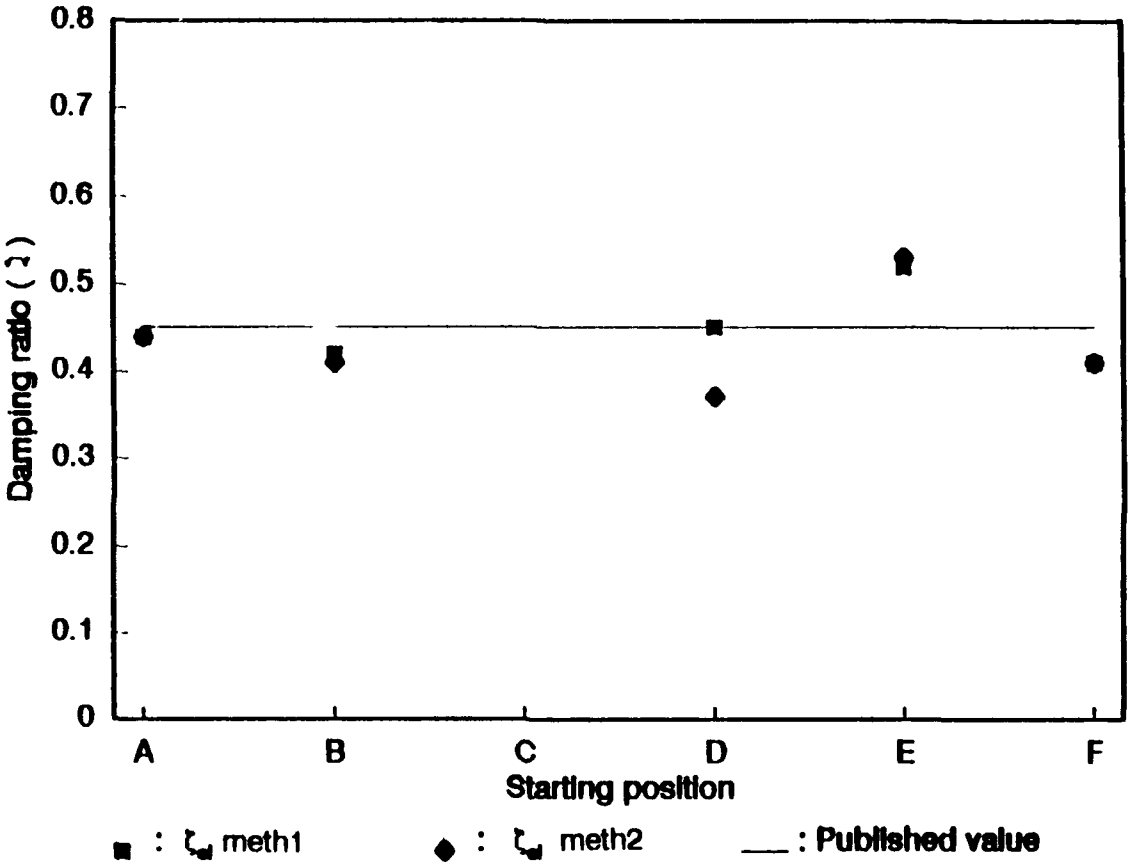

Figure 98. Comparison of the damping ratio values from the dynamic characteristic averaging method and the computed trace for U = 5 m s^{-1}. Both methods are in good agreement.

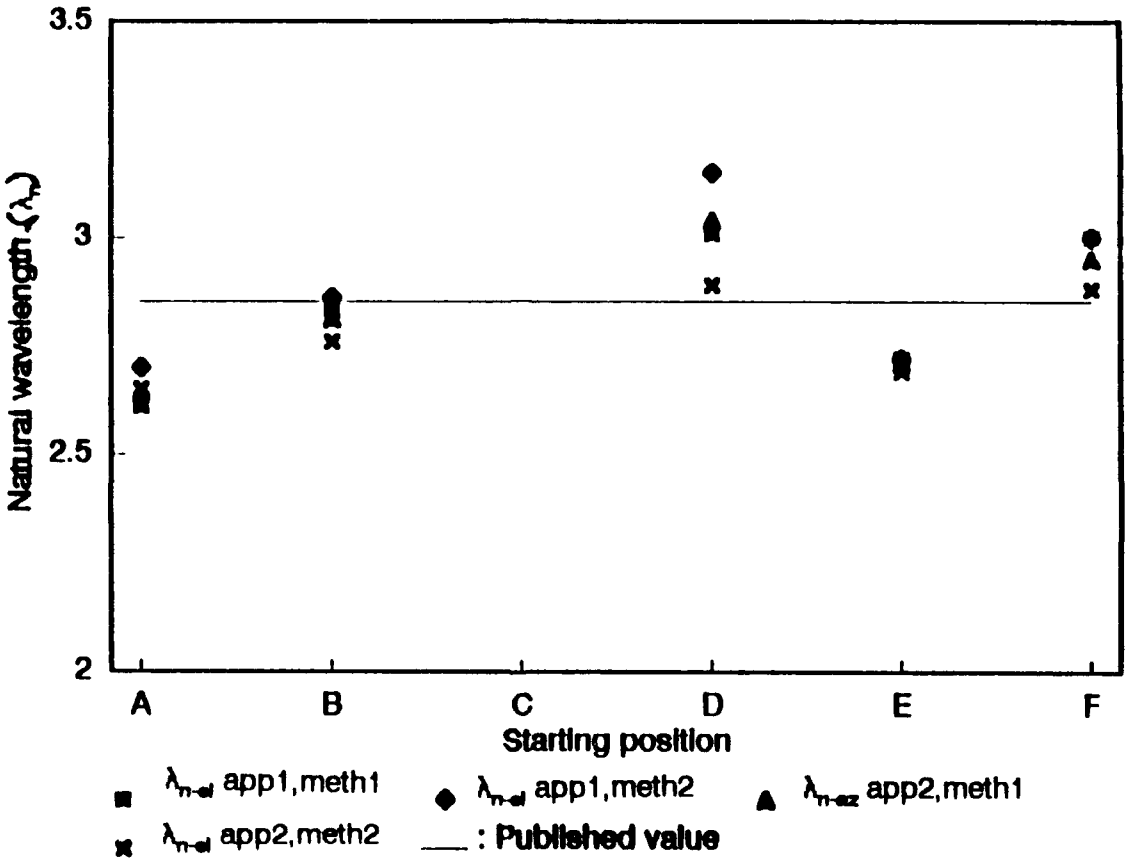

Figure 99. Same as in Figure 98, but for natural wavelength data.

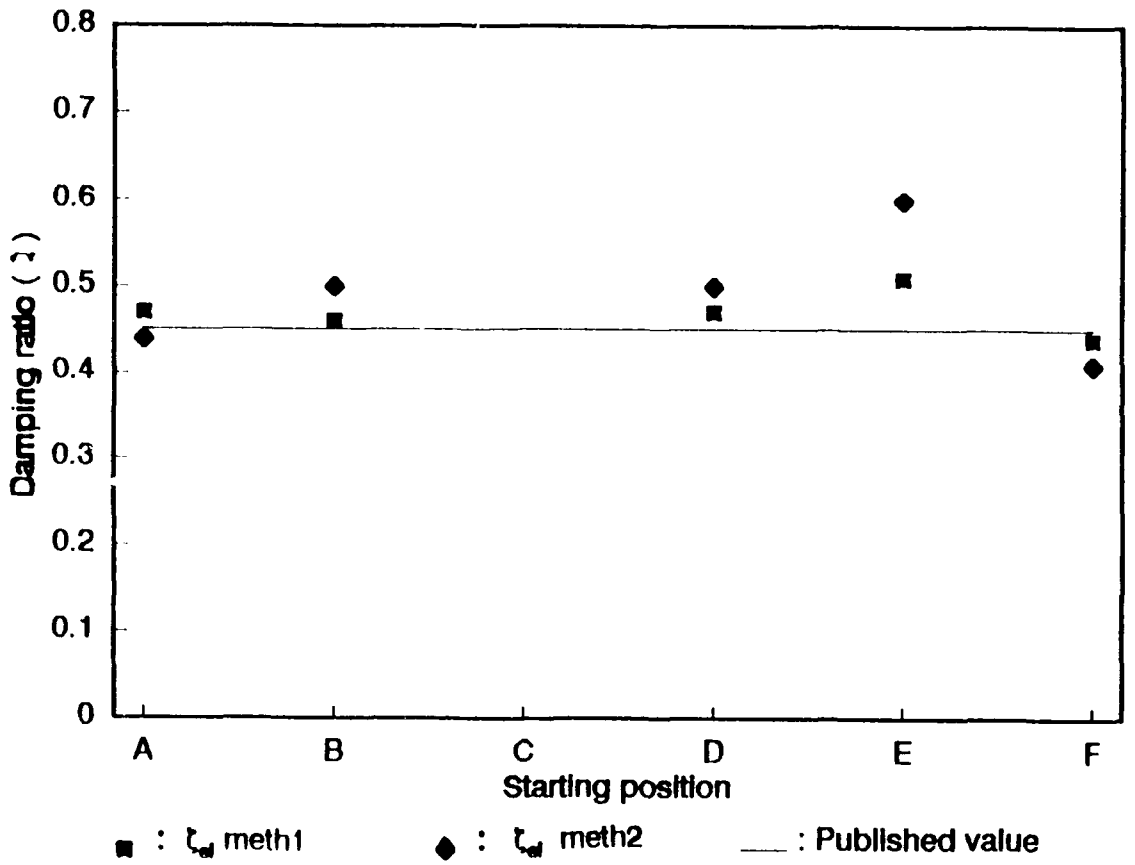

Figure 100. Same as in Figure 98, but for U = 10 m s^{-1}.

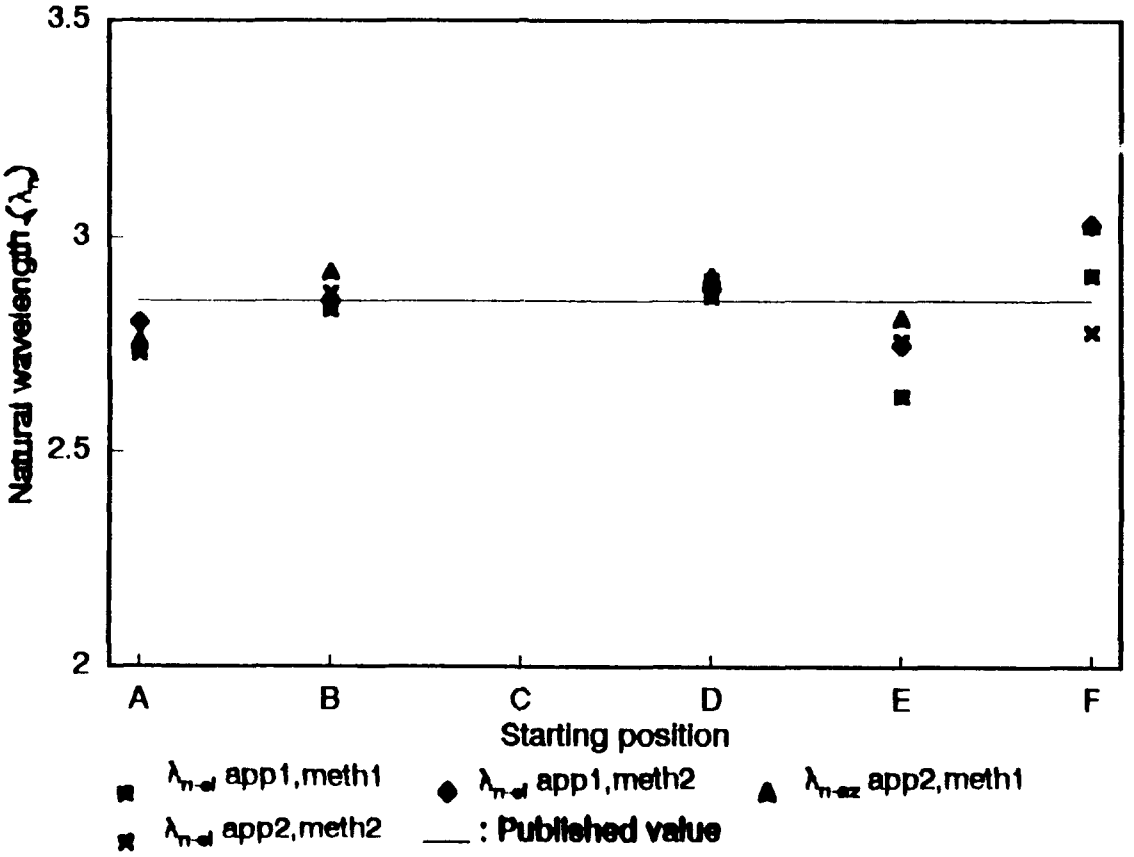

Figure 101. Same as in Figure 99, but for U = 10 m s^{-1}.

derived from both methods. The data point averaging method deviates little from the dynamic characteristic averaging method. A drawback of the point averaging method is that the confidence of the values is unavailable since one consolidated run is used to calculate the dynamic characteristics. However, the data point averaging method is preferable over hand-drawn analyses when the dynamic characteristic averaging method is found unreliable.

The data point averaged traces for position D in Figures 90 and 92 show a distinct set of trailing oscillations similar to those found in the Teledyne Geotech data. These oscillations are not easily seen in traces of individual runs as in Figure 88. Only with data point averaging are these oscillations unmasked. The frequency of oscillations is approximately 5 Hz for both tunnel speeds. As with the Teledyne Geotech azimuth data, these oscillations are not dependent on wind speed and are probably due to conditioning electronics or inconsistencies in the azimuth resolver. These oscillations may be the cause of the additional noise seen in Figure 89 where the oscillations are masked.

Trailing periodical oscillations are not seen in the elevation traces in Figures 91 and 93. Recall that the Climatronics and Teledyne Geotech vane assemblies attempt to return to the same elevation reference angle of 0°. Since the Climatronics' vane assembly has a mass of roughly 28 g and the Teledyne Geotech vane assembly has a mass of 196.8 g, the momentum of the Climatronics' vane assembly is considerably smaller than the Teledyne Geotech's momentum. Thus, the lighter Climatronics' vane assembly does not create the force necessary to produce the same trailing oscillations seen in the Teledyne Geotech elevation data.

Table 10 presents the final results of the Climatronics Dual Annulus Bivane. Azimuth results are from the data point averaging method and the elevation results are from the dynamic characteristic averaging method. Figures 102 to 105 compare model traces using the manufacturer's published dynamic characteristics and the results from this study.

Table 10. Final results for Climatronics Dual Annulus Bivane. These results are a mathematical average of values from positions B, C, D, and F. Azimuth results are from Table 9 and elevation results are from Table 8.

Air Speed: 5 m s^{-1}

ζ_{az} = 0.39±0.06	$\lambda_{n\text{-}az}$:	Approach 1 = 2.70±0.16 Approach 2 = 2.66±0.41
ζ_{el} = 0.43±0.04	$\lambda_{n\text{-}el}$:	Approach 1 = 2.93±0.08 Approach 2 = 2.95±0.09

Air Speed: 10 m s^{-1}

ζ_{az} = 0.38±0.06	$\lambda_{n\text{-}az}$:	Approach 1 = 2.52±0.26 Approach 2 = 2.30±0.07
ζ_{el} = 0.46±0.04	$\lambda_{n\text{-}el}$:	Approach 1 = 2.92±0.10 Approach 2 = 2.87±0.10

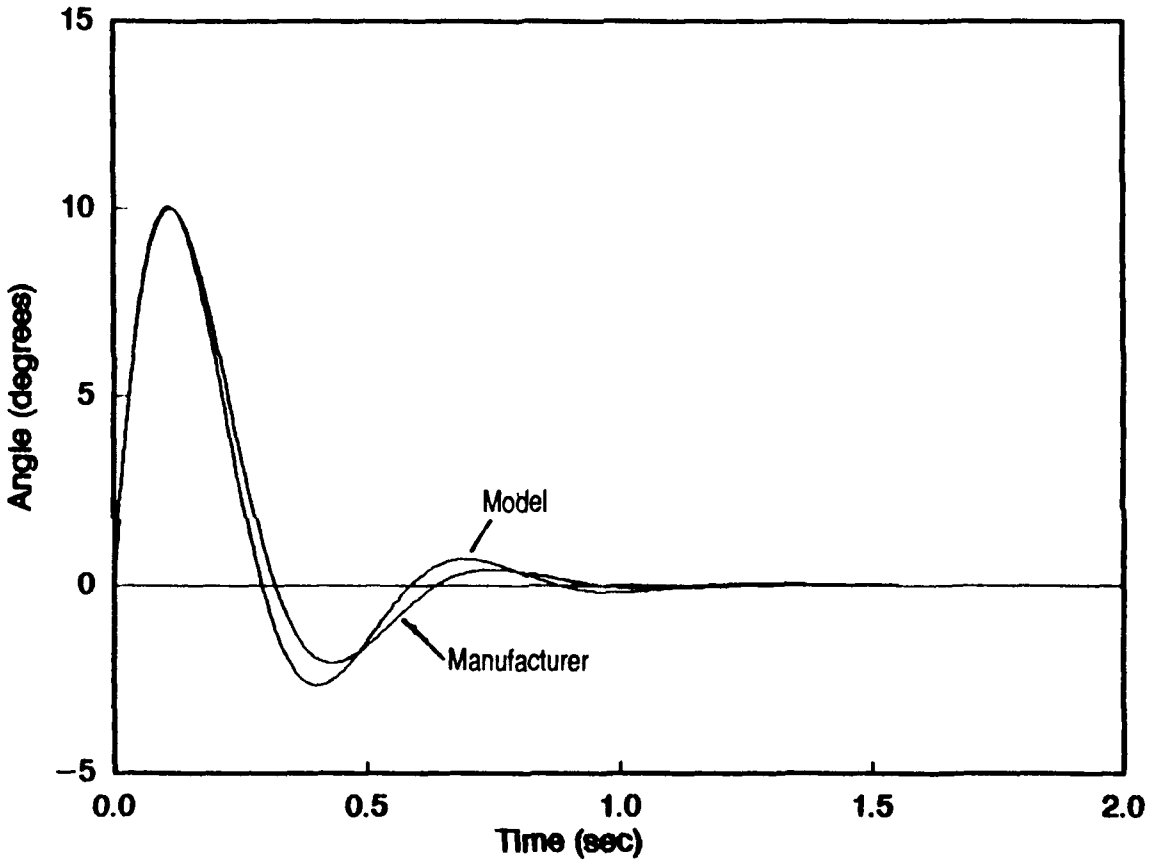

Figure 102. Comparison of azimuth traces computed from the final results and the manufacturer's published values using the model equation (38) for U = 5 m s^{-1} and Λ_0 = 192.32 deg s^{-1}.

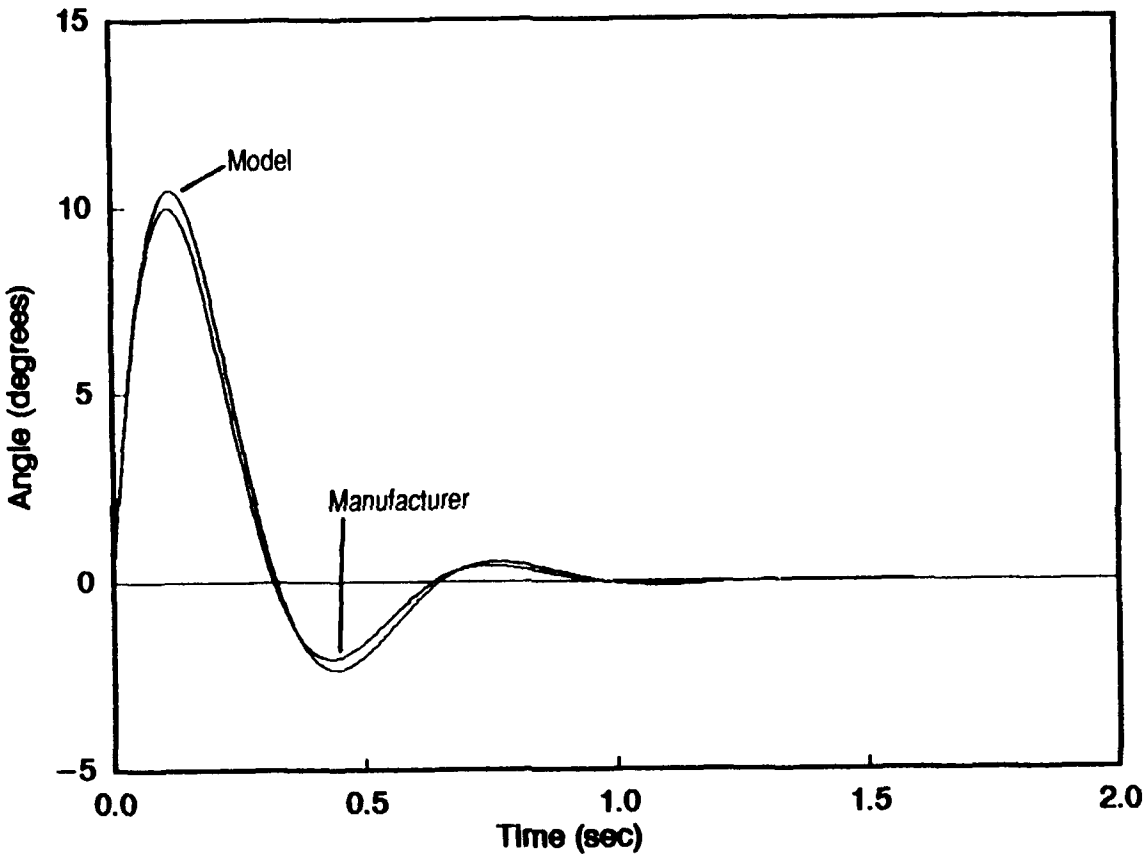

Figure 103. Same as in Figure 102, but for elevation data.

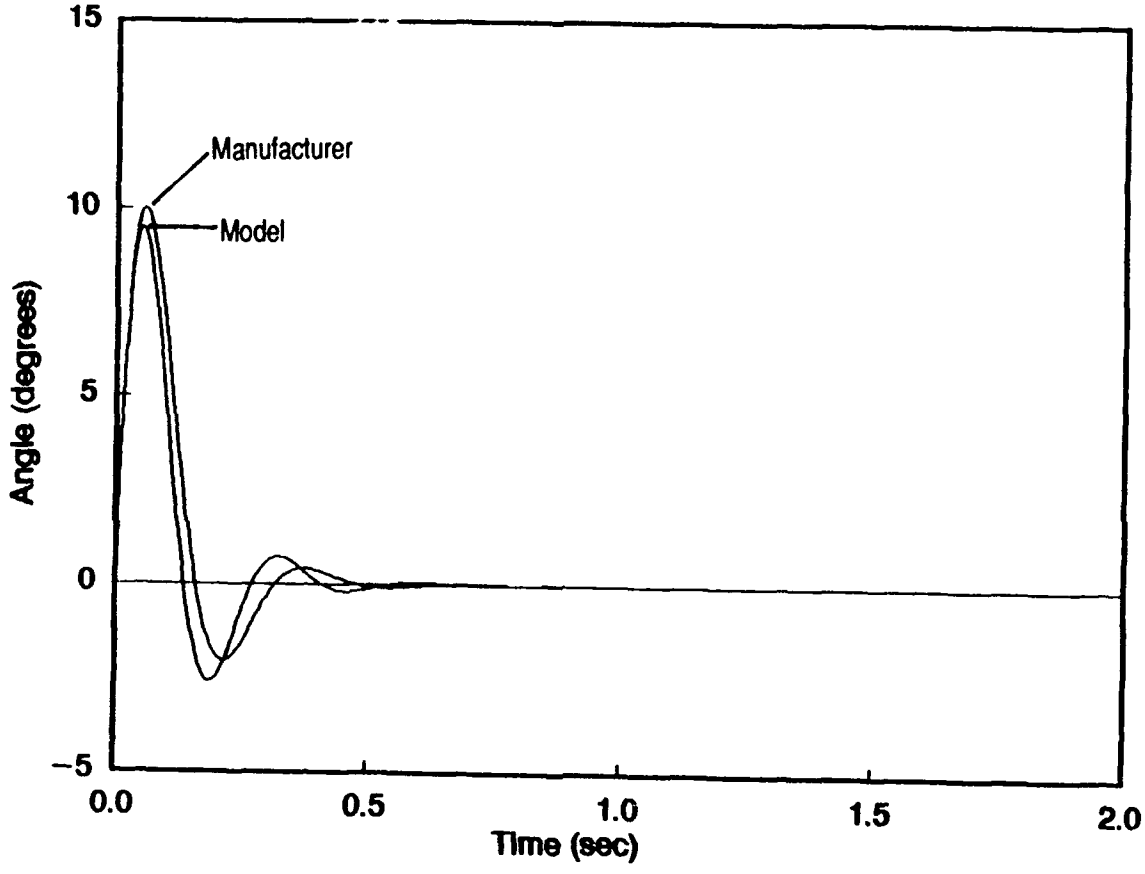

Figure 104. Same as in Figure 102, but for U = 10 m s^{-1} and Λ_0 = 384.64 deg s^{-1}.

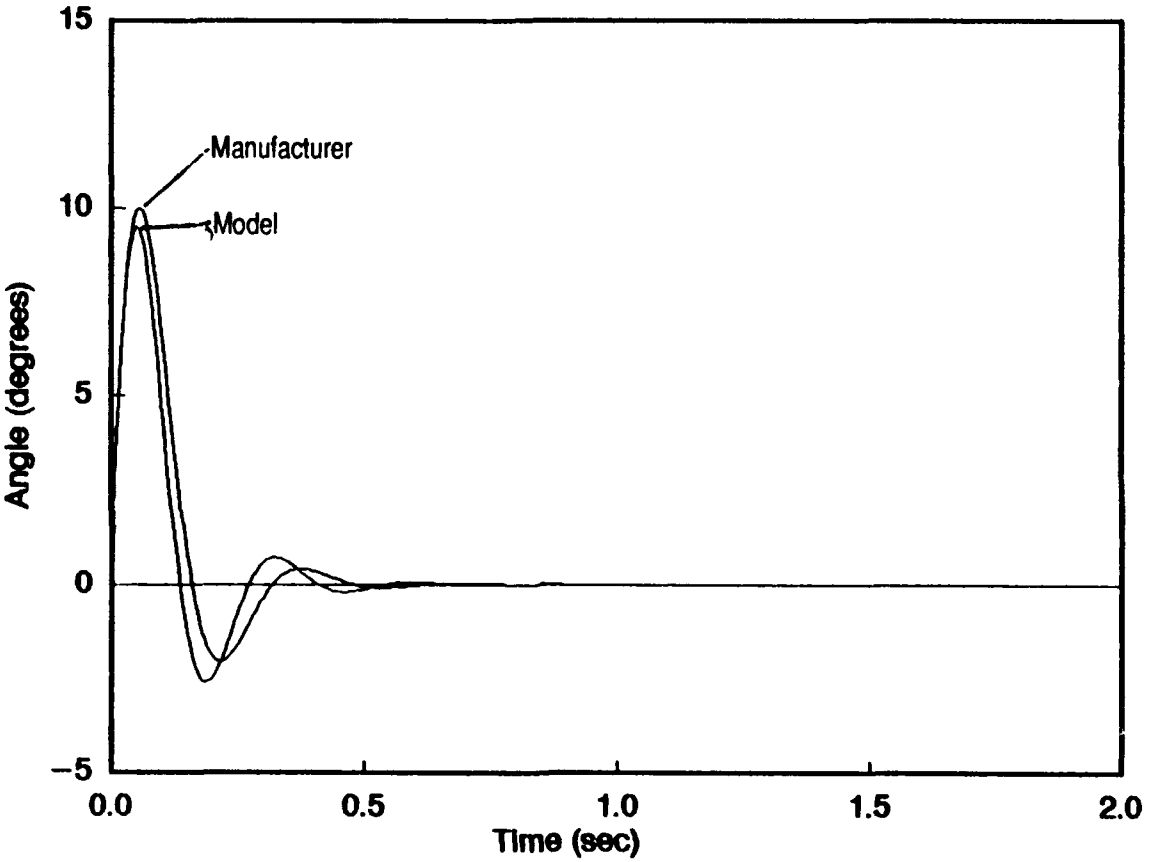

Figure 105. Same as in Figure 104, but for elevation data.

5. SUMMARY AND CONCLUSIONS

The goal of this study was to evaluate three different bivanes produced by R. M. Young, Teledyne Geotech, and Climatronics and determine which bivane displays the fastest and most accurate response to a change in wind direction. A subsequent study well determine if the bivane is suited to measure vertical momentum flux of horizontal momentum.

The evaluation consisted of two parts: static and dynamic tests. Static testing determined the degree of linearity of the voltage output as a function of known azimuth and elevation angles of each bivane. All three bivanes have output errors within the acceptable standards set by the ASTM. A best-fit regression line from the data was viewed as the ideal voltage output for the bivanes. The difference between the actual output and the regression value became the correction for that output. The corrections were used to adjust the voltage output from the dynamic response data.

Dynamic tests were performed in the large Civil Engineering wind tunnel at two wind speeds: 5 and 10 m s^{-1}. The vane assembly of each bivane was displaced at predetermined azimuth and elevation angles corresponding to six initial positions, A through F, so that when the vane was released the amplitude of the first peak was less than 15° and more near 10°. These angles are assumed small enough to consider aerodynamic effects about the fin as being negligible. Thus, the governing equation describing the bivane's dynamic response reduces to a simple second-order, underdamped system. The dynamic response consists of oscillations that contain overshoot and a characteristic wavelength. From these test results, the damping ratio and natural wavelength that characterize the behavior of the bivane are derived with respect to change in wind direction are derived.

The damping ratio and natural wavelength numbers were calculated using a scheme that involved the times of the first peak and the second zero-crossing. Conventional techniques that calculate these

dynamic characteristics use the amplitudes of the first and second peaks. In the dynamic tests performed in this study, the amplitude of the second peak was often difficult to measure and thus, the value was unreliable. Therefore, it was necessary to determine a different method to calculate the dynamic characteristics using more reliable values (i.e., times of the first peak and second zero-crossing).

A governing equation was used to model each bivane's output using the manufacturer's published dynamic characteristics for these bivanes and the results from the dynamic tests. When the amplitude of the first peak of the model was matched with the amplitude of a real data trace, the model accurately predicted the time of the second zero-crossing, but tended to overpredict the successive amplitudes and zero-crossings. Therefore, the bivanes actually damped out faster than what the model predicted. The governing equation does not take into account that mechanical friction opposes the motion of the vane. However, in this study, only the times of the first peak and second zero-crossing were necessary to calculate the dynamic characteristics. After T_1, equation (38) does not contribute to calculating ζ and λ_n.

The model from the governing equation can be used to determine the dynamic characteristics of the response if the velocity of the vane at the equilibrium angle, is known. This dynamic characteristic includes the forces about the tail and possibly can be used to determine how the aerodynamic affects are contributing to the bivane's response.

Determination of the final results of the bivanes was constrained to the nature of the individual bivanes. The response of the R. M. Young bivane was predictable. The data were easy to retrieve and interpret. The construction of the bivane was fairly rugged and the design was simple.

The Teledyne Geotech bivane used more elaborate methods to determine azimuth and elevation angles that eliminate friction at the contact points of the mechanical and electrical interfaces. The elevation data were found to have dynamic characteristics far different than what the manufacturer claimed. Upon inspection of the elevation data, significant oscillations with a consistent frequency were found trailing the initial vane response. These oscillations increased in direct proportion to increasing wind speed. It is felt that these oscillations are due to the fact that the cams in the elevation resolver are designed to force the vane assembly back to the horizontal position in near calm wind. This additional force is believed to

significantly affect the initial bivane response and produce dynamic characteristics different from the manufacturer's claim. The azimuth data also showed trailing oscillations, but at a lower frequency. These oscillations were not dependent on the wind speed and are believed to be caused by the conditioning electronics.

The Climatronics bivane consisted of a unique dual annulus vane assembly design that is suppose to react to changes in wind direction faster than vanes that use the more traditional cruciform tails. The R. M. Young and Teledyne Geotech bivanes use cruciform tails. The azimuth data from the Climatronics bivane was found to be too noisy for the software to calculate the dynamic characteristics. (The source of the noise is probably in the azimuth resolver and/or subsequent conditioning electronics.) Instead of hand-drawing a response curve through the data, the data points of all test runs were averaged to produce an average curve for a particular initial position and wind speed using locally-developed software for this purpose. These calculated curves were used to find the dynamic characteristics of the bivane at that initial position and wind speed. Reasonable numbers resulted from using this method. Elevation results calculated from the average dynamic characteristics of the test runs compared well with the results from the method used on the azimuth data. Thus, it is felt that the resulting azimuth dynamic characteristics are reliable and are fairly close to the manufacturer's published claims. The elevation response behaved well and was close to the manufacturer's claims.

It can be concluded from these test results of the three bivanes that the Climatronics Dual Annulus Bivane responds to wind changes the fastest. A comparison of the model traces of the three bivanes using the final results can be seen in Figures 106 to 109. In all the figures, the Climatronics response is the fastest to reach the equilibrium angle. The R. M. Young response is a close second, though its natural wavelength is nearly 60% longer than that of the Climatronics bivane. The Teledyne Geotech model curves react wildly to a change in wind direction and take considerable time to reach equilibrium. These curves are in response to the inferior data produced by the Teledyne Geotech bivane.

The forced oscillations in the Teledyne Geotech data are due to a design flaw and cannot be easily corrected. If the noisy azimuth signal from the Climatronics bivane is also due to a design problem, then the

R. M. Young bivane is the best bivane to be used in the second part of this study. However, if the noisy azimuth data in the Climatronics bivane is due to a defect in this particular azimuth resolver and can be easily corrected with a replacement, and since the output of the uncalibrated LVDT is easily corrected, then the Climatronics Dual Annulus Bivane is the best bivane for measuring momentum flux.

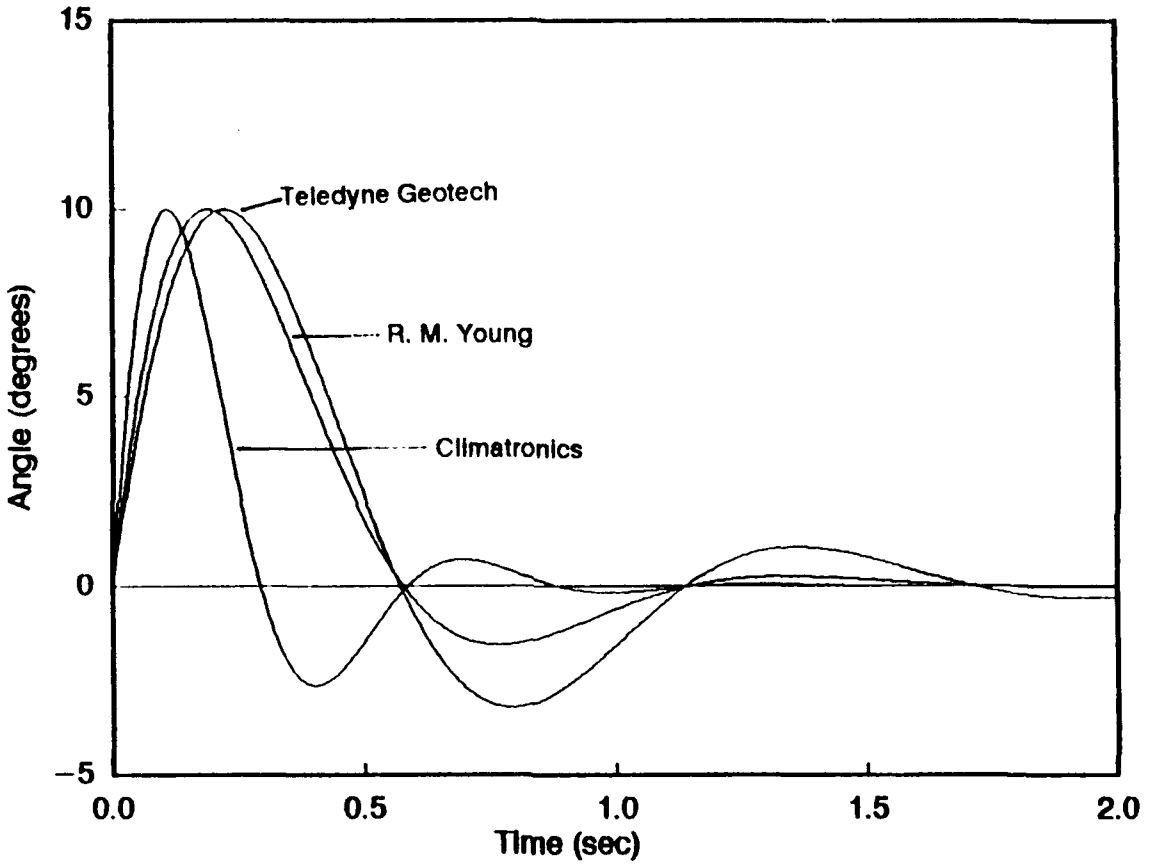

Figure 106. Comparison of the model traces from the three bivanes using the final azimuth results at 5 m s^{-1}.

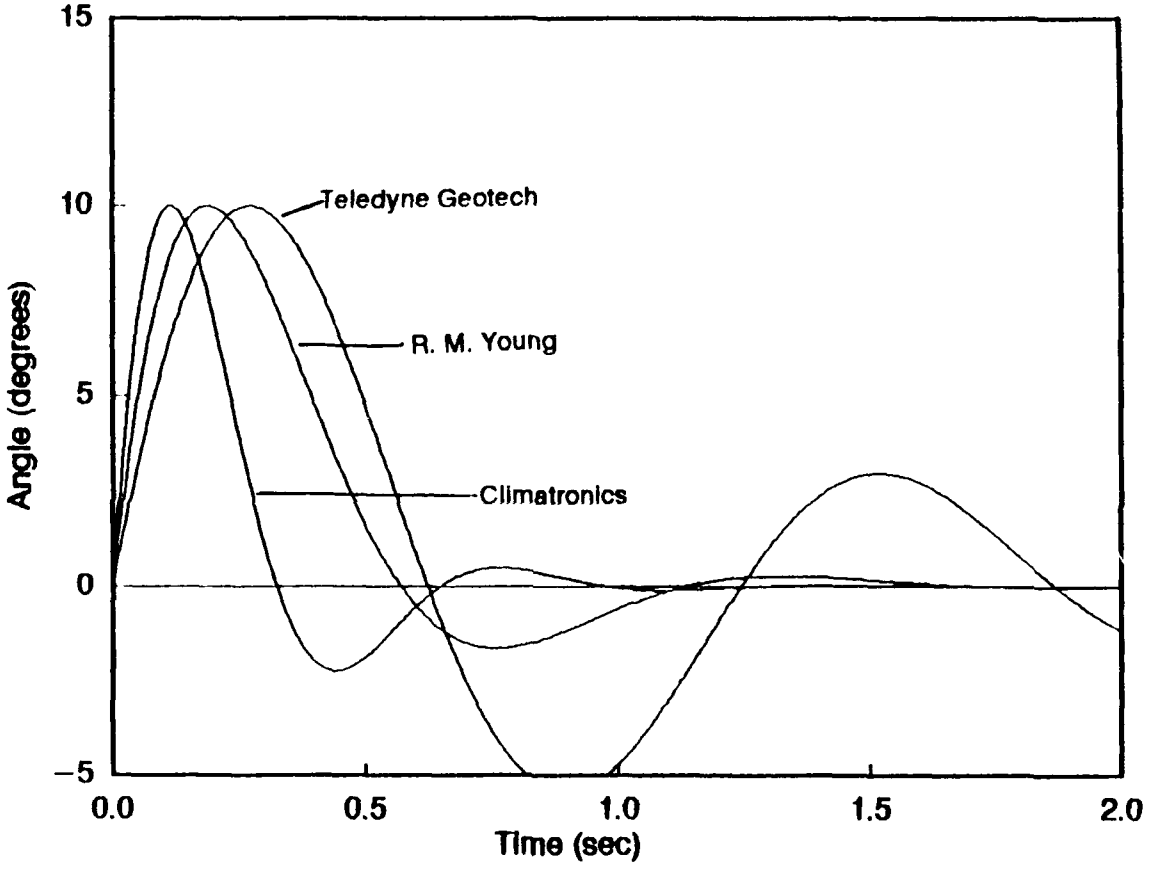

Figure 107. Same as in Figure 106, but for elevation final results.

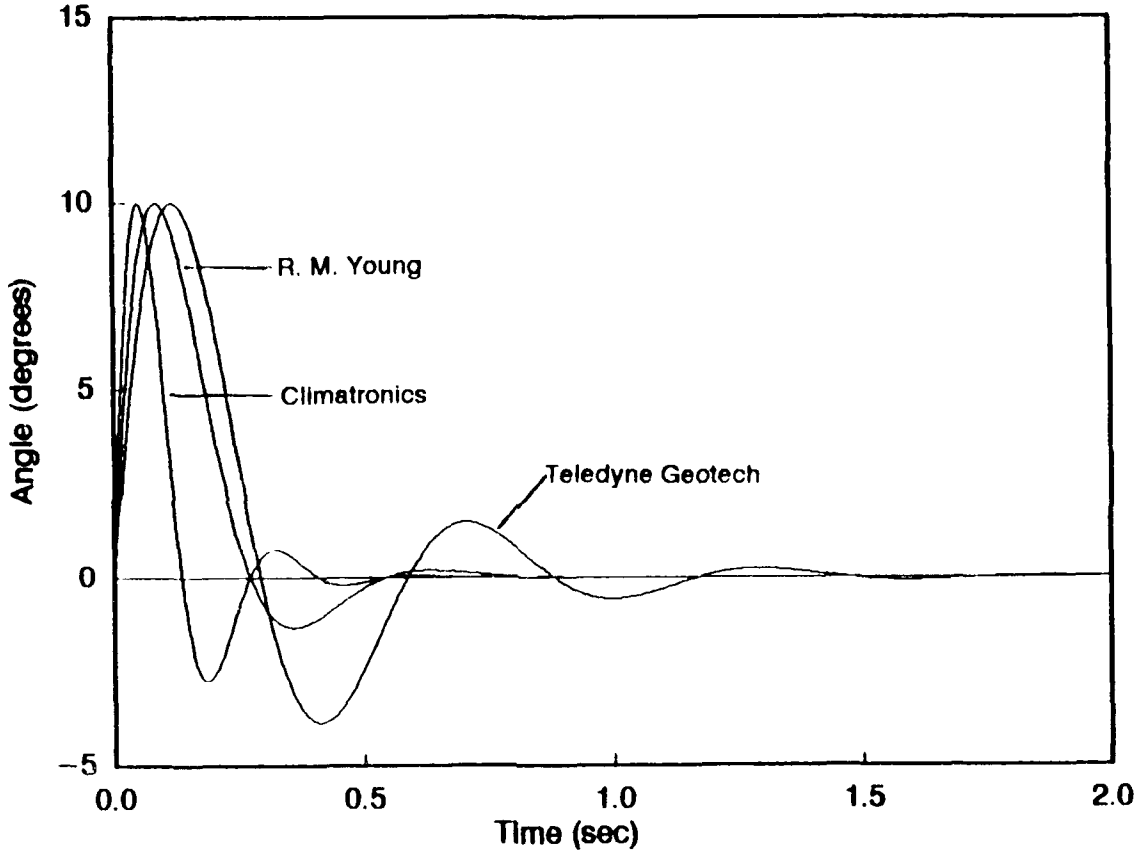

Figure 108. Same as in Figure 106, but for U = 10 m s^{-1}.

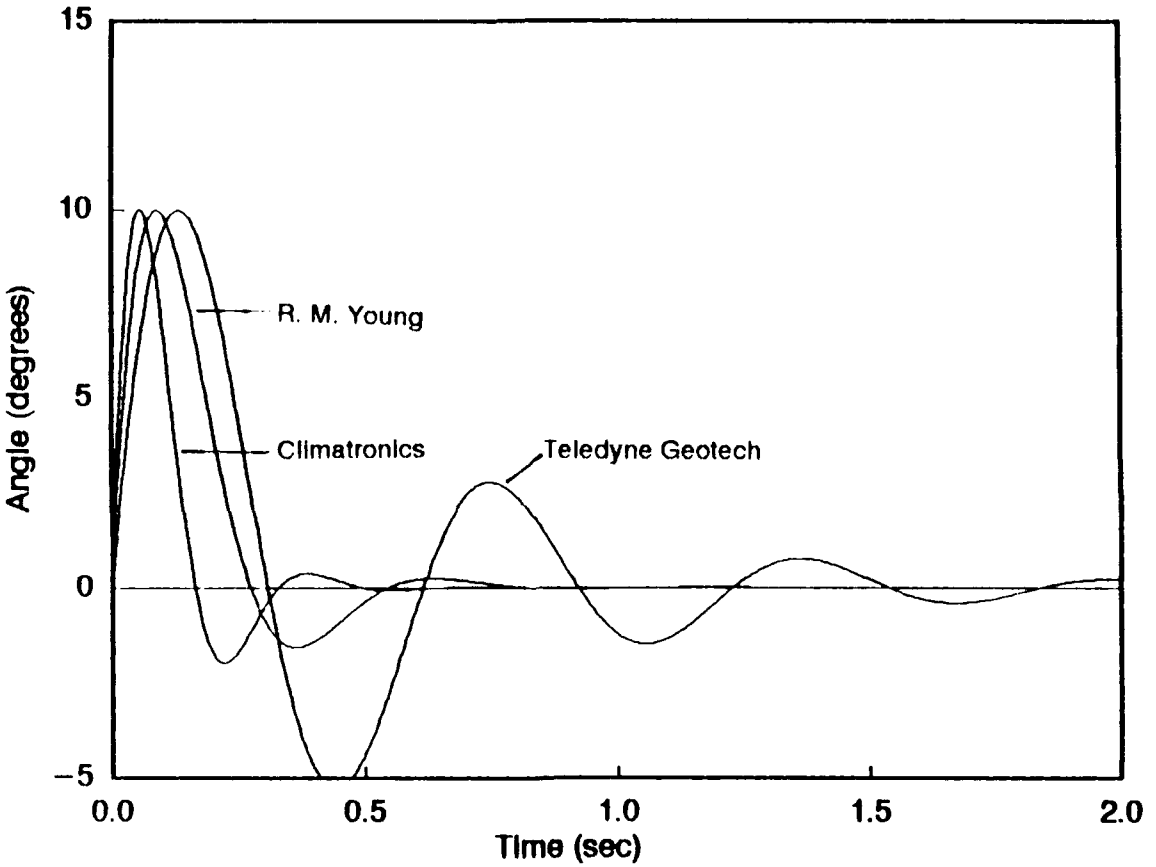

Figure 109. Same as in Figure 107, but for U = 10 m s^{-1}.

LIST OF REFERENCES

LIST OF REFERENCES

Baker, C. B., and Sethu Raman, 1987: Dynamic response of an annular bi-directional vane. Preprints Sixth Symposium Meteor. Observation and Instrumentation, New Orleans, Amer. Meteor. Soc., 177-180.

Chimonas, G., 1980: Reynolds stress deflections of the bivane anemometer. J. Appl. Meteor., 19, 329-333.

Climatronics Corporation, 1980: Dual Annulus Bivane, Climatronics Corp.,Bohemia, N. Y., 9 pp.

Garbell, M. A., 1947: Fins for aerological instruments. J. Meteor., 4, 82-91.

Lockhart, T. J., 1989: Quality Assurance Handbook for Air Pollution Measurement Systems, 4, Meteor. Measurements, USEPA, Research Triangle Park, N. C., 240 pp.

MacCready, P. B., and H. R. Jex, 1964: Response characteristics and meteorological utilization of propeller and vane wind sensors. J. Appl. Meteor., 3, 182-193.

Mazzarella, D. A., 1952: An all-weather, remote-recording bivane. Bull. Amer. Meteor. Soc., 33, 60-66.

R. M. Young Company, 1989: Product Catalogs: Sensitive Wind Instruments, R. M. Young Co., Traverse City, MI., 7 pp.

R. M. Young Company, 1979: Instructions: Gill Bivane, Gill Anemometer Bivane, R. M. Young Co., Traverse City, MI., 11 pp.

SethuRaman, S., and W. A. Tuthill, 1978: Response characteristics of a new bidirectional vane. Bull. Amer. Meteor. Soc., 59, 1114-1118.

Schlicting, H., 1968: Boundary-Layer Theory, McGraw-Hill, Inc., 748 pp.

Teledyne Geotech, 1987: Operation and Maintenance Manual, Teledyne Geotech, Garland, TX., 28 pp.

Wang, J. Y., and C. M. M. Felton, 1983: Instruments for Physical Environmental Measurements, Kendall/Hunt Publishing Company, 378 pp.

Wieringa, J., 1967: Evaluation and design of wind vanes. J. Appl. Meteor., 6, 1114-1122

Wyngaard, J. C., 1981: Cup, propeller, vane, and sonic anemometers in turbulence research. Ann. Rev. Fluid Mech., 13, 399-423.